

THE UNIVERSITY OF HULL

**An Effective Optimisation Method for Multifactor and
Reliability-related Structural Design Problems**

being a Thesis submitted for the Degree of Doctor of Philosophy

in the University of Hull

by

CHUNG KET THEIN

BEng Mechanical Engineering (Hull)

July 2011

Abstract

This thesis first presents a systematic design procedure which satisfies the required strength and stiffness, and structural mass for conceptual engineering structural designs. The procedure employs a multi-objective and multi-disciplinary (MO–MD) optimisation method (multifactor optimisation of structure techniques, MOST) which is coupled with finite element analysis (FEA) as an analysis tool for seeking the optimum design. The effectiveness of the MOST technique is demonstrated in two case studies.

Next, a reliability-related multi-factor optimisation method is proposed and developed, representing a combination of MOST (as a method of multi-factor optimisation) and the reliability-loading case index (RLI) (as a method of calculating the reliability index). The RLI is developed based on a well-known reliability method: the first-order reliability method (FORM). The effectiveness and robustness of the proposed methodology are demonstrated in two case studies in which the method is used to simultaneously consider multi-objective, multi-disciplinary, and multi-loading-case problems. The optimised designs meet the targeted performance criteria under various loading conditions.

The results show that the attributes of the proposed optimisation methods can be used to address engineering design problems which require simultaneous consideration of multi-disciplinary problems. An important contribution of this study is the development of a conceptual MO–MD design optimisation method, in which multi-factor structural and reliability design problems can be simultaneously considered.

Acknowledgements

First, I would like to express my sincere gratitude to my supervisor, Dr. Jing-Sheng Liu, who has provided support and guidance during this study and has shown great understanding as well as giving me the freedom to pursue my research.

I would also like to thank Dr. Gilbert and Mr. Ooi for useful advice and recommendations regarding the energy-harvesting problem.

Above all, I would like to thank my parents and my sister for their great care and thank Alicia Ng for her understanding and support, for which I am eternally grateful.

Publications

The following is a list of publication recently submitted:

- Thein, C.K., and Liu, J-S., Effective structural sizing/shape optimisation through a reliability-related multifactor optimisation approach, *Multidiscipline Modeling in Materials and Structures*, Submitted for publication.
- Thein, C.K., Ooi, B.L., Liu, J-S., Gilbert, J.M., Modelling and optimisation of a bimorph piezoelectric cantilever beam in an energy harvesting application, *Journal of Intelligent Material Systems and Structures*, Submitted for publication.

Table of Contents

Abstract	ii
Acknowledgements	iii
Publications	iv
Table of Contents	v
Table of Figures	x
Table of Tables.....	xvi
Glossary	xviii
1 Introduction.....	1
1.1 Introduction	1
1.2 Research objectives	4
1.3 Applications of the proposed optimisation methods	4
1.4 Overview of the dissertation.....	5
2 Sizing-, Shape-, and Topology-Optimisation Methods for a Structural Problem	8
2.1 Introduction	8
2.2 Description of the optimal design.....	9
2.3 Types of structural optimisation techniques	11
2.4 Review of existing optimisation methods	12
2.4.1 Metamorphic development	13
2.4.2 Adaptive weighted sum method	16
2.4.3 Genetic algorithm	18
2.4.4 Multifactor optimisation of structure techniques.....	23
2.4.5 Structural shape optimisation	24
2.4.6 Particle swarm optimisation	25
2.5 Summary.....	27
3 Methods for Analytical and Computational Reliability Analyses	28
3.1 Basis of a structural design concept	28
3.2 Graphical representation of load and resistance	29
3.3 Reliability techniques	29
3.3.1 First- and second-order reliability methods.....	30
3.3.2 Monte Carlo simulation	32

3.3.3	Latin hypercube sampling.....	33
3.3.4	Importance sampling	35
3.3.5	Response surface	36
3.3.6	Artificial neural network.....	37
3.4	Summary of reliability methods	39
3.5	Reliability analysis using commercial software	40
3.5.1	NESSUS	41
3.5.2	PROBAN	43
3.5.3	CalREL	44
3.5.4	FERUM	46
3.6	Summary.....	47
4	First-order Reliability-related Method, Reliability-based Optimisation, and Optimisation Methodology	48
4.1	Detailed description of the first-order reliability method.....	48
4.1.1	Cornell method	48
4.1.2	Hasofer and Lind method	50
4.1.3	Rackwitz and Fiessler method.....	53
4.2	Reliability loading-case index – A new first-order reliability-related method	54
4.3	Reliability-based optimisation (RBO) technique	57
4.3.1	Introduction.....	57
4.3.2	Description of an RBO problem	58
4.3.3	Early approaches.....	59
4.3.4	Approximate reliability technique	61
4.3.4.1	Double loop approaches	61
4.3.4.2	Single loop approaches	62
4.3.4.3	Decoupling approaches.....	64
4.3.5	Simulation-based RBO	65
4.3.5.1	Meta-models	65
4.3.5.2	Decoupling.....	66
4.3.5.3	Direct integration.....	68
4.4	Multifactor Optimisation of Structure Techniques (MOST).....	69
4.4.1	Optimisation methodology	69

4.4.2	Performance data matrix	69
4.4.3	Parameter profile matrix	70
4.4.4	Performance Assessment	71
4.5	Formulation of an optimisation problem	74
4.6	Summary.....	75
5	Multi-objective Optimisation – An Automotive Component Optimisation (Sliding Caliper).....	76
5.1	Introduction	76
5.2	Brake system.....	77
5.2.1	Drum brake	77
5.2.2	Disc brake	79
5.3	Validation analysis of optimised sliding caliper.....	80
5.3.1	Design Problem	80
5.3.2	Design constraints and boundary conditions	81
5.3.3	Convergence test.....	82
5.4	Results and discussions	85
5.4.1	MOST optimisation	85
5.4.2	Distributions of stress and displacement	86
5.4.3	Optimisation history and convergence	90
5.5	Summary.....	93
6	Multi-objective and Multi-discipline Optimisation – An Energy Harvesting Device Optimisation (Bimorph Cantilever Beam).....	94
6.1	Introduction	94
6.2	Background to energy harvesting	96
6.2.1	Vibration	96
6.2.2	Source of energy	96
6.2.2.1	Solar power.....	97
6.2.2.2	Vibration.....	98
6.2.2.3	Human power	98
6.2.2.4	Temperature variations	99
6.2.2.5	Summary of power scavenging	99
6.2.3	Types of vibrations	100
6.2.4	Model of the Conversion of Vibration to Electricity.....	103

6.2.5	Piezoelectric material.....	105
6.2.6	Piezoelectric converter (vibration to electrical).....	107
6.3	Analytical model of a piezoelectric generator	108
6.3.1	Review of the magnitude of voltage for a piezoelectric bender (Roundy, 2003)	108
6.3.2	Predicting the output power of piezoelectric generator designs with different geometrical shapes using finite element analysis	108
6.3.3	Theoretical frequency	111
6.3.4	Material properties	112
6.4	Verification of experimental, theoretical, and ANSYS simulation results.....	113
6.5	Maximum strain and width responses	115
6.6	Shape optimisation using the multifactor optimisation of structure techniques (MOST)	116
6.6.1	Design considerations	116
6.6.2	Design constraints and load	116
6.6.3	Finite element model of a bimorph cantilever beam	117
6.6.4	Formulation of the optimisation problem	120
6.7	Results and discussions	121
6.7.1	Optimisation results	121
6.7.2	Optimisation history	122
6.7.3	von Mises total strain energy.....	124
6.7.4	Vibration of the cantilever beam	126
6.7.5	Mass response of the optimised design	128
6.7.6	Optimised design and triangular design	128
6.8	Investigation of the optimum topology of a bimorph cantilever beam	130
6.8.1	Design domain, load, and boundary conditions.....	130
6.8.2	Optimum “topology” structure of the cantilever beam.....	131
6.8.3	Results and discussions.....	131
6.8.4	Sizing and shape optimisation using MOST	133
6.9	Summary.....	135
7	A New Development of Reliability-related Multi-factor Optimisation and its Applications	136
7.1	Multi-criteria optimisation.....	136

7.1.1	Design constraints.....	136
7.2	Example 1 – Star-like truss structure.....	137
7.2.1	Introduction.....	137
7.2.2	Design considerations.....	137
7.2.3	Design constraints and loads	139
7.2.4	Results and discussions.....	139
7.2.4.1	Optimisation results.....	139
7.2.4.2	Optimisation histories.....	141
7.3	Example 2 – Raised-access floor panel	145
7.3.1	Introduction.....	145
7.3.2	British Standard BS EN	146
7.3.3	Design constraints and loads	148
7.3.4	Finite element modelling of the panel	150
7.3.5	Optimisation of the raised-access floor panel.....	151
7.3.6	Results and discussions.....	151
7.3.6.1	Optimisation results.....	151
7.3.6.2	Optimisation histories.....	153
7.3.6.3	Stress distribution	157
7.4	Summary.....	161
8	Conclusions and Future Work	162
8.1	Summary of research	162
8.2	Conclusions	163
8.3	Recommendations for future work	166
9	References.....	168
10	Appendices.....	195
	Appendix A – Example of reliability-related multi-factor optimisation.....	195
a)	Result of static analysis	195
b)	Reliability loading-case index result	199
	Appendix B – Multifactor optimisation of structure technique (MOST): optimisation flow procedure	200
	Appendix C – Piezoelectric generator	206
a)	Mechanical derivation	206

List of Figures

Figure 1.1 –	MO–MD design for single and multiple disciplines (de Weck, 2004).....	2
Figure 1.2 –	Breakdown of the thesis and the proposed method, highlighting the reliability-related multifactor sizing/shape structural optimisation.....	7
Figure 2.1 –	Topology optimisation (discrete element), showing (a) the initial design, and (b) the optimised design (Rong and Liang, 2008).....	12
Figure 2.2 –	Topology optimisation (continuum approach), showing (a) the initial design, and (b) the optimised design (Ohsaki, 2001).....	12
Figure 2.3 –	Optimisation from structure A, showing (a) the initial structure, (b) iteration 10, (c) iteration 20, (d) iteration 30, (e) iteration 45, (f) iteration 60, and (g) iteration 69 (Liu <i>et al.</i> , 2000).....	14
Figure 2.4 –	Optimisation from structure B, showing (a) the initial structure, (b) iteration 10, (c) iteration 20, (d) iteration 30, (e) iteration 40, (f) iteration 50, and (g) iteration 53 (Liu <i>et al.</i> , 2000).....	15
Figure 2.5 –	The concept and procedures of AWS, showing (a) the weighted-sum method, (b) the initial step, (c) constraint imposition, and (d) refinement (Kim and de Weck, 2005).....	17
Figure 2.6 –	AWS method for the Pareto front, showing (a) the convex region, (b) non-convex regions with non-dominated solutions, and (c) non-convex regions with dominated solutions (Top: initial solution; Bottom: AWS solution) (Kim and de Weck, 2005).....	17
Figure 2.7 –	(a) Geometrical dimensions, applied load, and force locations for an 18-bar space truss structure, and (b) the optimum shape of the structure (Rahami <i>et al.</i> , 2008).....	19
Figure 2.8 –	Optimization of a cantilever beam, showing (a) loading case 1 and (b) loading case 2 (top: design domain; bottom: optimum design), and (c) combinations of the two initial solutions (Aguilar Madeira <i>et al.</i> , 2005).....	19
Figure 2.9 –	Optimal shape of a planar truss structure, as obtained by MOST. (a) Initial design; (b) Optimised design (Liu <i>et al.</i> , 1999).....	23
Figure 2.10 –	Two-dimensional plate with a hole, showing (a) the general dimensions, and the locations of the applied load and stress constraint, (b) the initial finite element design, and (c) the optimal finite element design (Campbell and Kelliher, 2000).....	25

Figure 2.11 – Layout of (a) a 25-bar space truss structure and (b) a 72-bar space truss structure.....	26
Figure 3.1 – Density distribution of load and resistance (Haldar and Mahadevan, 1995).....	29
Figure 3.2 – H–L reliability index	30
Figure 3.3 – The bulges method is used to search for the optimum solution for multiple design points, for x_1 values between -5 and -1 (left), for between 1 and 5 (middle), and for between -1 and 1 (right). (Der Kiureghian and Dakessian, 1998).....	31
Figure 3.4 – Random cumulative density function divided into five intervals.....	34
Figure 3.5 – 4×4 Latin domain for two random variables	34
Figure 3.6 – Optimal radius of the excluded sphere using adaptive radius-based IS (Grooteman, 2008)	35
Figure 3.7 – Multilayer feed-forward ANN.....	37
Figure 3.8 – (a) Simulation model for a vehicle crash, and (b) the relevant NESSUS problem statement (Riha <i>et al.</i> , 2004)	42
Figure 3.9 – Ductile frame and failure mechanisms (after Der Kiureghian, 2006)	45
Figure 4.1 – \hat{Y} space	49
Figure 4.2 – Definition of β in the standard normal space	50
Figure 4.3 – Rackwitz algorithm to solve the H–L reliability index	52
Figure 4.4 – Limit state of mass, stress, and displacement in the standard normal space	56
Figure 4.5 – Schematic diagram of an RBO problem (after Valdebenito and Schuëller, 2010a).....	59
Figure 4.6 – Example that employs a PDM.....	70
Figure 4.7 – Calculation of a data point in the case of two acceptable limits	71
Figure 5.1 – Brake system	77
Figure 5.2 – Simplified drum brake system.....	78
Figure 5.3 – Cross-sectional diagrams of (a) a fixed caliper and (b) a sliding caliper	79
Figure 5.4 – Types of disc: (a) top-hat shaped disc, and (b) ventilated disc	80
Figure 5.5 – (a) Numbers ‘1’ to ‘13’ are the key points as design variables, and (b) ‘d14’ is one of the sizing design variables	81
Figure 5.6 – (a) Sliding caliper overview, (b) design constraints, and (c) applied load (red area) and symmetry plane (green area)	82
Figure 5.7 – Initial design (bottom view)	83

Figure 5.8 – Initial finite element design of a sliding caliper	84
Figure 5.9 – Optimisation history, showing (a) the initial design, (b) $n_i = 29$, and (c) the optimised design at $n_i = 109$	85
Figure 5.10 – Contours of von Mises stress for (a) the initial design and (b) the optimised design (MPa).....	86
Figure 5.11 – Distribution of stress in a sliding caliper under mechanical load, showing (a) τ_{xz} shear stress, (b) τ_{xy} shear stress, (c) τ_{yz} shear stress, (d) most positive (tensile) stress, and (e) most negative (compression) stress (MPa).....	87
Figure 5.12 – Distribution of displacement along the x -axis (mm)	88
Figure 5.13 – Distribution of displacement along the y -axis (mm)	89
Figure 5.14 – Distribution of displacement along the z -axis (mm)	89
Figure 5.15 – Distribution of the displacement vector sum (mm).....	90
Figure 5.16 – Convergence of mass and maximum von Mises stress	91
Figure 5.17 – Convergence of the maximum displacement vector sum.....	92
Figure 6.1 – Continuous power density for various power sources.....	98
Figure 6.2 – Vibration spectrum of acceleration vs. frequency for a desk fan with variable	101
Figure 6.3 – Vibration spectrum of displacement vs. frequency for a desk fan with variable speed	102
Figure 6.4 – Vibration spectrum of a fan heater (acceleration vs. frequency).....	102
Figure 6.5 – Vibration Spectrum of a fan heater (displacement vs. frequency)	103
Figure 6.6 – Schematic diagram of a vibration converter.....	103
Figure 6.7 – Simulation of generated power against mechanical and electrical damping ratios	104
Figure 6.8 – Power output against frequency	105
Figure 6.9 – Schematic diagrams showing the 33 mode and 31 mode of a piezoelectric material.....	107
Figure 6.10 – Schematic of a piezoelectric bender	108
Figure 6.11 – Schematic diagrams of (a) a cantilever structure, and (b) an SDOF model	111
Figure 6.12 – Schematic diagram of the experiment setup (mm).....	113
Figure 6.13 – Comparison of theoretical calculations, ANSYS simulation, and experimental results for output power	114
Figure 6.14 – Strain distributions for a rectangular beam with varying widths	115

Figure 6.15 – Load and boundary conditions of the cantilever beam.....	117
Figure 6.16 – Convergence of average element stress and displacement.....	119
Figure 6.17 – Finite element discretisation of the initial solid cantilever beam	119
Figure 6.18 – MOST optimisation history of a bimorph cantilever beam showing the (a) initial design, (b) $n_i = 4$, (c) $n_i = 8$, (d) $n_i = 12$, (e) $n_i = 18$, and (f) the optimised design at $n_i = 27$ (red lines indicate the constraints are fixed along the x , y , and z axes).....	121
Figure 6.19 – Distribution of von Mises stress for the initial design (left) and the optimised design (right) (Pa)	122
Figure 6.20 – Optimisation convergence history of the structural volume (excluding the volume of the tip mass) and power.....	123
Figure 6.21 – Optimisation convergence history of the average element stress and displacement	123
Figure 6.22 – Distribution of strain energy for the initial and optimised designs	125
Figure 6.23 – Strain distribution according to the strain ratio	126
Figure 6.24 – Shapes of the first six modes of the beam (undeformed shape: dotted line and deformed shape: blue colour)	127
Figure 6.25 – Mass response of the optimised design	128
Figure 6.26 – Dimensions of (a) rectangular, (b) triangular, and (c) optimised shapes (unit in mm).....	129
Figure 6.27 – Power output of rectangular, triangular, and optimised shapes.....	129
Figure 6.28 – Design domain and shape constraints of the optimised design	130
Figure 6.29 – Optimisation of optimum “topology” designs, showing designs (a) to (h)	131
Figure 6.30 – Average strain and power density of the various optimum “topology” designs	132
Figure 6.31 – von Mises stress and structural volume of the various optimum “topology” designs	132
Figure 6.32 – Distribution of von Mises stress in the optimum “topology” design (h) (Pa)	133
Figure 7.1 – Initial layout of the star-like truss structure.....	138
Figure 7.2 – Optimised design, showing a (a) front view and (b) top view	140
Figure 7.3 – Stress distribution in a truss structure with the initial design, showing loading case 1 (left) and loading case 2 (right) (MX and MN indicate the maximum and minimum stress, respectively) (Pa)	140

Figure 7.4 – Stress distribution in a truss structure with the optimised design, showing loading case 1 (left) and loading case 2 (right) (MX and MN indicate the maximum and minimum stress, respectively) (Pa).....	141
Figure 7.5 – Optimisation convergence histories of sizing design variables and structural mass	142
Figure 7.6 – Optimisation convergence histories of truss dimensions	142
Figure 7.7 – Optimisation convergence history of the reliability loading-case index	143
Figure 7.8 – Optimisation convergence history of maximum stress	143
Figure 7.9 – Optimisation convergence history of maximum displacement	143
Figure 7.10 – Raised-access floor panels (The Access Flooring Company, 2008)	145
Figure 7.11 – Example of a steel-encapsulated HDPB floor panel (RG2 BS EN floor panel; see http://www.fieldmansaccessfloorsltd.com/)	146
Figure 7.12 – Loading cases in the present analysis	148
Figure 7.13 – (a) Discretisation of the initial structure, and (b) enlarged view of the panel	149
Figure 7.14 – Detail of design parameters	150
Figure 7.15 – Discretisation of the floor panel design, showing (a) the initial design and (b) the optimised design.....	151
Figure 7.16 – Distribution of von Mises stress for the optimised floor panel, showing loading case 1 (top left), loading case 2 (top right), loading case 3 (bottom left), and loading case 4 (bottom right) (unit: Pa).....	152
Figure 7.17 – Distribution of displacement for the optimised floor panel, showing loading case 1 (top left), loading case 2 (top right), loading case 3 (bottom left), and loading case 4 (bottom right) (unit: m)	153
Figure 7.18 – Optimisation convergence history of mass.....	154
Figure 7.19 – Optimisation convergence history of maximum von Mises stress for four different loading cases	154
Figure 7.20 – Optimisation convergence history of maximum displacement for four different loading cases	155
Figure 7.21 – Optimisation convergence history of reliability loading-case index for four different loading cases	155
Figure 7.22 – Distribution of the most positive (tensile) stress for the optimised floor panel, for loading cases 1 (top left), 2 (top right), 3 (bottom left), and 4 (bottom right) (unit: Pa).....	157

Figure 7.23 – Distribution of the most negative (compressive) stress for the optimised floor panel, for loading cases 1 (top left), 2 (top right), 3 (bottom left), and 4 (bottom right) (unit: Pa)	158
Figure 7.24 – Distribution of τ_{xz} shear stress for loading cases 1 (top left), 2 (top right), 3 (bottom left), and 4 (bottom right) (unit: Pa).....	159
Figure 7.25 – Comparison of maximum von Mises stress for the original and optimised panels	160
Figure 7.26 – Comparison of maximum displacement for the original and optimised panels	160

List of Tables

Table 2.1 –	GA methods.....	20
Table 2.2 –	Summary of the most well-known GA methods (from Konak <i>et al.</i> , 2006).....	21
Table 3.1 –	Summary of reliability methods	39
Table 3.2 –	Reliability software and relevant references	40
Table 4.1 –	Performance data matrix.....	70
Table 4.2 –	Parameter profile matrix.....	70
Table 5.1 –	Element size (sliding caliper)	83
Table 5.2 –	Attributes of the initial and optimised designs	92
Table 6.1 –	Comparison of Energy Sources (Roundy, 2003).....	97
Table 6.2 –	Solar power under different conditions	98
Table 6.3 –	Acceleration magnitude and fundamental frequency of various vibration sources (after Leland <i>et al.</i> , 2007).....	100
Table 6.4 –	SDOF equivalent mass for structural systems.....	111
Table 6.5 –	Material properties of PZT and brass shim	112
Table 6.6 –	Dimensions of piezoelectric generator	114
Table 6.7 –	Dimensions of the initial design.....	117
Table 6.8 –	Effect of element length on displacement and average element stress in a convergence test	118
Table 6.9 –	Design attributes of the initial and optimised designs of a cantilever beam	124
Table 6.10 –	Distribution of the strain ratio for the initial and optimised designs.....	125
Table 6.11 –	Natural frequency of the first six modes	127
Table 6.12 –	Comparison of power density among beams with different shapes.....	129
Table 6.13 –	Design attributes of the optimised and optimum “topology” structures	134
Table 7.1 –	\hat{Y} space variables of the star-like truss structure.....	138
Table 7.2 –	Coordinates of nodal points of the initial star-like truss structure.....	139
Table 7.3 –	Cross-sectional areas of elements of the initial star-like truss structure	139
Table 7.4 –	Attributes of the initial and optimised designs of the star-like truss structure	144
Table 7.5 –	Truss dimensions and size of the initial and optimised star-like truss structure	144
Table 7.6 –	Panel classification based on ultimate load	147

Table 7.7 – Panel classification based on deflection	147
Table 7.8 – BS EN 12825 standard	147
Table 7.9 – Initial dimensions of design parameters	149
Table 7.10 – Material properties of BMC	151
Table 7.11 – Performance of the original design under four different loading cases.	156
Table 7.12 – Performance of the optimised structure under four different loading cases.....	156

Glossary

Abbreviations

AWS	Adaptive Weighted Sum Method
CalREL	Cal-Reliability
FERUM	Finite element reliability using MATLAB
FORM	First-order reliability method
GA	Genetic Algorithm
H–L	Hasofer and Lind
IS	Importance sampling
LHS	Latin hypercube sampling
LSC	Limit state condition
MCS	Monte Carlo simulation
MD	Metamorphic development
MO–MD	Multi-objective and multi-disciplinary
MOST	Multifactor optimisation of structural techniques
NESSUS	Numerical evaluation of stochastic structures under stress
NN	Neural network
PROBAN	Probability Analysis
PSO	Particle swarm optimisation
R–F	Rackwitz and Fiessler
RLI	Reliability loading-case index
RS	Response surface
SORM	Second-order reliability method
SSO	Structural shape optimisation

Nomenclature

C_p	Capacitance of the piezoelectric device (F)
k	Coupling coefficient
c	Damping coefficient
ϵ	Dielectric constant of the piezoelectric material
m_{eff}	Effective mass (kg)
l_b	Length of base (mm)
l_f	Length of clamp (mm)
l_m	Length of tip mass (mm)
L	Load (N)
W	Magnification factor
m	Mass (kg) or Number of performances
m_{beam}	Mass of the beam (kg)
S1	Maximum principal stress/most positive stress (MPa)
S3	Minimum principal stress/ most negative stress (MPa)
MSNS	Modified standard normal space
f	Natural frequency (Hz)
n_i	Number of iterations
n	Number of loading cases
n_c	Number of piezoelectric material elements
d	Piezoelectric strain coefficient
P	Power output (W)
R	Resistance (N) or (Ω)
H	Standard normal space
b^*	Strain related to vertical displacement of the beam
V_s	Structural volume (mm ³)
t_c	Thickness of the piezoelectric material (mm)
t_{sh}	Thickness of the shim material (mm)
m_{tip}	Tip mass (kg)
z	Vertical displacement at the tip end (m)
V	Voltage (V)
W_p	Weighting factor
\hat{Y}	\hat{Y} space
Y	Young's modulus (GPa)

Y_c Young's Modulus for the piezoelectric material (GPa)

Greek letters

σ_{ave}	Average element stress (MPa)
ζ	Damping ratio
δ	Displacement (m)
ω	Radian driving frequency (radian per second)
ck	Individual reliability index
μ_{x_i}	Mean and standard
ω_n	Radian natural frequency (radian per second)
β	Reliability index
σ_{x_i}	Standard deviation
μ_i	Standard normal distribution
τ_{xy}	xy -shear stress (MPa)
τ_{xz}	xz -shear stress (MPa)
σ_y	Yield stress/strength (MPa)
τ_{yz}	yz -shear stress (MPa)

1 Introduction

1.1 Introduction

This thesis deals with many inter-related concepts, with a focus on solving a structural optimisation problem.

The primary goal of design engineers is to seek an optimum structural design according to the design requirements. An optimised design must not only achieve optimum performance, but also attain optimisation efficiency. The use of optimal designs can bring significant economic benefits, especially in the manufacturing of highly demanding products (e.g., mobile phone casings, which require an optimal shape and high reliability). The demands for lightweight materials (e.g., in aerospace applications), the efficient use of materials (e.g., composite material and telecommunication systems), and design performance (e.g., automotive components) have led to the development of design optimisation.

In the 1970s, optimisation was basically limited to problems involving the maximisation or minimisation of a single measure of performance, or objective. In the late 1970s, a multi-objective optimisation technique was developed to overcome this deficiency (Stadler, 1979; de Weck, 2004). This technique is capable of solving size variables, such as the cross-sectional areas of a truss, the thickness of a plate, and other geometrical dimensions. Although it was the most advanced technology at that time, multi-objective optimisation is only capable of solving for a single discipline; consequently, multi-objective and multi-disciplinary (MO–MD) optimisation method was introduced to address this problem (Edgeworth, 1881). MO–MD optimisation has increasingly been used as a tool in solving general linear/nonlinear and structural design problems in the field of engineering. MO–MD designs may be concerned with statics, dynamics, acoustics, heat flux, etc. This method has been applied in the automotive, mechanical structure, micro-electronic mechanical systems (MEMS), and aerospace industries. Basically, the MO–MD optimisation method provides the simplest context in which to consider the trade-offs between each objective and each discipline. In the ‘efficient, better, reliable’ stage, the method is used to seek an optimal solution between different disciplines and different objectives without compromising the target performance. Many studies have reported on the MO–MD optimisation method,

although their application has been limited to cases of single loading (Aoues and Chateaufneuf, 2008; Barakat *et al.*, 2004; Pandey *et al.*, 2007).

In terms of the MO–MD optimisation method, the optimisation procedure is becoming increasingly complicated, especially with the simultaneous consideration of multiple loading cases. Figure 1.1 provides a brief description of MO–MD optimisation problems for a single loading scenario. The objectives are always in conflict with each other in terms of seeking the optimal solution; consequently, a Pareto optimal set is used to overcome this problem. The optimum solution is obtained with the help of preference functions; i.e. preference methods and non-preference methods. In the case of preference methods (e.g., the global criterion technique), a typical preference function is required for the objectives and a single optimum solution is produced. For non-preference methods, in contrast (e.g., the weighting method, constraint method, and goal programming), a set of Pareto optimal solutions is generated.

Several non-preference methods have been reported in previous studies. For example, Watkins and Morris (1987) used a weighting method to solve laminated composite structures, where the objective function was combined with strain energy. Liu and Hollaway (1998) proposed a specific weighting method for solving MO–MD design problems under different loading scenarios. Díaz and Bendsøe (1992) used a similar technique—the average weighted mean method—to solve a topology optimisation problem under multiple loading scenarios.

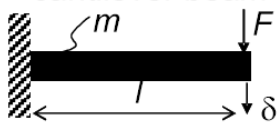
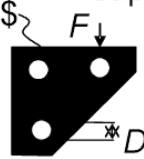
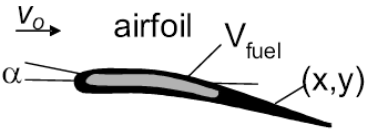
	Single discipline	Multiple discipline
Single objective	<p>cantilever beam</p>  <p>Minimize displacement s.t. mass constraints</p>	<p>support bracket</p>  <p>Minimize stamping costs (mfg) subject to loading constraints</p>
Multi-objective	<p>airfoil</p>  <p>Maximize C_L/C_D and maximize wing fuel volume</p>	<p>commercial aircraft</p>  <p>Minimize SFC and maximize cruise speed s.t. fixed range, payload</p>

Figure 1.1 – MO–MD design for single and multiple disciplines (de Weck, 2004)

Over time, structural models have become increasingly detailed and optimisation procedures have become increasingly complex; consequently, more precise data are

required for MO–MD analysis. Using an MO–MD optimisation method, the optimum design is always pushed to the limit of the design constraints, leaving no room for uncertainties. Thus, the assessment of safety and reliability (or probability of failure) is an increasingly vital component of the design process. Given the increasing importance of reliability, it is appropriate to incorporate reliability performance into the MO–MD optimisation method. The concept of “reliability” is used to assess the possibility that a structure subjected to unpredictable loads and geometry is able to satisfy specific safety requirements. Ultimately, the reliability or probability of failure can be determined from the multidimensional integral of the probability of the joint density function. This function is used to analyse the failure region and to calculate the reliability level; however, this process is extremely complicated in most engineering problems.

Structural reliability analysis can be classified into two types: (i) analytical methods and (ii) simulation methods. These two major groups have been used to predict/calculate the probability of failure for a structural system or an individual component. One of the most popular simulation methods is Monte Carlo Simulation (MCS), which was introduced in the 1940s to predict the behaviour of a system. In the following decades, additional simulation techniques were introduced, such as Latin Hypercube Sampling (McKay, 1979), Importance Sampling (Schuëller and Stix, 1987), and Direct Simulation (Bjæger, 1988). One of the disadvantages of the simulation methods is the need for vast computational resources. In contrast, the reliability index approach is popular because of its small computational cost. The first-order reliability method (FORM) is one of the most widely used methods in analysing structural reliability designs. This method was developed by Hasofer and Lind (1974) (herein, H–L) and extended by Rackwitz and Fiessler (1978) (R–F).

Structural optimisation and reliability analysis are the equivalent of two-level optimisation, which is computationally expensive compared with deterministic optimisation. In the present research, this problem is solved by developing the MO–MD optimisation method, which employs a new FORM procedure. The proposed methodology is applied to a problem involving multiple loading cases.

This thesis presents the development of a new MO–MD optimisation method that incorporates reliability performance. This research addresses design optimisation problems in which the design is required to satisfy multiple performance criteria, such as mechanical strength and stiffness, structural mass, reliability, and piezoelectric power

output, among others. This work encompasses the optimisation of sizing and shape, focusing on a number of engineering structural problems and a smart material problem. The first two examples demonstrate the efficiency of the proposed method (i.e., optimisation of a sliding caliper and a bimorph cantilever beam using piezoelectric materials). This method is subsequently extended to simultaneously considering a multi-loading case. The next two examples demonstrate the effectiveness of the method (i.e., optimisation of a star-like truss structure and a raised-access floor panel structure in which reliability performance is also maximised). An MO–MD optimisation method is developed to obtain the optimum solution for strength and stiffness, structural volume, reliability, etc.

1.2 Research objectives

Having identified the main research themes for this work, the following objectives were established:

- i) Develop a simple reliability method.
- ii) Demonstrate the efficiency and power of the multi-objective and multi-discipline optimisation method.
- iii) Develop and apply an automatic reliability and multifactor optimisation method.
- iv) Apply the proposed methodology in an industrial context.

1.3 Applications of the proposed optimisation methods

Four applications of the proposed optimisation method are presented in this thesis. The details of each case study (i.e., the design problem, optimisation setting, and results) are presented in the following chapters. First, a multi-objective problem is attempted under a single loading case; i.e., the optimisation of an automotive braking system (sliding caliper). The structure must satisfy all the design constraints in terms of strength and stiffness, and retain a low mass. The proposed method is then used to simultaneously solve a multi-disciplinary problem related to energy harvesting by a piezoelectric generator, concerned with optimisation of the shape of a cantilever beam and its effect

on the generation of piezoelectric power. The objective of this latter example is to maximise the generated power density while satisfying all the design constraints. The next two examples are multi-objective, multi-disciplinary, and multi-loading-case optimisation problems that are addressed by incorporating a reliability procedure to greatly enhance the proposed technique. The two examples are a star-like truss structure and a raised-access floor panel structure. The objectives of the optimisation are to simultaneously maximise the strength and stiffness, and minimise the structural mass, and to maximise the reliability index under multiple loading cases.

1.4 Overview of the dissertation

This thesis presents a multi-objective and multi-disciplinary optimisation technique that simultaneously considers multiple loading scenarios and the reliability index. The technique is applied to identify the optimal solution in problems relevant to industry, and the results are presented. The thesis is organised into 8 chapters, as summarised below.

Chapter 2 reviews the state of art of sizing-, shape-, and topology-optimisation methods for structural design optimisation. The advantages and disadvantages of each method are discussed. A brief summary of optimisation problems is presented.

Chapter 3 reviews the state of art of various reliability methods, followed by a review of well-known software-based reliability methods.

Chapter 4 presents a detailed discussion on the first-order reliability method, followed by a review of reliability-based optimisation, ranging from traditional methods to the latest techniques. A brief description is provided of a Multifactor Optimisation of Structure Techniques (MOST), which introduces a matrix system with which to evaluate all the performances and loading cases. A weighting system is introduced that takes into account the importance of each value in the matrix system, and an objective function is computed to evaluate the performance of the whole system. A brief explanation is provided of the proposed reliability method—the reliability loading-case index. Finally, the formulation of optimisation problems is discussed.

Chapter 5 presents a method for optimising the size and shape of a sliding caliper, employing the MOST method. This chapter presents a brief review of the history of braking systems in the automotive industry, followed by an account of the basic operation of a sliding caliper. Finally, the results of the analyses are presented and discussed.

In Chapter 6, a relatively complex problem is considered: a multi-objective and multi-disciplinary problem concerned with energy harvesting using a piezoelectric element. Reviews are presented of energy harvesting and piezoelectric material, followed by a brief explanation of a piezoelectric generator using the finite element method—bimorph cantilever beam. An existing technique (the Roundy method; Roundy, 2003) is verified, practical results are presented, and the proposed technique is discussed. The first example focuses on maximising the output power by obtaining the optimal geometrical shape for an idealised bimorph cantilever beam. The attributes of the design solution are discussed. The second example is concerned with maximising the power density for a bimorph cantilever beam. The current work focuses on a size and shape optimisation method using a pre-determined design solution from the first example. The concept is to simultaneously maximise the power density and minimise the structural volume. Finally, the results of the optimisation are presented and discussed.

Chapter 7 presents a combination of the MOST technique (as a method of multifactor optimisation) and a reliability loading-case (as a way of calculating the reliability index), which is known as the reliability related multifactor optimisation approach. The reliability loading-case index is developed from one of the most popular approaches in analysing structural reliability performance—FORM. Two examples are presented, demonstrating the effectiveness of the proposed methodology. The attributes of the designs are discussed.

Finally, Chapter 8 provides a summary of the results and conclusions, including the key findings and recommendations for future work. Figure 1.2 shows the relationships among the chapters in this thesis.

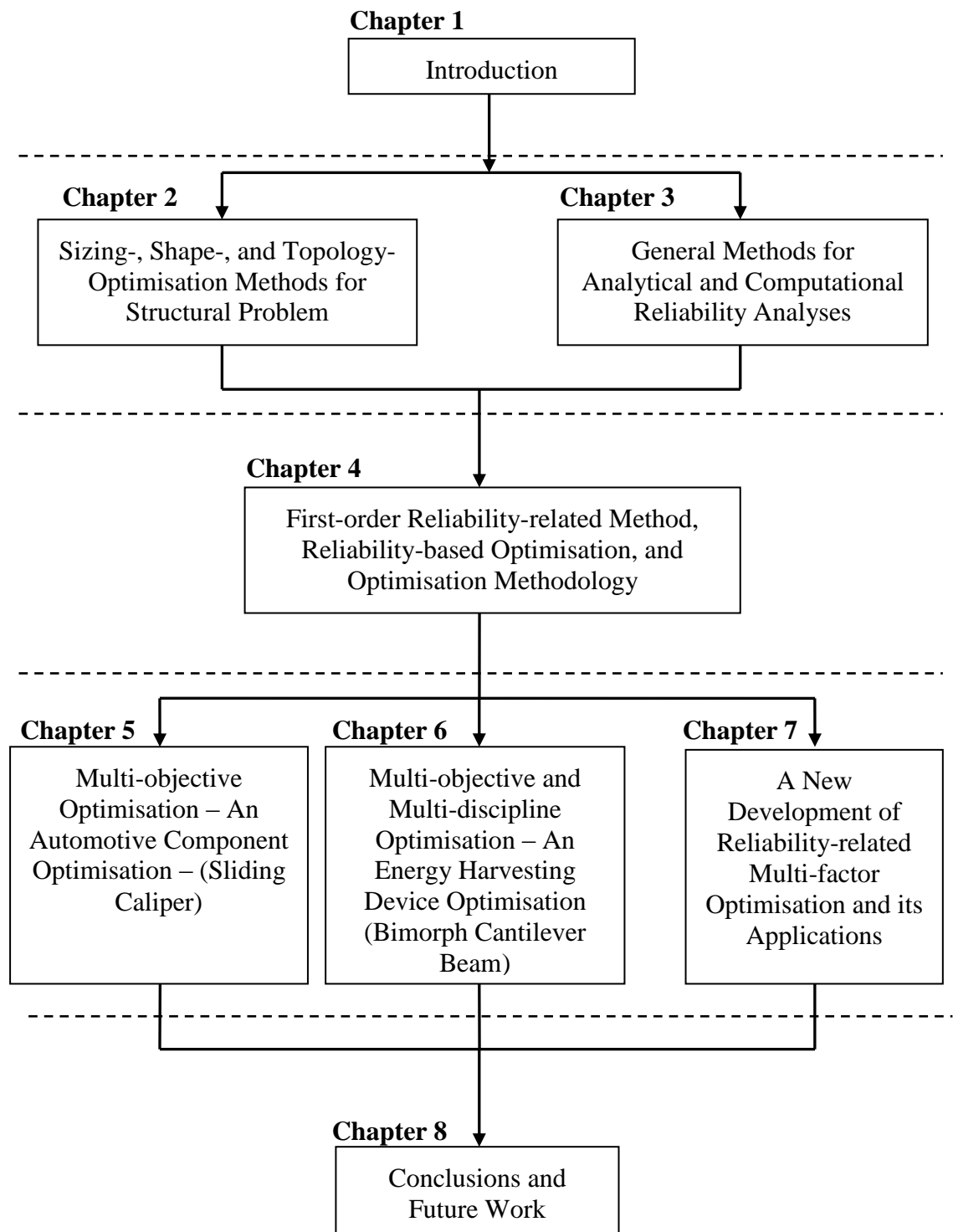


Figure 1.2 – Breakdown of the thesis and the proposed method, highlighting the reliability-related multifactor sizing/shape structural optimisation

2 Sizing-, Shape-, and Topology-Optimisation Methods for a Structural Problem

2.1 Introduction

Design optimisation methods are enabling technologies which are of use in the process of engineering design. Such methods are employed mainly in the aerospace and automotive industries to achieve weight reduction without compromising structural performance or accuracy. In recent years, much research interest has focused on developing and solving massive, complex calculations. Multi-objective, multi-disciplinary, and multi-loading-case optimisation has been investigated using improved engineering computational methods, such as finite element analysis applied to structural problems. A brief history of the development of structural analysis and optimisation is as follows (Papalambros, 1995; Saitou *et al.*, 2005; Venkataraman and Haftka, 2004):

- i) *Before 1980* – Structural analysis became popular and was used to calculate the results of physical experiments. Structural optimisation was rarely employed due to the high computational cost.
- ii) *1980s* – Structural optimisation became a tool for design. Many researchers focused on analysis and optimisation to improve the efficiency and accuracy of structural design (Bennet and Botkin, 1986).
- iii) *1990s* – Three-dimensional (3D) CAD was developed and combined with structural analysis to become an important method of design optimisation.
- iv) *2000s until present* – Structural optimisation is increasingly becoming an important tool in solving new conceptual, large-scale, robust, and reliability-based optimisation problems, including multi-objective and multi-disciplinary optimisation problems.

2.2 Description of the optimal design

Optimisation is concerned with achieving the best possible solution while satisfying all of the specified requirements (e.g., strength and stiffness requirements). Design optimisation is a procedure employed in the case that the user needs to transform the required information into a detailed specification of a system, or in the case that the user requires an object with a physical form and function (Liu, 1996). In general, the definition of optimal design problems involves an objective function, design variables, and design constraints. The typical mathematical expression can be defined as follows:

$$\begin{array}{ll} \text{Find} & X = (x_1, x_2, \dots, x_k) \\ \\ \text{To minimise/maximise} & f(X) \\ \\ \text{subject to} & h_i(X) \leq 0, \quad i = 1, 2, \dots, m \\ & g_j(X) = 0, \quad j = 1, 2, \dots, n \\ & x_i^{\min} \leq x_i \leq x_i^{\max} \quad i = 1, 2, \dots, k \end{array}$$

where X is the design variables, $f(X)$ is an objective function, m is the number of inequality constraints, n is the number of equality constraints, k is the number of design variables, and x_i^{\min} and x_i^{\max} are the minimum and maximum bounds of the design variable x_i , respectively. For example, the lower bounds are normally used to define the minimum cross-sectional area of a truss member.

A design variable is a parameter which can be controlled. Design variables are numerical quantities which define a design solution within the stated bounds during the optimisation process. They may be ‘continuous’ (values in a given range, such as the geometry of the design) or ‘discrete’ (i.e., can be integer numbers, such as the number of gear teeth). The type of design variable must be considered in the design, and they are bounded by maximum and minimum values.

An objective function is a function which is to be maximised or minimised. For example, the weight of an aircraft or aerospace structure is to be minimised, or structural stress is to be minimised to maximise the strength. Many optimisation problems involve multiple objective functions, and these objectives may conflict with each other. A simple method to overcome this problem is to form an overall objective function as a linear combination of the conflicting multiple functions.

A constraint is a condition which must be satisfied. Such constraints are statements of the limits of values for a specific condition. Design constraints are the conditional restrictions that must be satisfied in order to seek an optimal solution. These constraints collectively define a region referred to as the “feasible region”. Constraints may be equality or inequality. In some design problems, equality constraints are required (e.g., the required fundamental frequency of a structure). Inequality constraints state that the design variables are greater or smaller than a set of values (e.g., the maximum stress must be less than the yield stress of the material). The latter is the most flexible type of constraint, and it can be described for most engineering problems.

Basically, a recurring iterative process is required before a solution is converged in an optimisation. The optimisation problem is solved by using an optimisation procedure, which involves analyses and redesigns. Most design optimisation methods are employed with a numerical solver to assess the performance of a design. The present research focuses on the use of finite element analysis for structural optimisation. The optimisation process involves five fundamental steps:

- i) Model generation (initial design)
- ii) Numerical analysis
- iii) Sensitivity analysis
- iv) Model redesign (improved design)
- v) Optimum design

Step (i), which involves the initial design, may have a strong influence on the final optimal design and on the number of iterative cycles required for convergence. Liu *et al.* (2000) noted that the selection of the initial design determines whether an optimisation is converged and influences the number of iterative cycles.

Step (ii), numerical analysis, forms an important part of the design because the process verifies the designs such that all the constraints and loading conditions are properly defined. For structural optimisation, this step is commonly performed using finite element software (e.g., ANSYS).

Step (iii), the sensitivity analysis, involves the overall objective function and constraints functions with respect to design variables.

Step (iv) involves the optimisation process which seeks to find a better design by improving the system’s objective function. In sizing methods, the dimensions of a

structure or, for example, the cross-sectional area of truss members are varied. In shape methods, the shape of a structure is varied, followed by re-meshing of the optimisation model.

Steps (ii) to (iv) are repeated until the design satisfies the chosen constraints and until the design cannot be improved by further iterations.

Step (v) is the final stage in the optimisation process, at which point the design is converged.

2.3 Types of structural optimisation techniques

Optimisation techniques can be categorised into three types: sizing-, shape-, and layout/topology-optimisation methods. Sizing optimisation is normally applied to a structure constructed with truss, beam, and/or plate/shell members. Design variables may be, for example, the cross-section area of a truss member, details of a beam section, or the thickness of a plate/shell. This type of optimisation is relatively straightforward and does not require changes to the finite element model when a structure is modified.

Shape optimisation determines the optimal boundary of a structure for a given topology. The design variables are typically spline controlled points, used to determine the shape of the structure in 2D or 3D. Unlike sizing optimisation, shape optimisation requires changes to the finite element model during the optimisation process and increases the degree of difficulty of mesh generation.

Topology optimisation, which is also employed to determine the optimal solution, can be classified into discrete element and continuum approaches. The discrete element method is somewhat similar to the sizing and shape method. The design domain is represented as a finite set of possible locations of the structural members (Figure 2.1(a)). The size (i.e., the width and thickness) of the members is varied between the design domain and zero. If a member size is zero the member is non-existent. In this way, the optimised topology can be represented (Figure 2.1(b)). However, this method is only suitable for conceptual design, which is generally limited by the number and type of possible members defined in the design domain. In the continuum approach, the design domain is represented as a “void” region (Figure 2.2(a)), and the optimal structure can

be determined by varying the void region within the design domain (Figure 2.2(b)). Therefore, structures with various sizes and topologies can be represented.

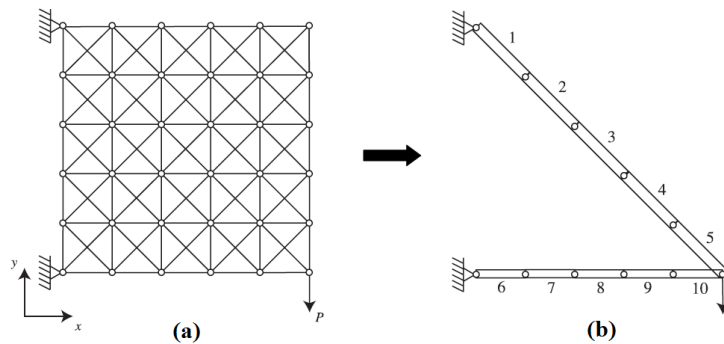


Figure 2.1 – Topology optimisation (discrete element), showing (a) the initial design, and (b) the optimised design (Rong and Liang, 2008)

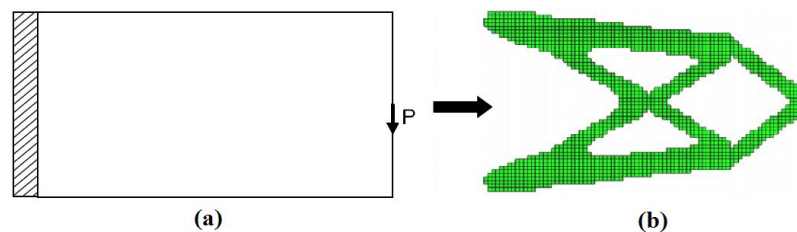


Figure 2.2 – Topology optimisation (continuum approach), showing (a) the initial design, and (b) the optimised design (Ohsaki, 2001)

Thus, sizing-, shape-, and topology-optimisation methods are required to solve different classes of problems. For a given problem, it is possible to simultaneously solve the shape and layout optimisations, or the sizing and shape optimisations.

2.4 Review of existing optimisation methods

Various methods for optimal structural designs have been developed to solve different classes of problems. In general, all optimisation methods are mainly concerned with finding the optimal design for which the objective function is minimised or maximised subject to the design constraints. This review examines the following optimisation methods used in engineering design problems:

- i) Metamorphic development
- ii) Adaptive weighted sum method
- iii) Genetic algorithm
- iv) Multifactor optimisation of structure techniques

- v) Structural shape optimisation
- vi) Particle swarm optimisation

The review focuses on sizing and shape methods because they represent the basis technique used to address the design problem.

2.4.1 Metamorphic development

Metamorphic development (MD) is an optimisation method that can be applied to continuum structures and truss members to find the optimal structural shape and topology by minimisation of structural compliance and mass, subject to stress and deflection constraints (Liu *et al.*, 2000). MD can start from a basic description of the structure, involving as little as the minimum number of nodes and elements connecting the applied loads and support points. The MD process can start from any degree of development of the structure, and a dense finite element mesh is not necessary, thereby reducing the computation cost.

The optimum solution obtained by MD is developed via simultaneous growth and degeneration approaches with the aim of ensuring satisfactory or improved overall performance. The rate of growth is controlled using a dynamic growth factor by adding material to decentralise high stress and removing material to eliminate relatively low stress. A design domain may be specified, containing sub-domains that can be finite or infinite in size. MD can be used to find an optimum shape which minimises the structural mass and the compliance stress subject to structural response constraints, and vice-versa.

Good examples of the MD method can be found in Liu *et al.* (2001) and Ngim *et al.* (2009). These examples sought to achieve minimum mass structures subject to the constraints on stress and deflection. Most of the optimum designs were developed starting from a simple structure. Figure 2.3 and Figure 2.4 show examples of the use of the topology optimisation to solve the same Michell structure design problem (Michell, 1904) starting from two different initial structures. The optimum solutions for the structural design problem are basically the same, as shown in Figure 2.3(g) and Figure 2.4(g), respectively.

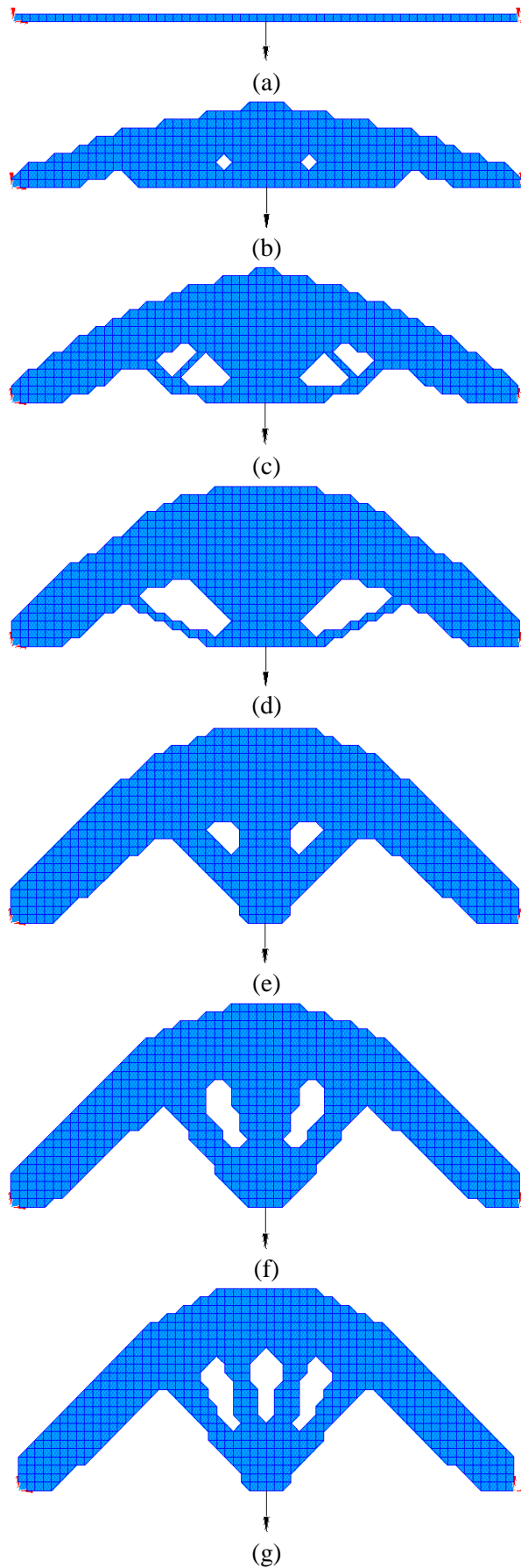


Figure 2.3 – Optimisation from structure A, showing (a) the initial structure, (b) iteration 10, (c) iteration 20, (d) iteration 30, (e) iteration 45, (f) iteration 60, and (g) iteration 69 (Liu *et al.*, 2000)

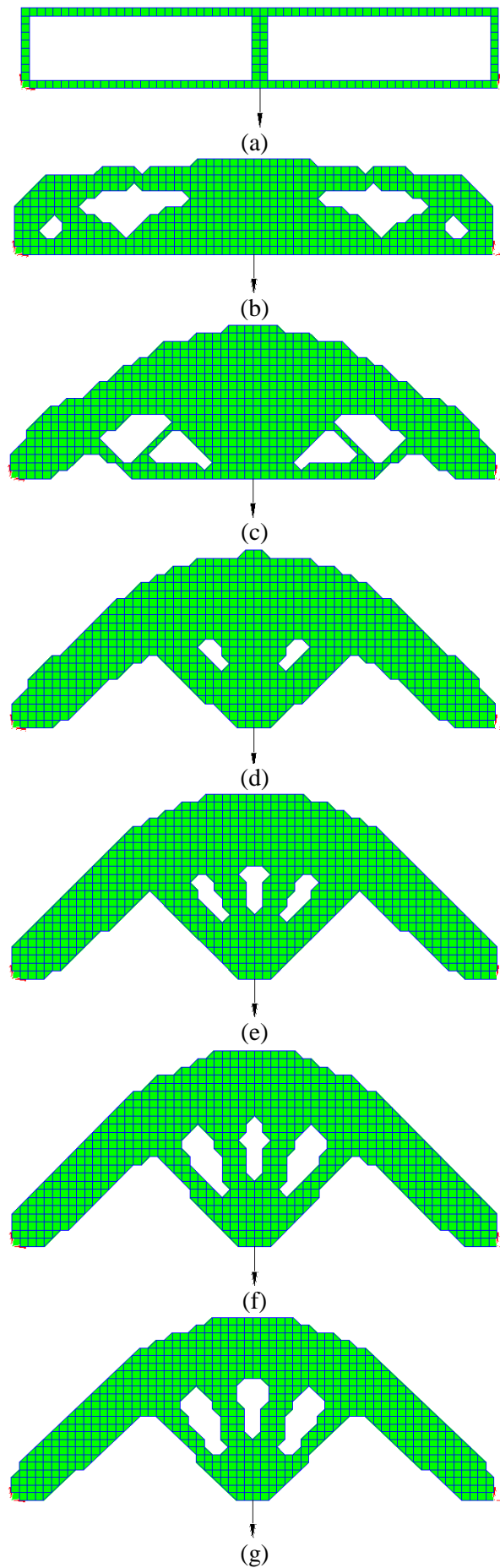


Figure 2.4 – Optimisation from structure B, showing (a) the initial structure, (b) iteration 10, (c) iteration 20, (d) iteration 30, (e) iteration 40, (f) iteration 50, and (g) iteration 53 (Liu *et al.*, 2000)

The fact that the same solution is obtained from different starting points confirms the robustness of the MD search methodology. Liu *et al.* (2000 and 2005) presented several examples of layout and topology optimisation using the MD method; i.e., a fixed-end beam, a C spanner, a 2D suspended apple, and a turbine disk. MD has also been used to optimise the design of micro-fibre holder clips (Liu and Lu, 2001), and has been extended to cover the design optimisation of axisymmetric structures, including the shape optimisation of cylindrical nozzles in a spherical pressure vessel (Liu. *et al.*, 2001) and design optimisation for manufacturing using Additive Manufacturing Technologies (AMT) (Ngim *et al.*, 2007).

MD is mainly used in solving layout/topology problems, and requires further development in terms of simultaneously solving multiple objective and multiple loading cases, for which the method may currently be inappropriate.

2.4.2 Adaptive weighted sum method

In the 1970s, the most widely used method for multi-objective optimisation was the weighted sum method. Stadler (1979 and 1984) applied the notion of Pareto optimality to the field of engineering optimisation. The goal of a design optimisation is to find the best design while satisfying all the design constraints. The weighted sum method transforms the multiple objectives into a scalar objective function. Each function is multiplied by a weighting factor (w) to give the individual objective function (J_i , $i = 1, 2, \dots, m_{ws}$), and the functions are summed. Thus, each individual objective determines a single optimal solution point of a Pareto front. For the weighted sum, the weights are changed systematically to obtain a different optimum solution. Zadeh (1963) was the first to employ this method, and Koski (1988) used the method to examine a multi-objective truss problem. Schy and Giesy (1988) applied the weighted sum method to multi-objective optimisation of an aircraft control system. Das and Dennis (1998) reported the following disadvantages of the weighted sum method: (i) it is difficult to obtain optimal solutions due to equality constraints in non-linear problems, (ii) it is necessary to filter out the Pareto and non-Pareto optimal solutions, and (iii) the Pareto front regions are not covered by this method in the case of more than two objective functions.

To overcome the above limitations, Kim and de Weck (2005) developed the adapted weighted sum (AWS) method, which has proved to be successful in finding the Pareto

optimal in non-convex regions and ignoring non-Pareto optimal solutions. The procedure employed by AWS is to refine the Pareto front (see Figure 2.5). This method is effective in solving multi-objective optimisation problems in which the Pareto front is i) a convex region, ii) non-convex regions with non-dominated solutions, and iii) non-convex regions with dominated solutions (see Figure 2.6).

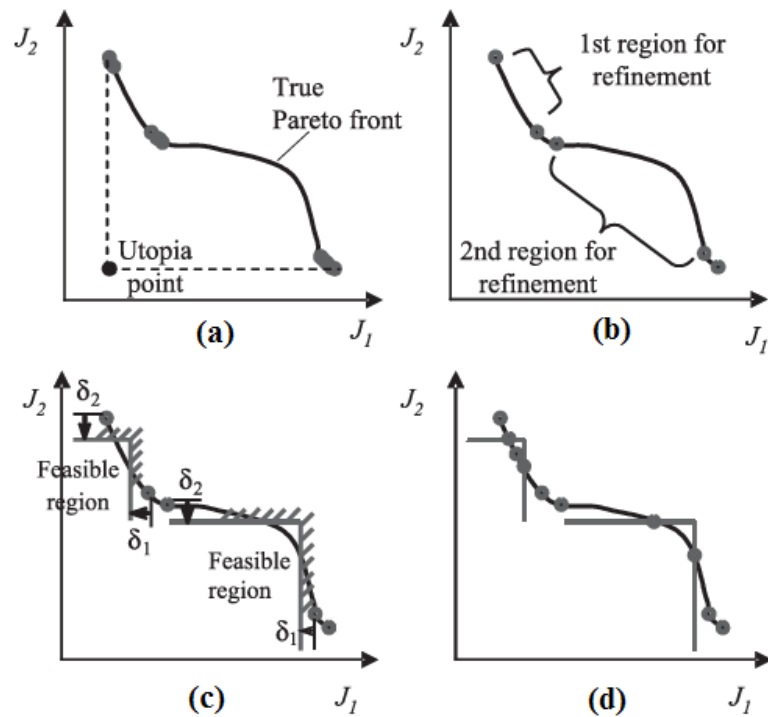


Figure 2.5 – The concept and procedures of AWS, showing (a) the weighted-sum method, (b) the initial step, (c) constraint imposition, and (d) refinement (Kim and de Weck, 2005)

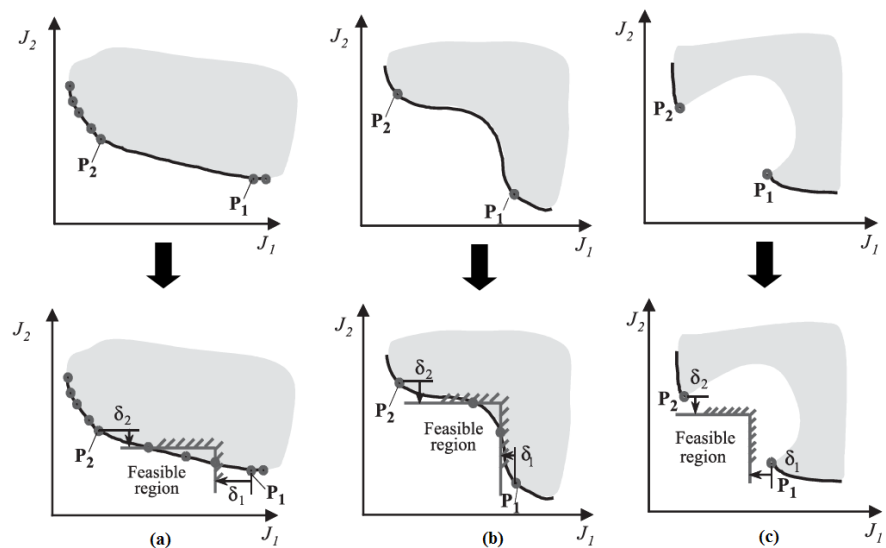


Figure 2.6 – AWS method for the Pareto front, showing (a) the convex region, (b) non-convex regions with non-dominated solutions, and (c) non-convex regions with dominated solutions (Top: initial solution; Bottom: AWS solution) (Kim and de Weck, 2005)

The drawback of AWS is that it is limited to two objective functions (Kim and de Weck, 2006). This method needs to be further developed to include multiple objective functions that can be used to solve more general problems, for which the method may currently be inappropriate.

2.4.3 Genetic algorithm

The Genetic algorithm (GA), introduced by Holland (1975), is a metaheuristic optimisation method. This method imitates natural phenomena and is applied to complex optimisation problems. Goldberg (1989) extended GA to the field of engineering structural optimisation. The GA is a stochastic search method based on the mechanisms of natural selection and genetics, with the extra capability of random search in regions of the design space with a significant potential gain. Based on Darwin's theory of evolution, a group of solutions (defined by their individual genes) is placed among the populations. Well-adapted solutions are forwarded to the subsequent iterations, whereas those which are less fit are discarded, which is similar to the process of evolution in nature. This leads to the optimum solution. GA is not limited by the discontinuous design space that is commonly used in mathematics programming. The main advantages of GA are as follows (Goldberg, 1989):

- i) does not require objective functions to be differentiable
- ii) searches all the possibilities in the design space, yielding a global optimal
- iii) works on a coding of the design variables that consists of continuous, discrete, and integers variables
- iv) does not require extensive problem formulation

GA has been used to solve various classes of problems in the fields of engineering structure, science, and finance. Erbatur *et al.* (2000), Jenkins (1991), and Oshaki (1995) used a GA to determine an optimum solution for engineering truss structures. The task is to find an optimum shape which minimises the structural weight of an 18-bar truss structure under a single loading case, as shown in Figure 2.7 (Rahami *et al.*, 2008). Aguilar Madeira *et al.* (2005) used GA to obtain a multi-objective optimisation of a structural layout, and tested the optimal design on a short cantilever subjected to two different loading cases. Although the cantilever beam was tested for two loading cases, the authors used two objective functions to represent the design problem, yielding two different solutions (Figure 2.8), although both structures are identical (compare Figure

2.8 (a) and (b)). This result means that if the force applied to the structure in Figure 2.8 (a) is upward, the structure may not be able to withstand the force. This also applies to the structure in Figure 2.8 (b). Nevertheless, the authors used this result and proceeded with further optimisation to obtain a single structure which can withstand two different loading cases (Figure 2.8 (c)).

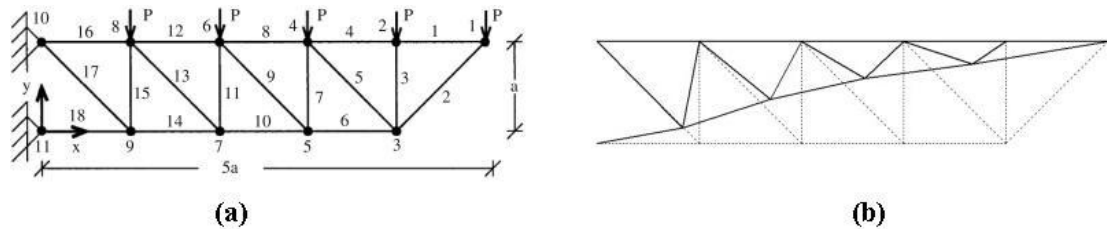


Figure 2.7 – (a) Geometrical dimensions, applied load, and force locations for an 18-bar space truss structure, and (b) the optimum shape of the structure (Rahami *et al.*, 2008)

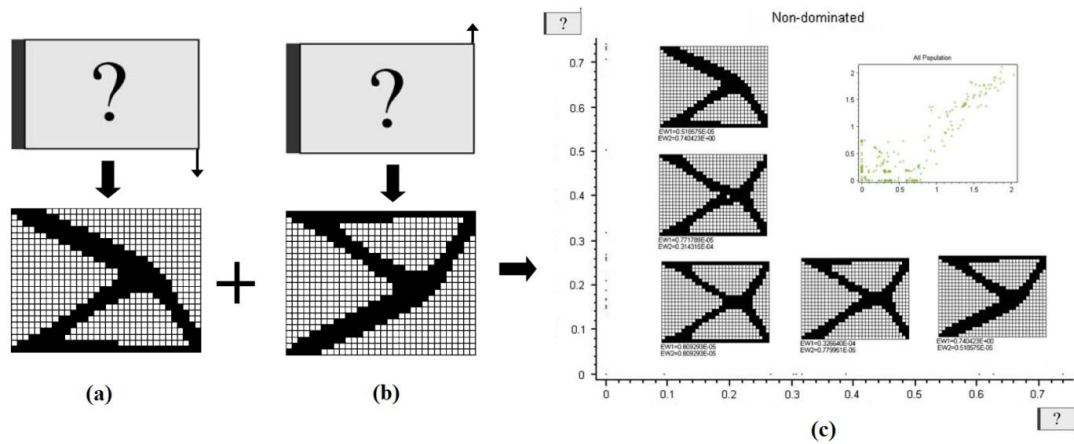


Figure 2.8 – Optimization of a cantilever beam, showing (a) loading case 1 and (b) loading case 2 (top: design domain; bottom: optimum design), and (c) combinations of the two initial solutions (Aguilar Madeira *et al.*, 2005)

GA has been applied mainly to single-objective optimisation problems (Fernandes *et al.*, 1998). To tackle multi-objective optimisation problems, the objective function in the GA method should be combined with a scalar fitness function, which utilises the search method in the feasible region to obtain an optimum solution. Schaffer (1985) proposed the first vector-evaluated GA (VEGA) as a multi-objective GA. Subsequently, several multi-objective algorithms have been developed (Fonseca and Fleming, 1993; Sarker and Liang, 2002). Table 2.1 lists the most widely employed GA methods. The application of GA to solving multi-objective optimisation has been reported by Tamaki *et al.* (1994) and Kita *et al.* (1996), among others.

Table 2.1 – GA methods

Algorithm name	Author(s)
Weight-based GA (WBGA)	Hajela and Lin (1992)
Multiobjective GA (MOGA)	Fonseca and Fleming (1993)
Niched Pareto GA (NPGA)	Horn <i>et al.</i> (1994)
Nondominated Sorting GA (NSGA)	Srinivas and Deb (1994)
Random Weighted GA (RWGA)	Murata and Ishibuchi (1995)
Strength Pareto Evolutionary Algorithm (SPEA)	Zitzler and Thiele (1999)
Pareto Archived Evolution Strategy (PAES)	Knowles and Corne (2000)
Pareto Envelope-based Selection Algorithm (PESA)	Corne <i>et al.</i> (2000)
Improved SPEA (SPEA2)	Zitzler <i>et al.</i> (2001)
Region based Selection in Evolutionary Multiobjective Optimisation (PESA-II)	Corne <i>et al.</i> (2001)
Micro-GA (Micro-GA)	Coello and Pulido (2001)
Multiobjective Evolutionary Algorithm (MEA)	Sarker and Liang (2002)
Fast Non-dominated Sorting GA (NSGA-II)	Deb <i>et al.</i> (2002)
Rank Density Based GA (RDGA)	Lu and Yen (2003)
Dynamic Multiobjective Evolutionary Algorithm (DMOEA)	Yen and Lu (2003)
Polar Coordinates GA (PCGA)	Kuang and Zheng (2005)

Many types of multi-objective GAs have been developed and applied (Corne *et al.*, 2001; Fonseca and Fleming, 1995a and 1995b). For example, Caello (2009) listed more than 4000 studies concerned with multi-objective GAs. Table 2.2 lists the most well-known multi-objective GAs along with their advantages and disadvantages.

Table 2.2 – Summary of the most well-known GA methods (from Konak *et al.*, 2006)

Algorithm	Fitness assignment	Diversity mechanism	Elitism	External population	Advantages	Disadvantages
VEGA	Each subpopulation is evaluated with respect to a different objective	No	No	No	First MOGA straightforward implementation	Tends to converge to the extreme of each objective
WBGA	Weighted average of normalized objectives	Niching predefined weights	No	No	Simple extension of single objective GA	Difficulties in nonconvex objective function space
MOGA	Pareto ranking	Fitness sharing by niching	No	No	Simple extension of single objective GA	Usually slow convergence, problem related to niche size parameters
NPGA	No fitness assignment, tournament selection	Niche count as tiebreaker in tournament selection	No	No	Very simple selection process with tournament selection	Problem related to niche size parameters, extra parameter for tournament selection
NSGA	Ranking based on non-domination sorting	Fitness sharing by niching	No	No	Fast convergence	Problem related to niche size parameters
RWGA	Weighted average of normalized objectives	Randomly assigned weights	Yes	Yes	Efficient and easy to implement	Difficulties in nonconvex objective function space
SPEA	Ranking based on the external archive of non-dominated solutions	Clustering to truncate external population	Yes	Yes	Well tested, no parameter for clustering	Complex clustering algorithm

PAES	Pareto dominance is used to replace a parent if offspring dominates	Cell-based density as tiebreaker between offspring and parent	Yes	Yes	Random mutation hill-climbing strategy, easy to implement, computationally efficient	Not a population-based approach, performance depends on cell size
PESA	No fitness assignment	Cell-based density	Pure elitist	Yes	Easy to implement, computationally efficient	Performance depends on cell size, requires prior information on objective space
SPEA2	Strength of dominators	Density based on the k-th nearest neighbour	Yes	Yes	Improved SPEA, ensure extreme points are preserved	Computationally expensive fitness and density calculation
NSGA-II	Ranking based on non-domination sorting	Crowding distance	Yes	No	Single parameter (N), well tested, efficient	Crowding distance works in objective space only
RDGA	Problem reduced to bi-objective problem with solution rank and density as objectives	Forbidden region cell-based density	Yes	Yes	Dynamic cell update, robust with respect to the number of objectives	Relatively difficult to implement
DMOEA	Cell-based ranking	Adaptive cell-based density	Yes (implicitly)	No	Includes efficient techniques to update cell densities, adaptive approaches to set GA parameters	Relatively difficult to implement
PCGA	Pareto front	Grid division using polar coordinates	No	No	Modification of MOGA	Uniform Pareto optimal front only

Despite the successful application of GA, several drawbacks have been identified. GAs often require many function evaluations, resulting in a high computational cost. For relatively small problems, GA solutions still require a large number of computational analyses (Jakiela *et al.*, 2000). Adeli and Kamal (1992) proposed a method for reducing the number of computational analyses for large optimisation problems. To minimise the overall computational effort for multi-objective, multi-disciplinary, and multi-loading-case optimisation, an alternative method is required to ensure the efficiency of the GA.

2.4.4 Multifactor optimisation of structure techniques

A multi-objective and multi-discipline optimisation method, MOST (Multifactor Optimisation of Structure Techniques; Liu and Hollaway, 2000; Liu and Lu, 2004), has been developed to accommodate and implement the optimisation. MOST is able to simultaneously optimise various objectives of structural performance for many loading cases. The method utilizes commercially available finite element codes (e.g., ANSYS) and combines finite element static/dynamic analysis with a unique optimisation technique. The MOST optimisation system can efficiently and systematically solve complex engineering design problems which may have multiple objectives and multiple loading cases, by creating a parameter profile analysis and seeking an optimum solution. This method has introduced an assessment system with scores and merit indices (range, 0–10) for all performance and loading cases. These features make MOST a powerful, cost-effective, and reliable tool with which to optimize complex structural systems.

The MOST technique has been applied to solve sizing- and shape-optimisation problems. For example, Liu and Hollaway (1998) presented an example of design structure–electromagnetic optimisation of large reflector antenna systems. The optimised solution obtained by MOST yielded improved performance under seven loading cases. Liu *et al.* (1999) sought to find the optimal design for a planar truss structure which is able to simultaneously sustain different loading cases (Figure 2.9).

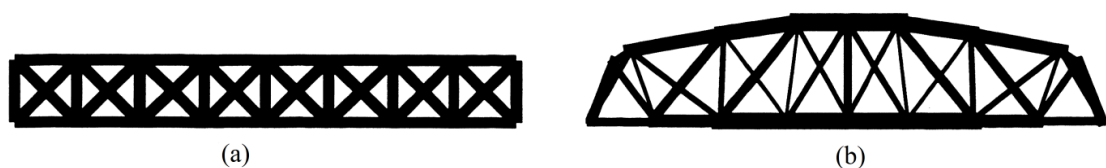


Figure 2.9 – Optimal shape of a planar truss structure, as obtained by MOST. (a) Initial design; (b) Optimised design (Liu *et al.*, 1999)

Thus, in the present research, MOST forms the basis of the sizing- and shape-optimisation method. The first two examples considered in this thesis (i.e., the sizing and shape optimisation of a sliding caliper and a bimorph cantilever beam; see Chapters 5 and 6) demonstrated sizing and shape optimisation under multiple objectives and multiple disciplines. These examples are only considered as single loading cases. The next two examples are cases with multiple objectives, multiple disciplines, and multiple loading.

2.4.5 Structural shape optimisation

The structural shape optimisation (SSO) method was first proposed by Zienkiewicz and Campbell (1973). The most commonly used SSO method is the Lagrangian method, in which several points are sequentially numbered along the structural boundary to enable the shape of the structure to be expressed using a spline/interpolation function. Thus, SSO can be implemented by moving the points within the restricted boundary. Sequential Linear Programming (SLP) is the optimisation method normally used in the SSO algorithm (John and Denis, 2000). The advantage of the SSO method is guaranteed convergence to the global optimum for design problems. SLP also involves a series of non-linear solutions. Griffith and Stewart (1961) were the first to suggest using SLP as a method for solving non-linear problems. However, this method may converge very slowly compared with other methods. Wilson (1963) proposed the Sequential Quadratic Programming (SQP) method to solve non-linear optimisation problems. The advantage of SQP is that it provides a significant, reliable, matrix factorisation which is frequently updated to provide a uniform treatment of ill-conditioning. However, it is difficult to execute SQP methods in such a way that the exact second derivatives can be used efficiently. Previous studies have applied SSO to solve shape-optimisation problems, including Atrek *et al.* (1984), Bugeda *et al.* (2008), Haftka and Gürdal (1992), Hartman and Neumann (1989), and Hinton and Rao (1993 and 1994). Figure 2.10 shows the benchmark problem of SSO, which is to optimise a 2D plate with a hole.

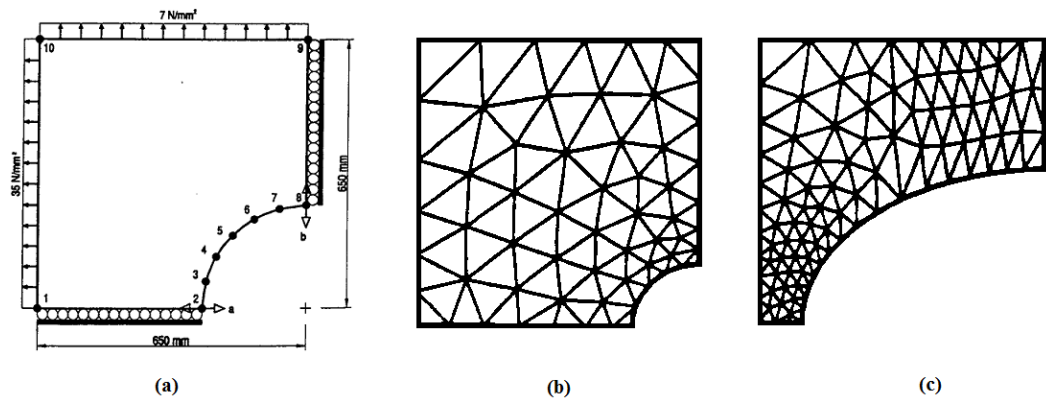


Figure 2.10 – Two-dimensional plate with a hole, showing (a) the general dimensions, and the locations of the applied load and stress constraint, (b) the initial finite element design, and (c) the optimal finite element design (Campbell and Kelliher, 2000)

Several good examples of shape optimisation have been reported previously. Kelliher *et al.* (1999) showed an example using a new hybrid boundary element and finite element SSO method. The design variables are to control the shape of the design, which is subjected to the design constraints. Afonso and Sienz (1999) further developed the SSO method by considering multiple objective functions, and Nadir *et al.* (2004) investigated the method in terms of multi-objective problems related to an abrasive water-jet-cutter manufacturing process, considering both structural performance and manufacturing cost. Although SSO is able to solve multi-objective and multi-disciplinary problems, this method has yet to be applied to simultaneously solving multi-loading cases, for which it may be inappropriate.

2.4.6 Particle swarm optimisation

Particle swarm optimisation (PSO) is a method based on a probabilistic search algorithm. This technique was originally developed by Kennedy and Eberhart (1995) to solve a continuous optimisation problem, based on the social behaviour of birds and fishes that adapt to their physical environment to avoid predators. The main concept is to randomly create particles, explore possible solutions, and seek the optimal solution. This technique has many similarities to other methods (e.g., GA). The system employs a random search technique and searches for the optimum point by updating after every iteration.

PSO has been used in many applications in engineering design problems. Applications in the field of structural optimisation are normally focused on engineering design problems, which involve sizing and shape optimisation. For example, Venter and

Sobieszczanski-Sobieski (2004) demonstrated a multidisciplinary optimisation of a transport aircraft wing. The authors investigated the basic PSO approach and applied it to minimise the weight of the wing structure and to maximise the flight range of the aircraft. Fourie and Groenwold (2002) applied the PSO method to size optimisation (e.g., a plane truss and a space truss) and shape optimisation (e.g., a torque arm); a similar study was performed by Schutte and Groenwold (2003). Omkar *et al.* (2008) presented a vector-evaluated PSO algorithm for the design optimisation of composite structures. The authors sought to minimise the weight of the structures and to minimise the cost by varying the number of layers, the composite thickness, and the stacking sequence. Perez and Behdinan (2007) reported the development and implementation of a PSO approach for the structural optimisation of truss structures (Figure 2.11). The main objective was to find the optimal design of a 25-bar space truss structure which is able to sustain varying forces under a single loading case. The authors also investigated a multi-objective and multi-loading-case problem for a 72-bar space truss structure, obtaining a better solution (compared with other methods) while satisfying all the design constraints. Although a better optimal solution was achieved, the authors did not consider a multi-disciplinary problem.

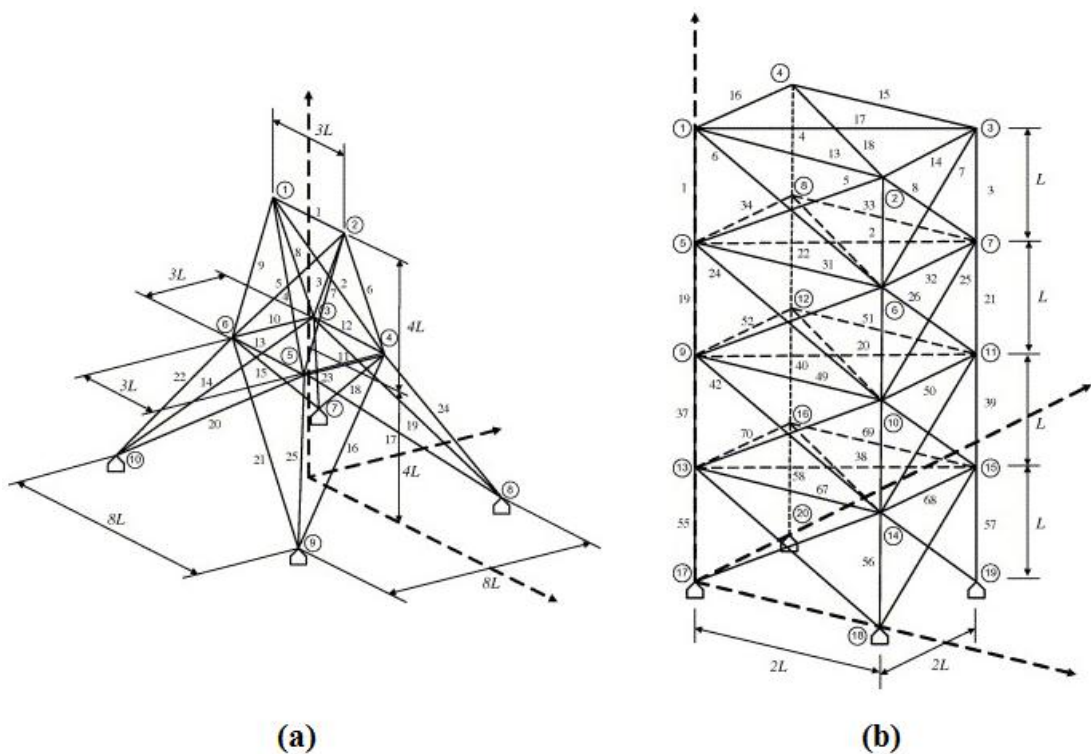


Figure 2.11 – Layout of (a) a 25-bar space truss structure and (b) a 72-bar space truss structure

PSO has been widely applied in engineering design problems, including process flow (Guo *et al.*, 2009), control design (Krohling *et al.*, 2002), power systems (Abido, 2002;

Wang *et al.*, 2010), and structural shape optimisation (Venter and Sobieszczanski-Sobieski, 2004). In structural problems, this method has mainly been applied to investigations of structural configuration and sizing optimisation problems. Compared with other methods, PSO has rarely been simultaneously applied to multi-objective, multi-disciplinary, and multi-loading-case problems. In general, an optimisation method for solving multi-objective, multi-disciplinary, and multi-loading-case design problems would require a large number of function evaluations. Despite the simplicity, effectiveness, and robustness of PSO, the computational cost is always a concern when using a design optimisation method. For example, Venter and Sobieszczanski-Sobieski (2004) reported an average of 9660 analyses to attain convergence for three separate design variables. In a multi-objective and multi-disciplinary optimisation, the number of combinations of sizing-, shape-, and layout-optimisation problems may be several orders of magnitude more than in the case of single-objective optimisation. Hence, the computational cost is greatly increased with increasing complexity of the design problem. Consequently, this method is not considered in the present study.

2.5 Summary

This chapter presented a historical chronology of structural analysis and optimisation, followed by a description of optimal design. In general, the definition of optimal design problems requires an objective function, design variables, and design constraints. Three basic optimisation methods were evaluated: sizing, shape, and topology optimisation. A general description of an optimisation process was presented, followed by a brief review of the various optimisation techniques (e.g., Genetic Algorithm, Particle Swarm Optimisation, and Multifactor Optimisation of Structures Technique). These methods are able to solve multiple objective problems which involve sizing and/or shape optimisation. The advantages and disadvantages of each method were evaluated.

The following chapter presents a brief review of various methods of reliability analysis.

3 Methods for Analytical and Computational Reliability Analyses

3.1 Basis of a structural design concept

Most engineering problems can be stated in terms of two simple terms: load and resistance. The basic principle of structural design is that the resistance should exceed the load:

$$R > L \quad (3.1)$$

where R is the resistance and L is the load. The basis of structural design is to ensure that the design can be used throughout the lifetime of the product. The basic idea of safety factors is that the resistance always exceeds the load; however, most of the quantities on both sides of the equation are uncertain. Consequently, it is necessary to calculate the probability of satisfying the criterion. A probabilistic approach is a means of evaluating a structural design to ensure the performance is satisfactory, known as “reliability analysis”.

Traditionally, a design problem is calculated using safety factors based on experience. Nevertheless, safety factors cannot always guarantee satisfactory design performance.

In a multi-objective, multi-disciplinary, and multi-loading-case problem, engineering design is usually an optimisation problem with two or more simultaneous, conflicting requirements (e.g., maximising safety factors, minimising structural cost, and maximising/minimising structural performance). Whereas classical safety-factor design does not provide sufficient information on the importance of the parameters in this optimisation problem, the probabilistic design method always provides this information and executes the design process.

3.2 Graphical representation of load and resistance

In probabilistic design, it is common to represent the resistance and load in terms of their distribution. Figure 3.1 shows the probability density functions of resistance and load, and the area of overlap. It should be noted that the overlapping area (striped region) is not equal to the probability of failure. The striped region is qualitatively proportional to the failure probability as long as the mean value of the load is less than the mean value of the resistance. The black area represents the probability of failure.

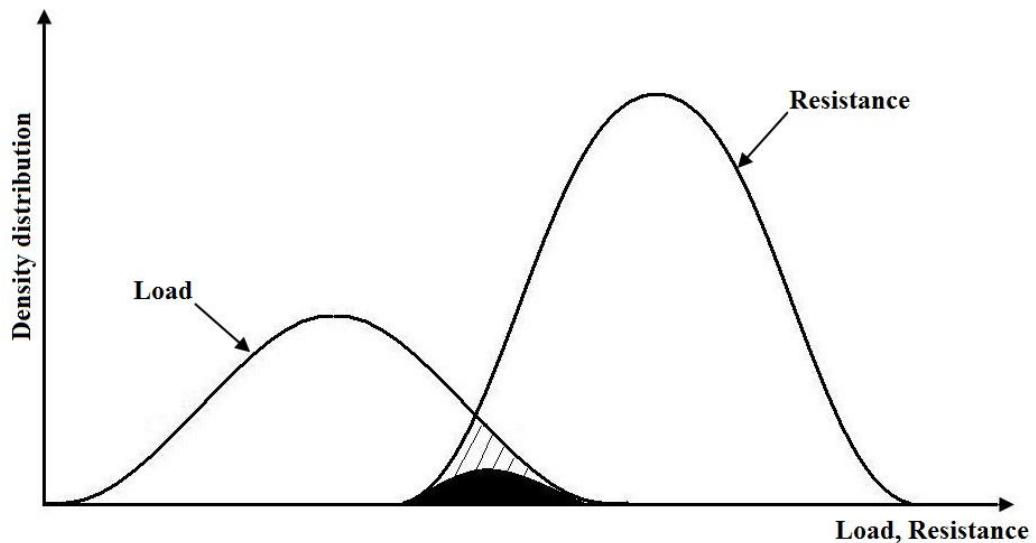


Figure 3.1 – Density distribution of load and resistance (Haldar and Mahadevan, 1995)

3.3 Reliability techniques

Reliability techniques have been developed to solve a class of problems which involves structural design, statistical data, etc. In general, structural designs are mainly concerned with maximising the reliability index subject to design constraints. The present review covers two main types of reliability techniques: analytical methods and simulation methods.

Analytical methods

- i) First- and second-order reliability methods (FORM and SORM, respectively)

Simulation methods

- ii) Monte Carlo simulation
- iii) Latin hypercube sampling

- iv) Importance sampling
- v) Response surface
- vi) Neural network

3.3.1 First- and second-order reliability methods

The first-order reliability method (FORM) is one of the most popular reliability methods in analysing structural reliability designs. Originally, Cornell (1969) used a first-order Taylor series approximation and second moment statistics to calculate the safety index, and proposed a term called the “safety index” or “reliability index”. However, this method encounters a serious problem in that it does not use distribution information for the variables. More importantly, Cornell’s safety index is not constant under different formulations of the same performance function. Consequently, this method was updated by Hasofer and Lind (1974) (herein, H–L), based on a linear system, to determine the limit state function in a standard normal space. H–L proposed a reliability index defined as the minimum distance from the origin to the limit state (see Figure 3.2). This method was later extended by Rackwitz and Fiessler (1978) (herein, R–F).

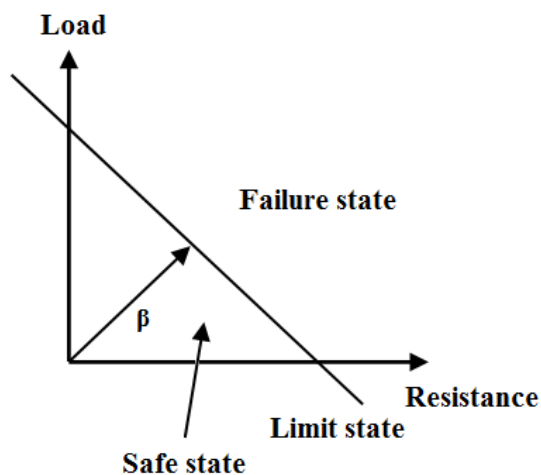


Figure 3.2 – H–L reliability index

R–F introduced two terms—the equivalent mean and the equivalent standard deviation—which were used to calculate the standard normal distribution. This approach was taken to ensure that all the random variables occur in the standard normal space, and is known as the first-order reliability method (FORM). Ditlevsen (1979a) presented a result for a non-linear problem, obtained using FORM, which was inconsistent with the actual reliability. Ditlevsen (1979b) calculated the approximation

of the non-linear limit state by considering tangent hyperplanes at the minimum distance from the origin; this approach is known as the second-order reliability method (SORM). SORM was first introduced by Fiessler *et al.* (1979), who devised the method to improve the actual FORM by constructing a curvilinear failure surface at the failure point. In recent decades, FORM has been used to evaluate the safety index and the location of the design point (Shinozuka, 1983). Chen and Lind (1982) proposed an extension of the R–F algorithm by using a three-parameter approximation, although this revised approach was only superior to the R–F method in certain cases.

Previous studies have reported the application of FORM in various case studies. Song and Lee (1992) demonstrated the use of FORM to predict the probability of failure against a pre-selected target value and information concerning the sensitivity of the result, which is related to the input variables. Der Kiureghian and Dakessian (1998) reported an improvement in estimating the failure probability using a system reliability analysis in a multi-design point problem using a bulge system (see Figure 3.3 and the ‘multi-design point’ of Ditlevsen and Madsen (1996)). To improve the FORM approach, recent studies have sought to make the method increasingly efficient and robust. For example, Santosh *et al.* (2006) developed an appropriate step-length selection (modified H–L and R–F method) which made the algorithm more robust. In addition, Xiang and Liu (2011) applied an inverse FORM to evaluate the fatigue life (a prediction problem, such as the growth of a fatigue crack) at an arbitrary level of reliability.

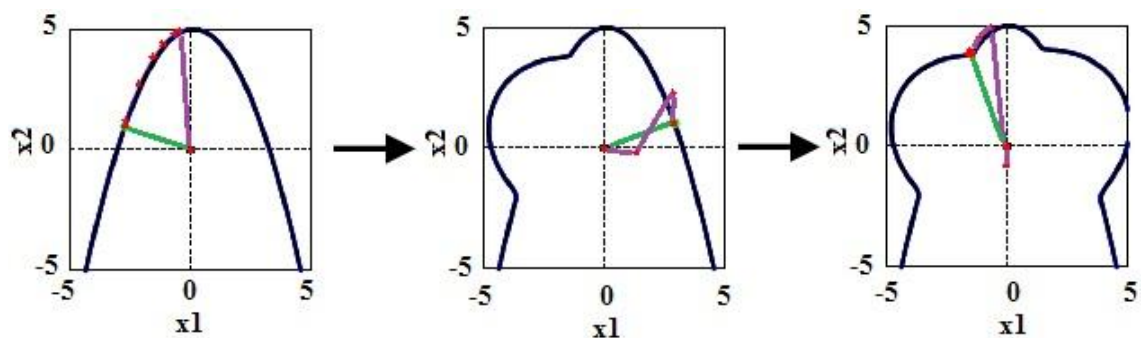


Figure 3.3 – The bulges method is used to search for the optimum solution for multiple design points, for x_1 values between -5 and -1 (left), for between 1 and 5 (middle), and for between -1 and 1 (right). (Der Kiureghian and Dakessian, 1998)

Several authors have demonstrated the potential of FORM as a probabilistic method for evaluating the reliability. The unique features of FORM provide it with the advantage of being simple and computationally inexpensive. In the present research, the FORM is adopted as the basis for calculating structural reliability.

3.3.2 Monte Carlo simulation

Monte Carlo Simulation (MCS) is a traditional technique used in reliability analysis, which is also known as a direct method. The principle that underlies this method is to develop a computer-based numerical model to predict the behaviour of a system. In MCS, random samples are collected for each variable and the model is evaluated using these realisations of the random variables and the generation of uniformly distributed numbers. The uniform random numbers are transformed to the distributions by the inverse transformation method or the acceptance–rejection method.

The MCS procedure involves four main steps: (a) defining inputs, (b) generating inputs, (c) performing a calculation, and (d) combining the results. Following this procedure, the probability of failure, as calculated using MCS, can be defined as

$$P_{F(MCS)} = \frac{N}{N_T} \quad (3.2)$$

where $P_{F(MCS)}$ is the probability of failure using MCS, N is the number of simulations in which failure occurs, and N_T is the total number of simulations. The accuracy of the procedure depends on the number of simulations. By repeating the procedure for N simulation cycles, N sets of output results are obtained. Statistical analysis can now be used to obtain the mean value, standard deviation, and distribution type for the output results. The accuracy of the system is expected to be further improved by increasing the number of simulations. Although the implementation of MCS in reliability analysis is remarkably straightforward, there exist a number of drawbacks. For highly reliable systems, the process may take a large number of simulations to achieve a specified target in the case that the probability of failure or the value of the reliability index is extremely high or low. In a structural reliability analysis in which the probability of failure is very small, the MCS process becomes inefficient. To enhance the efficiency of the simulation, the simulated iteration must concentrate on a certain region in the analysis; consequently, convergence is slow and the number of simulation cycles is increased.

Many researchers have presented the results of reliability analysis using MCS (Deng, 2006; Melchers and Ahammed, 2004; Pradlwarter and Schuëller, 2010). Papadrakakis and Lagaros (2002) applied the MCS method to calculate the stress/stiffness constraints and the reliability of a 3D multi-story frame. In the reliability analysis, the authors also considered material properties, member geometry, and loads. Although the probability

of failure showed a marked decrease, the computation time and structural weight increased markedly. Cardoso *et al.* (2008) used a combined MCS and a neural network to compute the probability of failure for a single-story steel frame. Yang *et al.* (2009) used the MCS method to evaluate the structural reliability in the case of random heterogeneous fractures. Su *et al.* (2010) applied the MCS method in 3D modelling of the effect of rough crack surfaces on the structural load capacity and on the reliability. Finally, Tekiner *et al.* (2010) used the MCS method to solve a multi-period, multi-objective problem, involving minimising the cost and air emissions (e.g., CO₂ and NO_x) over a long-term planning horizon.

In summary, MCS is a powerful tool for calculating structural reliability; however, it requires a large number of simulation cycles to obtain the optimum solution. Therefore, this method may not be appropriate for the present research, especially in the case of multi-objective and multi-disciplinary problems.

3.3.3 Latin hypercube sampling

Latin Hypercube Sampling (LHS), first proposed by McKay (1979) and later updated by Iman in 1981 (Iman, 1992), is a technique for reducing the number of MCS simulations, employing a constraints sampling method instead of random sampling as a direct simulation. The general idea of LHS is to force the sample into an area of interest by dividing the probability density function (PDF) into N_{LHS} non-overlapping intervals for each random variable, where N_{LHS} is the number of simulation cycles. The area beneath the PDF curve is the same for each interval; hence, the cumulative density function (CDF) can be obtained. Basically, the CDF region is in the range of 0–1. Figure 3.4 shows a CDF divided into five equal intervals.

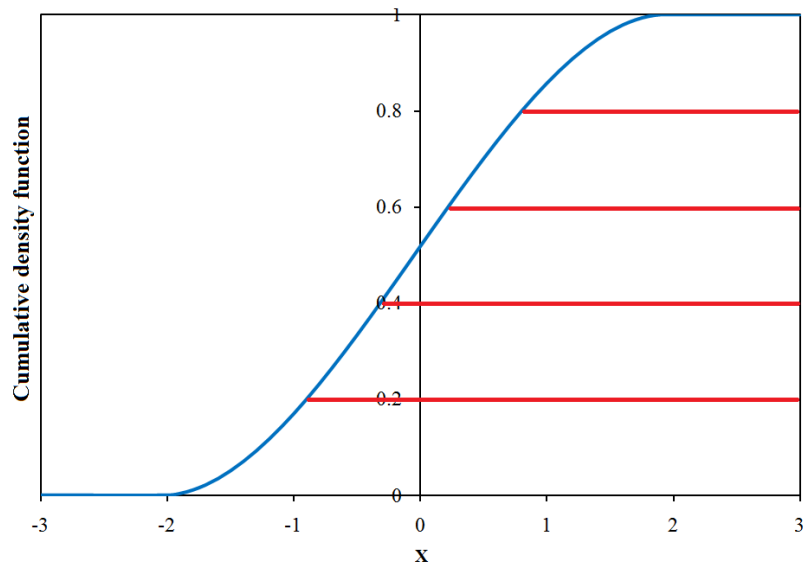


Figure 3.4 – Random cumulative density function divided into five intervals

The random variables are generated by choosing a CDF for each interval. Once the samples are generated, one value from each set is selected randomly and substituted into the performance function to determine precisely whether the structure survives or fails. This process can be described in a Latin domain (Figure 3.5).

A

	X			
		X		
B				X
			X	

Figure 3.5 – 4×4 Latin domain for two random variables

LHS has been extended for various purposes by several researchers; e.g., Iman and Conover (1982), Olsson and Sandberg (2002), Stein (1987), and Ziha (1995). Furthermore, Hossain *et al.* (2006) assessed the performance of LHS for uncertainty predictions of satellite rainfall observations in predicting flooding arising from storm events with moderate rainfall.

Although the LHS method enables a reduction in the number of simulations compared with MCS, it requires further development in terms of structural analysis, especially in dealing with multi-objective and multi-disciplinary problems.

3.3.4 Importance sampling

Importance sampling (IS) is a variance reduction technique that improves the efficiency of MCS. This method was developed to reduce the computational cost and to increase the accuracy of each simulation. IS depends on the magnitude of the probability of failure; i.e., the location of the failure point or design point, as described by Schuëller and Stix (1987). In this method, the sample is located in the tail of the distribution to ensure a sufficient number of simulations, rather than spreading the sample evenly. However, the design point is not known in advance, and the analyst can only guess the starting point of the simulation. Generally, the solutions are located with the mean values, close to the design point. This process is employed to obtain an unbiased sampling using a ‘weighted method’ estimator for the samples.

A benchmark structural reliability problem based on IS was reported by Engelund and Rackwitz (1993). This method has been applied to solve various problems. For example, Grooteman (2008) developed adaptive radial-based IS to determine the radius of a sphere, presenting an efficient and robust method that automatically determined the optimal radius of the excluded sphere, which is the optimum distance from the origin to the limit state surface (Figure 3.6). Ogawa and Tanaka (2009) improved the IS method in estimating an extremely small probability of system failure, and Zhang *et al.* (2010) combined IS and stratified sampling to calculate structural reliability under multiple failure modes.

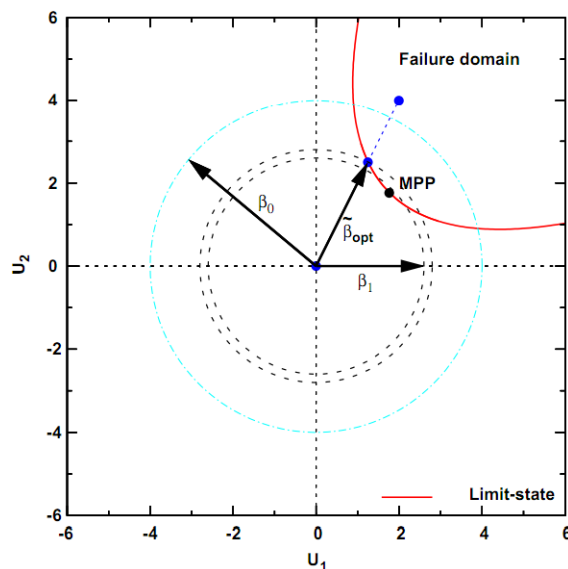


Figure 3.6 – Optimal radius of the excluded sphere using adaptive radius-based IS (Grooteman, 2008)

IS methods are more efficient than MCS, but require information about the limit state, especially the design point close to the origin in the standard normal space. The

procedure followed in gathering all the information is extremely time-consuming and can fail to find the optimum solution; consequently, the use of IS may not be appropriate in the present research.

3.3.5 Response surface

The response surface (RS) method was first introduced by Box and Wilson (1951), based on the use of design experiment data to obtain an optimal response. The authors suggested using a second-degree polynomial model to perform the analysis. They agreed that the model is an approximation technique, but the model is easy to develop and apply (Hill and Hunter, 1966). The RS is used to approximate the limit state functions. To obtain a solution of the RS, regression analysis is required; e.g., the least squares method or weighted regression. The RS method was examined by Schuëller *et al.* (1987) and Wu (1984). For n_v design random variables, the number of analyses required in Wu's method is $2n_v - 1$, whereas Schuëller's method require $4n_v + 3$. In the latter analysis process, the number of steps increases dramatically. For example, if two iterations are required for approximation of the RS with 20 initial experiment datasets a total of 40 structural analyses must be performed.

The RS method has been used in analysing the optimum aerobic biodegradable of dichloromethane in an aerobic pond (Wu *et al.*, 2009), the effect of various chemicals on a material's resistance to corrosion (Masmoudi *et al.*, 2006), and the effect of nanofiltration-modified membranes on the polymerisation technique (Khayet *et al.*, 2010). This method has been extended to other fields, especially engineering structural design. Nguyen *et al.* (2009) developed an RS method based on a double-weighted regression technique in analysing a three-bay, five-story rigid frame structure. The RS method is efficient, especially when used in conjunction with the finite element method. Ren and Chen (2010) developed a method of updating civil-engineering structures using the RS method and the finite element model.

The RS is constructed using various types of interpolation methods to calculate the reliability index. As mentioned above, the computational cost is higher when dealing with complicated problems. In this thesis, multi-objective, multi-disciplinary, and multi-loading cases are considered simultaneously in seeking an optimum design, resulting in an increase in the degree of analysis difficulty; consequently, a large number of simulation cycles would be required.

3.3.6 Artificial neural network

An artificial neural network (ANN) is a method designed to model a brain in executing a particular task. This method is generally used to simulate the behaviour of neurons in the human body (McCulloch and Pitts, 1943). An ANN consists of neurons connected according to a certain pattern. The simplest form of ANN structures consists of several inputs, a hidden layer, and one output. The most common approach is a multi-layer feed-forward network consisting of several layers, each composed of several neurons. This arrangement makes the whole process extremely complicated. There are generally more than one hidden layers in the ANN process, as shown in Figure 3.7. ANN is an approach that can create a relationship between two sets of data during a learning process and reproduce these data in a recall procedure.

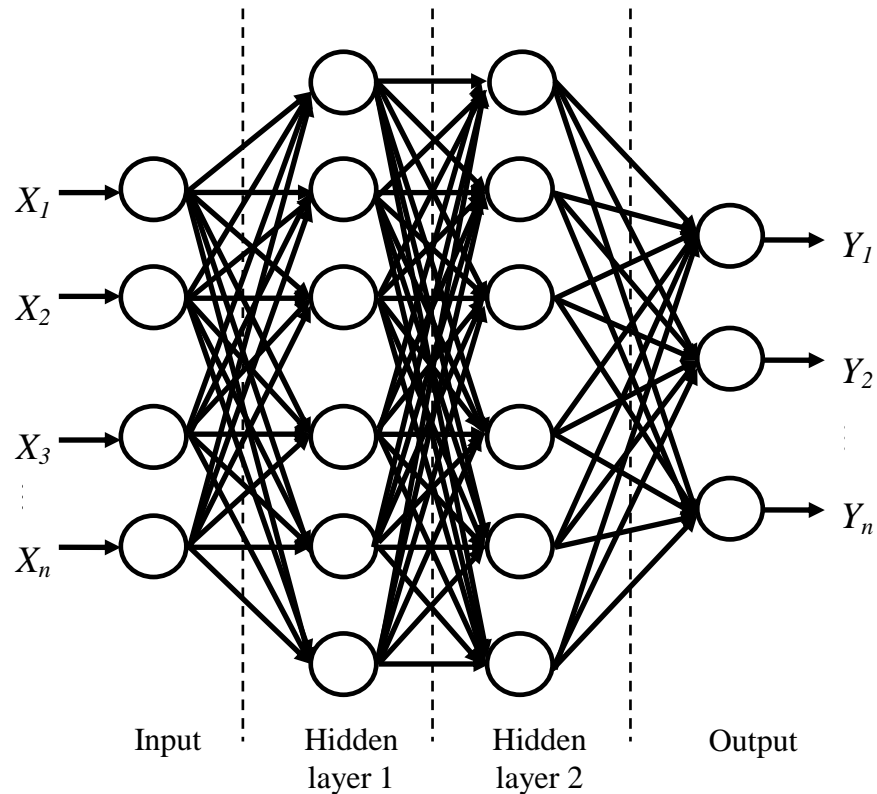


Figure 3.7 – Multilayer feed-forward ANN

In reliability analysis, an approximate implicit function is constructed to obtain performance values. The safety issue in an engineering structure can be defined in terms of design variables, dimensions, material properties, and load. Basically, the finite element method is used to analyse the response of complicated structures. The result of a finite element analysis is used to generate a performance function in terms of implicit

(design variables) and explicit (stress and displacement) forms. These data are then used to create an environment which is capable of learning (Masters, 1993). In reliability analysis, it is difficult to collect all the information related to the implicit performance functions. Nevertheless, ANN is a good universal method for approximating the implicit function. Consequently, ANN is an excellent learning technique for establishing the relationship between performance function and design variables.

Many researchers have combined the ANN approach with other methods to increase its efficiency and reliability. For example, Deng *et al.* (2005) presented a structural analysis for an implicit function in ANN. The authors applied the ANN method in conjunction with FORM, SORM, and MCS to analyse engineering problems. FORM or SORM proved to be useful for reliability problems with implicit and non-linear performance functions. Moreover, the ANN-based MCS required less computation time than did the traditional MCS and ANN. Similar results were reported by Elhewy *et al.* (2006). Lopes *et al.* (2010) showed that a large reduction in processing time could be achieved when a trained ANN is used to evaluate the failure probability.

The ANN approach has been applied in the field of engineering, especially in terms of structural reliability; however, few studies have applied ANN to multi-objective and multi-discipline engineering problems. Cheng and Li (2008) developed a new method for reliability analysis of structure by integrating a uniform design method with a generic ANN algorithm. The authors applied the method to a problem involving a non-linear truss structure and obtained an extremely small probability of failure, indicating a high level of reliability and consequently a high computational cost.

The ANN has several drawbacks: it is computationally expensive in the case of a large neural network system, as several hidden layers and several inputs must be considered simultaneously. In addition, each neural network must be well trained to yield consistent outputs from the training data, resulting in increased complexity. As a result, the ANN approach may not be appropriate for the present research.

3.4 Summary of reliability methods

The above review has demonstrated the vast difference between analytical methods and simulation methods. Although the latter are generally a more powerful tool for reliability analysis, their application to engineering design problems is limited by the large number of simulation cycles. In the present research, therefore, analytical methods have an advantage in terms of providing a robust, simple, and feasible method of obtaining a reliability solution. Table 3.1 lists the main features of the reliability methods introduced above.

Table 3.1 – Summary of reliability methods

Method	Requirements	Accuracy	Remarks
FORM	Transform random variables to standard normal space	Linear limit state functions	This method is required to transform random variables to standard normal space
SORM	As for FORM	Up to second-order functions	As for FORM. The results may be better or worse compared with FORM.
MCS	Not required	High accuracy	Simple and robust. Requires many simulation cycles
LHS	Assumption regarding tail distribution	Quality of the response of distribution	Reduces the number of MCS simulation cycles.
IS	Information about limit state	Similar to MCS	Improves the efficiency of MCS
RS	Approximation method used to approximate the limit state function	Must be carried out with regression analysis	Number of analyses depends on the number of iterations and the number of datasets
ANN	Required input, hidden layer and output.	Multi-layer feed-forward neural network for more than one hidden layer and output	Each neural network needs to be well-trained to yield the same output

3.5 Reliability analysis using commercial software

Several commercial computer programs have been developed for reliability analyses. This section describes the basis and application of these programs. Table 3.2 lists the available reliability software.

Table 3.2 – Reliability software and relevant references

Software	Reference
ANSYS PDS & DesignXplorer	Reh <i>et al.</i> (2006)
CalREL/FERUM/OpenSees	Der Kiureghian <i>et al.</i> (2006)
COSSAN	Schüeller and Pradlwarter (2006)
NESSUS	Thacker <i>et al.</i> (2006)
PERMAS-RA/STRUREL	Gollwitzer <i>et al.</i> (2006)
PHIMECA	Lemaire and Pendola (2006)
PROBAN	Tvedt (2006)
PROFES	Wu <i>et al.</i> (2006)
UNIPASS	Lin and Khalessi (2006)

NESUS, PROBAN, PHIMECA, and CalREL implement the FORM/SORM method. FERUM is considered a convenient method because the software is written in a script language similar to that of CalREL. FERUM not only considers the FORM/SORM method, but it incorporates other reliability methods such as simulation methods and reliability-based design optimisation. ANSYS PDS & DesignXplorer only considers the RS method. COSSAN, OpenSees, PERMAS-RA/STRUREL, and NESSUS can also be used for finite element analysis. Details of related reliability software can be found in the references listed in Table 3.2. To understand the capacities of these reliability software packages, four were selected for a more detailed investigation (NESSUS, PROBAN, CalREL, and FERUM), the results of which are provided below.

3.5.1 NESSUS

Numerical Evaluation of Stochastic Structures under Stress (NESSUS) is a reliability computer program developed in 1991 at the Southwest Research Institute (SwRI) in San Antonio, Texas, USA. This software has been developed over the past 25 years for the purpose of probabilistic analysis, sponsored by the NASA Lewis Research Center (Cleveland, USA). The program is actively being developed in order to enable the use of various methods; e.g., probabilistic analyses of structural systems and combining probabilistic analysis with numerical analysis to calculate the response of probability and reliability. Further information on this software can be found at the NESSUS Web site (<http://www.nessus.swri.org/>) and Thacker *et al.* (2006).

NESSUS seeks to balance efficiency and accuracy in complex structural problems, combining the structural analysis method with an approximate probabilistic algorithm. The basic idea is to estimate the structural reliability and identify the important random variables using a small amount of computational analysis. Random variables are used as inputs, including the dimensions of the problem, material properties, and loading conditions. The solution is the output, which includes deflection, stress, and frequency. Structural analysis is performed using either the displacement method or the boundary element method, which is used in sensitivity analysis. The output information is used to predict the probabilistic response and reliability.

Probabilistic analysis employs an advanced mean value technique. This method covers three main areas: (i) the performance function is located in the original space using the mean value of the random variables, (ii) the approximation is combined with the R–F and Chen and Lind (1982) methods to find the design point in the standard normal space, and (iii) a second-order approximation of the structural response can be made by a deterministic analysis at the design point, combined with the result of the previous step. Rajagopal *et al.* (1989) applied this method to turbine blades and high-pressure ducts, and Thacker *et al.* (2001) reported that the advanced mean value can handle complicated problems and yields satisfactory response functions.

NESSUS employs a graphical user interface (GUI), thereby enabling the use of commercial codes. The program employs 12 probabilistic reliability analysis methods, including FORM, SORM, the Advanced Mean Value (AMV), the RS method, and IS, among others. Furthermore, NESSUS can be used in conjunction with other interfaces,

such as ANSYS, MATLAB, LS-DYNA, and ABAQUS, resulting in great flexibility in terms of performing finite element analyses.

Previous studies have applied NESSUS in analysing system reliability. For example, Riha *et al.* (2004) simulated a vehicle crash using an LS-DYNA finite element model. This simulation evaluated the NESSUS problem statement for head-injury criteria, as shown in Figure 3.8. Rodriguez *et al.* (2002) and Thacker *et al.* (2003) employed NESSUS in an analysis of a containment vessel. A scale factor was defined to allow perturbations in the radius and thickness of the vessel, in order to withstand the maximum equivalent plastic strain occurring at the bottom of the vessel. The analysis revealed that the mean and standard deviation of the thickness of the vessel wall are the most sensitive parameters in improving the reliability.

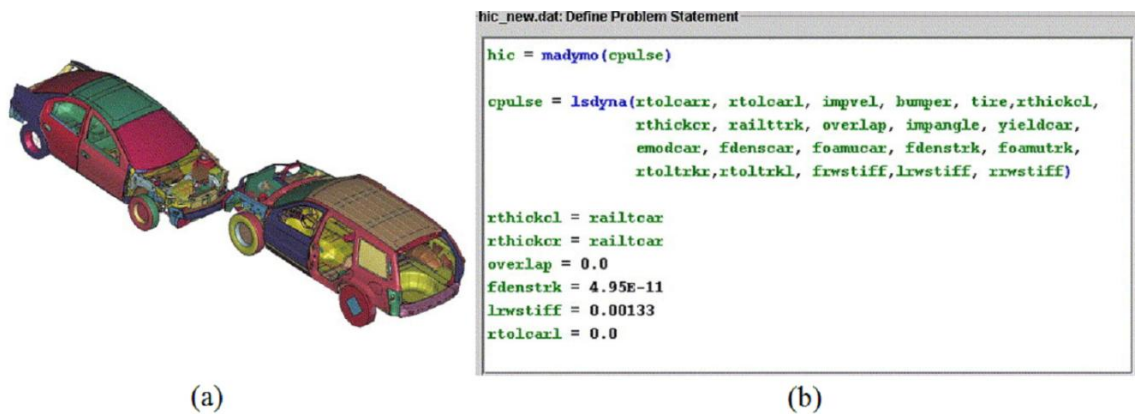


Figure 3.8 – (a) Simulation model for a vehicle crash, and (b) the relevant NESSUS problem statement (Riha *et al.*, 2004)

NESSUS is a useful tool in analysing a reliability problem, and is further enhanced by incorporating finite element analysis, thereby providing a complete engineering structural analysis. However, there is no evidence to suggest that this method is able to solve multi-loading cases simultaneously in seeking an optimal design, although the method has been recommended in verifying a topology reliability problem (Silva *et al.*, 2008). In summary, this method may not be appropriate for the present research, which involves problems with multi-loading cases.

3.5.2 PROBAN

PROBAN (PROBability ANalysis) is a reliability program developed at Det Norske Veritas (Høvik, Norway) of A.S. Veritas Research (Veritas Sesam Systems, 1991; Tvedt, 2006), intended to solve various types of probabilistic problems, including probability analysis, distribution analysis, first passage probability analysis, and crossing rate analysis. Each analysis is related to independent results. For example, the probability analysis is a measure of probability and sensitivity measurements, and the distribution analysis is a measure of the first four moments of a sample. PROBAN can be applied in various fields, including mechanical, structures, civil engineering problems, and offshore structures. This method is capable of estimating the probability of failure using FORM, SORM, MCS, or directional sampling.

PROBAN can be run on a graphical user interface and in batch mode, with the two methods being inter-linked. The user may also use their own equations/functions, combining them with the program in performing the analysis. This option provides flexibility for the user in terms of employing the method with little difficulty. Consequently, the software can be used to solve any problem according to the design requirement. PROBAN is not customisable software, but can be linked to other programs to obtain information for further analysis. PROBAN also contains a library of basic mathematical functions and standard probability distributions, comprising all the information required for a reliability study.

Once the functions are defined, a suitable distribution must be determined. The distributions are organised in the distribution library, and are fitted to the data. The data are either a solution from a PROBAN analysis or a user-generated result, depending on the user's preference. Subsequently, a problem is defined in terms of certain design variables. For example, a variable may be the product of two random variables, with each variable being an individual function. This approach provides flexibility in addressing a probabilistic problem. The next step is to develop the constraints of the problem, which are known as "events". The constraints may be equalities and/or inequalities, depending on the problem of interest. A suitable method must be chosen to perform the analysis. The result of a probability analysis, or a value of the reliability index, is calculated, and it is necessary to assess the efficiency of the selected method. The choice of method should be based on the nature of the design problem and on the computational cost.

PROBAN is a flexible tool which provides various methods and functions relevant to analyses of structural reliability; however, it is not considered for the present research because it is only able to predict the probability of failure or calculate the value of the reliability index. To obtain an optimal solution, PROBAN would require an optimisation procedure, especially in terms of simultaneously solving multi-objective and multi-loading cases. In this regard, PROBAN is unlikely to be appropriate for use in the present study.

3.5.3 CalREL

CalREL (Cal-RELIability) is a general-purpose structural reliability code developed by Liu *et al.* (1989) and written in FORTRAN-77. This method, developed for academic use and engineering practice, incorporates four general techniques: FORM, SORM, a sampling method, and a sensitivity method. CalREL is used to solve general structural-reliability problems. Basically, the method follows a number of simple procedures. For example, the limit state condition (LSC) is required, which provides a subroutine to calculate the function value. This subroutine, which is controlled by the user, must be compiled and linked with the reliability code, and is executed during the CalREL analysis. The LSC does not have to be an algebraic value, as long as it is differentiable with respect to the function. If the problem involves the use of finite element analysis, the LSC may be utilized. Thus, to compute the LSC value, the finite element software must be a subprogram under the CalREL subroutine. Several studies have examined the merging of CalREL with other software (Der Kiureghian and Zhang, 1999; Jang *et al.*, 1994; Liu and Der Kiureghian, 1991; Sitar *et al.*, 1987).

CalREL contains a rich library of probability distributions with three types of specifications: statistically independent random variables, dependent random variables with a Nataf joint distribution (Liu and Der Kiureghian, 1986), and a conditional distribution of dependent random variables (for details of this distribution, see Der Kiureghian *et al.*, 2006). When using the library distributions, the distributions parameter can be any random variable in the system. Next, the reliability in the CalREL system must be transformed into a standard normal space. Finally, a reliability analysis can be performed using the CalREL system.

As an example, consider a one-bay frame (after Der Kiureghian *et al.*, 2006) constructed with ductile members and subjected to random horizontal and vertical loads (Figure 3.9).

CalREL is used to estimate the system reliability, revealing the horizontal and vertical loads that can be supported by the system.

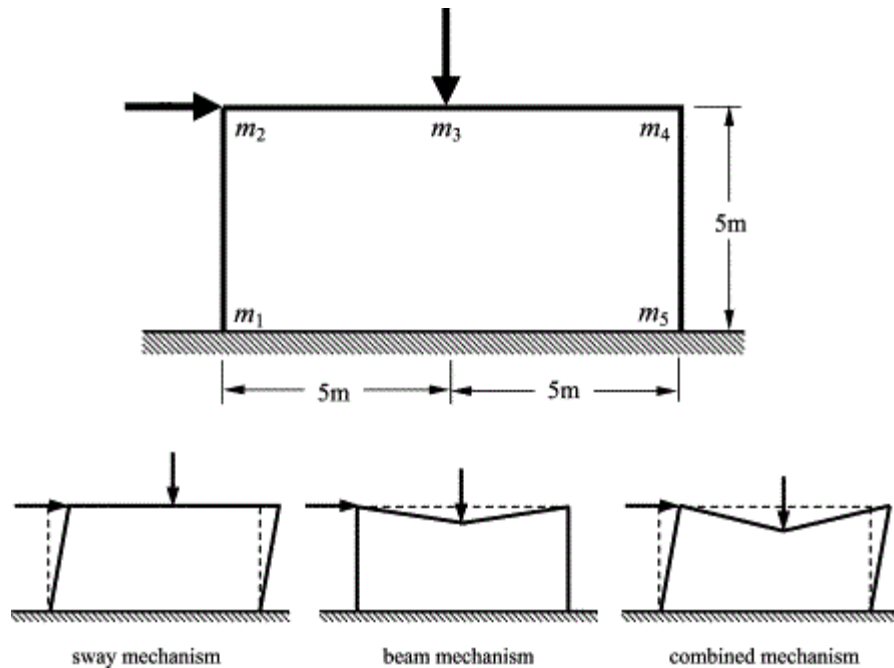


Figure 3.9 – Ductile frame and failure mechanisms (after Der Kiureghian, 2006)

The basic idea of CalREL is that it employs many reliability methods (these methods have been discussed in Section 3.3). The steps involved in using the CalREL system are summarised as follows:

- i) Select the analysis method (e.g., finite element analysis)
- ii) Choose a suitable probability distribution
- iii) Enter all the necessary data, including reliability and design variables
- iv) Select an appropriate reliability method
- v) Analyse the solution

Although CalREL is used to solve reliability problems, it requires further development to enable optimisation tasks that involve finding the optimum solution for each structural problem. Because this method is written in FORTRAN, its development requires expertise in computer programming. A more convenient method is discussed in the following section.

3.5.4 FERUM

Finite element reliability using MATLAB (FERUM) is an open-source MATLAB toolbox for structural reliability analysis which encompasses finite element analysis. This software, initially developed by Der Kiureghian and Haukaas in 1999 at the University of California, Berkeley, USA (Der Kiureghian *et al.*, 2006), employs a user-friendly platform: the user is able to simply give a command to execute the procedure. Because the software is written in MATLAB, the script language has simple rules while maintaining the characteristics of programming. This software is freely available from the FERUM Web site (<http://www.ce.berkeley.edu/FERUM>).

In FERUM, all of the reliability theory is written in MATLAB language. One of the special features of this software is the development of a new method to separate a specific LSC for a given random variable. Basically, FERUM is a collection of files that contain a command to execute the reliability analysis (e.g., FORM, SORM, and the sampling method). These files are available from the FERUM Web site (see above). FERUM has the following advantages: (i) the expression and algorithm is easy to execute in MATLAB, (ii) it takes advantage of the powerful debugging capabilities of MATLAB, and (iii) it benefits from the large number of advanced mathematical functions in MATLAB.

Several researchers have improved the FERUM software in seeking to solve various problems. For example, the original version of FERUM was extended by J. Song in solving problems regarding system reliability, and A. Hahnel extended the software with a detailed SORM analysis (for details, see Der Kiureghian *et al.*, 2006). Overall, the objective of FERUM is to provide users with a tool for immediate use and researchers with a tool for research purposes; it also represents a platform which combines structural reliability and finite element methods in solving structural reliability problems.

The latest version of FERUM (FERUM 4.x; Bourinet *et al.*, 2009) provides users with a simulation-based technique, global sensitivity analysis based on Sobol's indices, and reliability-based design optimisation. Therefore, this software provides a range of reliability tools in analysing structural problems. For further information on FERUM version 4.1, see the official Web site (<http://www.ifma.fr/Recherche/Labos/FERUM>).

To tackle more complicated structural problems, this method should be further developed to enable the simultaneous solving of multi-objective, multi-disciplinary, and

multi-loading-case problems. This method is highly recommended in reliability analyses which include structural problems; however, in its current form it is unlikely to be appropriate for use in the present research.

3.6 Summary

This chapter evaluated a basic structural design concept; i.e., employing the basic principles of resistance and load. The distribution of load and resistance was also discussed. The mean value of resistance is generally larger than the load, meaning that the structure is safe for operation. This evaluation was followed by a review of the most widely used methods of reliability analysis (e.g., FORM, MCS, RS) and a discussion on commercial computer-based reliability programs, of which more than 10 are available. Four reliability programs were examined in detail, including their advantages and disadvantages. The aim of this review was to provide an overview of how the tools for reliability analysis are implemented in the software.

The following chapter focuses on combining reliability and optimisation methodologies.

4 First-order Reliability-related Method, Reliability-based Optimisation, and Optimisation Methodology

4.1 Detailed description of the first-order reliability method

The first-order reliability method (FORM) is one of the most popular reliability methods in analysing the structural reliability of designs. In the following sub-sections, FORMs proposed by Cornell (1969), Hasofer and Lind (1974), and Rackwitz and Fiessler (1978) are described in detail.

4.1.1 Cornell method

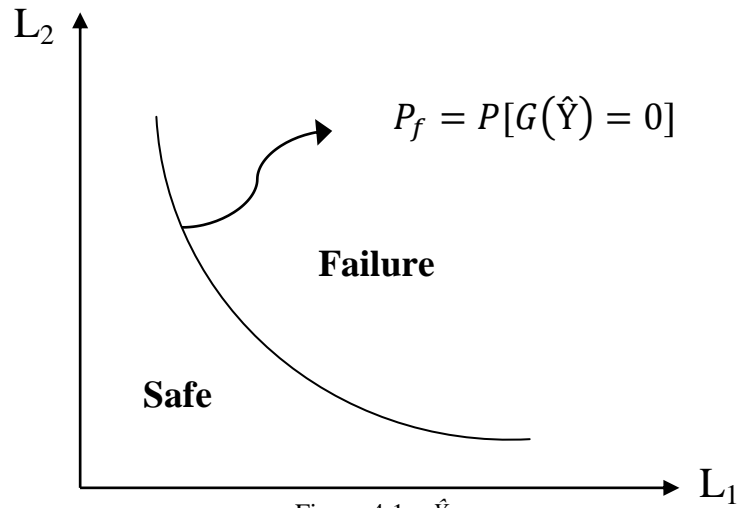
The development of FORM is related to the second moment method. Cornell (1969) used a first-order Taylor series approximation and second moment statistics to calculate a safety index. To evaluate the reliability term, it is convenient to start with a simple function. The two parameters are R (resistance) and L (load). The main objective of structural reliability analysis is to calculate the probability of failure P_f . The relationship between these two random variables (R and L) can be expressed as follows:

$$P_f = P(R - L < 0) \quad (4.1)$$

More often the limit state condition (LSC) is defined as a function of $G(\hat{Y}) = R - L$. The reliability index is related to the probability of failure, which for a given structure can be calculated by evaluating the following integration:

$$P_f = P\left[G(\hat{Y}) < 0\right] = \int_{G(\hat{Y}) < 0} \dots \int f_{\hat{Y}}(\hat{Y}_1 \dots \hat{Y}_n) d\hat{Y}_1 \dots d\hat{Y}_n \quad (4.2)$$

where $G(\hat{Y}) < 0$ is a failure domain, $P[\cdot]$ is a probability function, and $f_{\hat{Y}}(\hat{Y}_1, \dots, \hat{Y}_n)$ is a probability density function of all the relevant variables \hat{Y} . Integrating equation (4.2) is complicated because all the random variables have extremely small values and we do not possess the vital information for the density function. To evaluate the probability of failure, an LSC $G(\hat{Y})$ is defined and a function is used to determine the condition or stability of the structure. Figure 4.1 shows a \hat{Y} space region. The LSC is defined in terms of (i) $G(\hat{Y}) < 0$ (state of failure), (ii) $G(\hat{Y}) > 0$ (state of safety), and (iii) $G(\hat{Y}) = 0$ (limit state surface). The LSC defines the safe and unsafe regions.



Here, an LSC is introduced which employs the mean and variance of the random variables. The LSC, expressed in terms of R and L , is defined as:

$$H = R - L \quad (4.3)$$

It is assumed that R , L , and H are standard normal variables. The mean (μ) and standard deviation (σ) can be written as follows:

$$\mu_H = \mu_R - \mu_L \quad \text{and} \quad \sigma_H = \sqrt{\sigma_R^2 - \sigma_L^2} \quad (4.4)$$

Therefore, the probability of failure can be expressed as follows:

$$P_f = P[H < 0] = \Phi\left(-\frac{\mu_H}{\sigma_H}\right) \quad (4.5)$$

Cornell (1969) defined the probability of failure in terms of a safety index or reliability index (β). This term can be rewritten as follows:

$$\beta = \frac{\mu_H}{\sigma_H} \quad (4.6)$$

4.1.2 Hasofer and Lind method

The reliability index based on the Cornell method (Cornell, 1969) was updated by Hasofer and Lind (1974) (herein, H–L). In the H–L method, \hat{Y} space variables are transformed to a standard normal distribution and the whole process is carried out in standard normal space (μ_i), defined as follows:

$$\mu_i = \frac{(x_i - \mu_{x_i})}{\sigma_{x_i}} \quad (4.7)$$

where x_i is the i -th design variable, and μ_{x_i} and σ_{x_i} are the mean and standard deviation of the design variable, respectively. If none of the variables is normally distributed, it would be difficult to evaluate the reliability index. Consequently, Rackwitz and Fiessler (1978) (herein, R–F) proposed an improved transformation method from \hat{Y} space to standard normal space using equivalent normal variables.

The general idea regarding transforming the \hat{Y} space to the standard normal space is to solve the non-linear limit state (Hohenbichler and Rackwitz, 1981; Madsen *et al.*, 1986). Transformation to the standard normal space has been applied by Augusti *et al.* (1984) and H–L. The failure probability P_f can be expressed as a function of β ; i.e., $P_f = \Phi(-\beta)$, where β is the shortest distance from the origin to a point on the failure surface in the standard normal space μ_i , as shown in Figure 4.2.

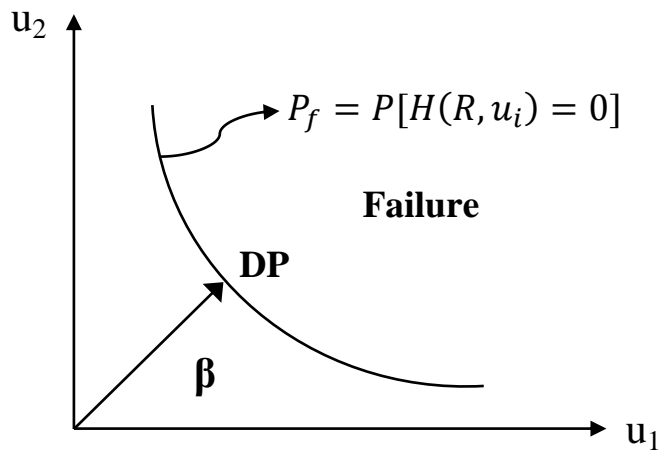


Figure 4.2 – Definition of β in the standard normal space

The procedures involved in employing the H–L method to calculate the reliability index are as follows. To calculate the reliability index in the standard normal space, these procedures require partial derivatives of the LSC with respect to x . The LSC $G(\hat{Y})$ is rewritten as $H(R, \mu_i)$ and defined as:

$$\frac{\partial x_i}{\partial \mu_i} = \sigma_{x_i} \quad (4.8)$$

$$\frac{\partial H}{\partial \mu_i} = \frac{\partial H}{\partial x_i} \cdot \frac{\partial x_i}{\partial \mu_i} = \frac{\partial H}{\partial x_i} \cdot \sigma_{x_i} \quad (4.9)$$

Because the origin in the standard normal space is the combination of all the \hat{Y} space variables, the minimum distance to the failure d_{\min} can be defined as

$$d_{\min} = \min (\mu_i^T \cdot \mu_i)^{1/2} = \min \sqrt{\sum_i (\mu_i)^2} \quad (4.10)$$

$$s.t. : H(R, \mu_i) \leq 0 \quad , \quad \mu_i^L \leq \mu_i \leq \mu_i^U \quad , \quad i = 1, 2, \dots, n$$

where $H(R, \mu_i)$ represents the LSC in the standard normal space and μ_i is the value of the i -th variable. The minimum distance between the limit state $H(R, \mu_i) = 0$ and the origin represents the reliability index. The solution of this problem is known as the Design Point, DP. To find the DP, the distance from the origin to the limit state surface needs to be minimised. Various methods have been proposed to find the DP (Wang and Grandhi, 1994; Wu *et al.*, 1990; Wu and Wirsching, 1987). In addition, Borri and Speranzini (1997) used a finite element analysis to determine the reliability index. For a given failure criterion, a reliability index β (in standard normal space) can be calculated as follows:

$$\beta = \frac{-\sum_{i=1}^n \frac{\partial H(\cdot)}{\partial x_i} \mu_i}{\left[\sum_{i=1}^n \left(\frac{\partial H(\cdot)}{\partial \mu_i} \right)^2 \right]^{1/2}} \quad (4.11)$$

To evaluate a new DP, it is necessary to evaluate a sensitivity factor, which can provide useful information in examining the response of the problem. The sensitivity factor is defined as follows:

$$\alpha_i = \frac{\frac{\partial H(\cdot)}{\partial \mu_i}}{\left[\sum_{i=1}^n \left(\frac{\partial H(\cdot)}{\partial \mu_i} \right)^2 \right]^{1/2}} \quad (4.12)$$

After calculating the reliability index and the sensitivity factor, the new DP can be calculated as follows:

$$x_{i+1} = \mu_{x_i} + \sigma_{x_i} \beta \alpha_i \quad (4.13)$$

where x_i is a design point ($i = 1, 2, \dots$). Rackwitz (1976) proposed an algorithm to calculate the H-L reliability index. The procedure can be summarised as follows (Figure 4.3):

- i) Develop an LSC
- ii) Initial guess of DP
- iii) Transformation of \hat{Y} space variables to standard normal space variables
- iv) Compute the partial derivatives at the initial guess
- v) Compute the reliability index
- vi) Compute new DP
- vii) Re-evaluate $\mu_i = -\beta \alpha_i$
- viii) Repeat steps iii) to vii) until β has converged

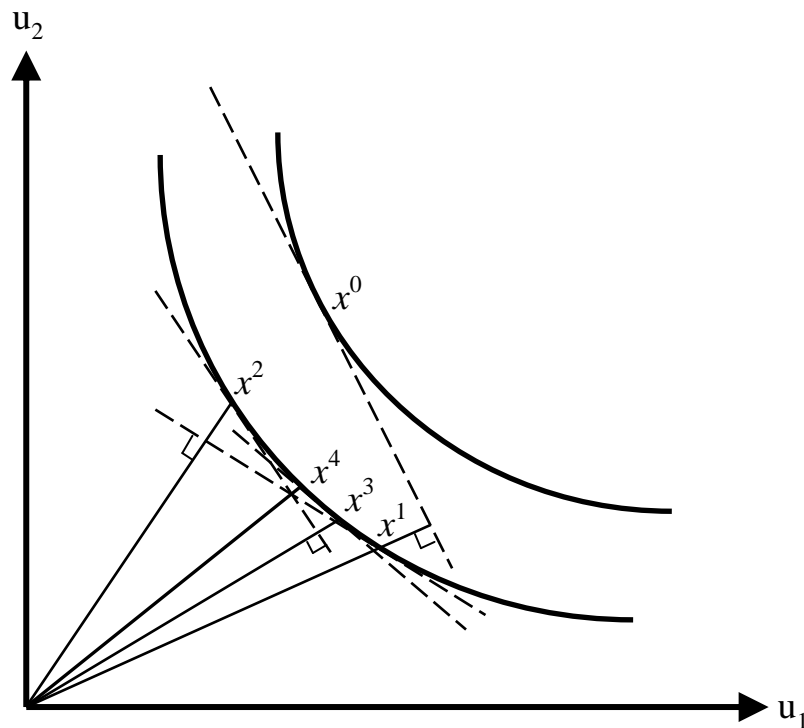


Figure 4.3 – Rackwitz algorithm to solve the H-L reliability index

4.1.3 Rackwitz and Fiessler method

The H–L method was extended by R–F, who suggested that the method could be further improved by using the equivalent standard deviation and the equivalent mean value. The R–F method used this “equivalent” approach to solve all the variables, which were not always normally distributed. The equivalent mean value and equivalent standard deviation in standard normal space are as follows:

$$\mu_{x_i}^e = x_i - \sigma_{x_i}^e \left[\Phi^{-1} \left(F_{x_i}(x_i) \right) \right] \quad (4.14)$$

$$\sigma_{x_i}^e = \frac{1}{f_{x_i}(x_i)} \phi \left[\Phi^{-1} \left(F_{x_i}(x_i) \right) \right] \quad (4.15)$$

Where

$\mu_{x_i}^e$ = equivalent mean value

$\sigma_{x_i}^e$ = equivalent standard deviation

ϕ = probability density in standard normal space

Φ^{-1} = cumulative distribution in standard normal space

f_{x_i} = probability density in \hat{Y} space

$F_{x_i}(x_i)$ = cumulative distribution in \hat{Y} space

x_i = design variables at DP

The procedure employed by the R–F method is similar to that of the H–L method. In the R–F method, the equivalent mean value and equivalent standard deviation are used to calculate the standard normal space distribution. The R–F method is also known as the “H–L and R–F method”, since it was originally developed by H–L and later extended by R–F.

4.2 Reliability loading-case index – A new first-order reliability-related method

As discussed earlier, the minimum distance from the origin to the failure surface must be calculated. This method requires the linearization of all the random variables in the transformation of \hat{Y} space into standard normal space. This is to ensure that the random variables are normally distributed. However, a simpler and more effective method is presented here to calculate the reliability index, as discussed below.

In this research, a reliability loading-case index (*RLI*) is proposed which is a new development of first-order reliability-related method. This method is based on the FORM developed by H–L and later extended by R–F. However, in the present approach a different method is presented involving the evaluation of the *RLI*. A unique optimisation technique, known as MOST, is used in conjunction with the *RLI* calculation to obtain a reliability-related optimum solution. The *RLI* is one of the objectives to be maximised in a MOST optimisation process. The evaluation of *RLI* does not require the calculation of LSC and therefore the optimisation process can be simplified. The *RLI* reflects all the possible outcomes such as the performances and cost of the design and it can be formulated as:

$$RLI_j = \max \sqrt{\sum_i (ck_{ij})^2} \quad (4.16)$$

$$i = 1, 2, \dots, m \quad \text{and} \quad j = 1, 2, \dots, n$$

where ck_{ij} is an individual reliability index, i indicates the i -th performance, and j indicates the j -th loading case. The ck_{ij} gives an individual performance rating for each system performance under a loading case. Each performance is weighted according to importance if desired, and the individual reliability index ck_{ij} is calculated as:

$$ck_{ij} = W_{p_i} \times MSNS_{ij} \quad (4.17)$$

$$i = 1, 2, \dots, m \quad \text{and} \quad j = 1, 2, \dots, n$$

where W_{p_i} is a weighting factor (range, 0–1) which reflects performance in the Modified Standard Normal Space (MSNS). Based on the H–L and R–F methods, a modified equation (i.e., MSNS) is applied to the design variables in the standard normal space. The modifications to $\mu_i = \frac{(x_i - \mu_{x_i})}{\sigma_{x_i}}$ (equation (4.7)) include (i) assigning a magnification

factor and (ii) taking the reciprocal of the modified standard normal space. First, a magnification factor is assigned to reflect the role of the objective functions in a particular performance. Second, the main objective is to maximise the RLI in the optimisation process. As a result, MSNS is the reciprocal to equation (4.7). In structural design, the equation for MSNS is related to structural mass and displacement, defined as

$$MSNS_{ij} = W \left(\frac{\sigma_{d_i}}{d_{ij}} \right) \quad (4.18)$$

$$i = 1, 2, \dots, m \quad \text{and} \quad j = 1, 2, \dots, n$$

where d_{ij} is a data point which indicates the performance parameters and loading case parameters (which will be discussed in Section 4.4), σ_{d_i} is the standard deviation of the performances, and W is the magnification factor applied to a particular parameter. W is used to amplify the MSNS values to ensure they are significant when the design variable is changed, thereby enabling the results to be easily assessed. It is assumed that W cannot be equal to 0. Preliminary calculations indicate that this factor should have a value in the range of 5–7. Its value is fixed to an appropriate value to solve a given type of problem. This factor W is not changed throughout the process in the case that equation (4.18) is used in an optimisation. This equation is only used to calculate the mass and displacement performances.

In structural design, structural mass and deflection are two of the primary objectives to be minimised. The optimisation system is applied to each particular parameter to achieve the required target; however, this approach depends on the magnification factor of each parameter. In the present research, finite element analysis software is used to determine the response of the structure, and the solution is used to calculate MSNS and RLI.

In engineering structural design, stress performance is assessed using equation (4.19) rather than equation (4.18). Normally, materials are designated an allowable stress that the design can sustain. If the allowable stress is exceeded, the material may undergo plastic deformation, which must be avoided. Therefore, the transformation to the standard normal space variable is used in terms of MSNS (referring to stress performance only), defined as:

$$MSNS_{ij} = \frac{d_{ij} - \sigma_y}{\sigma_{d_{ij}}} \quad , \quad d_{ij} < \sigma_y \quad (4.19)$$

where d_{ij} is data points associated with stress performance, the yield stress σ_y , and $\sigma_{d_{ij}}$ is the standard deviation. The stress at a particular loading case must be less than the yield stress, and the result of the MSNS should be negative.

MSNS involves the calculation of the individual performance of the design. The individual reliability index (ck_{ij}) calculations are summed to calculate the RLI. The means and standard deviations are the values based on the design parameters of the structure. Figure 4.4 shows the linearization of mass, stress, and displacement limit states ($G(\hat{Y}) = 0$).

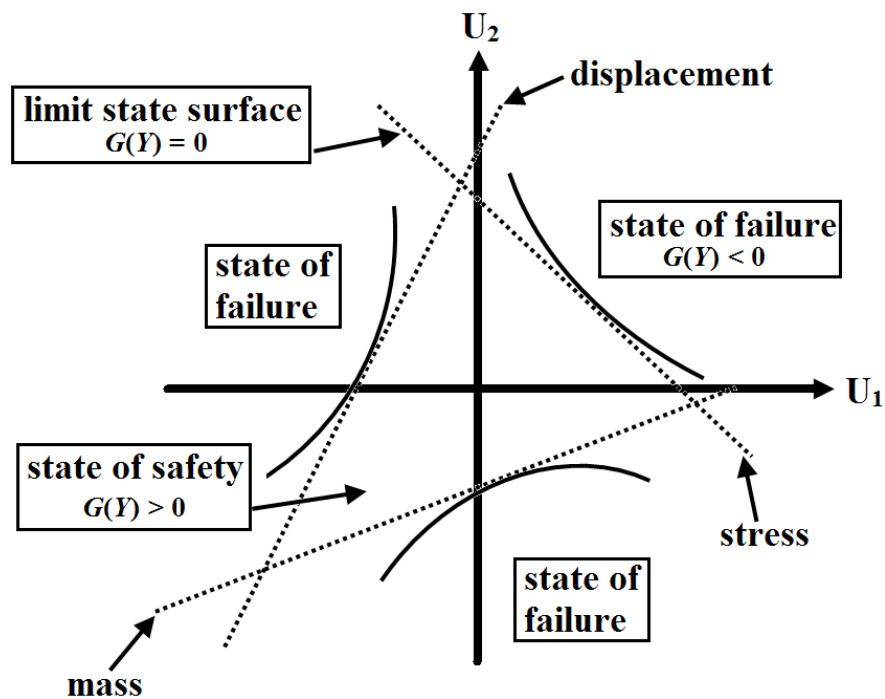


Figure 4.4 – Limit state of mass, stress, and displacement in the standard normal space

4.3 Reliability-based optimisation (RBO) technique

4.3.1 Introduction

The above discussions focussed separately on optimisation methodology and reliability analyses. These methods have been successfully applied to solve various types of problems. In structural engineering, several uncertainties are likely to be unpredictable in solving a given problem. This drawback is addressed using reliability analysis. Therefore, to solve a problem while considering the uncertainties of the problem and to seek an optimum solution, it is necessary to employ a reliability-based optimisation (RBO).

RBO is complicated because it simultaneously deals with a reliability problem and with an optimisation procedure. This method can be applied to a variety of problems, but it is most appropriate in the field of structural design. RBO not only solves optimisation problems, it also takes account of uncertainty in the modelling. Basically, the uncertainty is derived from the probabilities of occurrence and expected values. RBO performs well in terms of identifying unforeseen design problems, and is a powerful method in solving structural designs to determine the optimal solution while considering uncertainty (Enevoldsen and Sørensen, 1994; Papadrakakis *et al.*, 2005; Saitou *et al.*, 2005; Valdebenito and Schuëller, 2010a). Despite these advantages, the application of RBO to engineering design problems poses a great challenge to the engineer, because the RBO procedure is complicated and it is time consuming to solve a design problem, resulting in a high computational cost. Both reliability and optimisation require a repetitive process to evaluate the structural response for each set of design variables and uncertain parameters, continuing until the system has converged.

RBO is an effective method in solving several classes of optimisation and reliability problems. Previous studies have sought to efficiently solve the RBO. For example, Breitung (1994), Ditlevsen and Madsen (1996), and Rackwitz (2001) introduced approximate reliability techniques (as discussed in detail in Section 4.3.4) in solving and estimating the probability of failure and the cost. Schuëller *et al.* (2005) developed an advanced simulation method to solve a similar problem. Other researchers have focused on developing a method for reducing the simulation time, known as High Performance Computing (HPC). HPC employs parallel computing methods which are able to solve a problem within a minimum period (Johnson *et al.*, 2003; Leite and Topping, 1999; Pellissetti, 2009, Umesha *et al.*, 2005).

4.3.2 Description of an RBO problem

RBO has been in use for more than half of century and can be formulated in various ways. Moses and Kinder (1967) presented a weight minimisation while considering the safety level. Similar studies have followed. For example, Vanmarcke (1973) considered the minimum weight of a structural system based on reliability constraints. Both of these studies provided new insights into a matrix formulation of reliability analysis and reliability-based design by devising a novel way to present the RBO. A mathematical expression for an RBO problem is defined as follows (Freudenthal, 1956; Royset *et al.*, 2001; Vanmarcke, 1973):

$$\begin{aligned} & \min_x E[D(x, n_u)] \quad , \quad x \in \Delta_x \\ \text{s.t.} \quad & h_i(x) \leq 0 \quad , \quad i = 1, 2, \dots, n_D \end{aligned} \quad (4.20)$$

$$p_j(x) \leq p_j^{lim} \quad , \quad j = 1, 2, \dots, n_p \quad (4.21)$$

In this problem, x is the vector of design variables of the structure, n_u are uncertainty variables, h_i are constraints on the problem, D is the cost function of a problem, $E[\cdot]$ is an expectation, and p_j is the probability of occurrence at the j -th position. The value of p_j should be equal to or less than a certain limit p_j^{lim} . Equations (4.20) and (4.21) can be solved by using multi-dimensional integrals. The integration of the RBO is not shown here because this method is similar to equation (4.2) (see Section 4.1.1), which is used to evaluate the probability of failure; however, two performance conditions are to be evaluated in the RBO rather than one. This is necessary because the first condition is associated with the cost function and the second is needed to evaluate the probability of occurrence at a certain position. The performance condition is used to analyse a problem related to the whole system. To effectively solve an RBO problem, the performance condition is the so-called LSC. As mentioned above, the LSC can be divided into three components: state of failure, state of safety, and limit state surface.

There exists increasing demand for solving RBO in terms of practical applications. Figure 4.5 shows a schematic diagram of an RBO problem. The design variables of the optimisation algorithm are considered as the outer loop, which seeks the optimum solution. The problem generally starts from an initial state and the optimal solution is achieved after a number of iterations. For each iteration, the system performs the optimisation processes which employ multi-dimensional integrals to calculate the design solution (equations (4.20) and (4.21)). Before the integration is calculated, a

simulation is required to obtain each performance (e.g., in structural analysis, a finite element model is employed).

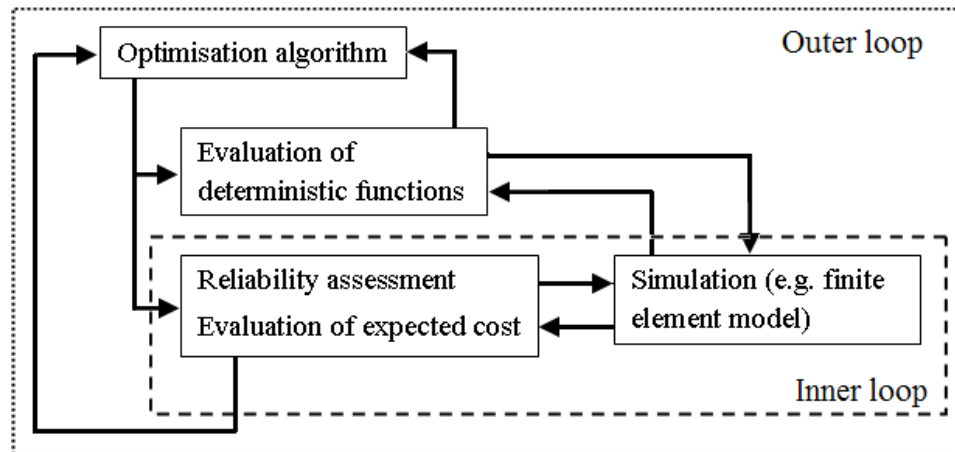


Figure 4.5 – Schematic diagram of an RBO problem (after Valdebenito and Schuëller, 2010a)

To describe RBO in detail, it is useful to recognise three different periods of the development of the technique:

- i) Early approaches
- ii) Approximate reliability techniques
- iii) Simulation-based RBO

Detailed descriptions are provided in the following three sections.

4.3.3 Early approaches

Several methods of reliability-based optimisation were developed during 1960–1980. During this period, the RBO problem was solved using a simplified method with a low computational cost, which was necessary because of the limited computational power available at the time. Hilton and Feigen (1960) proposed using the probability of failure as a constraint to minimise the structural weight. Consequently, the overall probability of failure is calculated by considering the individual probability of failure of components in the system/problem. Various optimisation methods were developed, such as Lagrange multipliers (Hilton and Feigen, 1960); consequently, optimality criteria were developed. Silvern (1963) and Switzky (1965) proposed that the probability of failure and the optimisation proportion weight should be of equal value. This technique was later extended by Murthy and Subramanian (1968), and the probability of failure can be approximated by

$$p(x) = Ae^{A_1x} \quad (4.22)$$

where A and A_1 are constants, with values which represent the dimension of the design variables. An assumption employed in this approach is to introduce a non-linear term related to probability. In simultaneously considering multiple failure modes, Moses and Kinser (1967) demonstrated that system reliability is affected by the weight of the structure, resulting in an overestimated design and an increased structural weight in the design solution. This problem was addressed by Moses (1997), who considered the correlation among failure modes. Using this simplification technique to estimate the probability of failure, the RBO can be solved with minimal computational cost.

Vanmarcke (1973) proposed a method of solving RBO using correlation coefficients by considering interactions between failure modes. This method introduces two subsets of failure events (basic and remainder), which allows the user to seek the optimum solution within the upper and lower bounds of the design variables. The method was successfully applied to an example that involved minimising the construction cost and failure cost. Charnes and Cooper (1959) developed chance-constrained programming for solving using the linearization of design variables, which was related to the reliability problem. Ditlevsen and Madsen (1996) used an explicit procedure to solve the linearization problem. The drawback of early approaches was their inefficiency in solving a large number of design variables, which involved simultaneously considering multi-objective and multi-loading cases. This inefficiency reflects the limited computational power available at the time. To develop an effective RBO, it is necessary to employ an approximate reliability technique, which is outlined in the following section.

4.3.4 Approximate reliability technique

As discussed above, many types of reliability approaches are available (e.g., FORM). Cornell (1969), H–L, and R–F have successfully developed FORM for practical applications, including the introduction of Design Point, DP (the shortest distance to the limit state surface). Thus, FORM is capable of predicting the probability of failure for a given problem. A reliability index (β) was also introduced, enabling the reliability of the problem to be computed. During this early period, FORM was capable of solving engineering design problems using analytical methods.

RBO has always been employed to minimise the objective function and to consider uncertainty. Basically, there exist three different approaches: (i) double loop, (ii) single loop, and (iii) decoupling.

4.3.4.1 Double loop approaches

The most direct approach in the approximate reliability method for solving an RBO problem is the double loop approach, which utilises the optimisation method to estimate the structural reliability. Two optimisation cycles are required: one for the optimisation loop and another for the reliability analysis. FORM is always employed in the reliability analysis to seek the DP. Nikolaidis and Burdisso (1988) proposed using FORM to solve a problem by minimising a cost function subject to a constraint, which is expressed as:

$$\min_x D(x) \quad (4.23)$$

$$\text{s.t. } \beta(x) \geq \beta_{min}$$

where $\beta(\cdot)$ is the reliability index and β_{min} is the minimum acceptable reliability index. The transformation of FORM is required, as mentioned by H–L and R–F. Therefore, the LSC is developed from the solution of the multi-dimensional integral, as mentioned above. Consequently, the LSC of failure is defined as $G(\hat{Y}) < 0$, where an inequality constraint is presented. This method is also known as the Reliability Index Approach (RIA), as proposed by Tu *et al.* (2001). Kwak and Lee (1987) presented a method for minimising the weight under several probability constraints, employing a sensitivity estimation method to solve the optimisation and reliability problems. This method was successfully used to calculate the reliability index using a Lagrange multiplier. The most important feature of this approach is that the optimum solution must be consistent with the DP in the Lagrange multiplier. This method highlights the efficiency of the

double loop using FORM. Lee and Kwak (1995) extended this method by using a Neumann expansion to solve a structural problem.

Other studies have developed methods for solving probability problems, employing a reliability index. For example, Enevoldsen and Sørensen (1994) presented a formula for solving RBO while considering the construction cost and failure cost, and Reddy *et al.* (1994) introduced an approximation concept for estimating the probability and its sensitivity. Yang and Nikolaidis (1991) used the double loop approach to solve various failure modes in reliability analysis.

A new methodology was proposed by Der Kiureghian *et al.* (1994), known as inverse FORM (iFORM). Tu *et al.* (2001) named this method the Performance Measure Approach (PMA). This method is relatively similar to RIA; however, the minimum acceptable reliability index is equal to the norm, which is the uncertain parameters derived from the iFORM (Lee *et al.*, 2002). This method is simpler than the RIA approach because it solves an optimisation problem with an equality constraint rather than with inequality constraints (Youn *et al.*, 2003).

The Dimension Reduction Method (DRM) is another classical approximate reliability method (Rahman and Xu, 2004; Xu and Rahman, 2004) which employs the double loop approach to solve an RBO problem. This method is also employed by iFORM for solving reliability problems.

The drawback of the double loop approach is that it focuses on a single function; i.e., minimising a cost function subject to a probability constraint. Although this method is not directly employed in the present research, it may be further developed to enable the solving of various types of problems.

4.3.4.2 Single loop approaches

The single loop approach is similar to the double loop approach. Basically, the single loop approach seeks to minimise the weight under several probabilistic constraints, utilising the mean values of the design variables which represent the uncertainty parameters in the problem. Consequently, in an RBO problem the probabilistic constraint is replaced with an approximation, meaning that the double loop problem is converted to a single loop problem.

This method, developed by Chen *et al.* (1997), has proved to be effective in solving a range of problems; however, the accuracy and efficiency of the method are influenced by several factors. For example, the initial starting point may affect the efficiency (Yang and Gu, 2004), and the method employs FORM to solve the problem, meaning that a highly non-linear problem may not be appropriate. This problem can be overcome by using a second-order reliability method rather than a first-order method.

Other methods that avoid the use of a double loop are Karush–Kuhn–Tucker (KKT) (Bonnans *et al.*, 2003; Kuschel and Rackwitz, 1997) and Lagrange multipliers. The optimisation involves finding the optimum solution, seeking the best DP. KKT is able to identify the DP when RBO is incorporated in the approach, meaning that the inner optimisation loop can be removed. This approach can simultaneously converge the solution and seek the DP and design variables. The KKT method employs a single loop approach, which still requires the calculation of the second-order derivatives. Moreover, Aoues and Chateauneuf (2010) stated that KKT is inconsistent because of stability problems. An approach similar to the KKT was recently developed. Agarwal *et al.* (2007) proposed probabilistic constraints using the iFORM method to solve the RBO (Kuschel and Rackwitz, 1997), and the second-order derivative is avoided by considering the quasi-Newton method (Bonnans *et al.*, 2003). Another application of the KKT method is to use a hybrid formulation for solving an RBO problem, related to the product of the objective function and the reliability of the structure (Kharmanda *et al.*, 2002).

The advantage of the single loop approach is that it converts the double loop into a single loop, which is achieved using KKT and Lagrange multipliers. However, the single loop approach still requires a second-order derivative in finding the optimum solution. Although the latter method (i.e., the iFORM method) is much simpler than the single loop approach (i.e., the KKT method), it still employs the double loop method in solving optimisation problems. The single loop approach is efficient in solving component reliability and linear performance functions from the viewpoint of reliability. Therefore, this method is appropriate in solving engineering problems related to a single/multiple objective function under a single loading condition. Nevertheless, the aim of this thesis is to simultaneously solve multi-objective and multi-loading cases, meaning that this method may not be appropriate for the present study in its current form.

4.3.4.3 Decoupling approaches

The decoupling approach is different from double and single loop methods, as it mainly uses an optimisation approach to perform an analysis, incorporating reliability analysis. An advantage of the decoupling approach is that it does not require a full reliability analysis because the optimum solution is determined by an optimisation procedure.

This method was firstly developed by Li and Yang (1994), who used it to solve a linear programming problem which involved constructing a linear approximation of the reliability index using sensitivity information. Subsequently, Tu *et al.* (2001) improved the method by considering a linear approximation of the probability. In addition, Chandu and Grandhi (1995) developed a linear and reciprocal approximation of the reliability index. Several studies have proposed methods for solving the reliability and optimisation method, including the application of recursion for estimating the DP and its sensitivity (Cheng *et al.*, 2006), and applying sequential linear programming and identifying active constraints (Chan *et al.*, 2006 and 2007).

Du and Chen (2004) proposed an approach in which all the design variables are assumed to have a Gaussian distribution and the mean value is employed, known as Sequential Optimisation and Reliability Assessment (SORA). SORA was developed to improve the efficiency of probabilistic optimisation. This method employs a single loop approach with cycles of optimisation and reliability assessment. For each cycle, optimisation and reliability assessment are decoupled. After the optimisation has been verified to satisfy the constraint under uncertainty, the reliability assessment is evaluated. This method is based on the constraint on the DP and the reliability information from the previous cycle. The key feature of this approach is the rapid improvement in each cycle and the improved computational efficiency; however, it does not guarantee an optimum solution can be attained. Although the method represents a significant improvement in uncertainty analyses of optimisation, it remains limited due to the nature of the single loop approach. Theoretically, this method is an indirect approach related to the double loop, as the reliability assessment is calculated after the optimisation has been verified, before the next cycle begins.

SORA is similar to the methodology employed in this thesis, but it was not employed in this case because it was necessary to perform the reliability analysis.

4.3.5 Simulation-based RBO

Another technique of RBO is the simulation method. Simulation-based RBO involves the development of an analytical model which is computer-based, with the aim of seeking the optimal solution in terms of reliability and optimisation assessment. As mentioned above, the Monte Carlo Simulation is commonly employed in RBO.

The simulation method can be used in predicting reliability for a certain degree of variability. For example, a structural problem may be analysed using two different simulations that yield different results in estimating the reliability; however, this problem can be overcome by using a large number of samples. Consequently, the system seeks all possibilities and calculates the reliability of the problem, ultimately yielding the optimal solution. A large number of calculations is expected to improve the accuracy of this procedure. Such techniques can be classified into the following types:

- i) Meta-models
- ii) Decoupling
- iii) Direct integration

4.3.5.1 Meta-models

The simulation model provides insight into the behaviour of a real system. Such models (e.g., finite element analysis and boundary element analysis) are always relevant to solving problems in structural engineering. Consequently, computational cost has shown a marked increase over time, especially in analyses of a large number of design variables or a large-scale structural system. A meta-model can be employed to reduce the computational cost by approximating the functions.

Meta-models employ a training system to ensure the consistent accuracy of the method. In this approach, all the data points are analysed to determine which are important. Cox and Reid (2000) stated that the data points are selected using an appropriate method such as Latin hypercube sampling (explained in Section 3.3.3). Bichon *et al.* (2008) proposed a method using an efficient global optimisation procedure to select specific data points, to ensure the accuracy of the method is highest when approaching the LSC or DP.

A meta-model is a method for approximating the performance function, which is evaluated if the uncertain parameters and design variables are available. A typical

example of a meta-model is the response surface (RS), as in Section 3.3.5. Foschi *et al.* (2002) proposed that the RS can be used in replacing the performance function of the system. Subsequently, FORM or importance sampling is used to evaluate the reliability. A similar technique was studied by Agarwal and Renaud (2004). RS can also be used in the intermediate responses.

Meta-models are also used in other reliability methods to reduce the computational cost. Papadrakakis *et al.* (2005) demonstrated the use of an artificial neural network (ANN) to approximate the computational cost of a finite element method, and Beyer and Schwefel (2002) stated that RBO can be solved using an MCS to evaluate the reliability. ANN has also been applied in solving the optimisation of dynamic systems (Zhang and Foschi, 2004). Bichon *et al.* (2009) introduced a meta-model to approximate the performance function in an RBO problem. In this method, the performance function is replaced by a Gaussian process meta-model, which enables the system to analyse the problem more effectively. Subsequently, the meta-model is combined with a different level of the RBO problem, such as the double loop, single loop, or decoupling approaches. Previous studies have focused on reducing the simulation effort, which is related to the cost (Missoum *et al.*, 2007).

The application of a meta-model is always an attractive approach in solving RBO problems because the method is computationally inexpensive; however, the training systems can be challenging in the case of complicated problems which involve a high-dimensional input vector.

4.3.5.2 Decoupling

As discussed above, the decoupling approach is a simulation technique for estimating reliability. It is possible to construct an approximation of the probabilities as an explicit function of the design variables. This method is used to maximise the efficiency of the optimisation loop (outer) by considering the design variables only, combined with the reliability loop (inner). The main idea of the decoupling method is to separate the double loop approach; i.e., the reliability problem is nested in the optimisation problem. Therefore, the problem is reduced to approximate the probability, which simplifies the RBO problem.

Murthy and Subramaniam (1968) and Lind (1976) employed the decoupling method to approximate a problem by means of an exponential function, and Gasser and Schuëller (1997) used this method to develop a global approximation of the failure probability. The global approximation considered the explicit function of the design variables. This approach involved constructing several interpolation points at the failure region using a simulation search. After the data are collected from the interpolation points in the design variables space, they are adjusted by an exponential function using a higher-order polynomial to predict the behaviour of the system. The global approximation method was later extended by Jensen (2005) and Jensen and Catalan (2007) to estimate the failure probability using local approximations. The advantage of a local approximation is the use of a lower order of polynomial function, which may also be combined into a sequential approximation optimisation problem (Jacobs *et al.*, 2004). In the sequential approximation method, a new approximation of a failure probability sub-domain is developed after a solution of the design variables has been identified. Therefore, the optimisation algorithm is repeated with the new approximation (sub-domain) until an optimum design is obtained.

Previous studies have sought to improve the approximation method. For example, Au (2005) developed an instrumental variability method in estimating a failure event by using Bayes' theorem and histograms to represent the probability distribution of the design variables. Ching and Hsieh (2007a and 2007b) extended the instrumental method by using a probability density function which utilises the maximum entropy principle (Jaynes, 1968; Ormoneit and White, 1999). The probability density function is able to estimate the failure probability using a global approximation method. Koutsourelakis (2008) further developed the instrumental variability method by using probabilistic classifiers at different stages of the reliability analysis. In addition, several authors have focused on the approximation method based on sensitivity analysis (Valdebenito and Schuëller, 2010b). The salient feature of this method is the consideration of design variables which correspond to the mean value (Zou and Mahadevan, 2006). The sensitivities are also used in estimating the reliability of the sample (Wu, 1994). Finally, the failure probability is approximated using an exponential function which is able to calculate the sensitivity using a large number of parameters.

Global and local approximations of the failure probability have a common drawback: because both methods utilise the exponential approximation method, the analysis of a large number of design variables requires the evaluation of a large number of functions,

resulting in a rapid increase in the exponential curve and a high simulation cost; consequently, this method may not be appropriate for the present research.

4.3.5.3 Direct integration

As mention in the previous section, the approximation method, when used to evaluate the failure probability, makes use of sensitivity information; however, this method can be used directly in a gradient-based optimisation to solve an RBO problem. The gradient method is based on calculating the derivatives of the objective and constraint functions. Although the number of analysis solutions is significant reduced, the sensitivities must be calculated repeatedly. The gradient method was presented by Royset and Polak (2004a and 2005b) using a simulation method such as MSC or IS. More specifically, this method requires the derivatives obtained using MCS or IS. The sensitivity information is later used in an optimisation method to obtain an optimum solution for the RBO problem.

Jensen *et al.* (2009) introduced an approach for solving RBO problems based on sensitivity information, subsequently extended by Valdebenito and Schuëller (2010b). In this method, the sensitivity information is combined with the optimisation method based on the feasible region. Thus, the line search method is performed to increase the efficiency of the procedure by using a polynomial approximation within the feasible region. This approximation is constructed using the probability estimation information and follows the procedure described by van Keulen and Vervenne (2004).

Another direct approach is stochastic subset optimisation (Au and Beck, 2001; Taflanidis and Beck, 2008a and 2008b), which allows the simultaneous evaluation of the structural reliability and identification of the optimum solution of the RBO problem. The advantage of this method is identification of the design variables, which improves the value of the objective function by simultaneously evaluating the structural reliability and identifying the optimal solution. By repeating this procedure many times, it is possible to obtain the optimum solution, which is required in the following optimisation process. Although this method is capable of solving a large number of variables while considering a non-linear performance function, a drawback is the high simulation cost.

4.4 Multifactor Optimisation of Structure Techniques (MOST)

This section deals with the combination of reliability analysis and the MOST technique, as adopted in part of this thesis.

4.4.1 Optimisation methodology

Structural design requirements often indicate that an optimisation procedure involves a number of quantity-variant objectives, constraints, loading cases, and design variables. Thus, an important part of the optimisation procedure is to establish a suitable method for evaluating this process; however, complex cross-relationships make it difficult to suitably appraise the design in order to yield an overall quantitative performance index which truly represents the character of the system. MOST tackles this problem by employing a systematic method for evaluation based on the concept of parameter profiles analysis, which is written in the FORTRAN programming language (Liu and Thompson, 1996; Thompson and Goeminne, 1993). This method evaluates a structural design by considering many individual performance parameters for a variety of loading cases, while also considering cost and mass.

4.4.2 Performance data matrix

The requirements for a complex structural design indicate that the optimisation must involve multi-objectives, multi-loading cases, and a large number of design variables. An $m \times n$ matrix (d_{ij}) , the so-called performance data matrix (PDM), is defined by a set of performance parameters P_i ($i = 1, 2, \dots, m$) and loading case parameters C_j ($j = 1, 2, \dots, n$). Thus, the data point d_{ij} is the i -th performance P_i of the structure for loading case C_j . The data points of the matrix are obtained by a finite element analysis and a reliability analysis of the structure. The matrix lists every performance of the structure at every individual loading case (see Table 4.1). Figure 4.6 shows an example of a PDM. The general procedure for obtaining the performance data is shown in Appendix A.

Table 4.1 – Performance data matrix

	C_1	C_2	...	C_n
P_1	d_{11}	d_{12}	...	d_{1n}
P_2	d_{21}	d_{22}	...	d_{2n}
\vdots	\vdots	\vdots		\vdots
P_m	d_{m1}	d_{m2}	...	d_{mn}

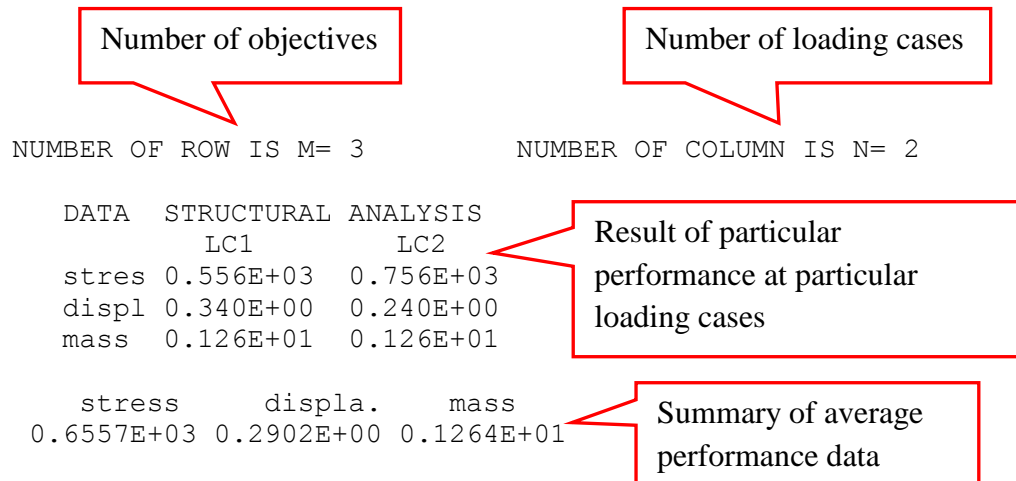


Figure 4.6 – Example that employs a PDM

4.4.3 Parameter profile matrix

A parameter profile matrix (PPM) is created to review the profile of the performances for different loading cases (see Table 4.2). The PPM assesses the character of the structure with respect to the actual performances relative to their acceptable limits and to the best values of the performances.

Table 4.2 – Parameter profile matrix

	C_1	C_2	...	C_n
P_1	D_{11}	D_{12}	...	D_{1n}
P_2	D_{21}	D_{22}	...	D_{2n}
\vdots	\vdots	\vdots		\vdots
P_m	D_{m1}	D_{m2}	...	D_{mn}

The data point D_{ij} in the PPM is a non-dimensional number in the range of 0–10 which is determined by the closeness of the actual performance d_{ij} to the acceptable limit and the best values of the performance.

In principle, the calculation of the data point D_{ij} for one acceptable limit (e.g., the lower limit) is as follows:

$$D_{ij} = \left(\frac{d_{ij} - l_{ij}}{b_{ij} - l_{ij}} \right) \times 10 \quad (4.24)$$

where d_{ij} is the actual performance value taken from the PDM, and l_{ij} and b_{ij} are the lower limit and the best value, respectively. Equation (4.24) is valid for $l_{ij} < d_{ij} < b_{ij}$; for $d_{ij} > b_{ij}$, $D_{ij} = 10$; and for $d_{ij} < l_{ij}$, $D_{ij} = 0$. The data points D_{ij} for the cases of acceptable upper limit and double acceptable limits (Figure 4.7) can be calculated in a similar way.

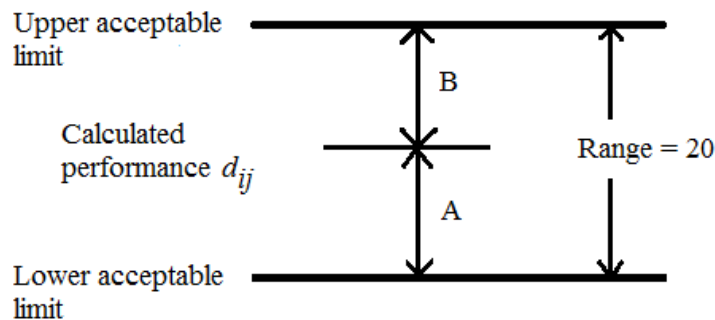


Figure 4.7 – Calculation of a data point in the case of two acceptable limits

4.4.4 Performance Assessment

Information obtained from the PPM allows the whole system to be evaluated. The mean and standard deviation (SD) are calculated for each parameter and each loading case for every column and row of the PPM matrix. The SD is a measure of the degree of dispersion of the data around the mean. A well-designed system should have low SDs and high means (close to 10). High SDs indicate that the system is likely to have significant problematic areas. A high SD obtained for a column indicates that the system, when under a specific loading case, will yield significantly problematic

performance. Similarly, a high SD for a given row indicates a fluctuation in the system performance under various loading cases for various parameters.

The system can be further analysed using the parameter performance index (PPI) and the case performance index (CPI). When i -th parameter is very vulnerable, some data points D_{ij} of the PPM will have values close to 0 and hence the PPI_i will also close to 0. Similarly, when the system is vulnerable at the j -th loading case, CPI_j will be close to 0. The highest values for PPI and CPI are 10. PPI and CPI values which are close to 10 indicate good designs, whereas values close to 0 should be avoided. The PPI and CPI can be defined as follows:

$$\begin{aligned} PPI_i &= \mathbb{Z}_i \times n \quad i = 1, 2, \dots, m \\ CPI_j &= \mathbb{N}_j \times m \quad j = 1, 2, \dots, n \end{aligned} \quad (4.25)$$

where

$$\mathbb{Z}_i = \frac{1}{\sum_{j=1}^n \left(\frac{1}{D_{ij}} \right)} \quad \text{and} \quad \mathbb{N}_j = \frac{1}{\sum_{i=1}^m \left(\frac{1}{D_{ij}} \right)} \quad (4.26)$$

The system can be reviewed by using the information in the indices, as follows:

- A comparison of PPIs indicates whether the system performs better with respect to some performances than to others.
- A comparison of CPIs shows whether the system performs better under certain loading cases than under others.

The mean values, CPIs, PPIs, and SDs provide an overall performance assessment for the system and loading cases. The mean values are not used directly to rate the performance, because high scores may hide low scores. These indices are calculated by summing the inverse of the data point as a performance rating. To simplify the calculations, the performance indices are categorized into the range 0–10, enabling different loading cases and parameters to be compared in order to gain an overall perspective of the characteristics of the system.

According to matrix profile analysis, the PPI is a measure of the vulnerability of each performance parameter and the CPI is a measure of the vulnerability of each loading case. Hence, the integration of PPI and CPI indicates the vulnerability of a particular parameter/loading case combination. To evaluate the design, an overall performance is

presented to formulate the performances and the loading cases, thereby providing a scientific quantitative evaluation for the system. An overall performance index (OPI), which takes the form of a qualitative score, can be established for the system by considering all the performances and all the loading cases. The OPI function lies in the range of 0–100. Each performance parameter and loading case is given a weighting system according to its importance. The OPI can be expressed as follows (for an un-weighted case):

$$OPI = \frac{100}{m \times n} \sum_{i=1}^m \sum_{j=1}^n PPI_i \times CPI_j \quad (4.27)$$

This optimisation technique has the advantage of forcing the performances to approach their best values. The nearer the performances to the acceptable limits, the more strict is the “punishment” (penalties). The optimisation problem stated above is further complicated by the fact that the objective does not always have continuous first and second derivatives. Consequently, the problem needs to be solved using a numerical process; however, a numerical calculation using the gradient method and a Hessian matrix may be computationally expensive or even impossible. Therefore, the objective function is maximised using the effective zero-order method, utilising conjugate search directions (Liu and Hollaway, 2000). For details of the MOST optimisation procedures, see Appendix B.

4.5 Formulation of an optimisation problem

In this research, a novel MOST has been extended to automatically accommodate and execute reliability-related multi-factor structural sizing/shape optimisations. Therefore, the design problem is to minimise structural mass, maximum stress, and maximum displacement, and to simultaneously maximise the RLI, subject to the design constraints for multi-loading cases. The optimisation to be solved is stated as follows:

$$\begin{aligned} &\text{find} \quad X = (x_1, x_2, \dots, x_k) \\ &\text{min} \quad \{m(X), \sigma_{\max,j}(X), \text{ and } \delta_{\max,j}(X)\} \\ &\quad \text{and/or} \\ &\text{max} \quad \{RLI_j(X)\} \\ &\text{s.t.} \quad \{\sigma_{\max,j} \leq \sigma_{\text{lim}} ; \delta_{\max,j} \leq \delta_{\text{lim}} ; m \leq m_{\text{lim}} ; RLI_j \geq RLI_{\text{lim}}\} \text{ and} \\ &\quad \{x_i^{\min} \leq x_i \leq x_i^{\max}, i = 1, 2, \dots, k\} \\ &\quad j = 1, 2, \dots, n \end{aligned}$$

where k is the number of design variables, m is the structural mass, σ_{\max} is the maximum stress of the structure, δ_{\max} is the maximum displacement of the structure, RLI is the reliability loading-case index, the subscript “lim” indicates a specified performance limit for the structure, and n is the number of loading cases. x_i^{\min} and x_i^{\max} are the lower and upper bounds of the design variables of x_i , respectively.

4.6 Summary

This chapter evaluated a detailed first-order reliability method (FORM). The reliability term was first developed by Cornell (1969). This method was further developed by Hasofer and Lind (1974) (H–L) and later extended by Rackwitz and Fiessler (1978) (R–F), and has proved to be successful in solving various types of problems. This account was followed by an outline of a reliability methodology: the reliability loading-case index (RLI), which represents a modification of the H–L and R–F methods. Subsequently, a reliability-based optimisation (RBO) was discussed. Various types of RBO were described in detail and their advantages and disadvantages considered.

In this research, a multifactor optimisation of structure techniques (MOST) has been extended to automatically accommodate and execute reliability-related multi-factor structural sizing/shape optimisations. This technique is able to consider individual performance and loading cases subject to the design constraints. Several examples, employing this technique, are presented in Chapters 5–7.

5 Multi-objective Optimisation – An Automotive Component Optimisation (Sliding Caliper)

5.1 Introduction

A braking system has been one of the most important safety components in automobiles. The development of the brake system has focused on increasing its efficiency. There are broadly three types of brake systems used in the automotive industry: drum brakes, disc brakes, and electromagnetic brakes. In recent developments, the brake system has been used in conjunction with advanced electronic technology to provide the most safe and reliable design. In such cases, the brake system converts brake energy into ‘electrical’ energy which is used to recharge the battery. Therefore, the electrical energy from the battery is used to generate the motion of the vehicle. This is known as a hybrid system. Many car manufacturers have adopted this new concept to create vehicles with low CO₂ emissions; e.g., the Toyota Prius¹⁰ and the new Toyota Auris hybrid (Toyota, see <http://www.toyota.co.uk>). Both of these cars use disc brakes as part of the innovative hybrid mechanism.

The disc brake was introduced by the British engineer Frederick William Lanchester (1868–1946) (Clark, 1995; Harper, 1998; Newcomb and Spurr, 1989), who in 1902 described a brake consisting of a disc which is firmly mounted to one of the vehicle wheels (Lanchester, 1902). In the following years, the carmakers Mercedes (Daimler Motor Gesellschaft) and Renault introduced drum brake systems (Newcomb and Spurr, 1989). Elmer Ambrose Sperry (1860–1930), an American inventor and entrepreneur, developed an electromagnetic actuated disc (Sperry, 1894, 1895, and 1896) which was placed in contact with another disc to act as a brake. Sperry discovered that the braking effect was generated in part by friction between the discs and in part by eddy currents. The designs of Lancaster and Sperry were significantly improved during the twentieth century. Lancaster’s design is a spot-type brake, whereas Sperry’s is a clutch-type brake, which was used in aircraft during the Second World War. In modern automobiles, spot-type disc brake systems are widely used on the front wheels of passenger vehicles.

Kinkaid *et al.* (2003) presented a detailed review of brake systems and brake squeal problem, including drum brakes and disc brakes. This chapter focuses on the sliding caliper, which is a component of a disc brake system.

5.2 Brake system

The brake system consists of brake pedal, brake line, hydraulic cylinder, and complete brake assembly. In a passenger vehicle, the most common brake types are drum brakes and/or disc brakes. Drum brakes are normally located at the rear and disc brakes located at the front of the vehicle. Each brake assembly is connected through brake lines, which are hydraulically linked to the master cylinder, as shown in Figure 5.1. When the brake pedal is pressed, the brake fluid in the master cylinder forces the fluid to each wheel of the brake assembly unit. Since the brake fluid cannot be compressed, the fluid pushes the piston outward in the brake assembly, resulting in slowing of the vehicle.

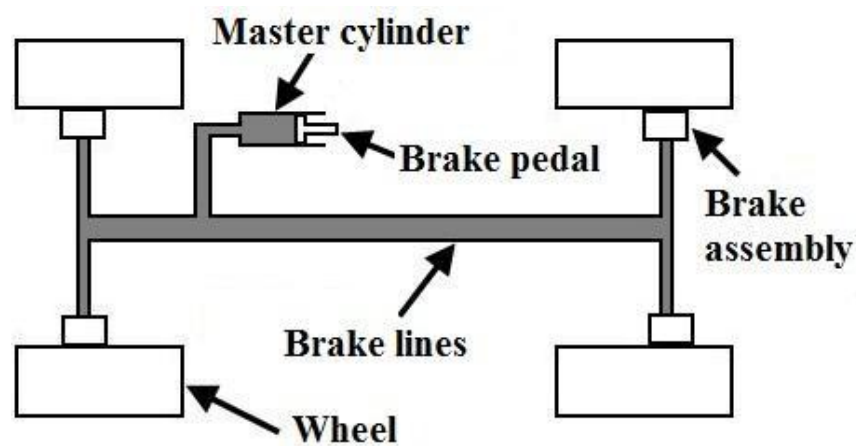


Figure 5.1 – Brake system

5.2.1 Drum brake

The drum brake, which is a basic brake system used in the automotive industry, consists of a backing plate, the brake drum, brake shoes, and other components which together form the complete drum brake. Brake drums are generally made of cast iron, and the inside of the drum is machine-smoothed. A pair of brake shoes, made of a frictional material, is in contact with the smooth surface. A drum brake also contains many small components; e.g., a backing plate, the cylinder wheel (piston), springs, the parking brake lever, and screws.

As mentioned above, the brake system is connected to the master cylinder through a series of brake lines. When the brake pedal is depressed, the brake fluid is forced under pressure into the wheel cylinder, which pushes the brake shoes outward and into contact

with the brake drum. When the brake is released, springs pull the brake shoes back to the original position. Over time, the brake shoes and brake drum become worn, meaning that the shoes need to move a greater distance to make contact with the drum brake. When this distance reaches a certain point, an automatic system adjusts the brake shoes to be closer to the brake drum. A simplified drum brake system is shown in Figure 5.2.

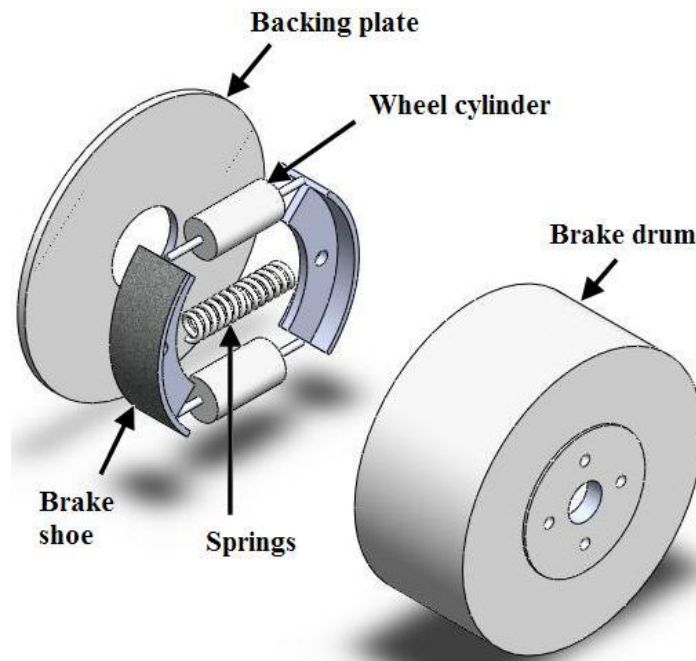


Figure 5.2 – Simplified drum brake system

Drum brakes are used in modern cars because they are cheaper to produce than other brake systems and because they are readily incorporated into the parking brake system. The parking brake is a long steel cable which connects the rear brakes and the hand lever. In drum brakes, the parking brake represents the addition of a simple system; i.e., by adding a lever. Consequently, the parking brake is separate from the hydraulic system and the mechanism is completely manual.

When a brake is applied, frictional force and heat are generated. The heat can be dissipated by adding a cooling fin to the outside of the drum. Excessive heat gives rise to problems such as expansion of the brake drums, the vaporisation of hydraulic fluid, and reduced effectiveness of the frictional material in the brake shoes, thereby reducing the efficiency of the brake and increasing the risk of malfunction.

5.2.2 Disc brake

A modern disc brake assembly comprises a rotor, caliper, brake pad, and hydraulic actuation system. The rotor or disc is firmly mounted on the axle at the site where the wheel is fixed to the rotor. Brake pads are placed either side of the rotor (i.e., inner and outer pads), and other small components are used to hold the pads. The brake pad is a frictional material which is pressed against the disc when the brake is applied. The caliper acts to hydraulically activate the pistons; consequently, heat is produced as the wheels are slowed.

Calipers may be fixed or sliding (Figure 5.3). A fixed caliper is firmly mounted on the vehicle axle, and uses at least one pair of opposed pistons to clamp onto the disc from each side when the brake is applied. For economy, a sliding caliper generally uses one piston and pushes the inner brake pad until it makes contact with the disc brake rotor. The sliding caliper, supported vertically by a mounting bracket attached to the axle housing, is allowed to travel in the opposite direction to the piston movement. More specifically, when the brake is applied, the piston is pushed outward, forcing the inner brake pad to press against the rotor. This forces the caliper to move in the opposite direction to that of the piston. As the result, both brake pads are pressed against the disc and the wheel speed is reduced.

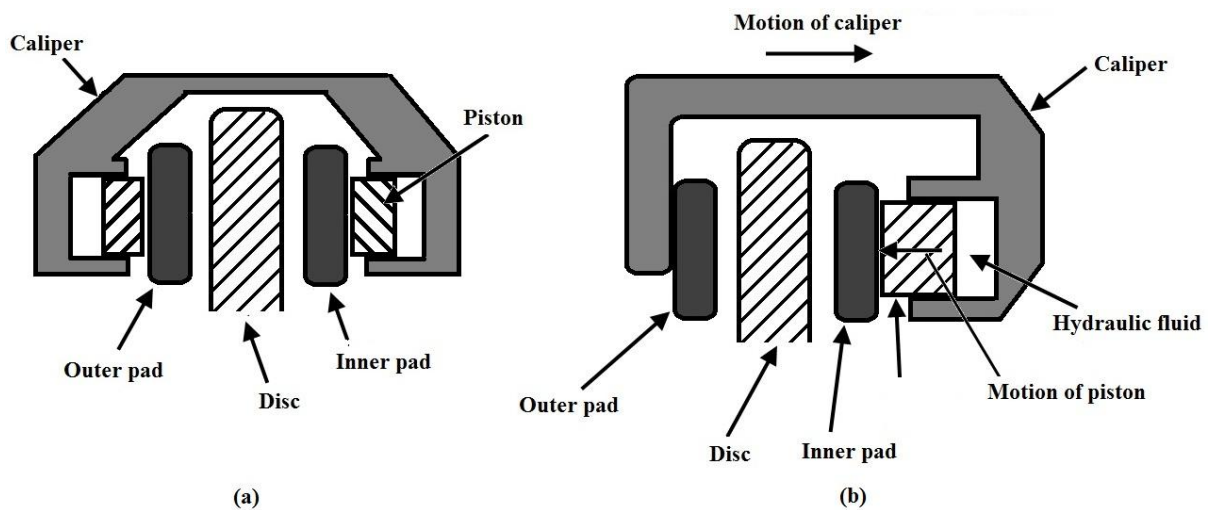


Figure 5.3 – Cross-sectional diagrams of (a) a fixed caliper and (b) a sliding caliper

The brake caliper, which is an important component of the disc brake system, comprises an assembly of a brake pad, seal, and pistons. The caliper needs to withstand the reaction from the brake effect and the heat generated by friction. Basically, the rotor is made of cast iron, which has high wear resistance. To protect the wheel bearings from the high temperatures generated during braking, the rotor has a top-hat shape

(Newcomb and Spurr, 1969) (Figure 5.4(a)), which increases the surface area and the path length that heat must travel to affect the bearings. A ventilated disc is used to reduce the heat more effectively, thereby enhancing the cooling effect. The two discs are connected by a series of thin ribs, as shown in Figure 5.4(b).

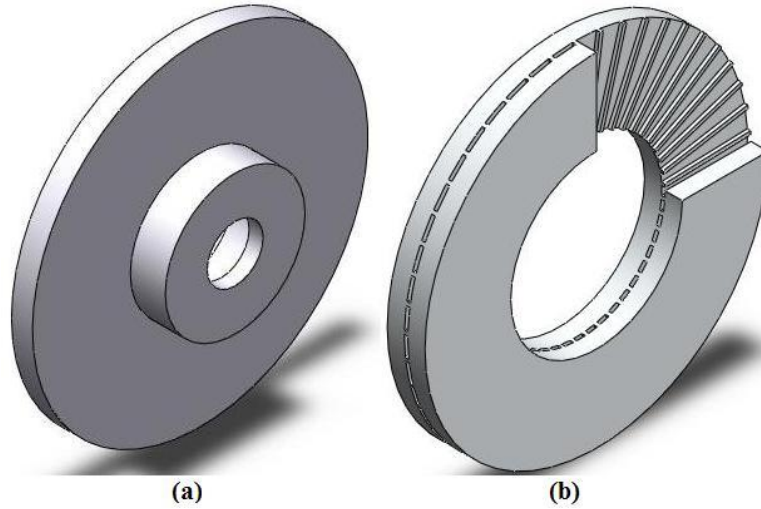


Figure 5.4 – Types of disc: (a) top-hat shaped disc, and (b) ventilated disc

5.3 Validation analysis of optimised sliding caliper

5.3.1 Design Problem

The design problem of a sliding caliper is to find an optimum solution while satisfying all the design constraints. This is done using a MOST (Multifactor Optimisation of Structure Techniques) technique by retaining a low mass and satisfying strength and stiffness standards, subject to the design constraints. The design optimisation problem to be solved may be formally stated as follows:

$$\begin{aligned}
 &\text{find } X = (x_1, x_2, \dots, x_k) \\
 &\text{min } \{m(X), \sigma_{\max}(X), \text{ and } \delta_{\max}(X)\} \\
 &\text{s.t. } \{\sigma_{\max} \leq \sigma_{\text{lim}} ; \delta_{\max} \leq \delta_{\text{lim}} ; m \leq m_{\text{lim}}\}, \\
 &\quad \{x_i^{\min} \leq x_i \leq x_i^{\max}, i = 1, 2, \dots, k\}
 \end{aligned}$$

where k is the number of design variables, m is the component mass, σ is the von Mises stress of the caliper, δ is the displacement of the component, and the subscript ‘max’ and ‘lim’ indicates a maximum and a specified limit of the design. The sliding caliper is optimised to carry a maximum pressure P , have a targeted deflection of $\delta_{\text{lim}} = 0.32$ mm

in any direction, satisfy a strength criterion of $\sigma_{lim} = 450$ MPa, and the structural mass (half of the model) of $m_{lim} = 1.24$ kg. x_i^{min} and x_i^{max} are the lower and upper bounds of the design variables of x_i , respectively. The model considers a single loading case.

5.3.2 Design constraints and boundary conditions

The optimisation method uses conjugate search directions (Liu and Hollaway, 2000) to search for the optimum solution, by changing the positions of the key points. The sliding caliper is modelled using sizing- and shape-design variables. There are 29 shape design variables and 7 sizing design variables. The former are defined using key points and are connected by lines and B-Splines. Each key point represents the coordinates of the design variables and two directions (i.e., x and y axes). Figure 5.5(a) shows that the key points act as design variables (only part of the design is shown). Sizing design variables are used to define the position and thickness of the guiding arm, the thickness of the outer pad support (Figure 5.5(b)), and other design variables. In this way, the initial finite element model is created.

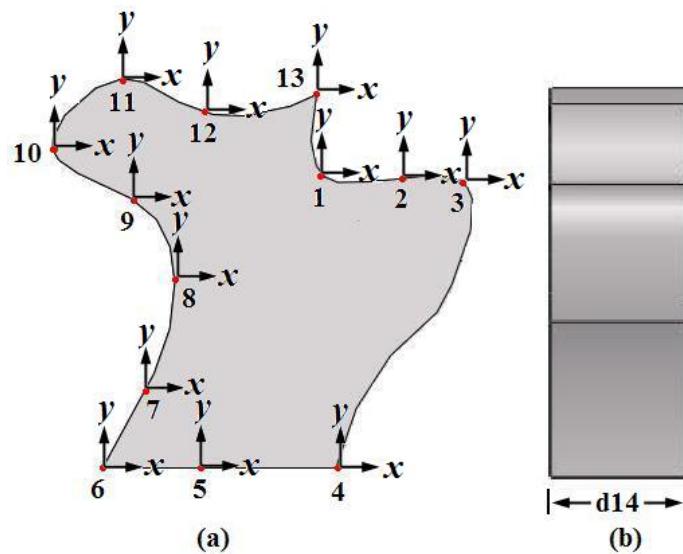


Figure 5.5 – (a) Numbers ‘1’ to ‘13’ are the key points as design variables, and (b) ‘d14’ is one of the sizing design variables

In this study, only half of the sliding caliper is modelled to reduce the computational cost. The caliper is divided into a guiding arm, the piston housing, the body, and an outer brake pad support (Figure 5.6(a)). The diameter of the sliding caliper is fixed at the site of the piston, and the distance between the piston and the end of the outer pad is also fixed. The distance between the piston housing and the outer brake pad support is set to enable the brake pad assembly and the disc to be located between them. The

sliding caliper is supported by the guiding arm and this small area is firmly mounted on the vehicle axle, as shown in Figure 5.6(b). For the guiding arm, only the x and y directions are fixed. The caliper is free to move parallel to the z -axis. During the analysis, the z -axis is fixed at the location of the outer brake pad, as indicated as the red line in Figure 5.6(b). A uniform pressure P is applied to the cylinder wall at the location of the piston of the sliding caliper, as indicated by the red region in Figure 5.6(c). A symmetry plane (the xz -plane) is considered during the analysis.

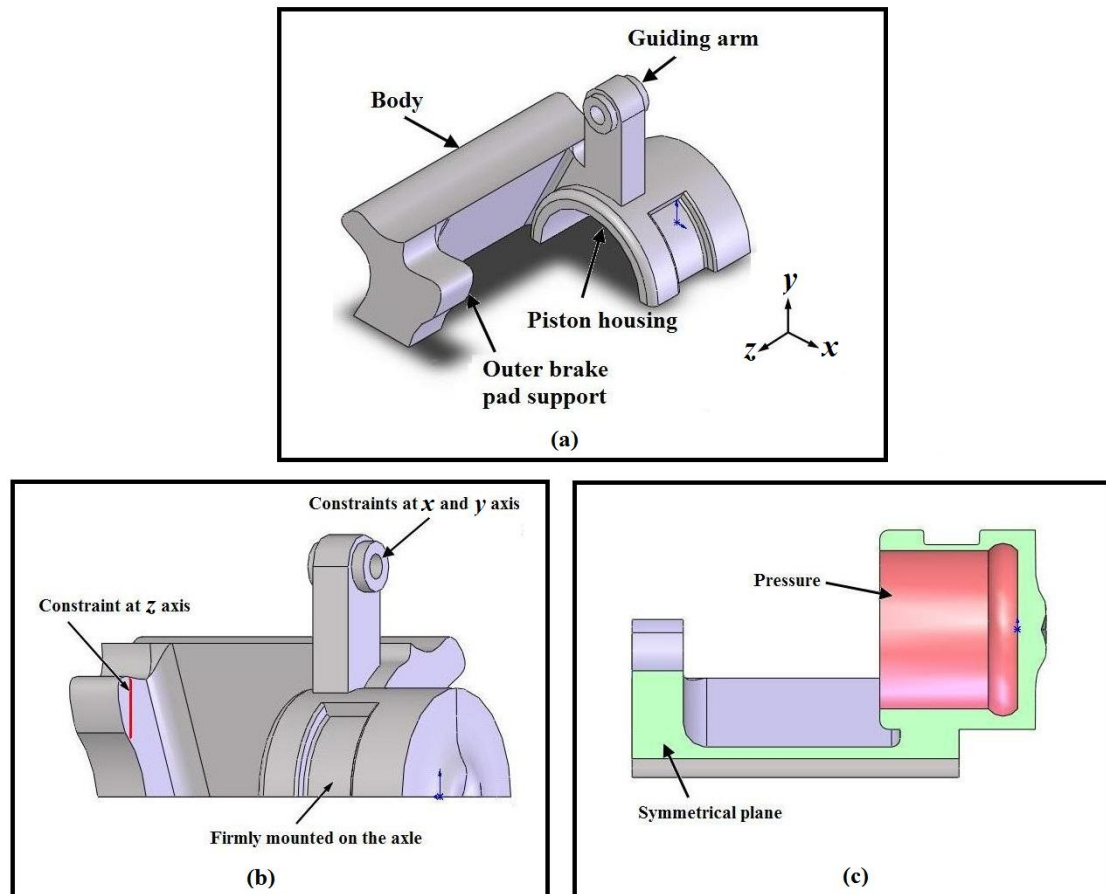


Figure 5.6 – (a) Sliding caliper overview, (b) design constraints, and (c) applied load (red area) and symmetry plane (green area)

5.3.3 Convergence test

The static structural response of the sliding caliper is modelled using the finite element analysis software ANSYS in conjunction with the MOST technique. In this study, the sizing and shape optimisation considers a three-dimensional design where variations in displacement occur along the x , y , and z axes. To ensure that the mesh density is sufficient, a displacement convergence test is performed by decreasing the element size. Table 5.1 shows the effect of incremental decreases in element length, starting with a

basic element length of 12 mm, on the overall displacement vector sum (for the area indicated by the red circle in Figure 5.7) and the number of elements.

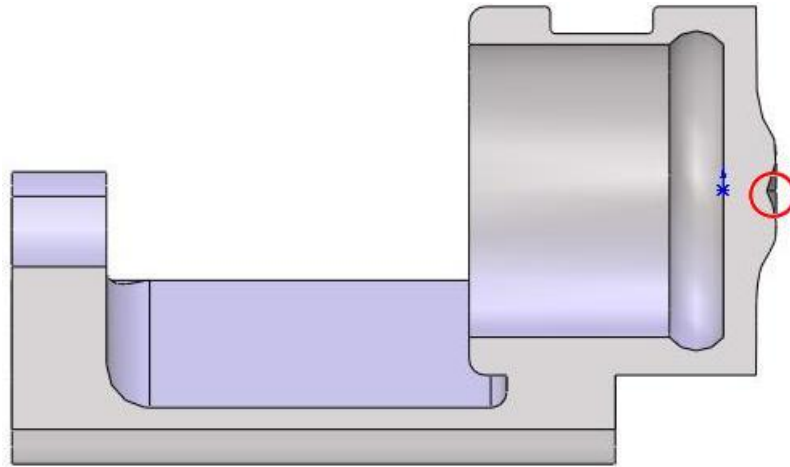


Figure 5.7 – Initial design (bottom view)

Table 5.1 – Element size (sliding caliper)

Element length/mm	No. of elements	Displacement vector sum/mm
12	2276	0.30792
6	8962	0.27936
3	53950	0.27771
1.5	401975	0.27773

Table 5.1 shows that no further accuracy is gained by reducing the element length beyond 3 mm (corresponding to 53,950 elements). In addition, any further reduction would result in a marked increase in the total number of elements and in the number of consecutive analyses. Therefore, an element length of 3 mm is selected for the analysis of the sliding calliper.

Figure 5.8 shows the discretisation of the initial sliding caliper. For simplicity, only half of the model is considered. The SOLID92 element is used to generate the finite element model, which uses 10-node tetrahedral structural elements. This design adapts well to the free meshing of irregular shapes. The initial model consists of 53,950 elements with a uniform mesh size of 4.5 mm^2 and a constant element length of 3 mm.

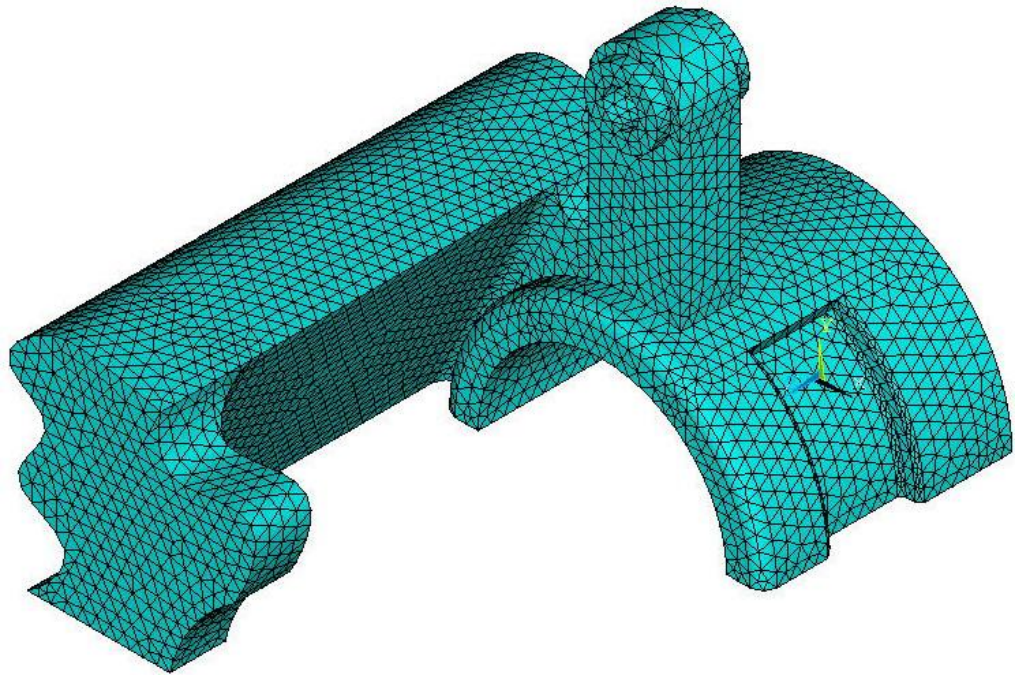


Figure 5.8 – Initial finite element design of a sliding caliper

5.4 Results and discussions

5.4.1 MOST optimisation

Optimisation of the sliding calliper required 109 MOST iterations (n_i) to attain convergence, as shown in Figure 5.9. Initially, the shape of the design is changed. More specifically, areas of low stress are removed, as indicated by comparing $n_i = 0$ with $n_i = 29$. From $n_i = 29$ onwards, the sizing- and shape-design variables are focused on finding the optimum size in each particular region; finally, the optimal solution with perfect design is found at $n_i = 109$.

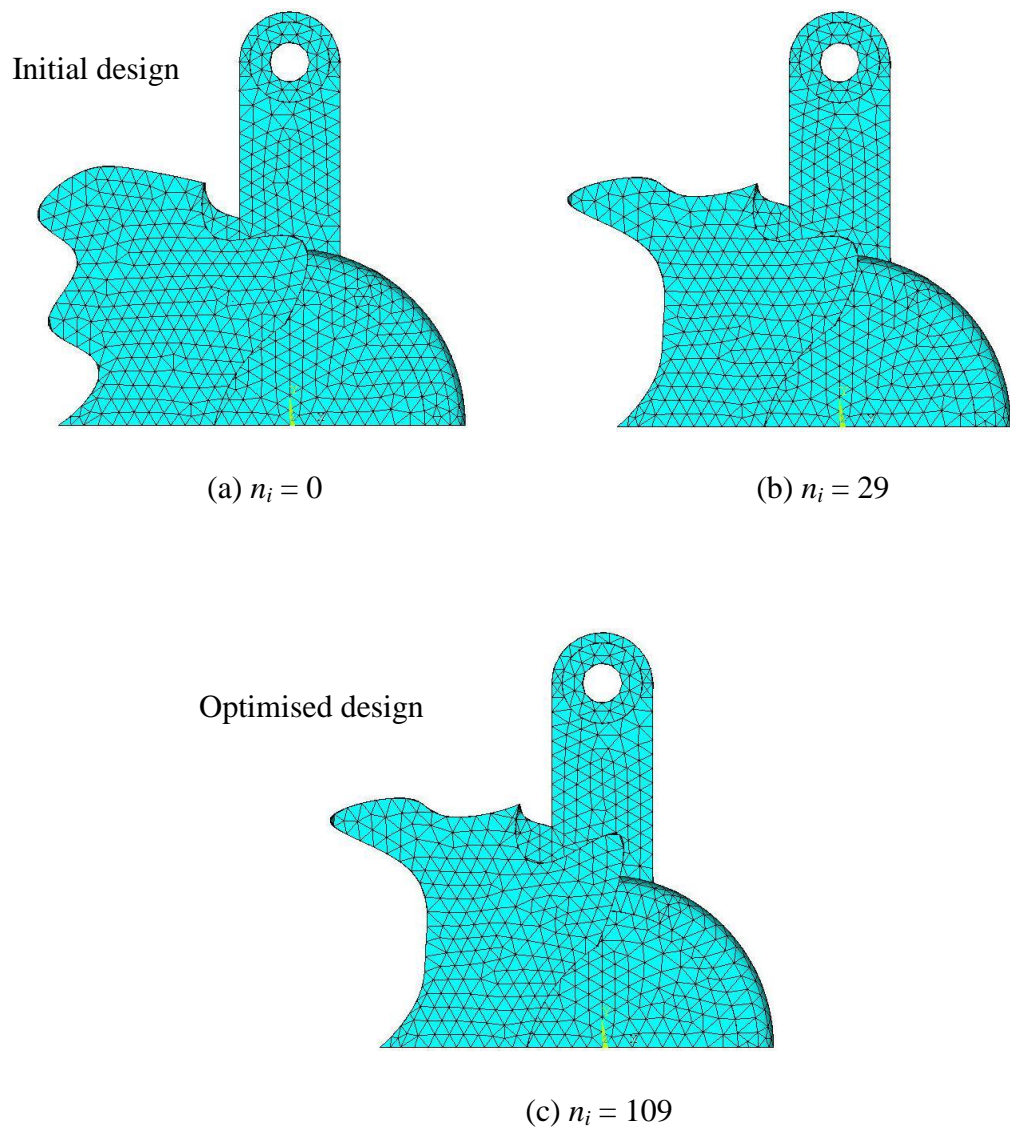


Figure 5.9 – Optimisation history, showing (a) the initial design, (b) $n_i = 29$, and (c) the optimised design at $n_i = 109$

As mentioned above, the dimensions and positions of the design variables are changed, yielding the optimum size and shape of the caliper. Figure 5.10 shows contours of the von Mises stress for the initial and optimised design.

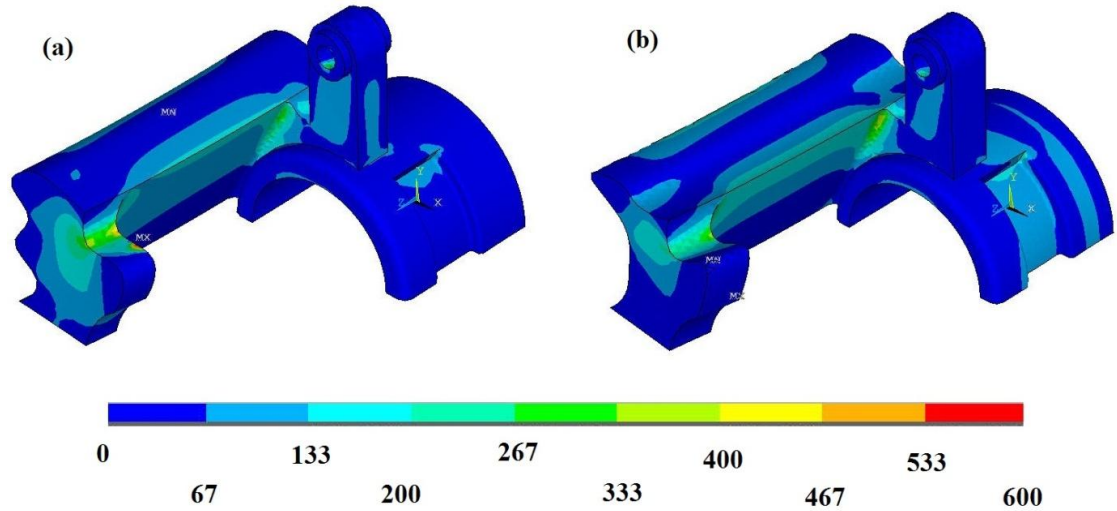


Figure 5.10 – Contours of von Mises stress for (a) the initial design and (b) the optimised design (MPa)

5.4.2 Distributions of stress and displacement

Figure 5.11 shows the distribution of the xz -shear stress (τ_{xz}), xy -shear stress (τ_{xy}), yz -shear stress (τ_{yz}), and maximum (most positive) (S1) and minimum (most negative) (S3) principal stresses for the optimised sliding caliper. The design solution obtained using a finite element model and the MOST technique consisted of 69,827 nodes.

The plots showing the distributions of τ_{xz} , τ_{xy} , and τ_{yz} in Figure 5.11(a–c) reveal shear stresses of approximately -208 to 190 MPa, -152 to 129 MPa, and -185 to 107 MPa, respectively. The principal stress contours of the most positive (tensile) and negative (compressive) stresses are shown in Figure 5.11(d and e), respectively. The most positive (tensile) stresses are developed on the fillet, as shown in Figure 5.11(d). This result was expected because the fillet in this area undergoes bending due to the loads. The maximum principal stresses (S1) were approximately -177 to 438 MPa. In contrast, the most negative (compressive) stresses were found at the far end of the caliper, where the outer brake pad is located (Figure 5.11(e)). The minimum principal stresses (S3) were approximately 41 to -430 MPa. These figures are within the limits of tensile and

compressive stress for the material (MatWeb – cast iron, see <http://www.matweb.com>). Hence, the sliding caliper structure is expected to remain safe under these stresses.

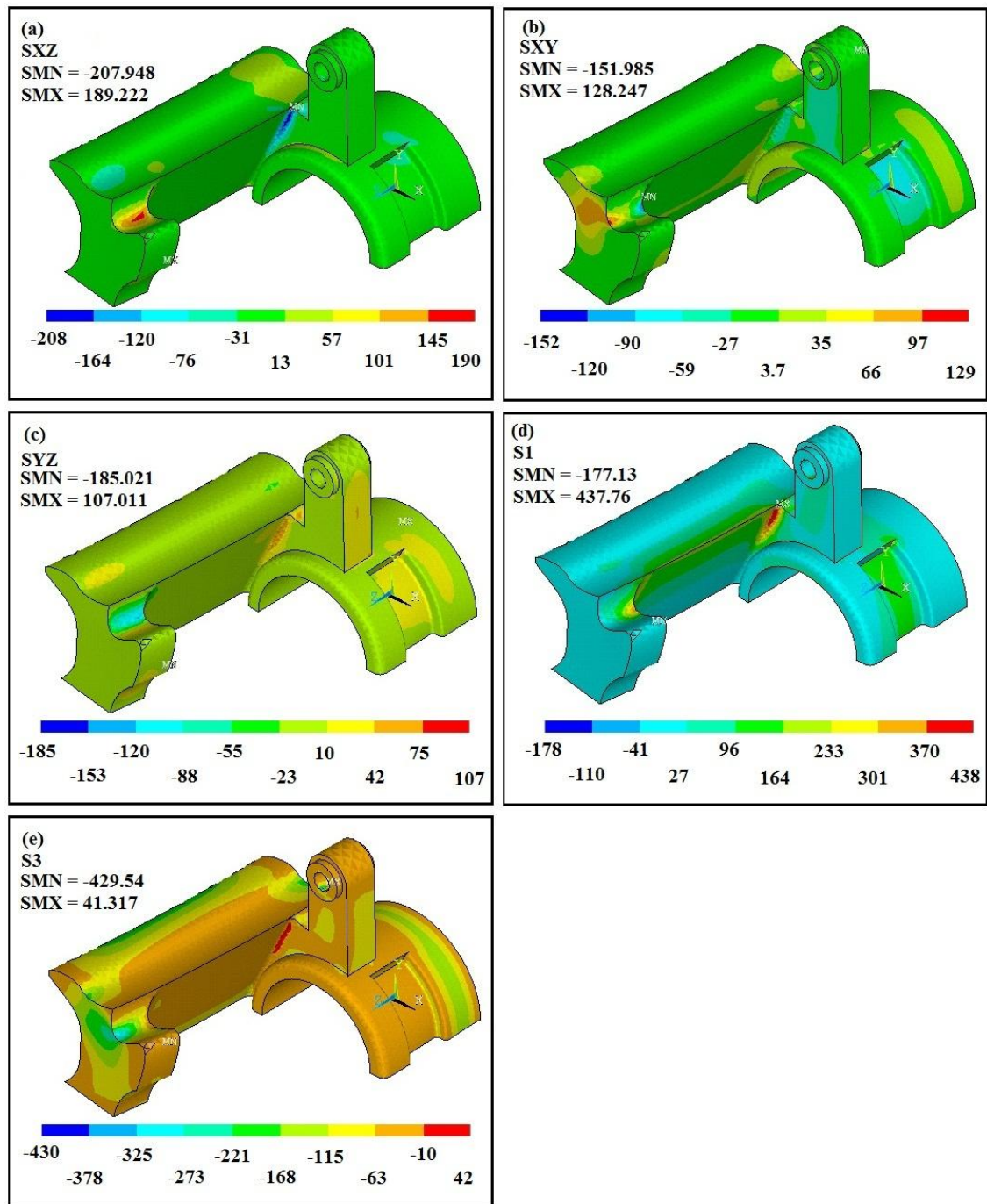


Figure 5.11 – Distribution of stress in a sliding caliper under mechanical load, showing (a) τ_{xz} shear stress, (b) τ_{xy} shear stress, (c) τ_{yz} shear stress, (d) most positive (tensile) stress, and (e) most negative (compression) stress (MPa)

The distribution of displacement parallel to the x , y , and z axes (Figure 5.12 to Figure 5.14, respectively) is approximately -0.22 to 0.048 mm, -0.011 to 0.010 mm, and -0.314 to -0.047 mm, respectively. Negative values indicate displacement in the opposite

direction to the x , y , and z directions shown in each figure. Displacement along the x and y axes is relatively small at the site of the piston (Figure 5.12 and Figure 5.13). Displacement along the z -axis is slightly larger (Figure 5.14) but does not affect the movement of the piston when the brake is applied. Figure 5.15 shows the distribution of the displacement vector sum for the sliding caliper. The displacement ranges from ~ 0.119 to 0.316 mm. The maximum displacement vector sum is found at opposing corners of the caliper (as indicated by the red vectors). These results are within the displacement constraint ($\delta_{lim} = 0.32$ mm).

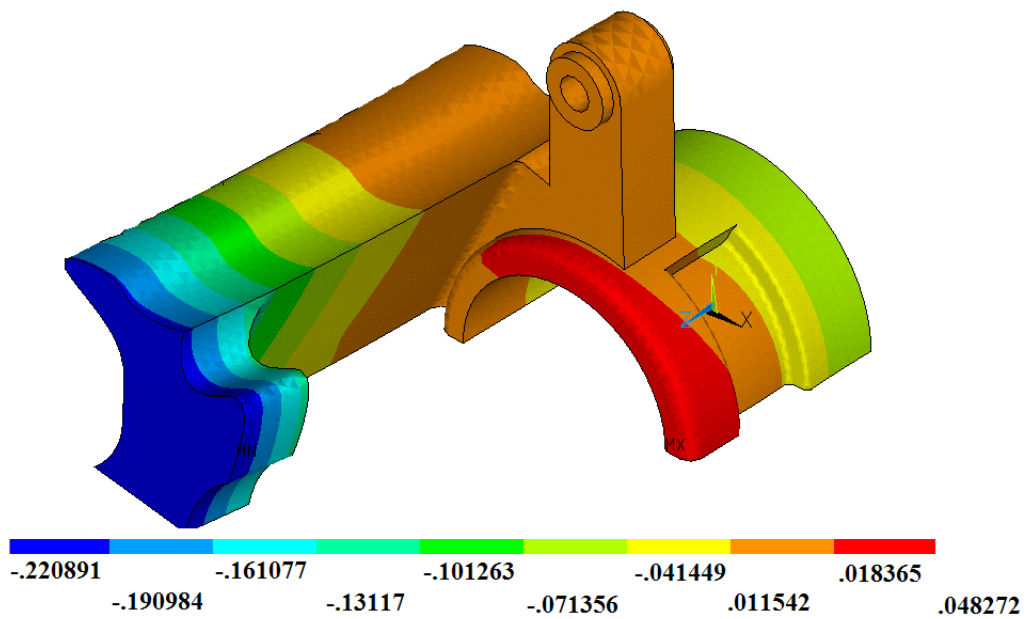


Figure 5.12 – Distribution of displacement along the x -axis (mm)

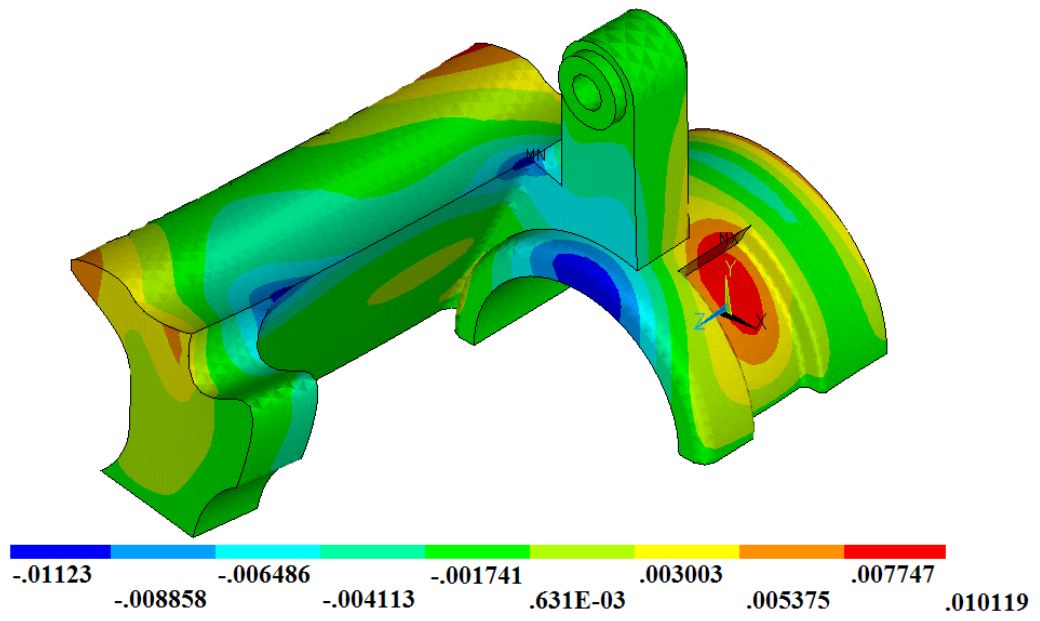


Figure 5.13 – Distribution of displacement along the y-axis (mm)

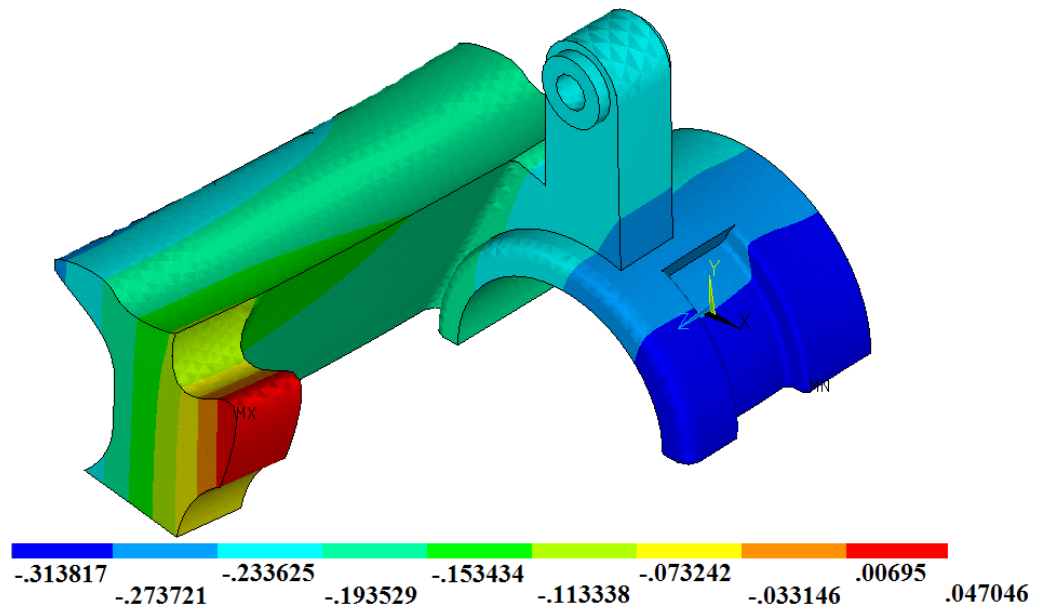


Figure 5.14 – Distribution of displacement along the z-axis (mm)

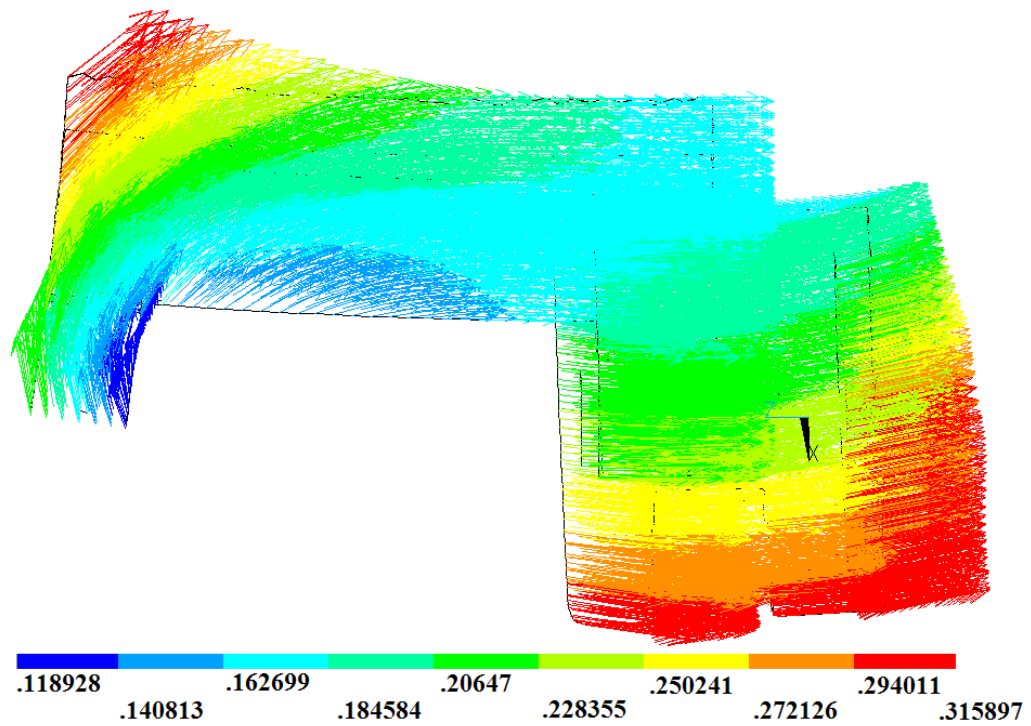


Figure 5.15 – Distribution of the displacement vector sum (mm)

5.4.3 Optimisation history and convergence

Figure 5.16 and Figure 5.17 show variations in the objective functions and the optimisation history with increasing number of iterations. Figure 5.16 shows a decrease in structural mass up to $n_i = 10$, a sharp decreasing trend until $n_i = 21$, a slight increasing trend until $n_i = 26$, a sharp decrease at $n_i = 28$ due to the higher sensitivity of the structure arising from a change in shape, a gradual increase until $n_i = 58$, and finally a flat trend before converging to an optimal solution at $n_i = 109$. The maximum von Mises stress shows a steep decrease in the first two iterations followed by a flat trend until $n_i = 11$, and increases at $n_i = 12$ and $n_i = 18$, corresponding to the higher sensitivity of certain areas. The maximum von Mises stress and structural mass show similar trends at $n_i = 28$, as indicated by the green line in Figure 5.16.

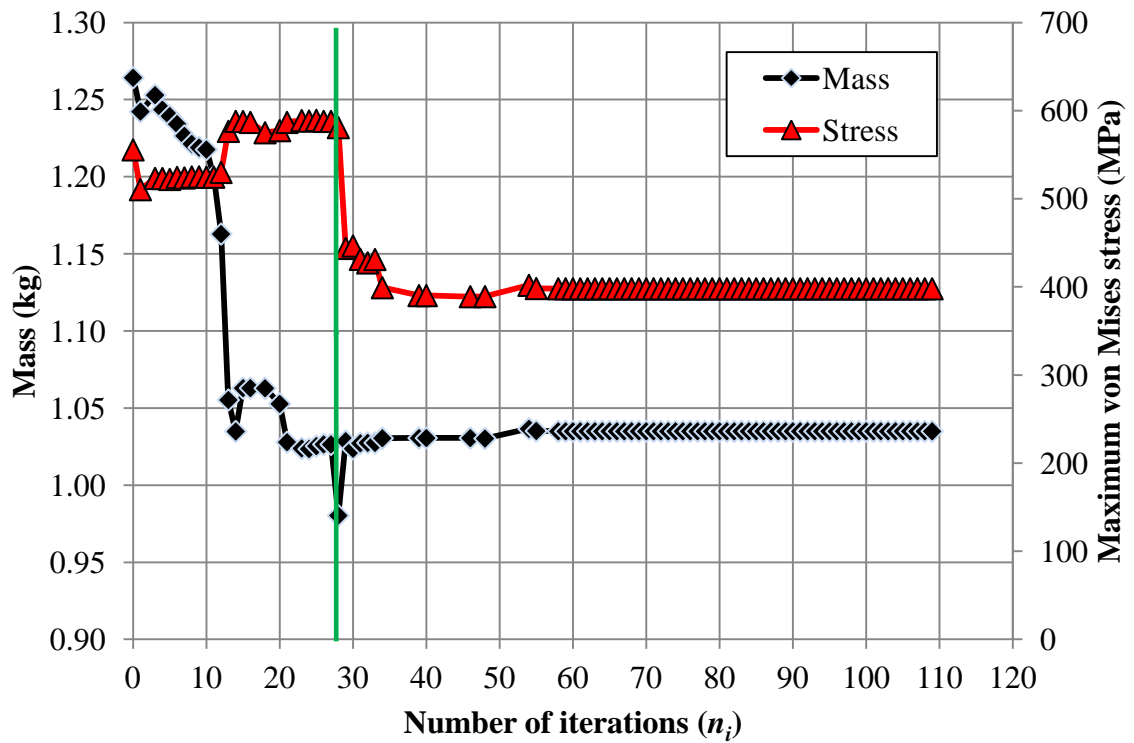


Figure 5.16 – Convergence of mass and maximum von Mises stress

With the removal of material, the maximum von Mises stress is reduced from approximately 580 MPa to 398 MPa before convergence to an optimal solution at $n_i = 109$. Consequently, the mass has been reduced from approximately 1.26 kg to 1.04 kg, representing a 17% savings in material.

In Figure 5.17, the displacement vector sum fluctuates up to $n_i = 28$ and thereafter shows a gradual decreasing trend until the optimal solution is achieved. The displacement vector sum is reduced from 0.340 mm to 0.316 mm. The design attributes are given in Table 5.2.

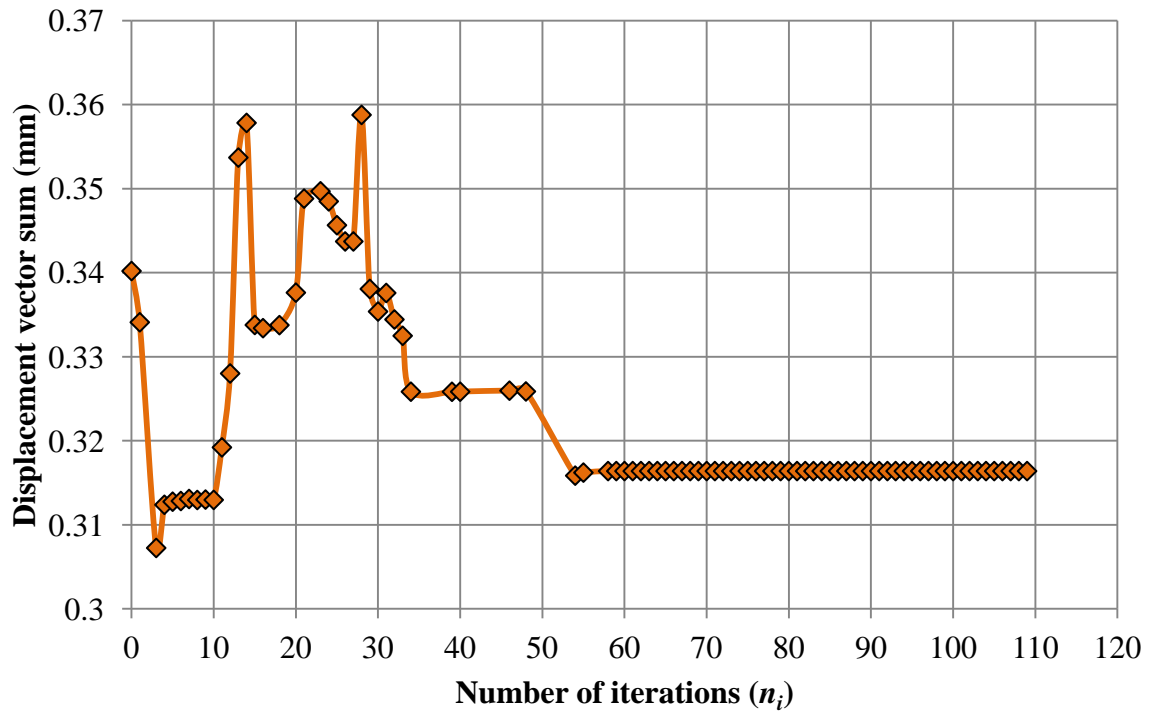


Figure 5.17 – Convergence of the maximum displacement vector sum

Table 5.2 – Attributes of the initial and optimised designs

Design attribute	Initial design	Optimised design
Mass (kg)	1.26	1.04
Maximum von Mises stress (MPa)	556	398
Maximum displacement vector sum (mm)	0.340	0.316

5.5 Summary

The optimisation of a sliding caliper was presented as an example to demonstrate the capabilities of the optimisation methodology. The model was defined using key points and connected by line and B-spline curve fitting, used to generate the finite element model. In this example, the aim was to optimise the caliper shape by minimising the structural mass, the maximum von Mises stress, and the maximum displacement. The positions of key points affected the shape of the structure; consequently, the stresses at each element changed during the optimisation. The proposed method was successfully applied in optimising the sliding caliper design. In the next chapter, the effectiveness of MOST is demonstrated for multi-objective and multi-disciplinary problem.

6 Multi-objective and Multi-discipline Optimisation – An Energy Harvesting Device Optimisation (Bimorph Cantilever Beam)

6.1 Introduction

In this chapter, a multi-objective and multi-discipline optimisation problem is investigated. The optimisation method is applied to an energy harvesting problem. In this research, a piezoelectric generator is considered to provide energy to power up certain devices for transmitting data.

Piezoelectric materials are widely used in medical devices, robotic systems, microscope cantilevers, and electric transducers (Ha and Kim, 2002), as such materials are excellent transducers in converting vibrational energy into electrical energy. The vibrations cause the piezoelectric element to generate an AC voltage potential across the element's electrodes. Energy for a wireless sensor can be found from many sources, including pressure, vibrations, ultraviolet (UV) light, and heat. Among these, vibrational energy is the most attractive source of electrical energy in the wireless sensor environment. The conversion of vibrational energy into electrical energy is desirable in an energy-harvesting scheme, which focuses on the wireless sensor's field. With this advanced technology, a wireless sensor can be used to monitor the performance of various devices including electrical motors, pumps, compressors, aerospace technology, and military equipment. Each structure (e.g., to monitor pump performance) vibrates at its resonance frequency and each device is designed to resonate at a particular frequency.

In the context of energy harvesting, the development of renewable energy is important in terms of protecting the environment. In advanced electronic technology, the major reduction in size and power consumption of CMOS (complementary metal-oxide semiconductor) circuit boards makes it easier to locate wireless sensors in inaccessible locations or hazardous environments.

As mention above, piezoelectric materials are excellent transducers in generating electrical energy converted from vibrational energy. Consequently, such materials are used in situations where electrical energy is not always available. However, the powered device requires a minimum amount of energy to operate, meaning that the power output

or the power density of the device is the key factor in designing an efficient and reliable product which is able to produce long-lasting energy.

The great potential of piezoelectric materials has stimulated numerous research efforts in this field. For example, Roundy (2003) used a rectangular piezoelectric cantilever beam to generate electrical energy from vibrational energy, and Roundy (2005) reported that the power density of a beam can be increased by using a smaller volume. The author found that strain is distributed more evenly in the case of a trapezoidal cantilever beam, which generates more than twice the energy of a rectangular beam for a given volume. Several researchers have focused on maximising the power density of a piezoelectric generator. Mateu and Moll (2005) performed an analytical comparison between rectangular and triangular cantilevers in which they assumed uniform stress across the width of the cantilever. This revealed that a triangular cantilever with the same beam volume as a rectangular beam has a higher average strain and maximum deflection for a given load, thereby producing more power per unit volume. Miller *et al.* (2008) showed an increase in the weighted strain of a cantilever with the addition of a slit through the middle of the beam, yielding a weighted strain that is more than twice that of a rectangular cantilever. Hence, the authors concluded that a typical solid rectangular cantilever beam is non-optimized for the micro-scale energy scavenging generator.

The power output of a piezoelectric generator is generally determined from the results of experiments. Roundy (2003) developed a general equation for calculating the power output of a rectangular beam, which has subsequently led to another approach to predicting the power output: FEM has been used to analyse the behaviour of piezoelectric material (Xu and Koko, 2004). However, few researchers have used FEM in optimising the best “topology” design to predict the power output/density of a piezoelectric cantilever beam.

The power output of a cantilever beam is directly related to the shape. Is a trapezoidal cantilever beam the best design in order to generate the maximum power density? To answer this question, the sensitivity of power density to beam shape is analysed in this research. In addition, hole openings within the cantilever beam are considered, in order to seek an optimum “topology” structure which maximises the power density by using the minimum structural volume. In this research, FEM is also incorporated into the optimisation to simulate the behaviour of a cantilever beam, with the aim of

simultaneously increasing the power output/power density. This background demonstrates the need to optimise the geometrical shape of a cantilever beam to yield the maximum power density.

Given the design problem focused in this Chapter, it is necessary to understand the basic application of piezoelectric material in the field of energy harvesting. Therefore, a basic background is firstly provided for energy harvesting and piezoelectric material. This is followed by verification of the proposed methodology. Next, the optimum geometrical shape of the piezoelectric generator is investigated with regard to power output. Finally, the best topology of the piezoelectric cantilever beam is searched for to maximise the power density.

6.2 Background to energy harvesting

6.2.1 Vibration

Vibration occurs when an object oscillates about a point. This process is continuous until the external energy source is removed. Vibration occurs when a rotating object is unbalanced; e.g., a conveyor belt will vibrate when the motor is running (due to vibration from the motor). The frequency, measured in Hertz (Hz), is the number of times a complete cycle per second.

6.2.2 Source of energy

Because energy can be transformed from one form to another, it is available if there exists an appropriate way to harvest it. There are many potential energy sources, such as nuclear energy, solar energy, wind energy, biomass, and vibration, as summarized in Table 6.1.

Table 6.1 – Comparison of Energy Sources (Roundy, 2003)

	Power Density (W/cm ³) 1 Year Lifetime	Power Density (W/cm ³) 10 Year Lifetime	Source of Information
Solar (Outdoor)	15,000 (direct Sun) 150 (cloudy day)	15,000 (direct Sun) 150 (cloudy day)	Common knowledge
Solar (Indoor)	6 (office desk)	6 (office desk)	Roundy (2003)
Shoe Inserts	330	330	Starner (1996)
Vibrations	200	200	Roundy <i>et al.</i> (2003)
Acoustic	0.003 (75 dB) 0.96 (100 dB)	0.003 (75 dB) 0.96 (100 dB)	Theory
Temperature Gradient	15 (10°C gradient)	15 (10°C gradient)	Stordeur and Stark (1997)
Battery (non- rechargeable, Lithium)	45	3.5	Common knowledge
Battery (rechargeable, lithium)	7	0	Common knowledge
Fuel Cell (methanol)	280	28	Common knowledge
Nuclear Isotopes (Uranium)	6×10^6	6×10^5	Common knowledge

6.2.2.1 Solar power

Solar power is one of the main sources of renewable energy on earth. To harvest solar energy, three main methods are employed: (i) heat from the sun is used to heat water in a glass panel on the roof of a building, thereby heating the panel; (ii) photovoltaic cells generate electricity from sunlight; and (iii) a solar furnace, comprising a huge array of mirrors, gathers the sun's energy into a small space and produces very high temperature. In the presence of sunlight (especially at midday), the power density of solar radiation on the earth's surface is approximately 100 mW/cm², which is able to power a 100 W light bulb from a solar panel with an area of 1 m² (Andy Darvill, 2009). Silicon solar cells are a mature technology in which the efficiency of a single-crystal silicon cell ranges from 12% to 25%. Thin-film polycrystalline solar cells are also commercially available, costing less than single crystal silicon, but with lower efficiency (Roundy *et al.*, 2003). As shown in Table 6.2, outdoor solar energy is much stronger than indoor

solar energy. Typical office lighting provides only several $\mu\text{W}/\text{cm}^3$ for conversion into electricity, which is insufficient to run low-power-consumption appliances. Table 6.2 compares the solar density power from various sources (after Roundy, 2003).

Table 6.2 – Solar power under different conditions

	Outside, midday	4 inches from 60 W bulb	15 inches from 60W bulb	Office lighting
Power ($\mu\text{W}/\text{cm}^3$)	14,000	5000	567	6.5

6.2.2.2 Vibration

Mechanical vibration energy has demonstrated high potential in terms of conversion to electrical energy. For example, Shenck and Paradiso (2001) successfully used piezoelectric generators to produce $336 \mu\text{W}/\text{cm}^3$ of power. For further information on vibration, see Glynn-Jones *et al.*, (2001). Figure 6.1 compares the lifetime of vibrational energy with solar power and battery power (Roundy, 2003). In this figure, the solar and vibration power are not a function of time and the power density of battery (both rechargeable and non-rechargeable) energy shows a gradual decline.

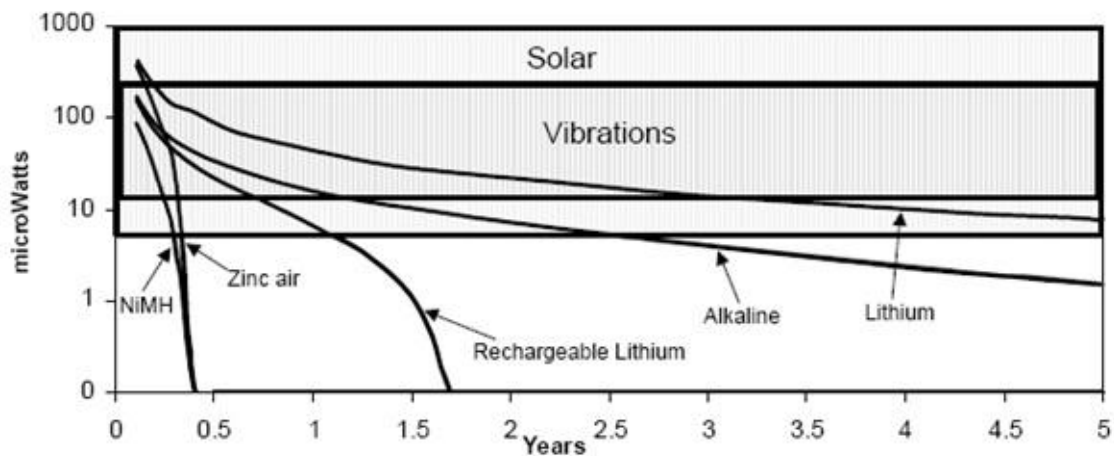


Figure 6.1 – Continuous power density for various power sources

6.2.2.3 Human power

There are two types of human power: (i) active human power, which requires power to generate motion, and (ii) passive human power, which is a scavenging power derived from daily activities. Passive human power has been scavenged from people walking across a floor. For example, Rome *et al.* (2005) demonstrated a ‘suspended-load’

backpack which generates up to 7.4 W, representing a 300-fold increase in efficiency over previous shoe devices (20 mW) (Kymissis *et al.*, 1998). This technique relies on the conversion of mechanical energy from the vertical movement of carried goods (20–38 kg in weight) to electricity during normal walking. This method was tested at Tokyo Station’s Marunouchi North Exit from 16 October 2006 to 8 December 2006. The aim is to generate electricity by using the energy from the vibrations created by people walking on the floor. The power generated from the vibrations is used to contribute to the energy required by, for example, automatic ticket gates and electro-luminescence displays. A power-generating floor was installed at six ticket gates, generating up to 10,000 watt-seconds per day (enough to illuminate a 100 W light bulb for 100 seconds) (Galhardi *et al.*, 2008). Starner (1996) showed that a 68-kg person produces 67 W of energy during normal walking (based on a foot-fall of 5 cm, wearing high heels, and walking at 2 steps/sec). Gilbert and Balouchi (2008) reported that shoe generators can produce 100 mW with a vertical deflection of 14 mm, based on a spring and freewheel mechanism.

6.2.2.4 Temperature variations

In general, energy can be harvested from the environment. By using a thermoelectric, a generator produces power from a change in environmental temperature. Stordeur and Stark (1997) demonstrated a thermoelectric micro-device that generated $15 \mu\text{W}/\text{cm}^3$ of power from a temperature difference of 10°C . This is a promising method that may be improved to ultimately become more efficient than other approaches, although the level of output is presently lower than that from other methods.

6.2.2.5 Summary of power scavenging

Solar power and vibration-based energy scavenging are promising methods for producing power from the environment. Both methods can be used to run devices with low power consumption. The most appropriate energy source in terms of wireless sensor nodes in a building is vibration energy, although this is not necessarily the best energy-scavenging solution overall.

6.2.3 Types of vibrations

Vibration is a type of energy that may occur in any setting. The vibration sources of interest in the present research include domestic and office appliances, and office equipment. The potential output power (P) is as follows (Roundy *et al.*, 2003):

$$P = \frac{m\zeta_T A^2}{4\omega\zeta_T^2} \quad (6.1)$$

where m is the mass, A is the acceleration, ω is the angular frequency of the vibration, and ζ_T is the total damping ratio. The potential output power is therefore proportional to A^2/ω , meaning that to obtain a higher output power, the design should target a low fundamental frequency. Table 6.3 lists various vibration sources and their maximum acceleration magnitude of vibration and maximum frequency.

Table 6.3 – Acceleration magnitude and fundamental frequency of various vibration sources (after Leland *et al.*, 2007)

Vibration source	Acceleration, A (m/s ²)	Frequency, f_{peak} (Hz)
Car engine compartment	12	200
Mobile phone (vibration mode)	12.3	170
Breadmaker	1.03	121
Washing machine	0.5	109
Blender casing	6.4	121
Clothes dryer	3.5	121
Desktop computer casing	0.5	120
Desktop computer casing (with CD drive running)	0.54	120
Standalone heater	1.5	34
Door frame immediately after door closes	3	125
Small microwave oven	2.5	121
HVAC vents in office building	0.2-1.5	60
Freezer	0.1	50
Windows next to busy road	0.7	120
Second-story floor of busy office	0.2	100

The potential vibration is important in designing a vibration converter because the design should resonate at the fundamental natural frequency in order to obtain the optimum output, and because the magnitude and frequency must be known. Figure 6.2–Figure 6.5 show spectrum analyses of a desk fan with variable speed and a fan heater.

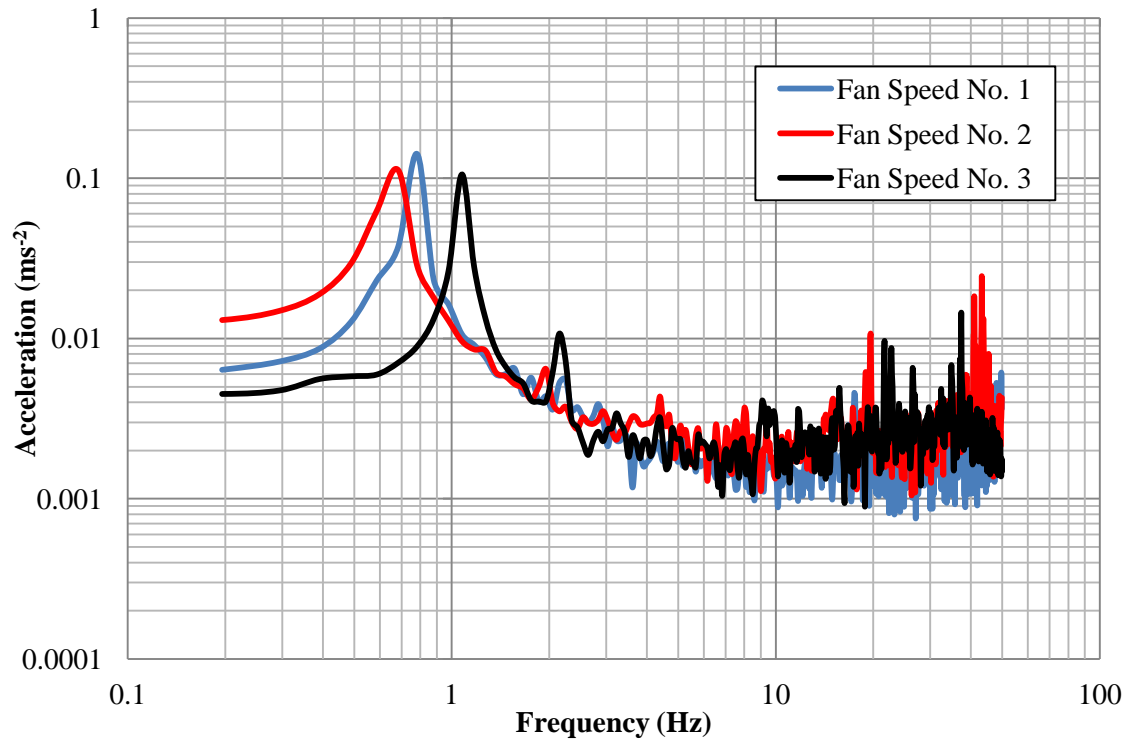


Figure 6.2 – Vibration spectrum of acceleration vs. frequency for a desk fan with variable

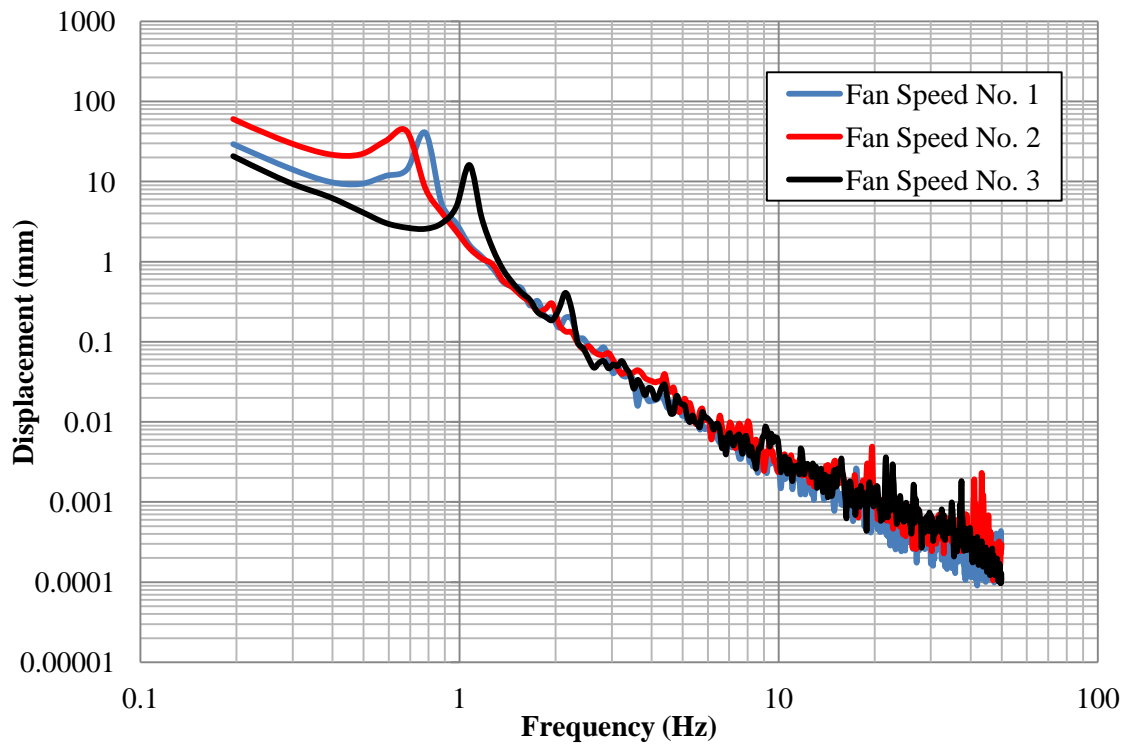


Figure 6.3 – Vibration spectrum of displacement vs. frequency for a desk fan with variable speed

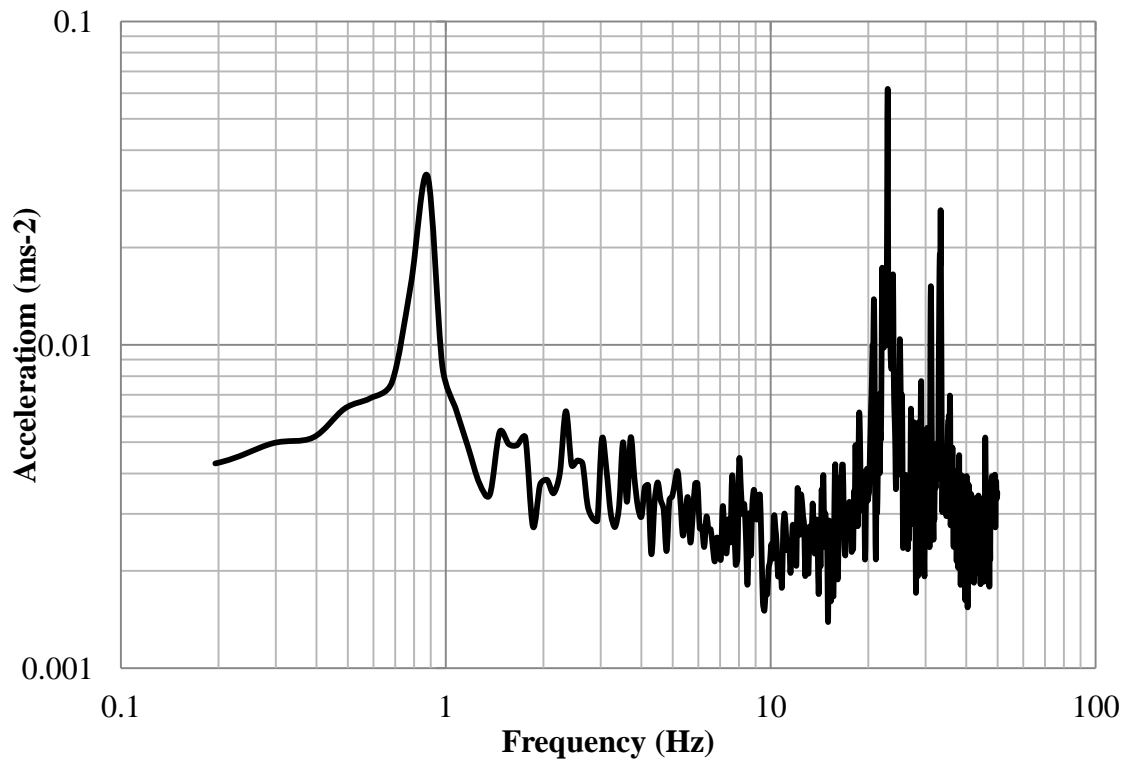


Figure 6.4 – Vibration spectrum of a fan heater (acceleration vs. frequency)

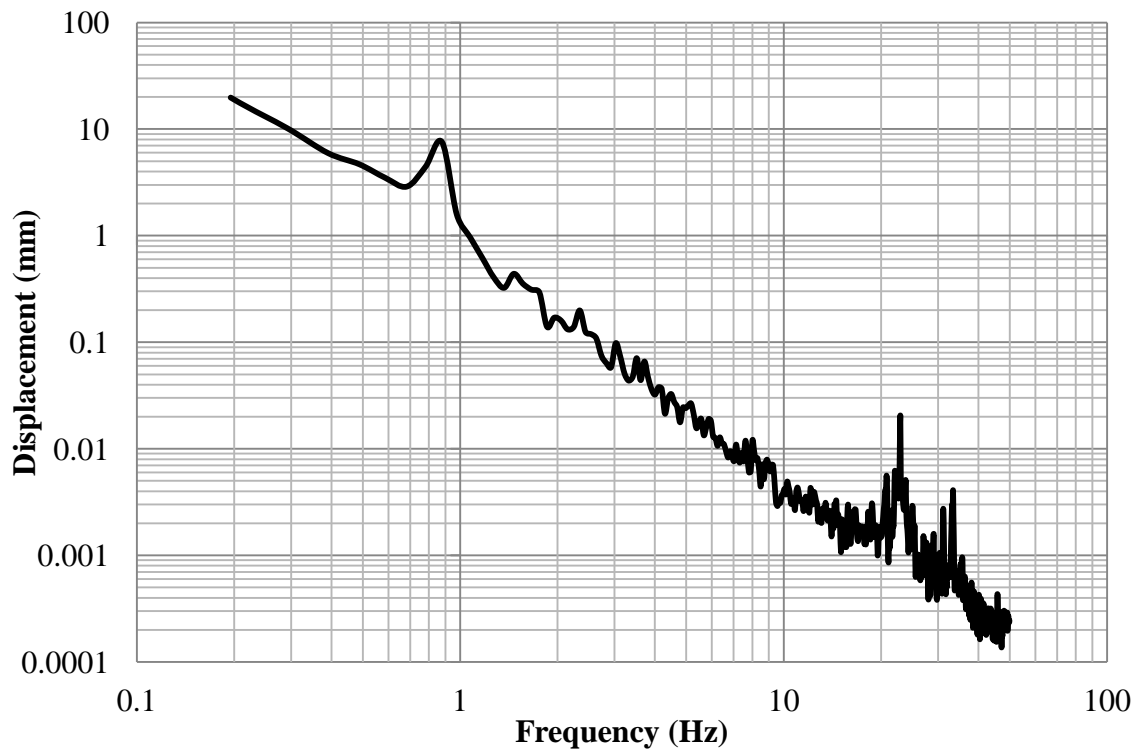


Figure 6.5 – Vibration Spectrum of a fan heater (displacement vs. frequency)

6.2.4 Model of the Conversion of Vibration to Electricity

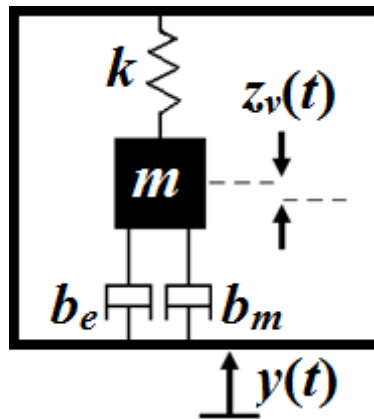


Figure 6.6 – Schematic diagram of a vibration converter

Williams and Yates (1996) proposed a simple model for converting vibrations to electricity (Figure 6.6). This model is described as follows (Roundy, 2003):

$$m\ddot{z}_v + (b_e + b_m)\dot{z}_v + kz_v = -m\ddot{y} \quad (6.2)$$

where m is the mass, k is a spring constant, b_e is an electrically induced damping coefficient, b_m is a mechanical damping coefficient, z_v is a spring deflection, and y is an input displacement. The power that is successfully converted to the electrical system is

equal to the power removed from the mechanical system by b_e . The electrically induced force is $b_e \dot{z}_v$. Because power is the product of force and velocity, the power can be stated as follows:

$$P = \frac{1}{2} b_e \dot{z}_v^2 \quad (6.3)$$

Equations (6.2) and (6.3) can be combined to derive the vibration expression for power:

$$P = \frac{m \zeta_e Y^2 \left(\frac{\omega}{\omega_n}\right)^3 \omega^3}{\left[1 - \left(\frac{\omega}{\omega_n}\right)^2\right]^2 + \left[2 \zeta_T \frac{\omega}{\omega_n}\right]^2} \quad (6.4)$$

where ζ_e is the electrical damping ratio, ω_n is the resonant angular frequency, ω is the angular frequency of the vibration, and ζ_T is the total damping ratio. If the resonant angular frequency is equivalent to the resonant frequency of the vibration, equation (6.4) can be simplified as follows by substituting the acceleration $A = Y\omega^2$:

$$|P| = \frac{m \zeta_e A^2}{4 \omega \zeta_T^2} \quad (6.5)$$

According to Roundy (2003), the power is affected by the electrical damping ratio ζ_e and the mechanical damping ratio ζ_m . Figure 6.7 shows that the generated power is optimised when $\zeta_e = \zeta_m$. There is a large penalty in the case that ζ_e is less than ζ_m , and a small penalty in the case that ζ_e exceeds ζ_m . Hence, to develop a highly damped system, ζ_m should be equal to or less than ζ_e , because most of the damping is electrically induced.

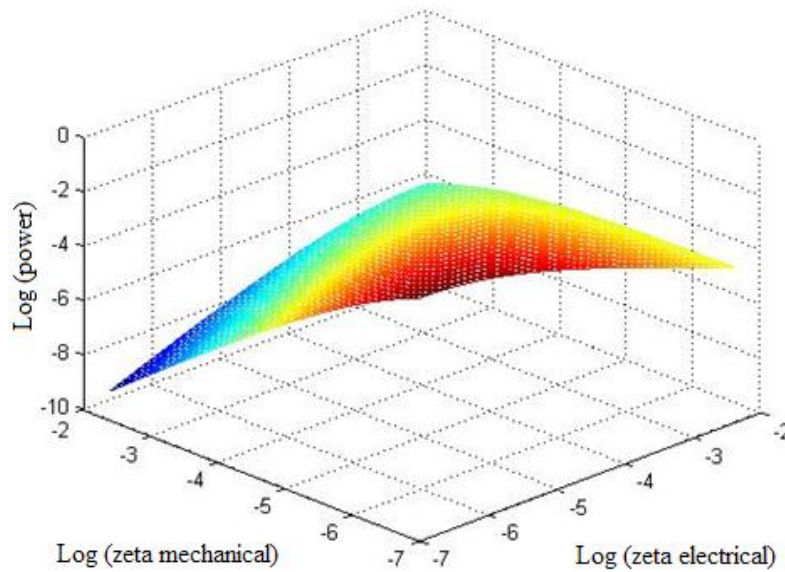


Figure 6.7 – Simulation of generated power against mechanical and electrical damping ratios

Figure 6.8 shows the output power versus frequency, assuming the electrical and mechanical damping ratios are equal. The resonance frequency for this simulation is 100 Hz and the input vibration frequency is varied from 10 to 1000 Hz.

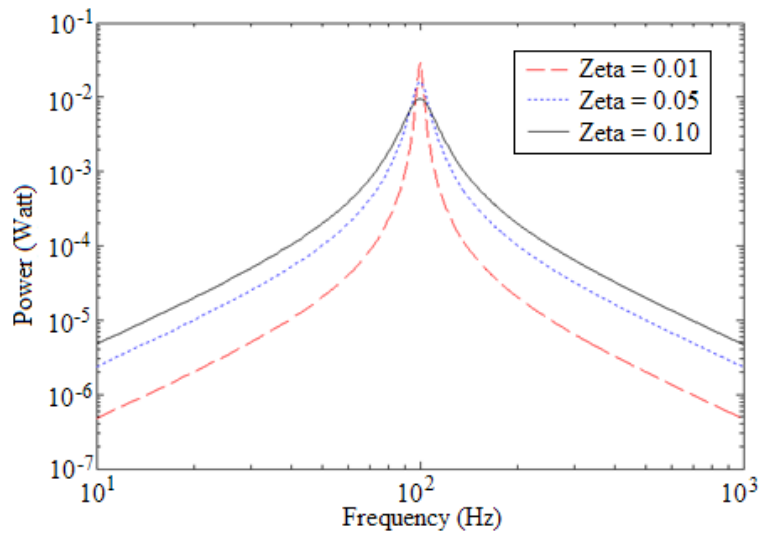


Figure 6.8 – Power output against frequency

The generated power is maximised when the vibration frequency is equal to the resonant frequency. There is a large penalty in the case of a small difference between the natural frequency and the frequency of the input vibration, and the output power decreases as the driving frequency moves away from the natural frequency.

To generate the maximum output, the natural frequency and the environment frequency must be very similar, and the electrical damping ratio must be larger than the mechanical damping ratio.

6.2.5 Piezoelectric material

The term “Piezo” is derived from the Greek word *piezein*, which means “to press”. In 1880, the brothers Pierre and Jacques Curie (both French physicists) discovered an unusual piezoelectric effect of crystals (e.g., quartz and Rochelle salt) during an experiment, whereby piezoelectric materials can generate electricity when a force or pressure is applied. This phenomenon occurs because the crystals have been polarized. In 1881, Lippmann discovered the fundamental thermodynamic principles behind this phenomenon; i.e., the crystal is exposed to an electric field when subjected to tension or compression, with the strength of the field being proportional to the tension or compression (Mason, 1950).

Piezoelectric materials have been applied in various ways in terms of energy harvesting (Roundy, 2003; Shenck and Paradiso, 2001). As describe above, there are two types of piezoelectric material: (i) those with a direct effect and (ii) those with a converse effect. The direct effect involves the conversion of mechanical strain in electrical charge, while the converse effect involves the conversion of electrical strain into mechanical strain energy. The most commonly used piezoelectric material is lead zirconate titanate (PZT), a piezoelectric ceramic.

In recent years, many researchers have focused on the performance of a cantilever beam with various geometries, in order to find potential design geometries that can increase the scavenging performance in terms of output power density (e.g., Goldschmidtboeing and Woias, 2008). Sodano *et al.* (2005a and 2005b) performed experiments to investigate piezoelectric devices in terms of their ability to transform vibrations into electrical energy using a cantilever generator. Sodano *et al.* (2004) used a bimorph Quick Pack QP40N (Mide Technology Corporation) cantilever beam (total volume: 1947 mm^3 ; piezoelectric volume: 240 mm^3), without proof mass attached to the free end, to generate $1.10\text{--}11.90 \text{ }\mu\text{W}$ of power at $25\text{--}50 \text{ Hz}$. Sodano *et al.* (2002) investigated a single layer of PSI-5H4E PZT (Piezo Systems Inc.) plate ($40 \times 60 \times 0.27 \text{ mm}$) bonded onto an aluminium plate ($40 \times 80 \times 1 \text{ mm}$), revealing that the cantilever beam can generate $1.7\text{--}2.0 \text{ mW}$ of power.

Poulin *et al.* (2004) compared the ability of piezoelectric and electromagnetic power generation from human movement to power up low-consumption electronic devices. Lu *et al.* (2004) designed and tested a micro-scale cantilever beam energy-harvesting system ('31' transverse mode type piezoelectric micro-generator) in terms of supplying power to run micro-electromechanical technology (MEMS) applications. The cantilever beam ($5.0 \times 1.0 \times 0.1 \text{ mm}$) generated about 1.6 mW of power at 7 kHz , which is enough to run a MEMS application. Hwang and Park (1993) proposed an alternative method to determine the response, yielding the values of parameters that are otherwise extracted from an FEM (finite element method) calculation. The FEM is used to calculate the static responses of a PZT bimorph beam in a PZT plate element. Other studies have used FEM to investigate piezoelectric composite beams and plates (Lam *et al.*, 1997; Saravanos *et al.*, 1997; Tzou and Tseng, 1990; Wang, 2004; Yao and Lu, 2003).

6.2.6 Piezoelectric converter (vibration to electrical)

Piezoelectric materials are materials that physically deform in the presence of an electric field, or conversely, produce an electrical charge when mechanically deformed. As described above, the direct effect and the converse effect are the two different behaviours of piezoelectric material. The constitutive equations for a piezoelectric material are as follows (Ikeda, 1996):

$$\delta = \sigma/Y + dE \quad (6.6)$$

$$D = \epsilon E + d\sigma \quad (6.7)$$

where δ is mechanical strain, σ is mechanical stress, Y is the modulus of elasticity, d is the piezoelectric strain coefficient, E is the electric field, D is electric displacement, and ϵ is the dielectric constant of the piezoelectric material. Without the piezoelectric coupling term, dE , equation (6.6) is simply Hooke's Law (Benham *et al.*, 1996). Likewise, without the coupling term, $d\sigma$, equation (6.7) is simply the dielectric equation, or a form of Gauss's law for electricity (Solymar, 1984).

Figure 6.9 shows the two different modes of a piezoelectric material. The x , y , and z axes are labelled 1, 2, and 3, respectively. Typically, a piezoelectric material is used in the 33 mode, meaning that both voltage and stress act in three directions. However, the material can also be operated in 31 mode, in which the voltage acts in direction three and the mechanical stress acts in direction one. The most common type of 31 mode is a bimorph, in which two separate sheets are bonded together, sometimes with a central shim between them (Roundy, 2003). Detailed information on piezoelectric material can be found in the product catalogue produced by Piezo System Inc. (Piezo System, 2009).

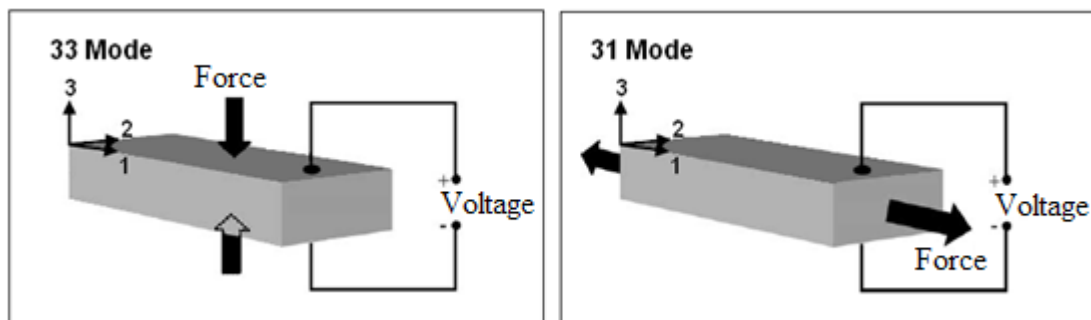


Figure 6.9 – Schematic diagrams showing the 33 mode and 31 mode of a piezoelectric material

6.3 Analytical model of a piezoelectric generator

6.3.1 Review of the magnitude of voltage for a piezoelectric bender (Roundy, 2003)

Piezoelectric elements are both mechanical and electrical, and are modelled as a transformer (Flynn and Sanders, 2002). Roundy (2003) proposed that the magnitude of voltage transferred to the load for a piezoelectric bender can be given as follows (assuming that the driving frequency is not matched with the natural frequency):

$$V = \frac{-j\omega \frac{Y_c d t_c b^*}{\epsilon}}{\left[\frac{1}{RC_p} \omega_n^2 - \left(\frac{1}{RC_p} + 2\zeta \omega_n \right) \omega^2 \right] + j\omega \left[\omega_n^2 (1+k^2) + \frac{2\zeta \omega_n}{RC_p} \omega^2 \right]} \quad (6.8)$$

where V is the voltage through the piezoelectric material, ω is the driving frequency, Y_c is Young's Modulus for the piezoelectric material, d is the piezoelectric strain coefficient, t_c is the thickness of the piezoelectric material, b^* is strain related to vertical displacement of the beam, ϵ is the dielectric constant of the piezoelectric material, R is the load resistance, C_p is the capacitance of the piezoelectric device, ω_n is the natural frequency of the system, ζ is the damping ratio, and k is a coupling coefficient. Equation (6.8) can be calculated using finite element analysis.

6.3.2 Predicting the output power of piezoelectric generator designs with different geometrical shapes using finite element analysis

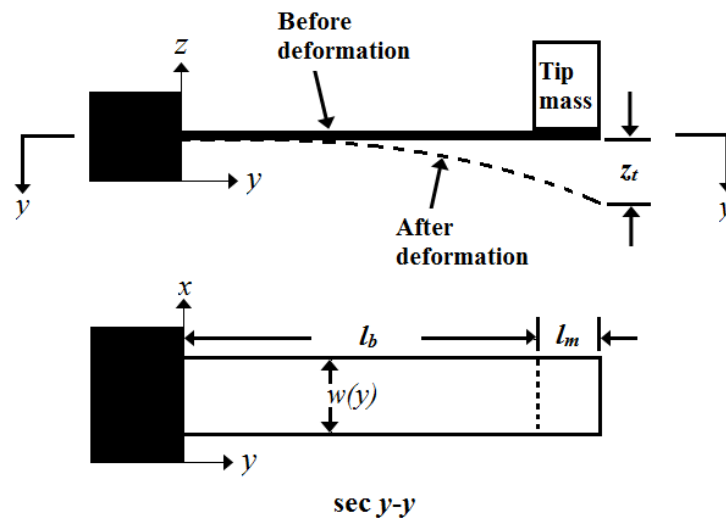


Figure 6.10 – Schematic of a piezoelectric bender

The model of interest, shown in Figure 6.10 is modified from the piezoelectric cantilever beam reported by Roundy *et al.* (2003). In the model, the left end is fixed and the right end is free. A tip mass is applied to the free end of the beam. The beam consists of three layers: the top and bottom layers are piezoelectric material, and the middle layer is a brass shim. The electrode, used to produce energy, is placed on the top and bottom surfaces. The electrode can be easily etched away, meaning that only the portion of the beam covered by the electrode is active as a piezoelectric element. The electrode length (l_e , not shown in the figure) is always equal to or less than the length of the beam (l_b). When the beam is deformed, a stress is induced on the top and bottom surfaces. To calculate the stress applied to the beam, it is always related to the Young's Modulus (E) and the tensile or compressive stress of the beam, expressed as follows:

$$E = \frac{\text{Stress}}{\text{Strain}} = \frac{\sigma}{\varepsilon} \quad (6.9)$$

$$\sigma = \frac{M(y)b}{I} \quad (6.10)$$

where $M(y)$ is the bending moment as a function of the distance (y) from its base, y is the position along the beam, b is the distance from the centre of the shim to the centre of the piezoelectric material, and I is the second moment of the area. The stress and strain in a piezoelectric material are the **average element stress and strain**. Therefore, the average element stress in the piezoelectric material covered by the electrode is expressed as follows:

$$\sigma_{ave} = \frac{1}{l_e} \int_0^{l_e} \frac{M(y)b}{I} dx \quad (6.11)$$

where σ_{ave} is the average element stress. However, if the beam is an irregular shape, the second moment of the area is difficult to calculate. Equation (6.10) is only valid for a regular shape. In a finite element analysis, the solution of the average element stress can be obtained in post-processing, meaning that calculation of the second moment of the area is not necessary to calculate the average element stress of the beam, especially if the shape is irregular. The average element stress (σ_{ave}) can be stated as follows:

$$\sigma_{ave} = \frac{1}{n_c} \sum_{c=1}^{n_c} \sigma_c \quad (6.12)$$

where n_c is the number of piezoelectric material elements. This equation assumes that all the elements are of equal size.

This chapter focuses on the modelling and analysis of a piezoelectric bender. Several terms from equation (6.8) need to be redefined to accommodate the results of the finite element analysis. By utilising the relationship between Hooke's Law for elastic material

(Benham *et al.*, 1996) and the solution from the finite element analysis, b^* in equation (6.8) can be defined as follows:

$$b^* = \frac{\sigma_{ave}}{Y_c z_t} \quad (6.13)$$

where z_t is the vertical displacement at the tip end (see Figure 6.10). The capacitance of the beam is the volume of the piezoelectric material. If the shape of the beam is irregular, the capacitance is calculated by integrating the width of the beam as a function of the distance (y) from its base, as follows:

$$C_p = \int_0^{l_e} \frac{n_c \epsilon w(y)}{t_c} dx \quad (6.14)$$

where n_c is the number of piezoelectric layers and $w(y)$ is the width of the piezoelectric material in terms of the electrode length (l_e). The damping ratio of the system can be stated as follows:

$$\zeta = \frac{c}{2m_{eff}\omega_n} \quad (6.15)$$

where m_{eff} is the effective mass and c is a damping coefficient. The effective mass and natural frequency can be found from the finite element analysis. The power transferred to the load is simply V^2/R . Equation (6.8) can be further simplified to yield equation (6.16) if we assume that the natural frequency (ω_n) matches the driving frequency (ω). The power output (P) of the beam is then formulated as follows:

$$P = \frac{1}{2\omega_n^2 (4\zeta^2 + k^4)} \frac{RC_p^2 \left(\frac{dt_c \sigma_{ave}}{\epsilon z_t} \right)^2}{(RC_p \omega_n)^2 + 4\zeta k^2 (RC_p \omega_n) + (2\zeta)^2} A_{in}^2 \quad (6.16)$$

The optimum resistance can be derived as:

$$R_{opt} = \frac{2\zeta}{\omega_n C_p \sqrt{4\zeta^2 + k^4}} \quad (6.17)$$

For details of the derivation of the system, including the mechanical and electrical sides, see Appendix C.

6.3.3 Theoretical frequency

The theoretical natural frequency can be calculated if the effective mass of the system is known. A schematic cantilever beam structure is shown in Figure 6.11, where a tip mass (m_{tip}) is attached to the free end of the beam, which is fixed to a vibrating base. The cantilever beam is assumed to be a rigid body. Therefore, the structure is modelled as a system with a single degree of freedom (SDOF). The structure consists of an effective mass (m_{eff}), spring stiffness (k), damper coefficient (c), and a vibrating base (\ddot{y}). In general, the effective mass can be stated as follows:

$$m_{eff} = B_f m_{beam} + m_{tip} \quad (6.18)$$

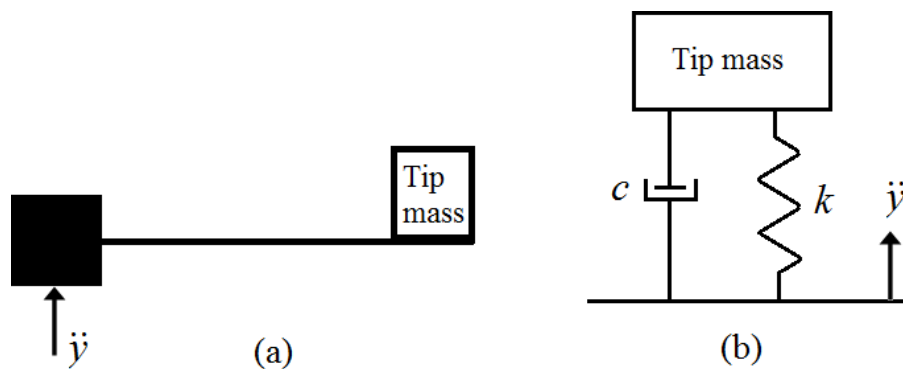


Figure 6.11 – Schematic diagrams of (a) a cantilever structure, and (b) an SDOF model

where m_{eff} is the effective mass, m_{tip} is the tip mass (applied load), m_{beam} is the mass of the beam, and B_f is a constant value that depends on the structure (see Table 6.4; Wahab, 2008).

Table 6.4 – SDOF equivalent mass for structural systems

Type of support	B_f
Axial bar	0.101
Simple supported beam	0.4857
Fixed-free beam	0.2357
Fixed-fixed beam	0.37
Fixed-simply supported beam	0.46

In this research, a cantilever beam (fixed–free beam) is considered with a constant B_f value of 0.2357 (Ng and Liao, 2005). As a result, the effective mass can be used to calculate the theoretical frequency. The frequency is defined as follows:

$$f = \frac{1}{2\pi} \sqrt{\frac{k}{m}} \quad (6.19)$$

where f is the natural frequency, k is the spring stiffness, and m is the mass attached to the system. More specifically, the mass m is the effective mass of the system. In the cantilever beam, the spring constant can be defined as follows (Gere and Timoshenko, 1991):

$$k = \frac{3EI}{l^3} \quad (6.20)$$

where l is the length of the beam. The spring constant is different for each mode. The focus is to determine the theoretical natural frequency. Therefore, the fundamental frequency is stated as follows:

$$f = \frac{1}{2\pi} \sqrt{\frac{3EI}{l^3 m_{eff}}} \quad (6.21)$$

Equation (6.21) is only valid if the effective mass of each mode is equal to the individual spring constant. For a higher order of mode, it is difficult to determine the spring constant and effective mass theoretically, especially for an irregularly shaped cantilever beam. However, this problem can be overcome by using finite element analysis to determine the frequency of each mode.

6.3.4 Material properties

The values of the mechanical and electric properties of the piezoelectric material (PZT-5A4E) and of the brass shim are given in Table 6.5 (Gallas *et al.*, 2003; see also Piezo System, 2009).

Table 6.5 – Material properties of PZT and brass shim

	Piezoelectric material (PZT-5A4E)	Shim material (brass)
Elastic Modulus (GPa)	66	117
Max. allowable stress (MPa)	24 ¹	200
Max. deflection (μm)	300	–
Poisson's ratio	0.31	0.324
Density (kg/m ³)	7800	7165
Relative dielectric constant	1800	–
d31 (m/V)	–190 × 10 ⁻¹²	–

¹Dynamic peak tensile strength (Bert and Birman, 1998)

6.4 Verification of experimental, theoretical, and ANSYS simulation results

Ooi (2010) performed an experiment to verify the validity of a model using equation (6.8) for a rectangular cantilever beam. A vertical vibration generated from a shaker (model number LDS-V406/8) was used to excite the cantilever and the vibration was also monitored using an accelerometer (MTN1800). The voltage generated by the piezoelectric material for a given load resistance was captured by an oscilloscope (Agilent MSO-6054A), along with the accelerometer signal. The obtained data from the oscilloscope were transmitted to the MATLAB for further investigations of the power and frequency response. The cantilever beam (known as a ‘bimorph’ system) is composed of two layers of piezoelectric materials and a layer of shim material. The effective piezoelectric cantilever (PZT-5A4E), which has dimensions of $23.5 \times 12.7 \times 0.51$ mm and a tip mass of 4.1 grams (Figure 6.12 and Table 6.6), was excited by a sinusoidal wave with an acceleration magnitude of 4.905 ms^{-2} at frequencies of 50–90 Hz. The experiments yielded a damping ratio of 0.02858. The output was obtained across a range of load resistances, and a multi-frequency response was plotted on a horizontal axis, as shown in Figure 6.13.

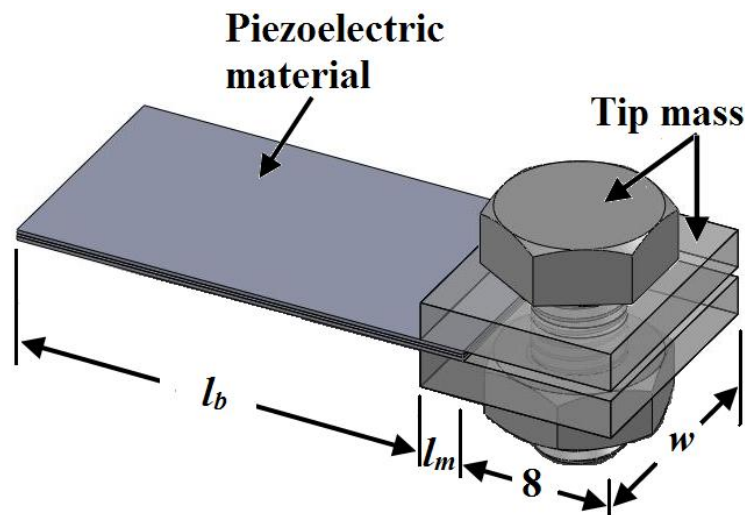


Figure 6.12 – Schematic diagram of the experiment setup (mm)

Table 6.6 – Dimensions of piezoelectric generator

Parameter	Value
Thickness of piezoelectric material (t_c)	0.19 mm
Thickness of shim material (t_{sh})	0.13 mm
Length of tip mass (l_m)	2.00 mm
Length of base (l_b)	21.5 mm
Effective length of piezoelectric material PZT ($l_e = l_m + l_b$)	23.5 mm
Width (w)	12.7 mm

Figure 6.13 compares 14 sets of data ($k = 1, 2, 3, \dots, 14$). All the experimental results show a resonant frequency (f_{re}) at around 73 Hz; however, for clarity of presentation, they are separated by an offset frequency ($f_{off} = 10$ Hz) in order to plot them on a single graph. Hence, the resistance-offset frequencies (f_k) on the horizontal axis for each set of data can be expressed as follows:

$$f_k = f_{re} + f_{off} \times k \quad (6.22)$$

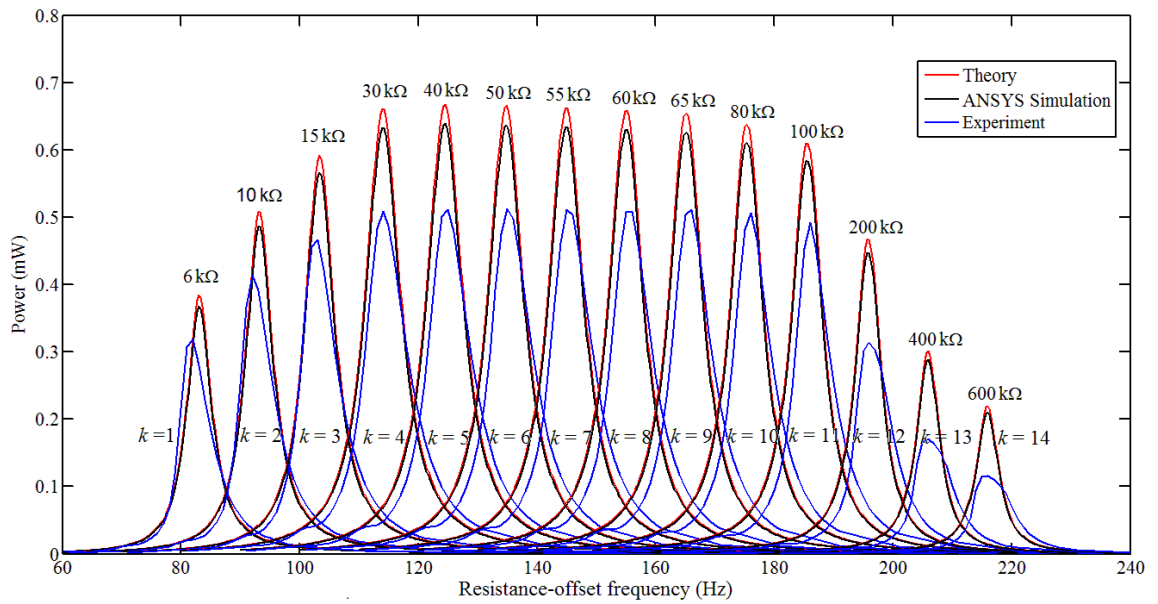


Figure 6.13 – Comparison of theoretical calculations, ANSYS simulation, and experimental results for output power

In this research, the main aim is to maximise the power output which is calculated by using equation (6.16). However, this equation must be verified before proceedings with the analysis. Therefore, a comparison is made between the existing technique (the Roundy method; Roundy, 2003), experimental results, and the proposed technique. Under the same setup in each case, but varying the resistance, equation (6.8) is calculated and plotted in Figure 6.13 (“theory”). To calculate the power output using the

proposed method, a finite element analysis is employed. A finite element model of a rectangular piezoelectric cantilever beam was developed for use in predicting the behaviour of the beam under a concentrated load at the free end, as shown in Figure 6.12. The average element stress and the vertical deflection are obtained in the analysis. The obtained values are substituted into equation (6.16) and the results are plotted in Figure 6.13 (“ANSYS simulation”).

The maximum power is produced when the resistance is 30–65 kΩ, as shown in Figure 6.13. The results of the finite element simulation and the theoretical calculation differ by approximately 4.50%, whereas the experiment results are markedly different from these two sets of results. There are many factors that may affect the experiment result, including the surrounding environment, the position of the tip mass, and the sensitivity of the apparatus. Hence, the error in the experiment is about 20% compared with the finite element analysis. However, the frequency response for each load resistance and the effect of the load do show similar trends to both theory and simulation.

6.5 Maximum strain and width responses

The aim of this section is to predict the behaviour of the piezoelectric material in terms of strain distribution and power output. Figure 6.14 compares the different strain distributions.

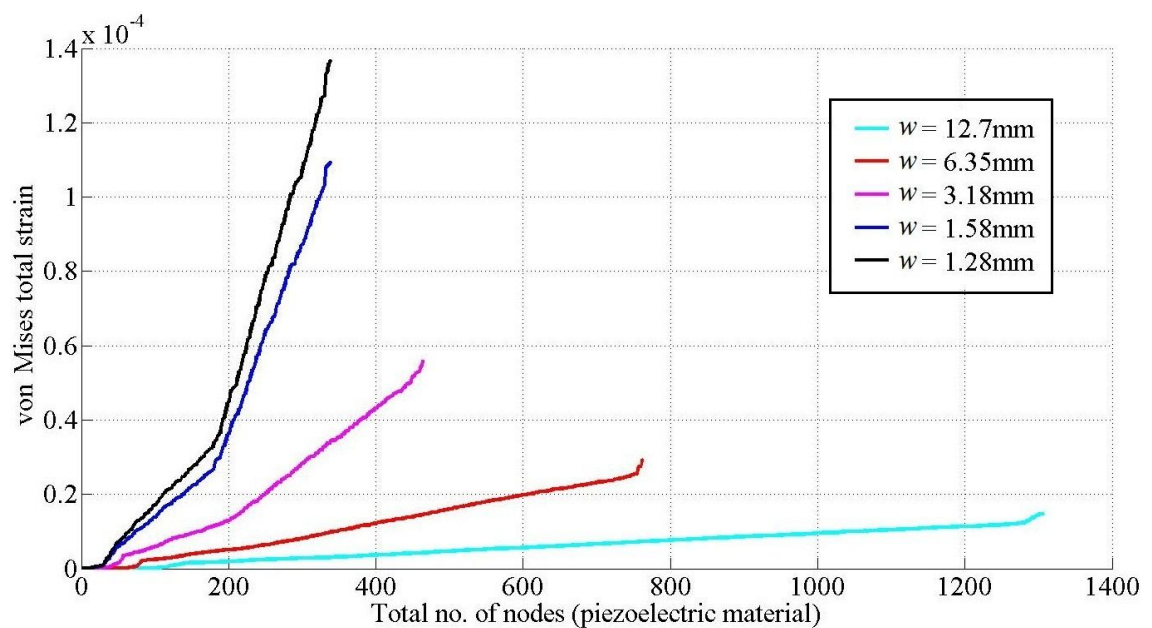


Figure 6.14 – Strain distributions for a rectangular beam with varying widths

The analysis considered a cantilever beam with widths of 12.7, 6.35, 3.18, 1.58, and 1.28 mm (Figure 6.14); all the other dimensions remained constant. The maximum von Mises strain showed a marked increase with decreasing width. As a result, the maximum strain, obtained for a width of 1.28 mm, is approximately nine times higher than that for a width of 12.7 mm.

The beam with a width of 12.7 mm has an even distribution of strain compared with the beam with a width of 1.28 mm. The strain data indicate that the design with a width of 12.7 mm provides the optimal power output, because for a given maximum strain constraint, the power output is greatest for the design with a width of 12.7 mm. This result reflects the fact that the power output for a cantilever beam is affected by the input acceleration, as evident in equation (6.16). Therefore, the analysis now considers the design of a cantilever beam using piezoelectric materials, in terms of power output and maximum strain.

6.6 Shape optimisation using the multifactor optimisation of structure techniques (MOST)

6.6.1 Design considerations

The main objective is to find the optimum geometrical shape of a bimorph cantilever beam that yields the maximum power and has the minimum structural volume.

6.6.2 Design constraints and load

Figure 6.15 shows a schematic diagram of the design domains, geometric constraints, load, and boundary conditions of the design. In this finite element model, the design is modelled as a cantilever beam. Points *A* and *D* are fixed at three coordinates (*x*, *y*, and *z*). A concentrated pressure is applied at the free end of the cantilever beam (between *B* and *C*). The initial dimensions of the beam are listed in Table 6.7.

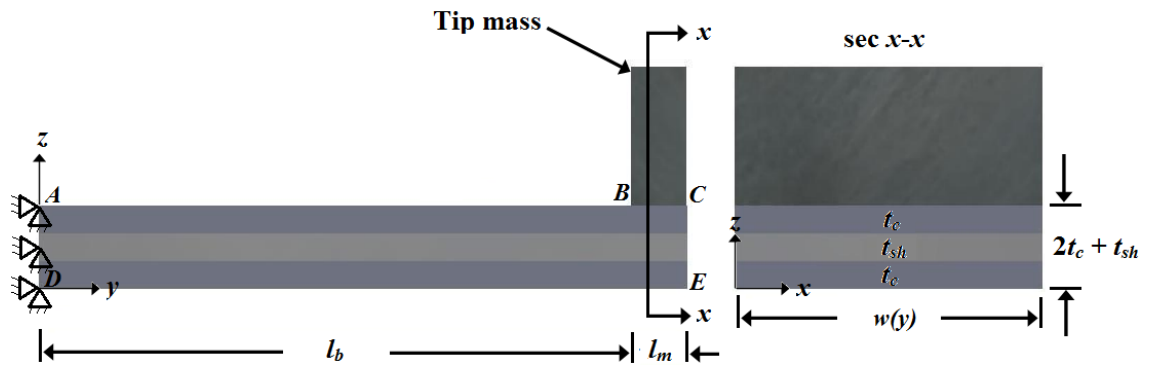


Figure 6.15 – Load and boundary conditions of the cantilever beam

Table 6.7 – Dimensions of the initial design

Parameter	Initial value
Thickness of piezoelectric material (t_c)	0.19 mm
Thickness of shim material (t_{sh})	0.13 mm
Effective length of piezoelectric material PZT ($l_e = l_m + l_b$)	23.5 mm
Length of tip mass (l_m)	2.00 mm
Length of base (l_b)	21.5 mm
Width ($w(y)$) $1 \leq w(y) \leq 12.7$ mm	12.7 mm

6.6.3 Finite element model of a bimorph cantilever beam

The maximum power of a rectangular cantilever beam can be enhanced by reducing the structural volume. The beam is modelled using finite element software (ANSYS) in conjunction with the Multifactor Optimisation of Structure Techniques (MOST). Shape optimisation is performed on three orthogonal planes, where the variation of stress is produced by the tip mass. The ANSYS SOLID92 element is used to generate the model rather than the SOLID98 element, although both elements are 10-node tetrahedral shapes with a large deflection and stress stiffening behaviour. SOLID98 is a tetrahedral coupled-field solid and SOLID92 is a 3D structural solid element. SOLID92 was selected to generate the model because it adapts well to the free meshing of irregular shapes. The solution from the analysis is used to calculate the value of b^* in equation (6.13), which is later substituted into equation (6.16) to compute the power output. Therefore, for generating the model there is little difference between SOLID98 and SOLID92 if the mesh density is sufficient.

To ensure that the mesh density is adequate, a displacement convergence test is performed by decreasing the element size. Table 6.8 shows the effect of an incremental

decrease in element length (starting with the basic element length of 3.2 mm) on the overall displacement in the z -direction (indicated as point E in Figure 6.15) and on the average element stress of the piezoelectric element.

Table 6.8 – Effect of element length on displacement and average element stress in a convergence test

Element length/mm	No. of elements	Displacement in z -direction (μm)	Average element stress (MPa)
3.2	847	8.286	0.2138
1.6	2714	8.432	0.2355
0.8	9620	8.485	0.2443
0.4	39052	8.505	0.2423

Sufficient accuracy is attained if the element length is less than 0.8 mm, although a reduction in element length beyond 0.8 mm results in a marked increase in the total number of elements and a corresponding increase in the number of consecutive analyses. Figure 6.16 shows that the average element stress of the cantilever beam is converged at approximately 10k elements, corresponding to an element length of 0.8 mm. In contrast, the displacement continues to increase in the case of larger numbers of elements. Although the beam is converged at an element length of 0.8 mm, the deflection at point E (see Figure 6.15) is smaller than that for an element length of 0.4 mm. However, this does not affect the accuracy of the solution. Therefore, an element length of 0.8 mm is selected for analysis of the cantilever beam. The initial model consists of 9620 elements (both piezoelectric and shim elements) with a constant element size of 0.32 mm^2 , using a uniform element length of 0.8 mm (Figure 6.17).

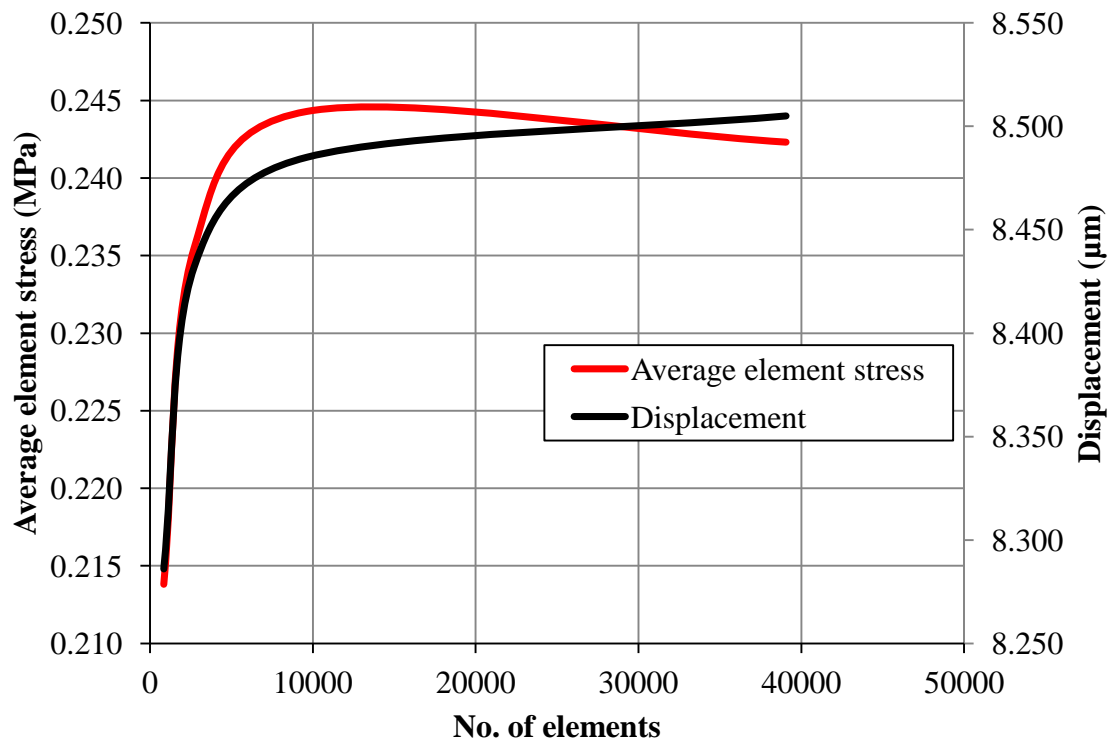


Figure 6.16 – Convergence of average element stress and displacement

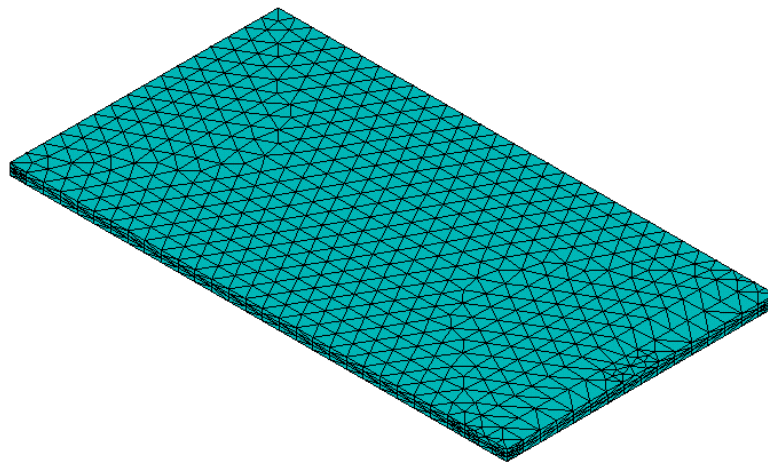


Figure 6.17 – Finite element discretisation of the initial solid cantilever beam

6.6.4 Formulation of the optimisation problem

In this study, the optimal shape of engineering structures is determined using MOST. The design problem is therefore to maximise the power output and the average element stress, and simultaneously minimise the structural volume, subject to the design constraints. The optimisation to be solved is stated as follows:

$$\begin{aligned}
 & \text{find} \quad X = (x_1, x_2, \dots, x_k) \\
 & \text{min} \quad \{V_s(X)\} \\
 & \quad \text{and} \\
 & \text{max} \quad \{P_j(X) \text{ and } \sigma_{\text{ave},j}(X)\} \\
 & \text{s.t.} \quad \{V_s \leq V_{s,\text{ini}}; P_j \geq P_{\text{ini},j}; \sigma_{\text{ave},j} \geq \sigma_{\text{ini},j}; \delta_{\text{ini},j} \leq \delta_j \leq \delta_{\text{lim},j}; \sigma_{\text{max},j} \leq \sigma_y\} \text{ and} \\
 & \quad \{x_i^{\text{min}} \leq x_i \leq x_i^{\text{max}}, i = 1, 2, \dots, k\} \\
 & \quad j = 1, 2, \dots, n
 \end{aligned}$$

where k is the number of design variables, V_s is the structural volume (excluding the volume of the tip mass), σ_{ave} is the average element stress of the structure, δ is the displacement of point E (see Figure 6.15), σ_{max} is the maximum von Mises stress of the structure, and P is the power output. The subscript ‘ini’ indicates the initial value for the structure (here, the initial iteration when $n_i = 0$), and n is the number of loading cases (here, $n = 1$). The subscript ‘lim’ indicates a specified performance limit for the structure. In this research, the cantilever beam is optimised to carry a tip mass of 4.1 grams with a maximum vertical displacement of $\delta_{\text{lim}} = 300 \mu\text{m}$ at any node, satisfying a maximum strength of $\sigma_y = 24 \text{ MPa}$ (see Table 6.5). x_i^{min} and x_i^{max} are the lower and upper bounds of the design variables of x_i , respectively. There are eight design variables in the structural model, which represent the width of the cantilever beam. In this case, the lower and upper bounds are set to 1 and 15 mm, respectively.

6.7 Results and discussions

6.7.1 Optimisation results

The optimisation is started from a rectangular cantilever beam. The optimisation took $n_i = 27$ iterations to converge, as shown in Figure 6.18. The von Mises stress of the initial and optimised structures is shown in Figure 6.19.

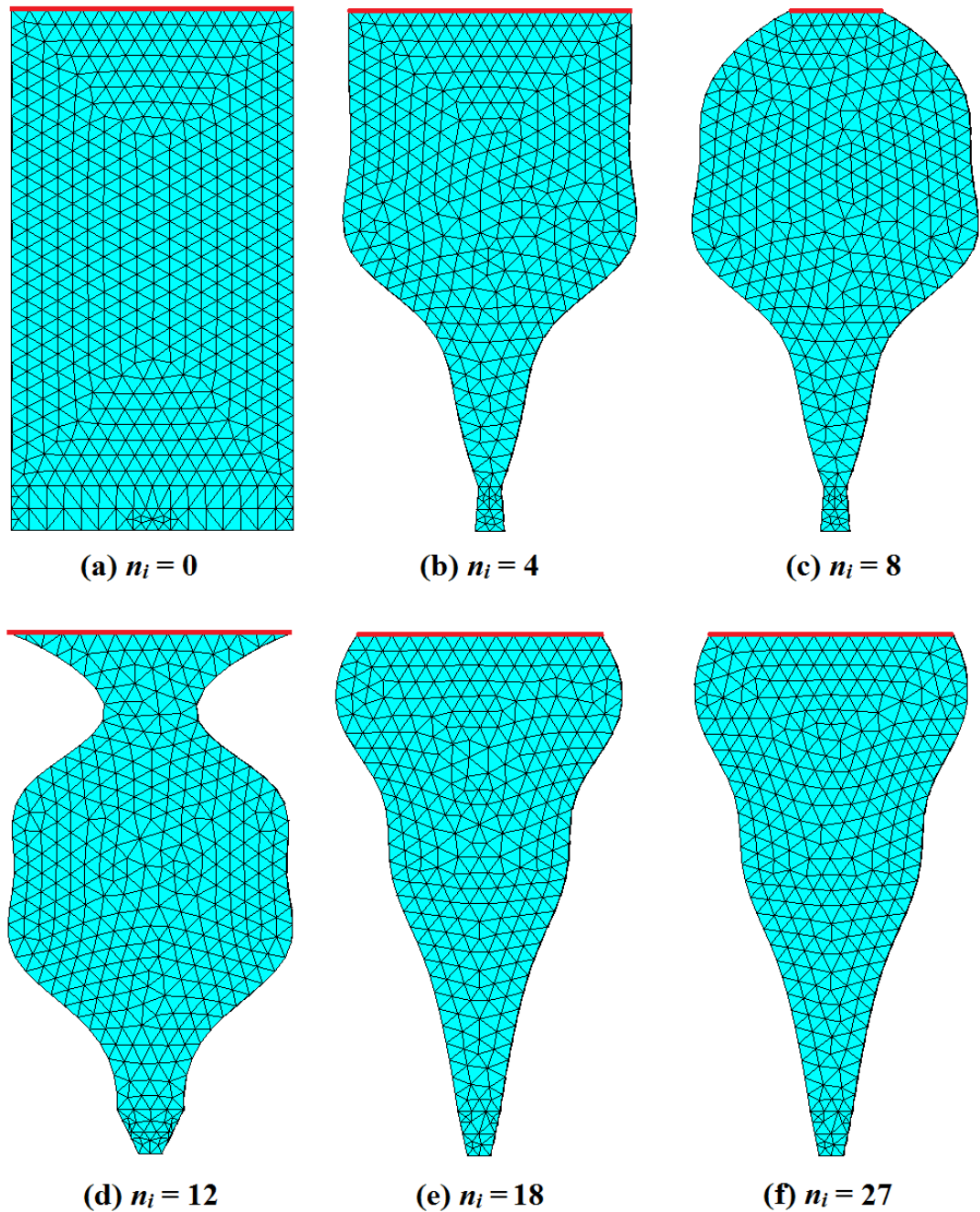


Figure 6.18 – MOST optimisation history of a bimorph cantilever beam showing the (a) initial design, (b) $n_i = 4$, (c) $n_i = 8$, (d) $n_i = 12$, (e) $n_i = 18$, and (f) the optimised design at $n_i = 27$ (red lines indicate the constraints are fixed along the x , y , and z axes)

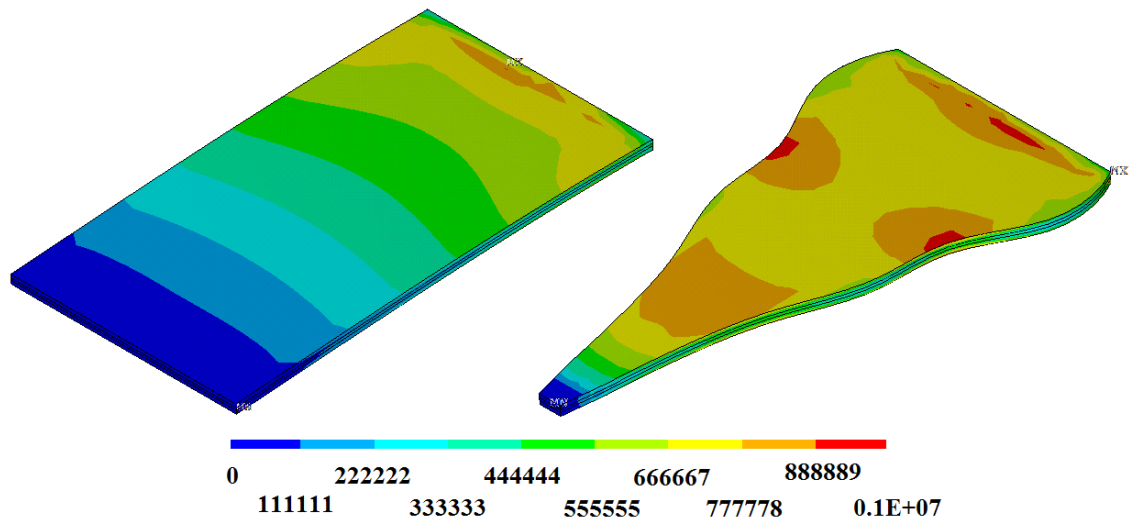


Figure 6.19 – Distribution of von Mises stress for the initial design (left) and the optimised design (right) (Pa)

The outer boundaries of the cantilever beam are described by a B-spline function, represented by the eight design variables. Topology optimisation is not considered in this problem. Movement limits are applied to the outer boundaries of the cantilever beam to prevent excessive distortion of the finite element mesh. One of the objectives of the optimisation is to increase the power output. From equation (6.16), the power output is related to the average element stress. During the optimisation, areas of low stress/strain are removed, resulting in areas of higher stress within the structure, accompanied by an increase in the average element stress due to a decrease in the number of elements. The maximum von Mises stress of the initial and optimised designs is 0.89 and 1.00 MPa, respectively (Figure 6.19).

6.7.2 Optimisation history

The shape optimisation of the cantilever beam required $n_i = 27$ iterations to converge, as shown in Figure 6.20, which depicts the evolution of the structural volume and the maximum power output. A sharp increase in the output power is seen up to $n_i = 5$, because the width at the free end of the beam (where the tip mass is located) is reduced to a tenth of its original size. This is followed by a sharp decrease in power output up to $n_i = 8$, due to the removal of material from the structure and changing values of the natural frequency, damping ratio, resistance, and capacitance. Subsequently, power output fluctuates before converging to an optimal solution at $n_i = 27$. The opposite trend is observed for the structural volume. The average element stress is increased by approximately 15% between $n_i = 5$ and $n_i = 10$, due to the removal of material and the

consequent higher average stress for each element in the structure (Figure 6.21). The displacement (at point *E*) shows an increasing trend up to $n_i = 10$, followed by a fluctuation before converging to the optimum value at $n_i = 27$.

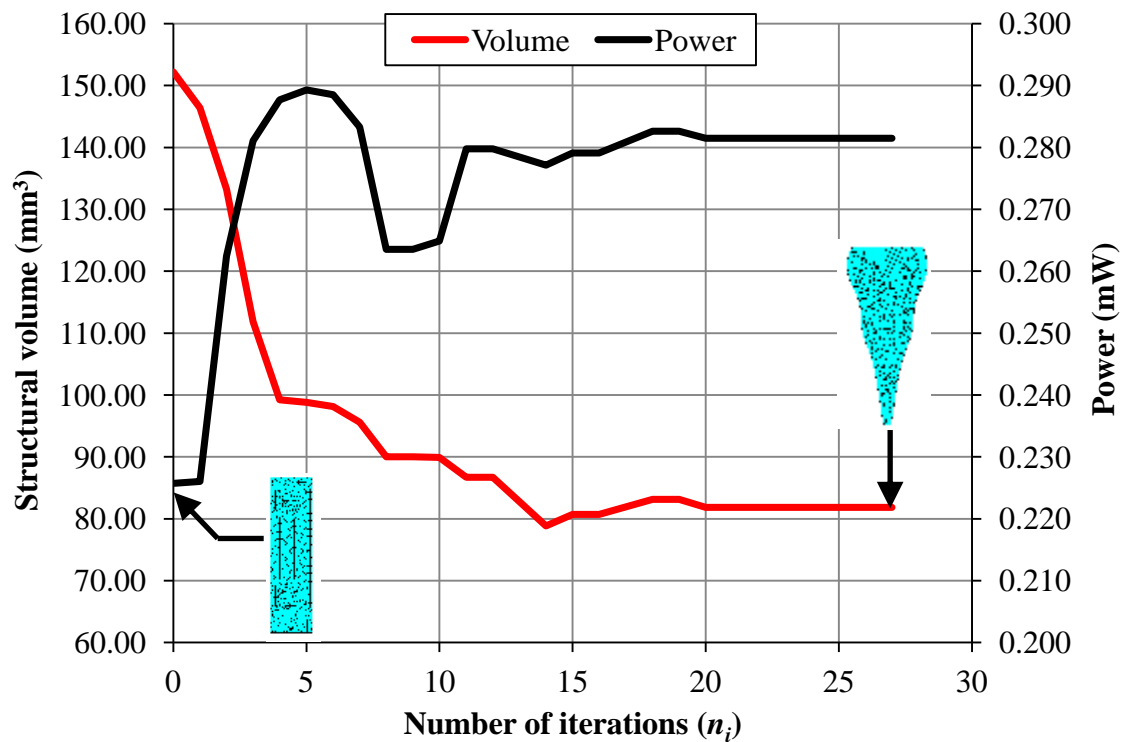


Figure 6.20 – Optimisation convergence history of the structural volume (excluding the volume of the tip mass) and power

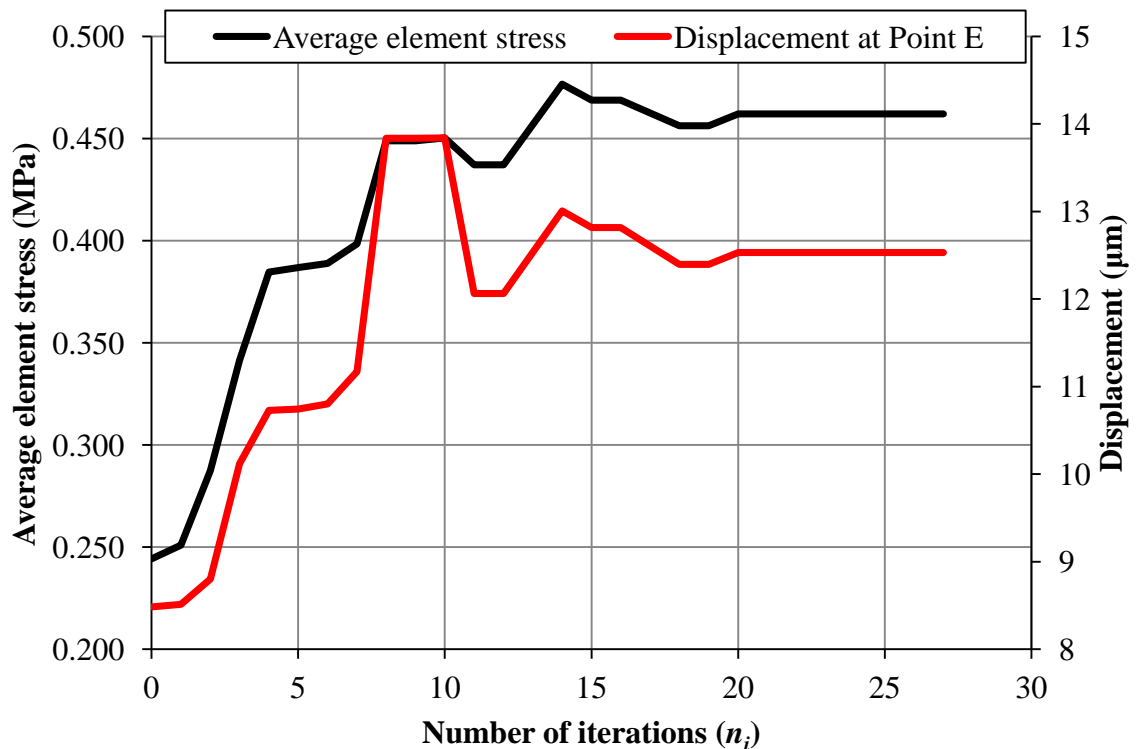


Figure 6.21 – Optimisation convergence history of the average element stress and displacement

Figure 6.20 shows that the power is increased from approximately 0.226 to 0.282 mW, which corresponds to an increase of approximately 25% compared with the initial design. The total structural volume (piezoelectric and shim material) is reduced significantly from 152.21 to 81.83 mm³ during the optimisation, corresponding to a 46.2% saving in materials. To increase the maximum power output, the vertical deflection of the cantilever beam is increased by about 47% from 8.48 to 12.50 μm (see Figure 6.21). The design attributes of the initial and optimised designs are listed in Table 6.9.

Table 6.9 – Design attributes of the initial and optimised designs of a cantilever beam

	Initial design	Optimised design
Power (mW)	0.226	0.282
Volume of piezoelectric material (mm ³)	113.41	60.97
Volume of shim material (mm ³)	38.80	20.86
Maximum von Mises stress (MPa)	0.89	1.00
Average element stress (MPa)	0.24	0.46
Displacement at point <i>E</i> (μm)	8.48	12.50
Capacitance (nF)	50.07	26.92
Frequency (Hz)	113	93

6.7.3 von Mises total strain energy

The von Mises total strain energy is assessed to determine whether the elements are subjected to high or low stress. To compare the initial and optimised designs at the same scale, each piezoelectric strain (or node) is divided by the maximum strain (or node) at each design (see equation (6.23)).

$$\text{Normalised strain(or node)} = \frac{\text{each piezoelectric strain (or node)}}{\text{Maximum strain(or node)}} \quad (6.23)$$

Figure 6.22 shows the normalised von Mises total strain energy of the initial and optimised designs. The optimised design has a higher strain than the initial design, and the initial design shows a uniform increase in strain energy. In contrast, the optimised design shows a rapid increase in strain energy from the origin.

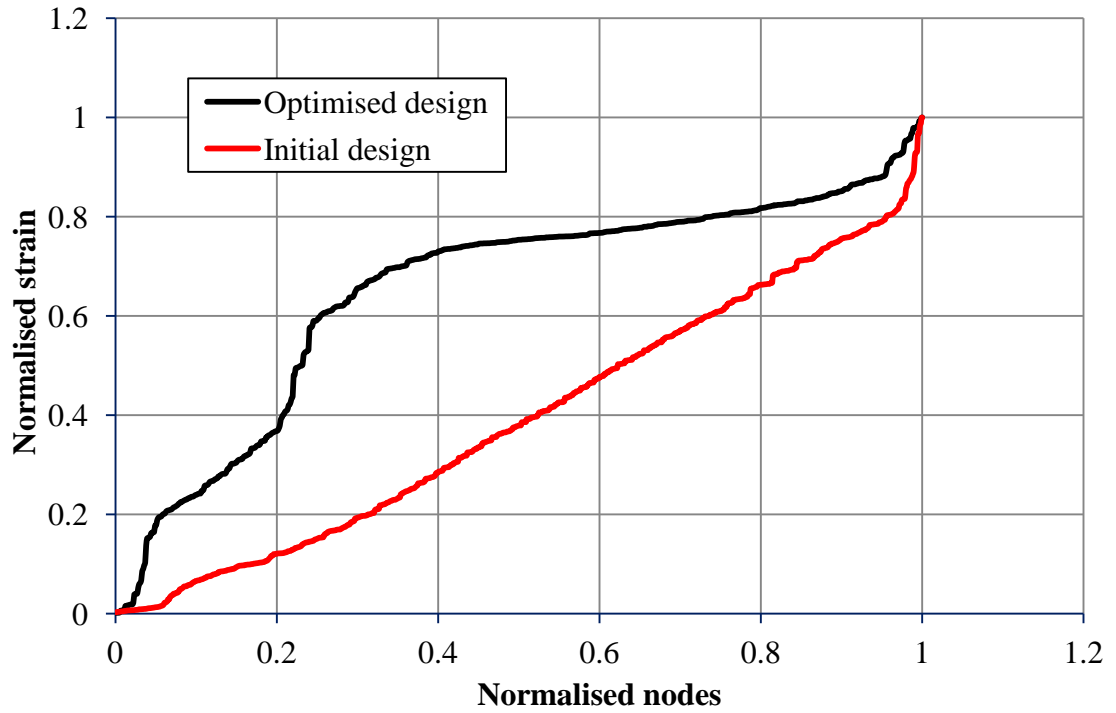


Figure 6.22 – Distribution of strain energy for the initial and optimised designs

From Figure 6.22, it is difficult to determine which design provides the most even strain distribution. To enable a comparison of the initial and optimised designs at the same scale, the strain values for the piezoelectric nodes are divided by the maximum strain in each design to obtain the strain ratio (see equation (6.24)). The attributes of the strain ratio of the initial and optimised designs are shown in Table 6.10 and Figure 6.23.

$$\textit{Strain ratio} = \frac{\textit{Strain of each piezoelectric node}}{\textit{Maximum strain}} \quad (6.24)$$

Table 6.10 – Distribution of the strain ratio for the initial and optimised designs

	Percentage of strain ratio > 0.5	Percentage of strain ratio > 0.75
Initial design	37.8	10.5
Optimised design	76.9	51.3

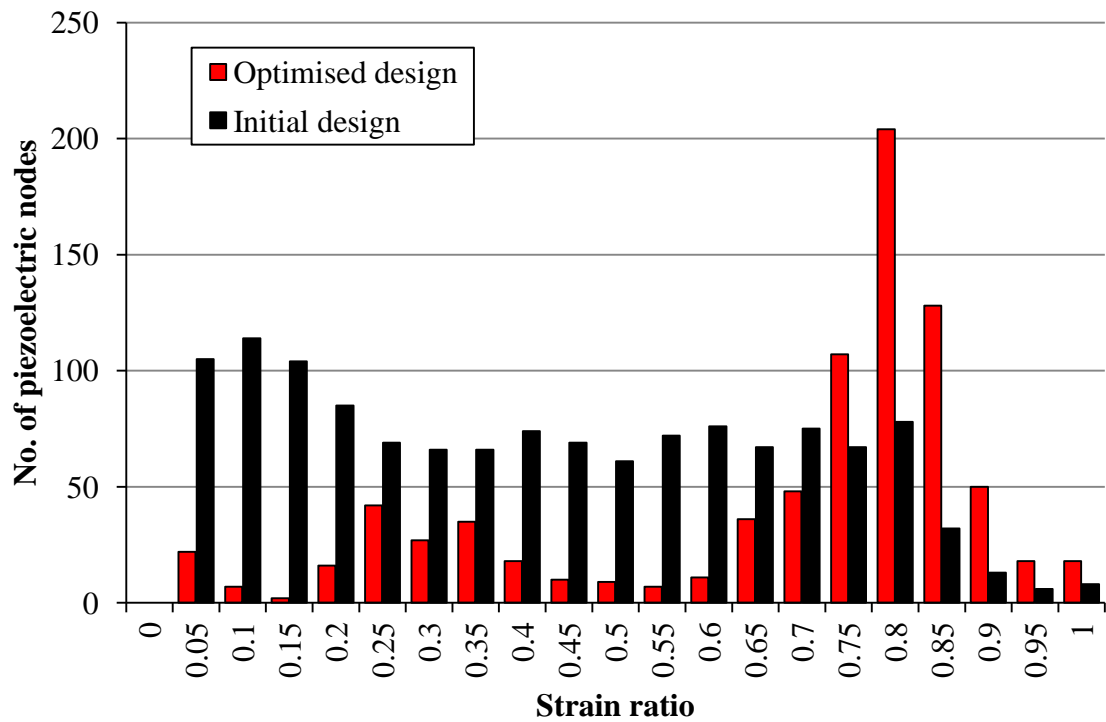


Figure 6.23 – Strain distribution according to the strain ratio

The optimised design gives the best strain distribution according to the strain ratio, with 76.9% and 51.3% of the nodes having a strain ratio greater than 0.5 and 0.75, respectively (Table 6.10). Figure 6.23 shows the distribution of the strain ratio of the initial and optimised designs. The initial design shows a wide spread in the strain ratio, whereas the optimised design has a better strain distribution that is concentrated around a strain ratio of 0.80. In the optimised design, more than 75% of the nodes have a strain ratio greater than 0.50.

6.7.4 Vibration of the cantilever beam

This section considers the modal frequencies of the cantilever beam. The theoretical natural frequency and the natural frequency of the finite element analysis of the initial design are 111.35 and 113.01 Hz, respectively. The difference between the theoretical and finite element results is approximately 1.5%, which is relatively small. Therefore, the finite element results are used in this study to determine the natural frequency of the cantilever beam. To gain a deep understanding of the vibration of different mode shapes, the first six natural frequencies of the optimised design are shown in Figure 6.24. Table 6.11 lists the modal frequencies of the beam, as predicted by finite element analysis.

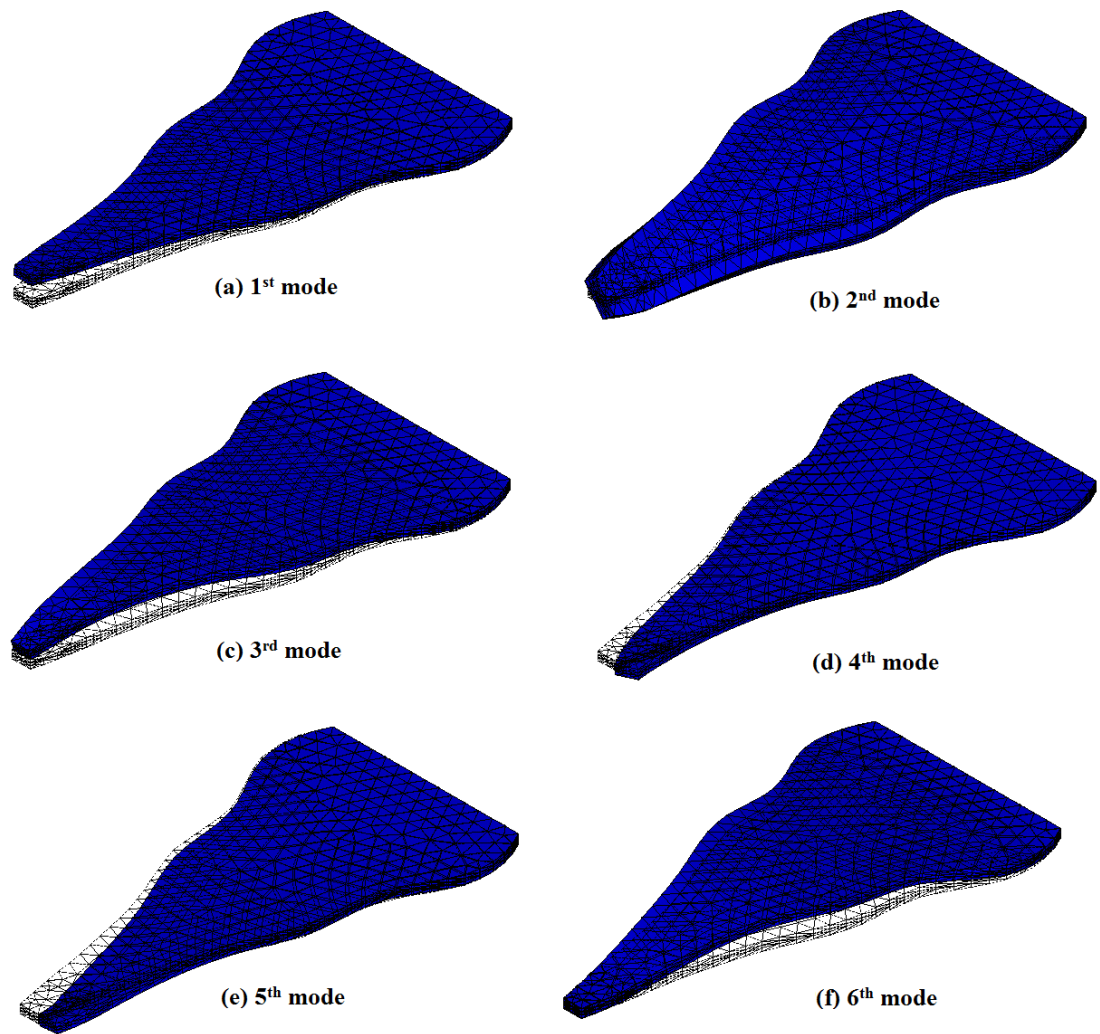


Figure 6.24 – Shapes of the first six modes of the beam (undeformed shape: dotted line and deformed shape: blue colour)

Table 6.11 – Natural frequency of the first six modes

	1 st mode	2 nd mode	3 rd mode	4 th mode	5 th mode	6 th mode
ANSYS (Hz)	93	194	337	1211	2623	2869

6.7.5 Mass response of the optimised design

The maximum power output is determined by factors such as the natural frequency, damping ratio, resistance, capacitance, average element stress, and displacement. Figure 6.25 compares the power output obtained using tip masses of different sizes (2.0, 4.1, 4.7, 5.5, and 6.5 grams), for resonance frequencies of 60–150 Hz.

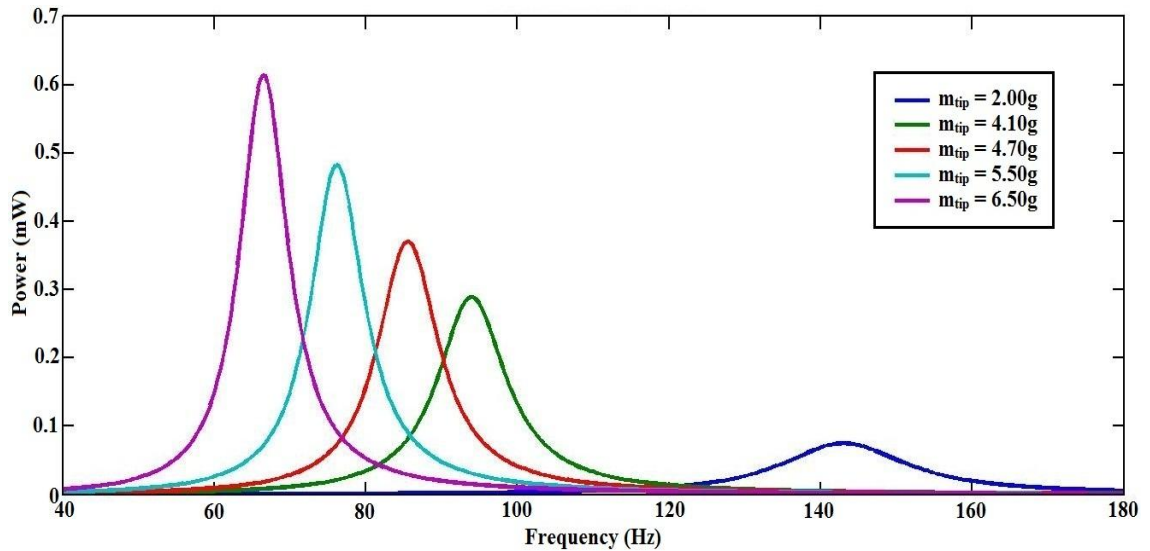


Figure 6.25 – Mass response of the optimised design

The highest power outputs of the system are found at the natural frequencies of 66, 76, 85, 93, and 140 Hz, respectively. The maximum power output shows an increase with increasing tip mass. The maximum power output is approximately 0.649 mW at 67 Hz, using a tip mass of 6.5 grams. The natural frequency varies with the tip mass.

6.7.6 Optimised design and triangular design

Table 6.12 lists the power density (per unit volume of piezoelectric material) and the dimensions of a rectangular beam, triangular beam, and the optimised shape (Figure 6.26). Roundy (2005) reported that a triangular shape produces more than twice the power density of a rectangular shape. Figure 6.27 compares the power output of three shapes for a given volume. The power output of the rectangular shape is approximately half that of the other two shapes.

Table 6.12 – Comparison of power density among beams with different shapes

	Rectangular shape	Triangular shape	Optimised shape
Volume of piezoelectric material (mm ³)	113.41	61.30	60.97
Power density (μW/mm ³)	1.99	4.49	4.62

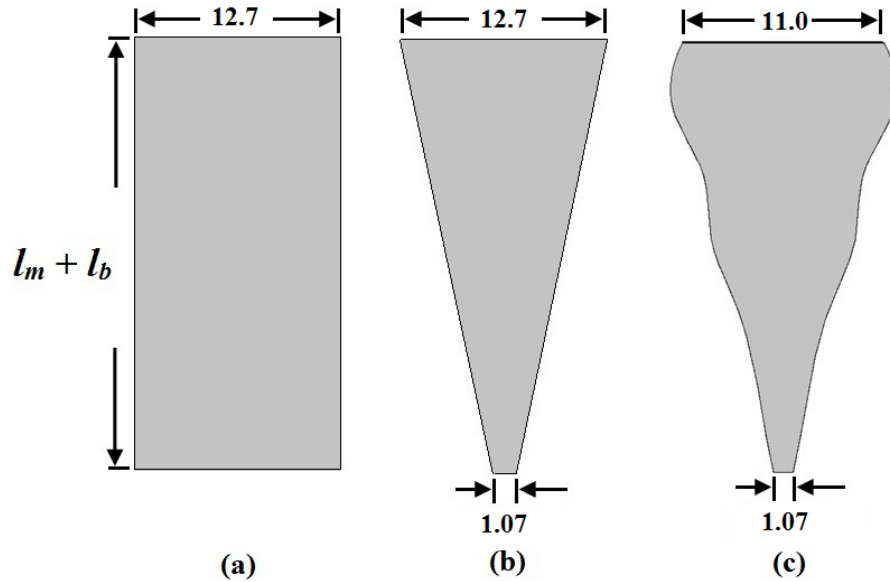


Figure 6.26 – Dimensions of (a) rectangular, (b) triangular, and (c) optimised shapes (unit in mm)

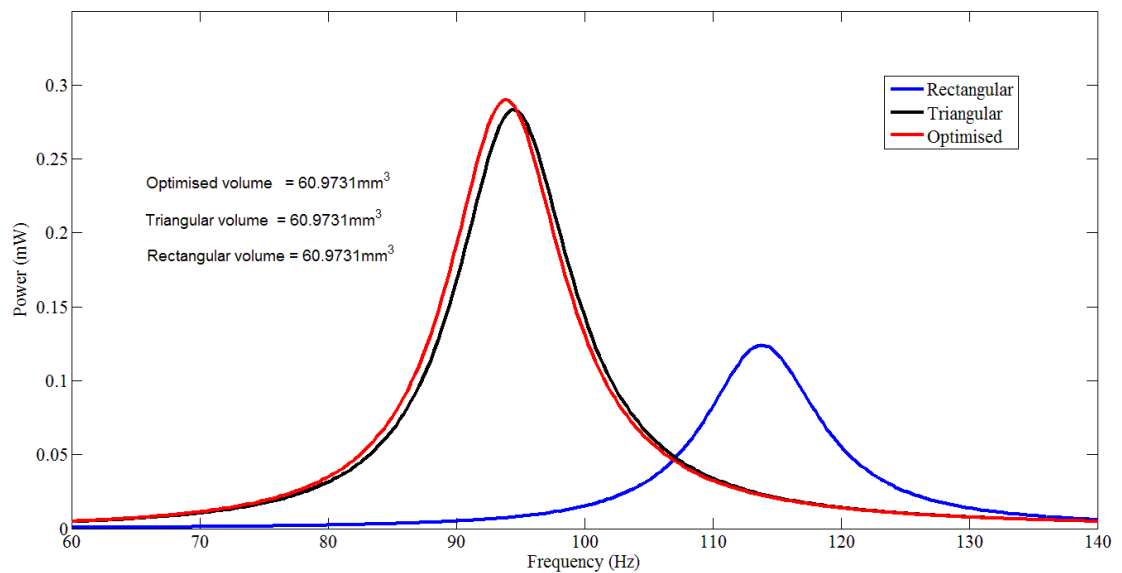


Figure 6.27 – Power output of rectangular, triangular, and optimised shapes

6.8 Investigation of the optimum topology of a bimorph cantilever beam

To increase the strain energy of the bimorph cantilever beam, additional holes within the cantilever beam region are considered. Miller *et al.* (2008) used this approach to release the gaseous etch to remove the underlying silicon (which is used to glue layers of material), obtaining a strain increase of at least 30%. Their result indicates that the strain of the bimorph cantilever beam can be increased.

The aim of the optimisation performed in this research is to maximise the power density, which is directly related to maximising the power output and minimising the structural volume. Manufacturing capability is not considered during the optimisation procedure. The optimisation is performed by adding/moving holes and changing their sizes/shapes utilising the sizing and shape optimisation method to seek the optimum “topology” of a bimorph cantilever beam.

6.8.1 Design domain, load, and boundary conditions

The schematic diagram in Figure 6.28 shows the design domain of the design. The load and boundary conditions of the cantilever beam remain unchanged (see Figure 6.15). All elements within the non-design domain are kept ‘frozen’. The removal of material occurs within the confines of the design domain.

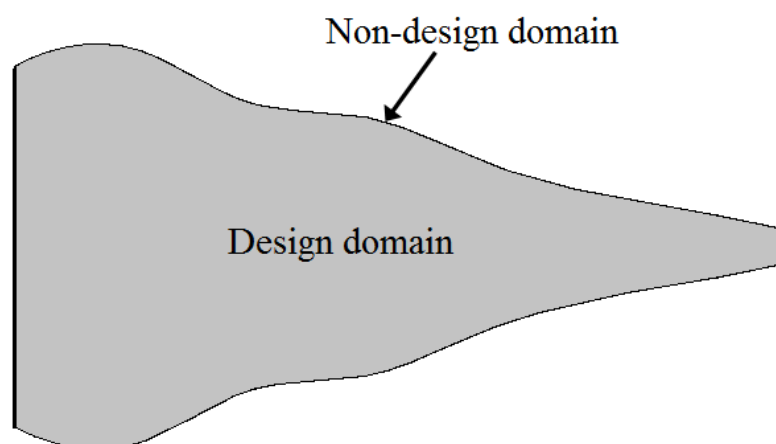


Figure 6.28 – Design domain and shape constraints of the optimised design

6.8.2 Optimum “topology” structure of the cantilever beam

The optimised design of the bimorph cantilever beam is modelled using ANSYS, as shown in Figure 6.18(f). The bimorph cantilever beam with the previously optimised design is taken for further possible improvement. Eight different designs were created, with different numbers and sizes of holes in the design domain.

6.8.3 Results and discussions

Figure 6.29 show the sizing and shape optimisations using the MOST technique for the various designs.

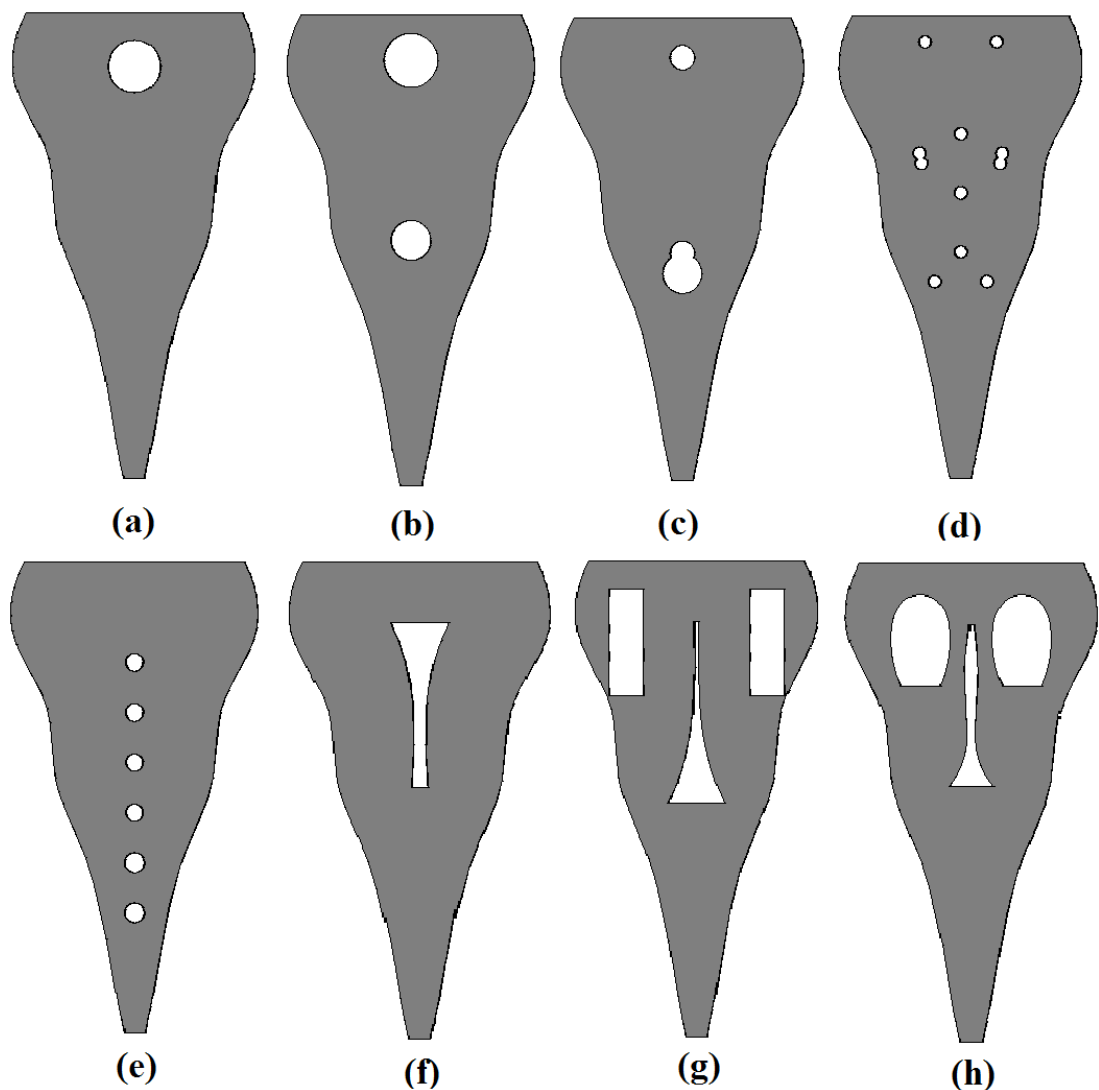


Figure 6.29 – Optimisation of optimum “topology” designs, showing designs (a) to (h)

Looking at Figure 6.29, it is difficult to assess, based on the shape alone, which design yields the highest power density. The design is determined by the average strain, power

density, maximum von Mises stress, and structural volume across the piezoelectric element. Figure 6.30 shows the power density and average strain for each design, while Figure 6.31 shows the structural volume and von Mises stress.

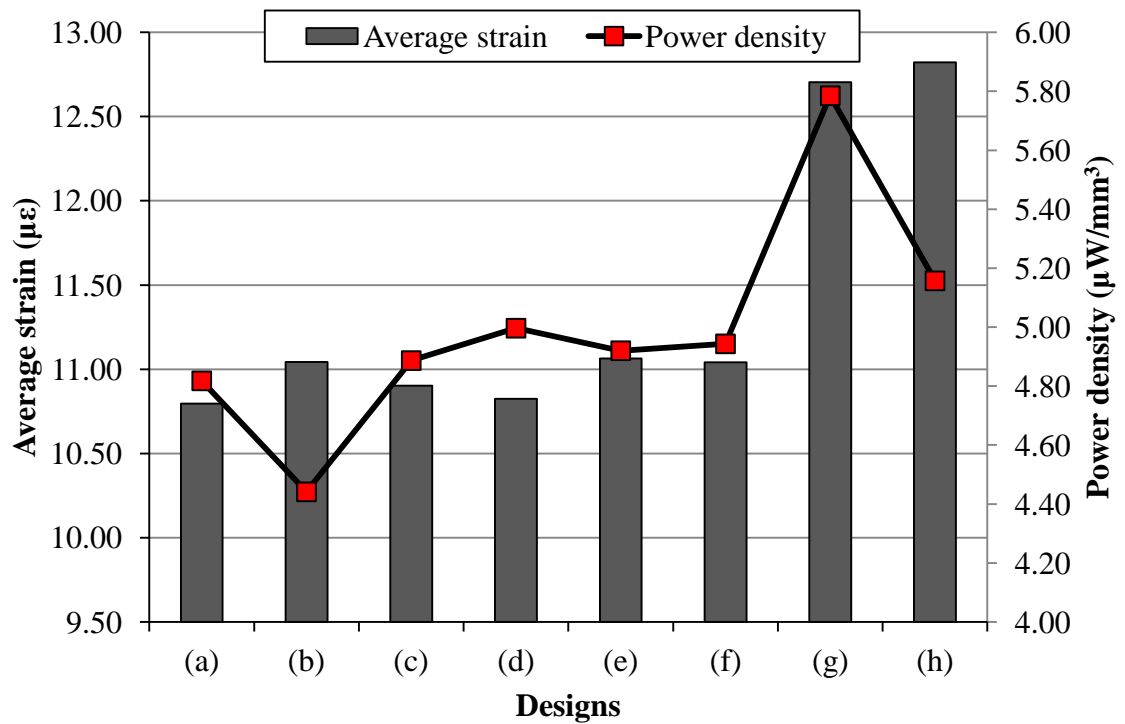


Figure 6.30 – Average strain and power density of the various optimum “topology” designs

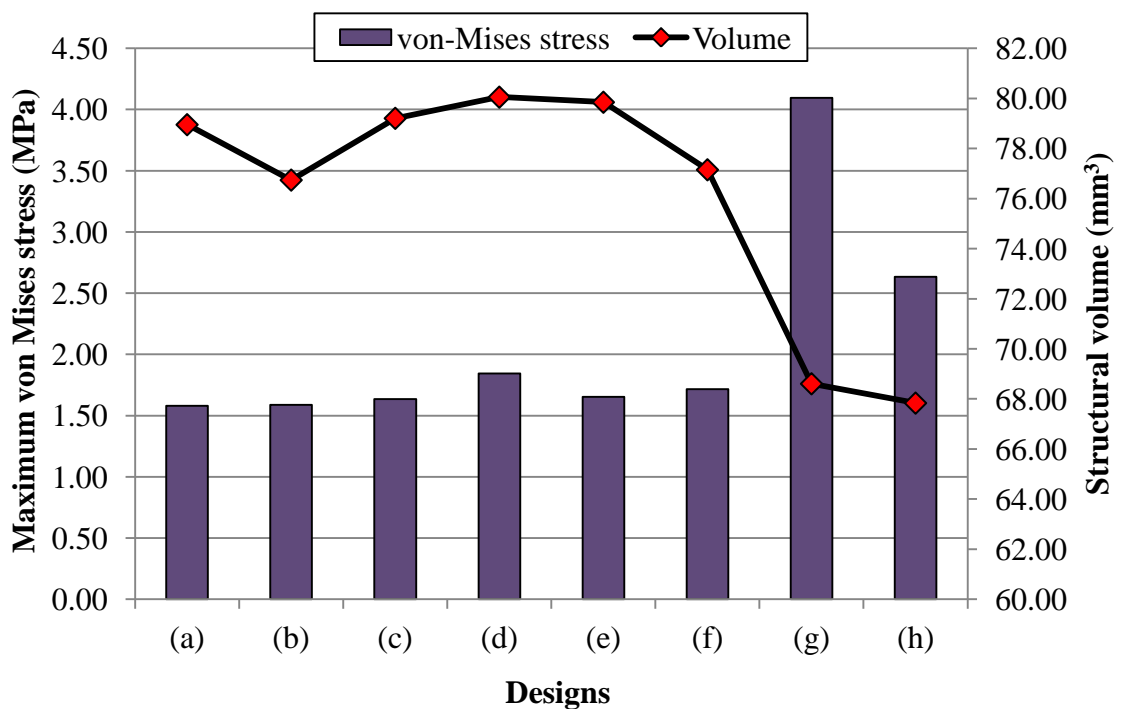


Figure 6.31 – von Mises stress and structural volume of the various optimum “topology” designs

Figure 6.30 and Figure 6.31 show that designs (a) to (f) yield the lowest average strain, power density, and maximum von Mises stress. Conversely, designs (g) and (h) show the highest values. Among these designs, design (h) has the smallest structural volume, enabling the production of a cantilever beam at a lower cost. Although design (g) achieved the highest power density, it yielded a higher maximum von Mises stress than design (h). Therefore, design (h) is the best optimum “topology” design and is chosen as the design of the cantilever beam.

6.8.4 Sizing and shape optimisation using MOST

Figure 6.32 shows the von Mises stress distribution for the optimum “topology” structure of design (h). The optimised structure (Figure 6.18(f)) and optimum “topology” structure show a slightly reduced maximum power output. However, the power density per unit volume for the later design is increased by approximately 11% compared with the optimised design. The structural volumes of the optimised and optimum “topology” designs of the cantilever beam (excluding the tip mass) are 81.83 and 67.84 mm³, respectively. The attributes of the both optimised designs are listed in Table 6.13.

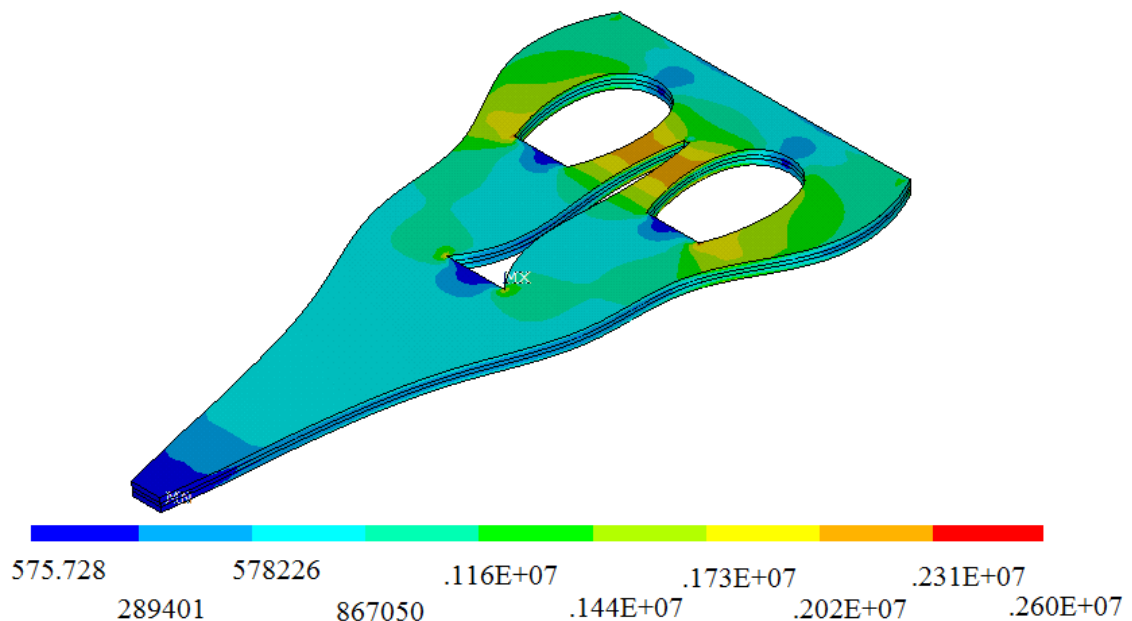


Figure 6.32 – Distribution of von Mises stress in the optimum “topology” design (h) (Pa)

Table 6.13 – Design attributes of the optimised and optimum “topology” structures

	Optimised design	Optimum “topology” design (h)
Power (mW)	0.282	0.261
Volume of piezoelectric material (mm ³)	60.97	50.55
Volume of shim material (mm ³)	20.86	17.29
Average element stress (MPa)	0.46	0.61
Displacement at point <i>E</i> (μm)	12.50	18.30
Capacitance (nF)	26.92	22.31
Frequency (Hz)	93	78
Power density (μW/mm ³)	4.62	5.16

The power density of the optimum “topology” design is 11.7% higher than that of the optimised design (Table 6.13), reflecting the fact that the volumes of the piezoelectric and shim materials are reduced, yielding a 17.1% saving in material. The reduced structural volume is accompanied by a reduction in the capacitance of the structure; consequently, the power output is also reduced. Although the average element stress of the optimum “topology” design is higher than that of the optimised design, the power output is lower because the power equation of the cantilever beam does not rely on the average stress only: it also depends on the frequency, damping ratio, resistance, and capacitance. The power output of the optimum “topology” structure is 0.261 mW, which is 7.4% lower than that of the optimised design. Conversely, the average element stress of the optimum “topology” design is 32% higher than that of the optimised design. Similarly, the displacement at point *E* is increased by 46.4% compared with the optimised design.

6.9 Summary

This chapter presented the sizing and shape optimisation of a bimorph cantilever beam, as an example of a piezoelectric generator. An existing technique (the Roundy method; Roundy, 2003) was verified, practical results were presented, and the proposed technique was discussed. A rectangular cantilever beam with a fixed tip mass was considered. The cantilever beam design was successfully optimised to yield a high power density and a low structural volume. The design was further enhanced by seeking an optimum “topology” (introducing holes within the cantilever beams). The power density of the optimum “topology” design was significantly improved and the structural volume reduced.

In the following chapter, multi-objective, multi-discipline, and multi-loading cases are considered simultaneously, and a reliability factor is included in the optimisation process.

7 A New Development of Reliability-related Multi-factor Optimisation and its Applications

7.1 Multi-criteria optimisation

This chapter presents multi-objective, multi-discipline, and multi-loading cases using reliability-related sizing/shape optimisation in conjunction with the Multifactor Optimisation of Structure Techniques (MOST). To demonstrate the effectiveness of the proposed method, two numerical examples are presented, considering a star-like truss structure and a raised-access floor panel structure. For the reliability problem, the maximum stress, maximum displacement, and structural mass are assumed to be independent of each other. The limit state conditions of both examples are given in \hat{Y} space.

7.1.1 Design constraints

As part of this study, a novel MOST has been extended to automatically accommodate and execute reliability-related multi-factor structural sizing/shape optimisations. One of the objectives of the present research is to develop the reliability loading-case index (RLI) (see Chapter 4.2), which is used in the optimisation by considering RLI, structural strength and stiffness, and structural mass. Therefore, the design problem is to minimise the structural mass, maximum stress, and maximum displacement, and to simultaneously maximise the RLI, subject to the design constraints for multi-loading cases. The optimisation problem to be solved can be stated as follows:

$$\begin{aligned} & \text{find } X = (x_1, x_2, \dots, x_k) \\ & \text{min } \{m(X), \sigma_{\max,j}(X), \text{ and } \delta_{\max,j}(X)\} \\ & \quad \text{and} \\ & \text{max } \{RLI_j(X)\} \\ & \text{s.t. } \{ \sigma_{\max,j} \leq \sigma_{\text{lim}}; \delta_{\max,j} \leq \delta_{\text{lim}}; m \leq m_{\text{lim}}; RLI_j \geq RLI_{\text{lim}} \} \text{ and} \\ & \quad \{x_i^{\min} \leq x_i \leq x_i^{\max}, i = 1, 2, \dots, k\} \\ & \quad j = 1, 2, \dots, n \end{aligned}$$

where k is the number of design variables, m is the structural mass, σ_{\max} is the maximum stress of the structure, δ_{\max} is the maximum displacement of the structure, RLI is the reliability loading-case index, the subscript 'lim' indicates a specified performance limit

for the structure, and n is the number of loading cases. x_i^{\min} and x_i^{\max} are the lower and upper bounds of the design variables of x_i , respectively.

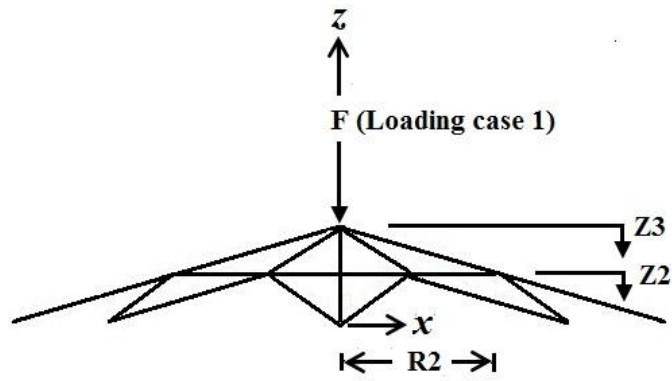
7.2 Example 1 – Star-like truss structure

7.2.1 Introduction

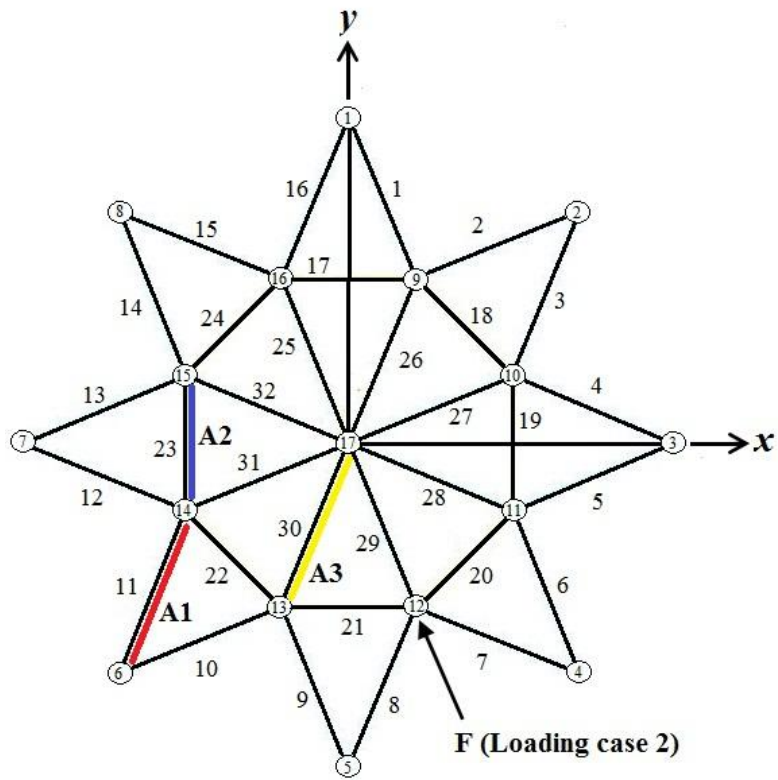
Truss structures are often used in construction projects to provide rigidity and support. A truss is constructed with straight members and joints between members, known as pin-jointed nodes. Each member is subjected to either tensile or compressive stress. In this study, a star-like truss structure is considered in order to demonstrate the effectiveness of the proposed methodology.

7.2.2 Design considerations

Consider a three-dimensional star-like structure with 17 nodal points and 32 bar elements, as shown in Figure 7.1. A finite element model of the structure is developed using ANSYS LINK8 elements. The initial structure has an external diameter of 1000 mm and a height of 100 mm. The material density is 7850 kg/m^3 , the Young's modulus is 210 GPa, the yield stress is 500 MPa, and the Poisson's ratio is 0.3. Table 7.1 lists the standard deviation (σ_{d_i}) and weighting factor (W_{p_i}) of the maximum stress, maximum displacement, structural mass, and RLI. In this example, the magnification factor (W) is set to 6.67 (see Chapter 4.2).



(a)



(b)

Figure 7.1 – Initial layout of the star-like truss structure

Table 7.1 – \hat{Y} space variables of the star-like truss structure

Performance	Standard deviation (σ_{d_i})	Weighting factor (W_{P_i})
Maximum stress (MPa)	50	0.354
Maximum displacement (mm)	0.5	0.021
Mass (kg)	2	0.525
RLI	-	0.100

7.2.3 Design constraints and loads

The design requirement of the star-like truss structure is to find the optimal solution in terms of satisfying the design constraints regarding strength and stiffness, and retaining a low mass. The truss members are assigned a stress limit (σ_{lim}) of 100 MPa. A maximum displacement limit of 1 mm is imposed on all nodes in all directions (x , y , and z). The minimum cross-sectional area (x_i^{min}) for each design variable is set to be 20 mm². The truss structure is considered for two loading cases simultaneously, as shown in Figure 7.1; i.e., a load applied in the z -direction at the centre of the truss structure ($F = 10$ kN), and a load applied at an angle of 22.5° to the y -direction ($F = 10$ kN). Nodal point coordinates are given in Table 7.2, and element cross-sectional areas in Table 7.3. Figure 7.1 shows the structural model with six design variables, which includes three cross-sectional areas (A1, A2, and A3) and three truss dimensions (R2, Z2, and Z3).

Table 7.2 – Coordinates of nodal points of the initial star-like truss structure

Node	x (mm)	y (mm)	z (mm)
1	0.000	500.000	0.000
2	353.550	353.550	0.000
3	500.000	0.000	0.000
9	103.553	250.000	50.000
10	250.000	103.553	50.000
17	0.000	0.000	100.000

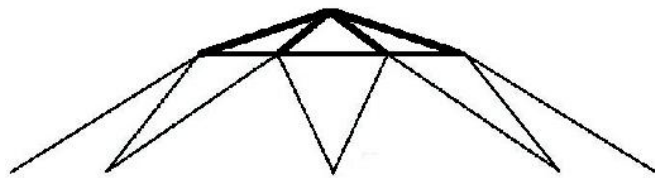
Table 7.3 – Cross-sectional areas of elements of the initial star-like truss structure

Element	Design variables	Area (mm ²)
1–16	A1	100
17–24	A2	100
25–32	A3	100

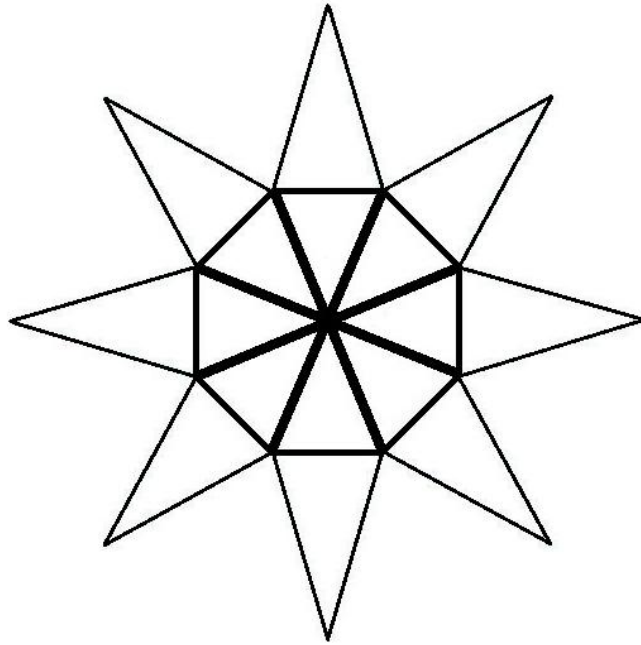
7.2.4 Results and discussions

7.2.4.1 Optimisation results

The solution of the star-like truss optimisation required $n_i = 96$ iterations to converge. The optimised design is shown in Figure 7.2. The magnitudes of stress for the elements in the initial and optimised designs are shown in Figure 7.3 and Figure 7.4, respectively.



(a)



(b)

Figure 7.2 – Optimised design, showing a (a) front view and (b) top view

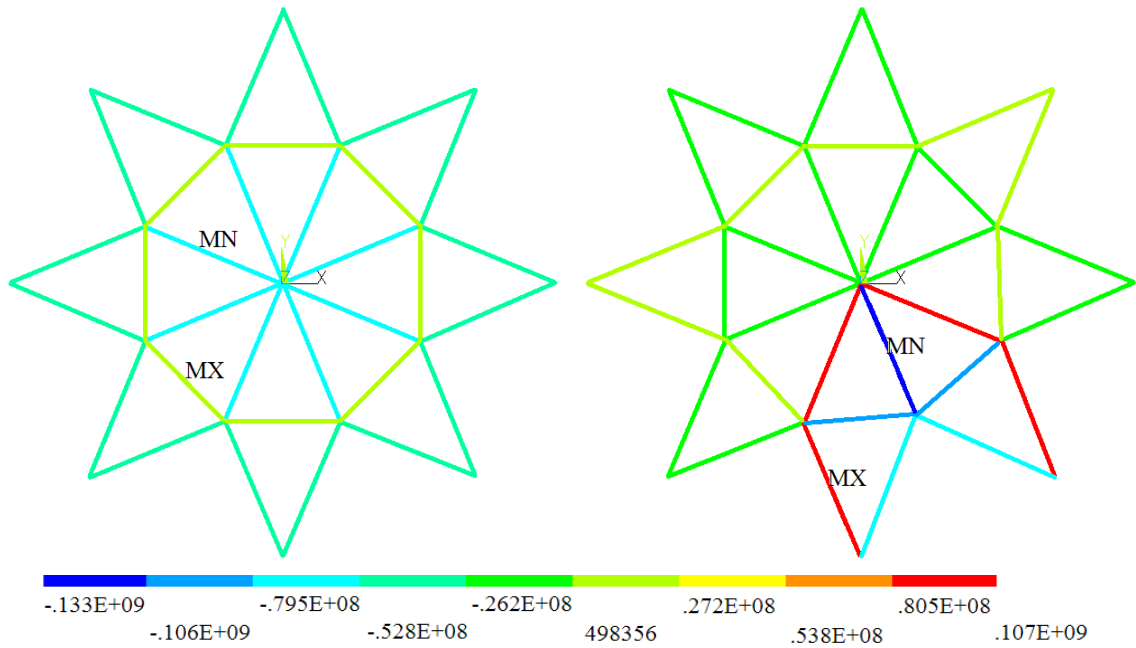


Figure 7.3 – Stress distribution in a truss structure with the initial design, showing loading case 1 (left) and loading case 2 (right) (MX and MN indicate the maximum and minimum stress, respectively) (Pa)

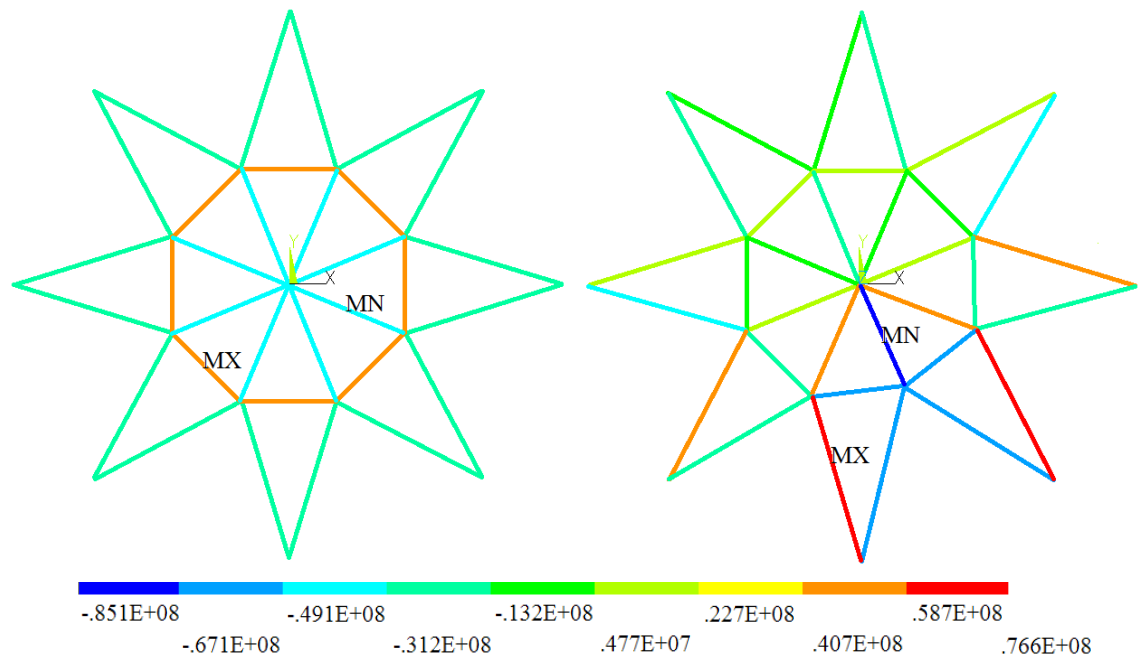


Figure 7.4 – Stress distribution in a truss structure with the optimised design, showing loading case 1 (left) and loading case 2 (right) (MX and MN indicate the maximum and minimum stress, respectively) (Pa)

7.2.4.2 Optimisation histories

Two different loading cases are simultaneously considered in this optimisation. The convergence histories in Figure 7.5 and Figure 7.6 show the trends in structural mass, sizing design variables, and geometrical design variables versus the number of iterations. The histories of RLI, maximum stress, and maximum displacement are shown in Figure 7.7–Figure 7.9, respectively.

Figure 7.5 shows an initially sharp decrease in structural mass. As a result, the cross-sectional areas of truss members A1 and A2 are reduced by approximately 48% and 33%, respectively, up to $n_i = 54$. In contrast, the cross-sectional area of A3 is increased by about 18%. At the same time, the maximum stress and maximum displacement show marked decreases (Figure 7.8 and Figure 7.9). To attain convergence, the height of the truss (Z2 and Z3) shows a marked increase (Figure 7.6).

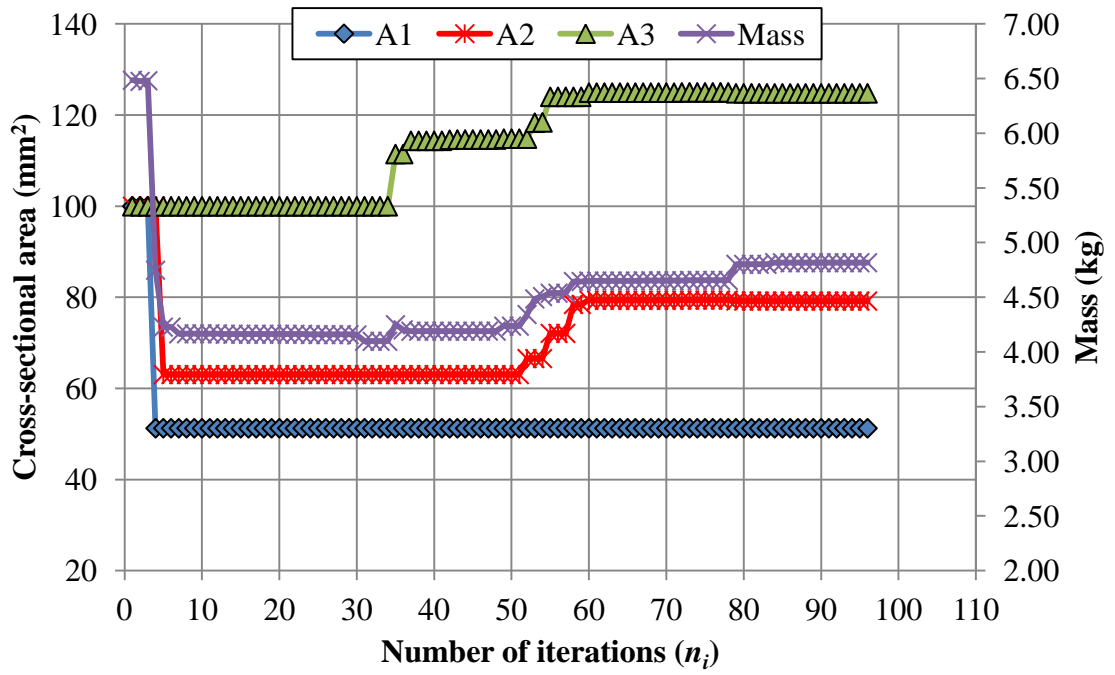


Figure 7.5 – Optimisation convergence histories of sizing design variables and structural mass

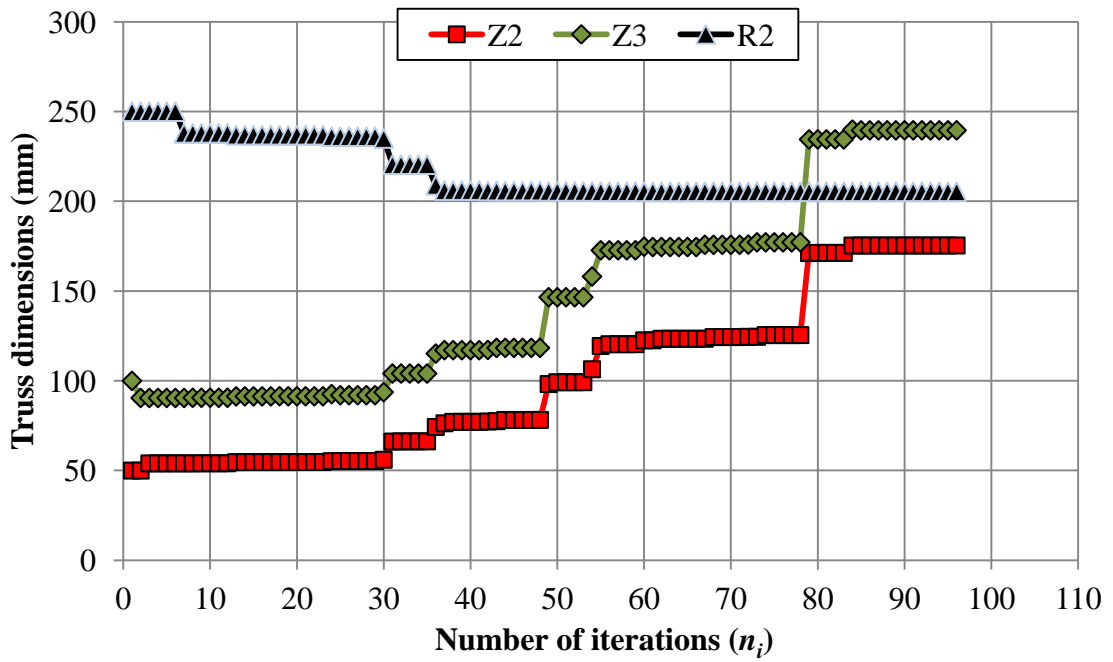


Figure 7.6 – Optimisation convergence histories of truss dimensions

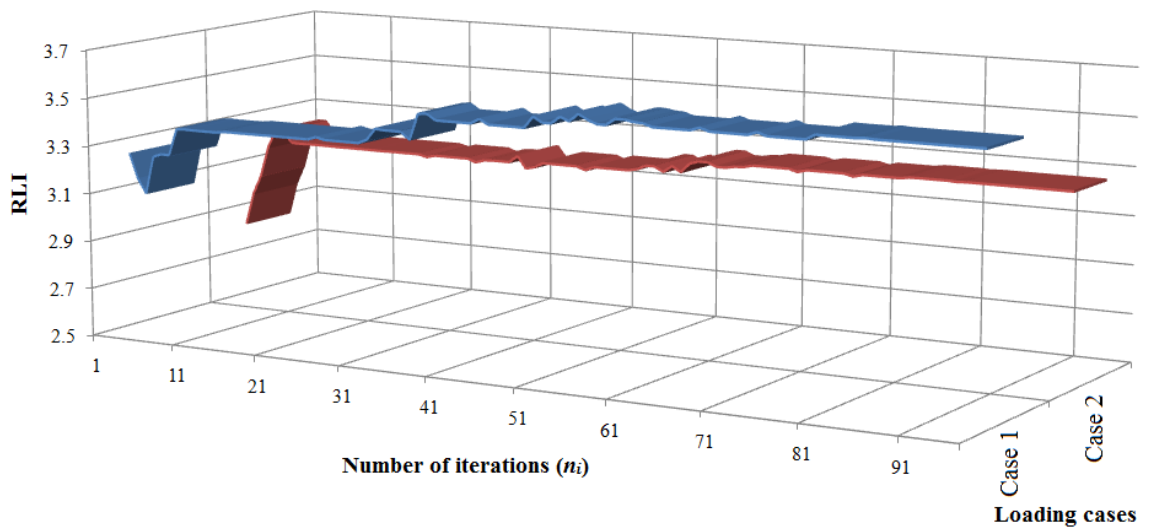


Figure 7.7 – Optimisation convergence history of the reliability loading-case index

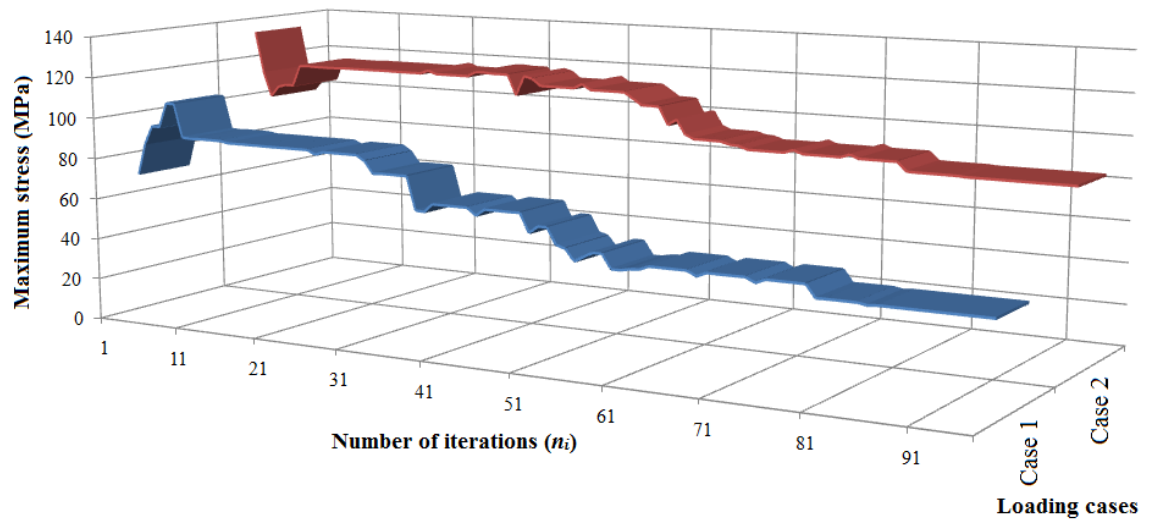


Figure 7.8 – Optimisation convergence history of maximum stress

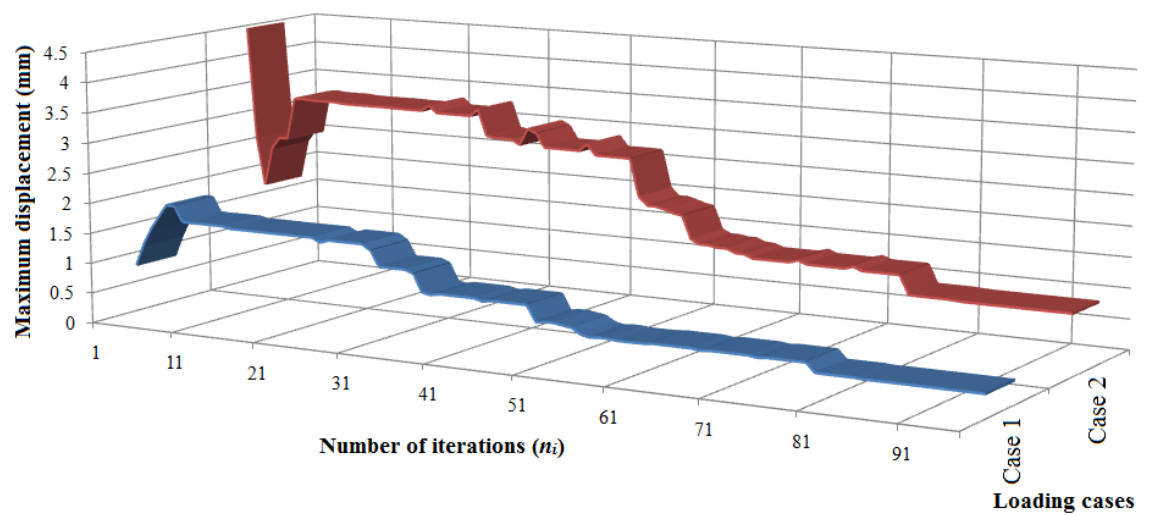


Figure 7.9 – Optimisation convergence history of maximum displacement

The initial minimal RLI and structural mass are 2.81 and 6.49 kg, respectively. Based on the properties of the material and the application of the star-like truss structure, σ_{lim} and δ_{lim} are set to be 100 MPa and 1 mm, respectively. The structural mass is required to be less than 4.9 kg. From these values (100 MPa, 1 mm, and 4.9 kg) and equation (4.16) in Chapter 4, the minimum acceptable value of RLI is 3.17. The design attributes are given in Table 7.4. The optimal design achieved a minimal RLI of 3.28 (a 16.5% increase compared with the initial value) and a structural mass of 4.82 kg (a 25.7% reduction). The optimised design satisfies all the design constraints and criteria. The design variables of the optimised design are given in Table 7.5.

Table 7.4 – Attributes of the initial and optimised designs of the star-like truss structure

		Loading case 1	Loading case 2
Maximum stress (MPa)	Initial	68.79	132.85
	Optimised	42.83	85.07
Maximum displacement (mm)	Initial	0.797	4.463
	Optimised	0.330	0.956
Mass (kg)	Initial	6.485	
	Optimised	4.817	
Reliability loading-case index	Initial	3.23	2.81
	Optimised	3.55	3.28

Table 7.5 – Truss dimensions and size of the initial and optimised star-like truss structure

Design variable	Initial design	Optimised design
A1 (mm ²)	100	51.28
A2 (mm ²)	100	79.19
A3 (mm ²)	100	124.80
R2 (mm)	250	205.38
Z2 (mm)	50	175.43
Z3 (mm)	100	239.60

7.3 Example 2 – Raised-access floor panel

7.3.1 Introduction

Here, the structural design of a raised-access floor panel is considered in order to examine the effectiveness of the proposed method. Such panels are used to provide an under-floor space for services. The panel is horizontal and is supported by adjustable vertical pedestals. The panel is elevated by the pedestals to create a space between the concrete floor slab and the raised-access floor (Figure 7.10). The panels are removable to allow rapid access to the under-floor area. The space can be used for the installation of, for example, electric power cables, data and telecommunication cables, environment control and air-conditioning equipment, and fire detection and suppression devices. The panels may be installed in general offices, computer rooms, laboratories, studios, auditoriums, etc. (The Access Flooring Company, 2008).

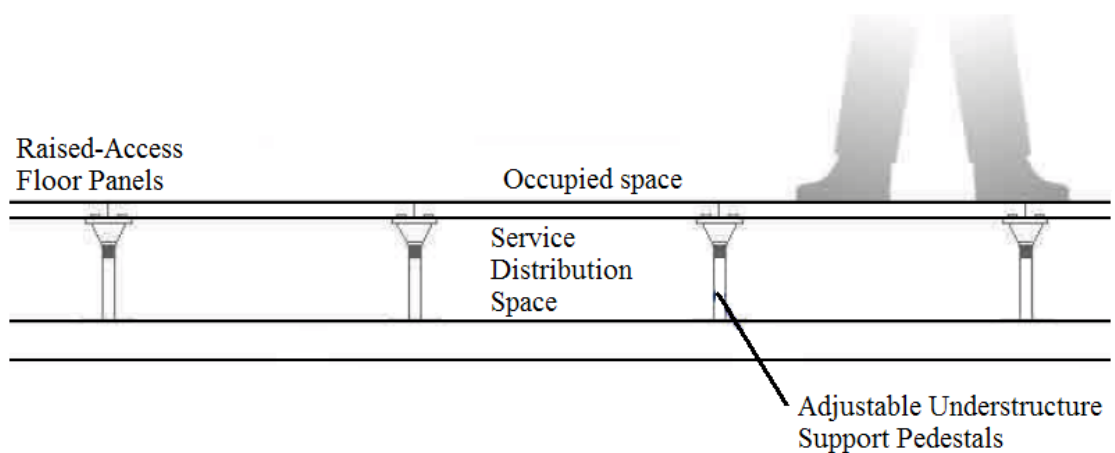


Figure 7.10 – Raised-access floor panels (The Access Flooring Company, 2008)

The panels are normally made of a combination of steel sheets and chipboard, thereby providing sufficient strength under specific loads. In commercial products, for example, the panels are made of a high-density particle board (HDPB) core encapsulated in a corrosion-resistant galvanised steel sheet (Figure 7.11). The panel may have various finish surfaces (e.g., vinyl, timber, stone, or glass) which are bonded directly onto the panel, thereby combining practicality and aesthetics.

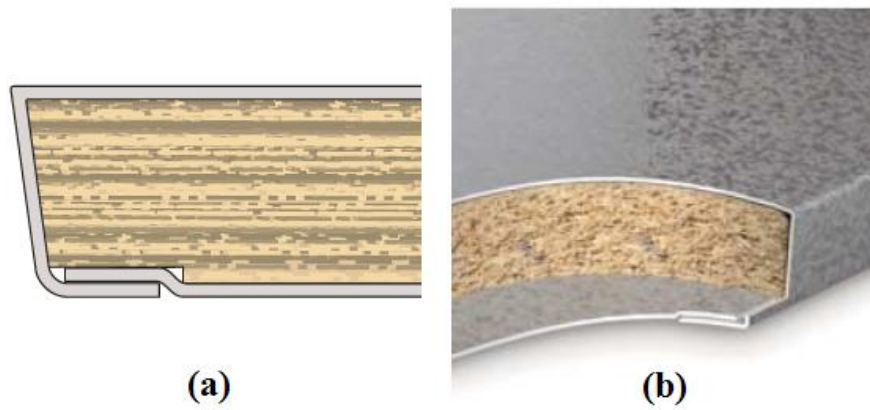


Figure 7.11 – Example of a steel-encapsulated HDPB floor panel (RG2 BS EN floor panel; see <http://www.fieldmansaccessfloorsltd.com/>)

No previous studies have investigated the use of bulk moulding compound (BMC) material in raised-access floor panels. In terms of mechanical and electrical properties, BMC has a high strength/stiffness–weight performance ratio, excellent dielectric properties, low thermal conductivity, and low tooling cost. Hence, in this research, BMC material is used in the design of a raised-access floor panel, which must satisfy the design constraints.

7.3.2 British Standard BS EN

British Standard BS EN 12825:2001 applies specifically to raised-access floor panels. This document states the required standards for raised-access floor systems in terms of ultimate load, safety factors, deflection under working load, and dimensional tolerances. Here, the raised-access floor panel is tested to its ultimate load, under a point load (25×25 mm area), until failure.

Raised-access floor panels have various classes of performance and should not exceed the limit requirements on stiffness and strength. The ultimate load is generally between 4 and 12 kN (Table 7.6), and the factor of safety is at least 2. The maximum deflection may be 2.5, 3.0, or 4.0 mm (Table 7.7). The panels are generally available in three sizes: 500×500 mm, 600×600 mm, and 750×750 mm.

Table 7.6 – Panel classification based on ultimate load

Class	Ultimate load (kN)
1	≥ 4
2	≥ 6
3	≥ 8
4	≥ 9
5	≥ 10
6	≥ 12

Table 7.7 – Panel classification based on deflection

Class	Deflection (mm)
A	≤ 2.5
B	≤ 3
C	≤ 4

BS EN flooring systems are classified using a standardised code; for example, a classification of 3/A/3/2 is explained as follows:

- ✎ ‘3’ indicates the ultimate load (in this case, ≥ 8 kN)
- ✎ ‘A’ indicates the deflection (in this case, ≤ 2.5 mm)
- ✎ ‘3’ indicates the factor of safety
- ✎ ‘2’ indicates the dimensional tolerances

Table 7.8 shows an example of the BS EN 12825 standard for various applications.

Table 7.8 – BS EN 12825 standard

Application	BS EN 12825 Classification		
	Light Use	Standard Use	Heavy Use
General Office	1/A/3/2	3/A/3/2	5/A/3/2
	1 kN working load	2.5 kN working load	3.3kN working load
Light Industries	4/A/3/2	6/A/3/2	6/A/3/2
	3 kN working load	4 kN working load	5 kN working load

7.3.3 Design constraints and loads

The structural design requirement of the raised-access floor panel is to find the optimum solution. The structure must satisfy all the design constraints in terms of strength and stiffness, and retain a low mass. In this example, σ_{lim} and δ_{lim} are set to be 100 MPa and 2.4 mm, respectively. In terms of boundary conditions, the nodes at the four corners of the panel are fixed (i.e., zero displacement). The analysis considers four different loading cases simultaneously (Figure 7.12): a central load ($F = 3$ kN), an edge load ($F = 3$ kN), a diagonal load ($F = 3$ kN), and a uniform distribution load ($P = 15$ kN/m²). Figure 7.13 shows a schematic diagram of the initial structure.

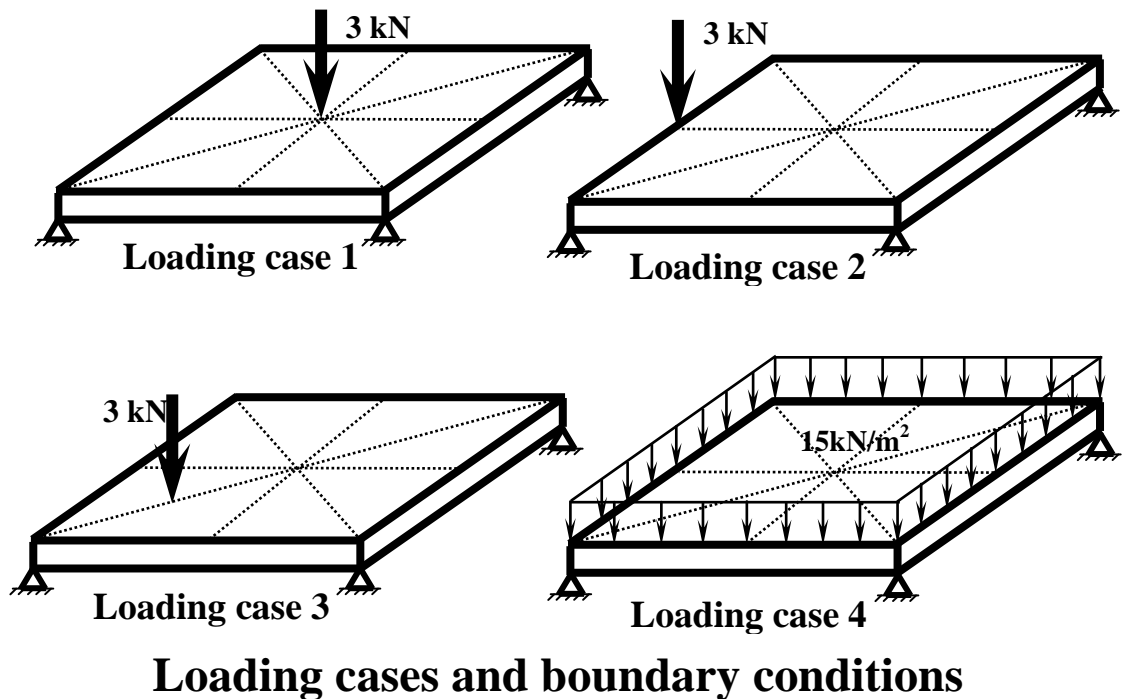


Figure 7.12 – Loading cases in the present analysis

Figure 7.13(a) shows the discretisation of the initial square symmetrical panel with a width of L mm and ribs with height H mm (Figure 7.13(b)). Table 7.9 lists the dimensions of 22 design variables in the structural model, including 11 cross-sectional thicknesses (T_1, T_2, \dots, T_{11}), 10 rib heights (Z_1, Z_2, \dots, Z_{10}), and the surface sheet thickness (TS). The exact positions of the design variables are shown in Figure 7.14. The minimum and maximum cross-sectional thicknesses ($x_{T_i}^{min}$ and $x_{T_i}^{max}$, respectively, where $i = 1, 2, \dots, 11$), rib heights ($x_{Z_i}^{min}$ and $x_{Z_i}^{max}$, respectively, where $i = 1, 2, \dots, 10$), and surface thickness (x_s^{min} and x_s^{max} , respectively) for each design variable are set to 1 and 20 mm, 1 and 51 mm, and 1 and 5 mm, respectively.

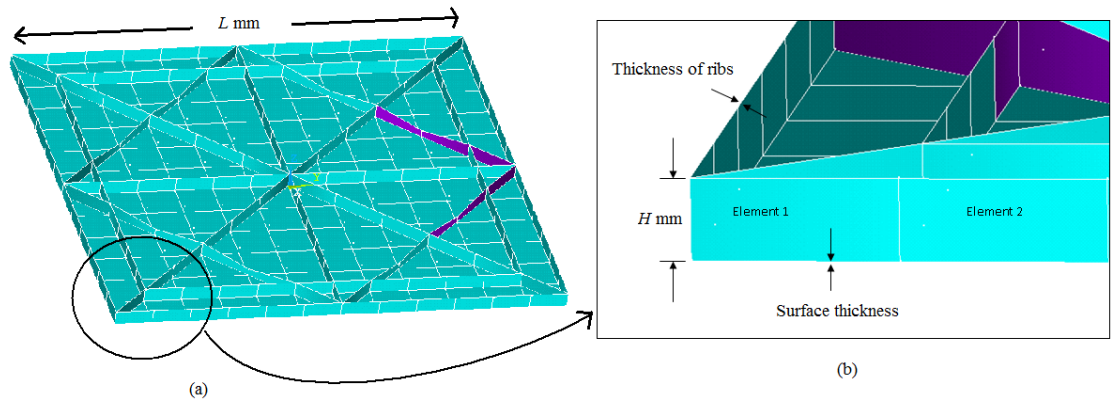


Figure 7.13 – (a) Discretisation of the initial structure, and (b) enlarged view of the panel

Table 7.9 – Initial dimensions of design parameters

Unit: mm	Z1	Z2	Z3	Z4	Z5	Z6	Z7	Z8	Z9	Z10	TS
Initial	20	10	4								
Unit: mm	T1	T2	T3	T4	T5	T6	T7	T8	T9	T10	T11
Initial	5	20	20	20	20						

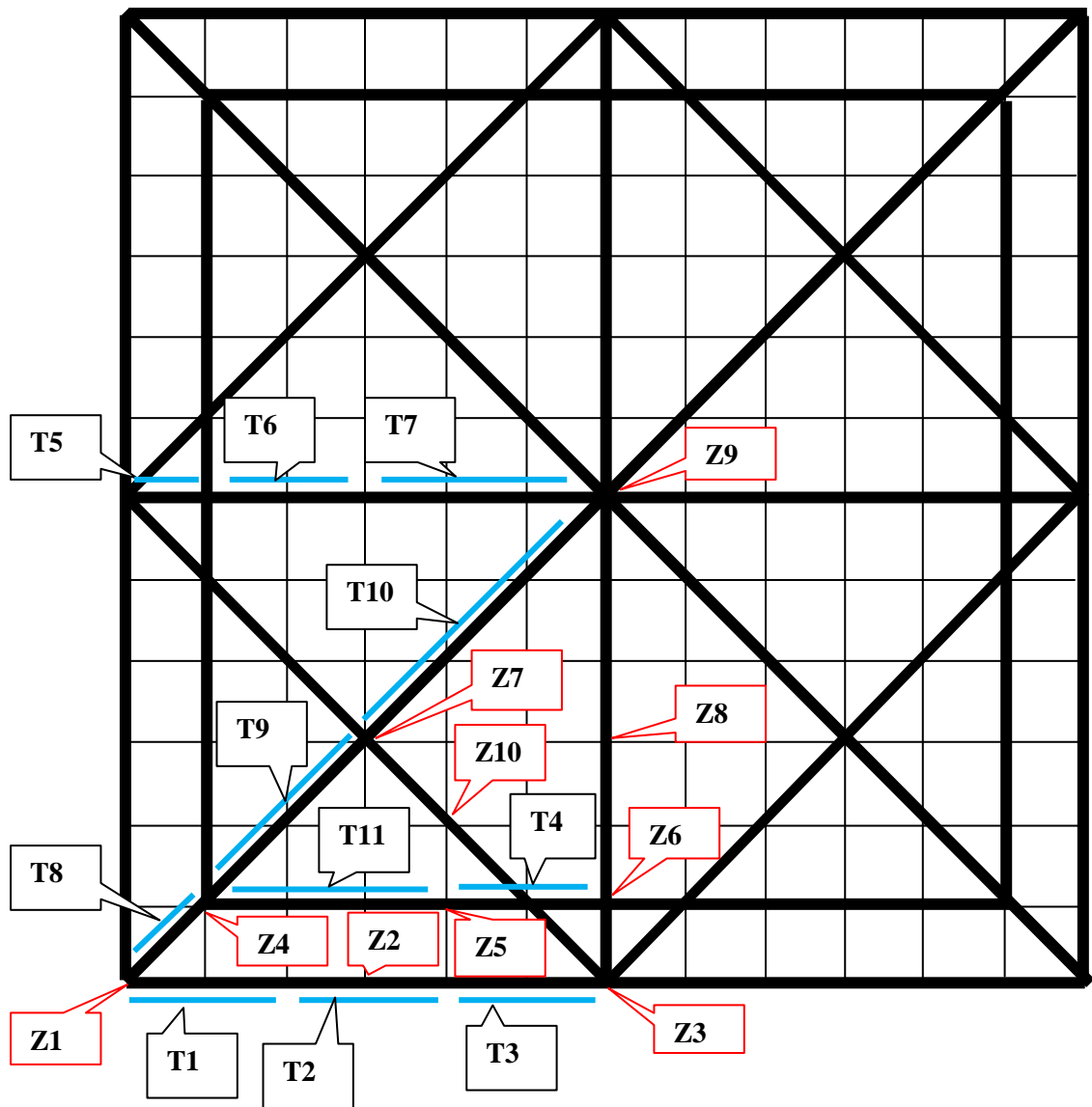


Figure 7.14 – Detail of design parameters

7.3.4 Finite element modelling of the panel

The raised-access floor panel is modelled using the finite element software ANSYS in conjunction with MOST. The ANSYS SHELL63 element is used to generate the finite element model, which consists of 304 quadrilateral elements. MOST uses the ‘input file’ approach in ANSYS to perform an optimisation procedure. The finite element modelling is executed using ANSYS commands rather than the graphical user interface. The ‘input file’ contains information on the improved design produced during each iteration; these data are required by the finite element code during the optimisation.

7.3.5 Optimisation of the raised-access floor panel

The most critical tasks in designing a raised-access floor panel are to optimise the structural performance, maximise RLI, and minimise the weight. It is desirable to design a panel with a minimum structural weight and that sustains the maximum load. BMC material is used to form the panel by injection-molding. BMC is an isotropic and linear elastic material. Table 7.10 lists the properties of the BMC materials used in the present analysis.

Table 7.10 – Material properties of BMC

Material property	Value
Young's Modulus (Y)	17 GPa
Yield Strength (σ_y)	100 MPa
Density (ρ)	2000 kg/m ³
Poisson's ratio (ν)	0.30

7.3.6 Results and discussions

7.3.6.1 Optimisation results

The sizing and shape optimisation of the raised-access floor panel required $n_i = 199$ iterations to converge. The initial and optimised finite element designs are shown in Figure 7.15. Figure 7.16 and Figure 7.17 show the distributions of von Mises stress and displacement for the optimised floor panel, respectively.

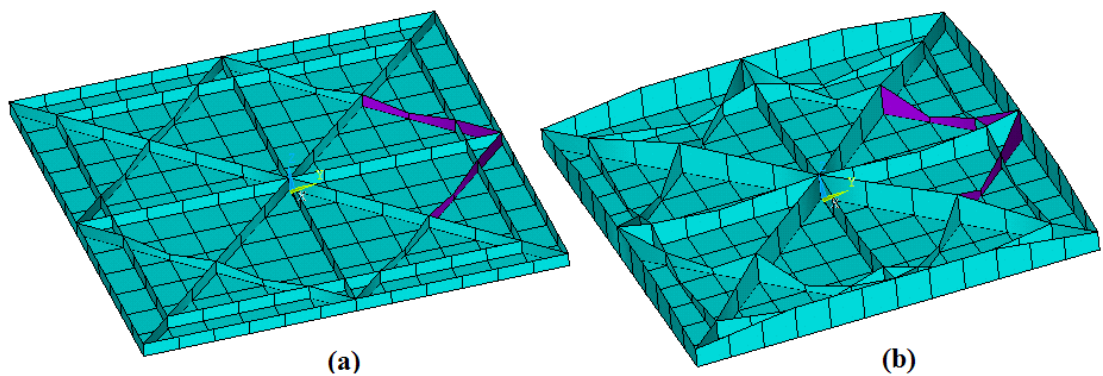


Figure 7.15 – Discretisation of the floor panel design, showing (a) the initial design and (b) the optimised design

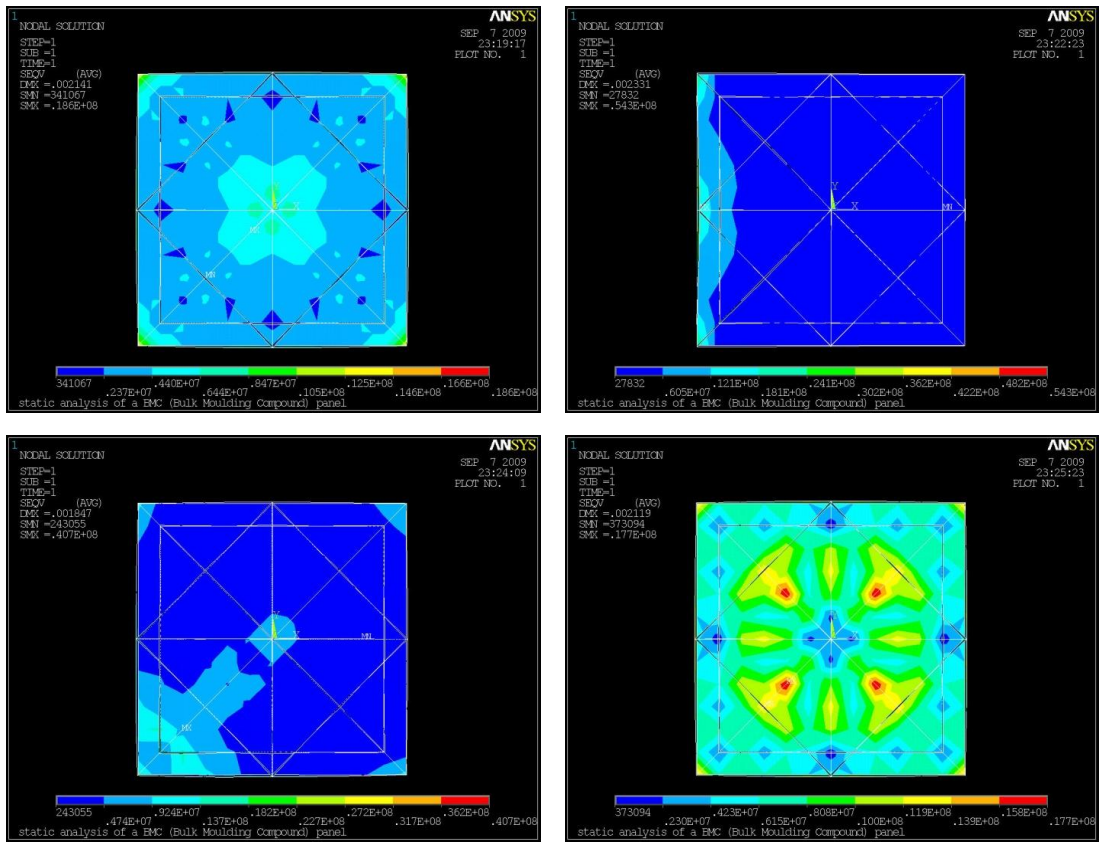


Figure 7.16 – Distribution of von Mises stress for the optimised floor panel, showing loading case 1 (top left), loading case 2 (top right), loading case 3 (bottom left), and loading case 4 (bottom right) (unit: Pa)

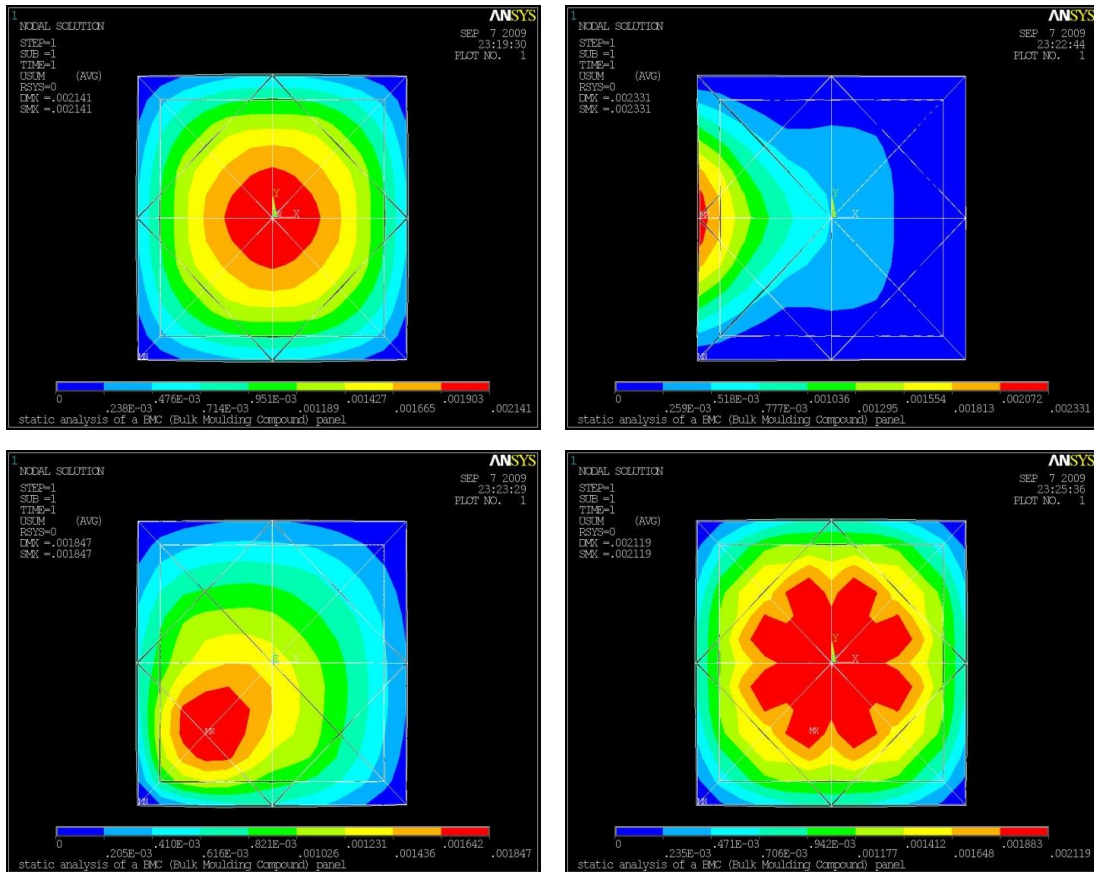


Figure 7.17 – Distribution of displacement for the optimised floor panel, showing loading case 1 (top left), loading case 2 (top right), loading case 3 (bottom left), and loading case 4 (bottom right) (unit: m)

7.3.6.2 Optimisation histories

In this optimisation, four different loading cases are considered simultaneously (centre load, diagonal load, edge load, and uniform distribution load). The convergence histories (Figure 7.18–Figure 7.21) show the trends in structural mass, maximum von Mises stress, maximum displacement, and reliability loading-case index with increasing number of iterations, for each loading case.

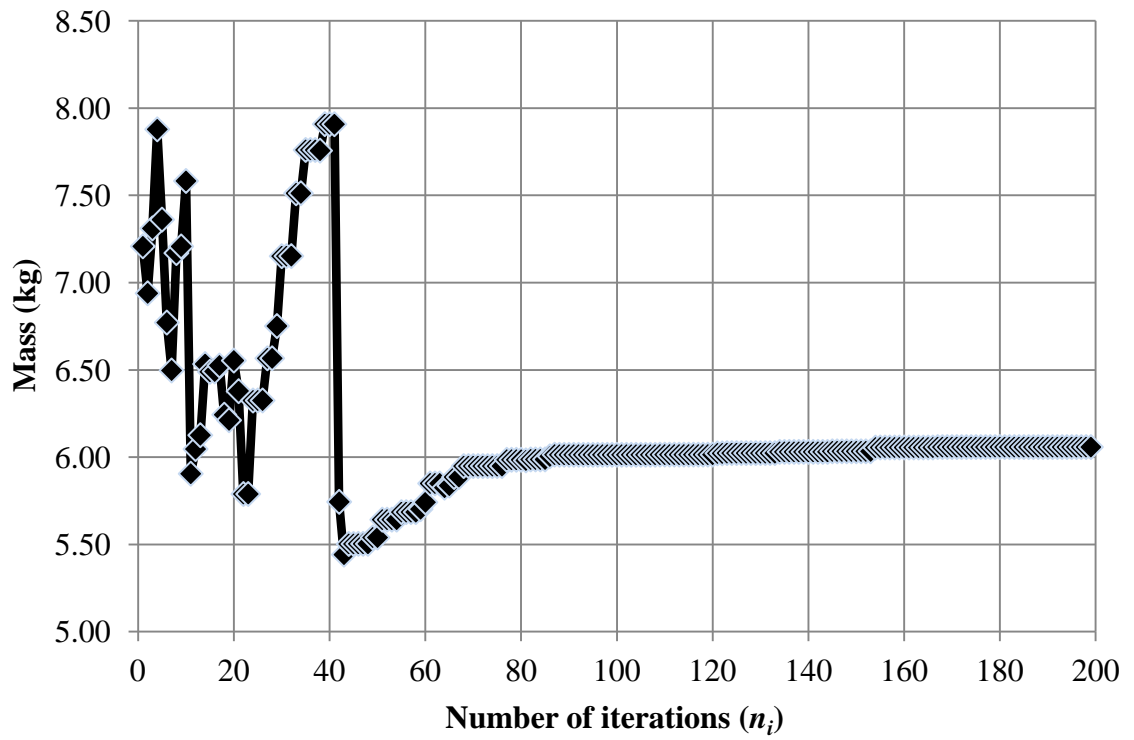


Figure 7.18 – Optimisation convergence history of mass

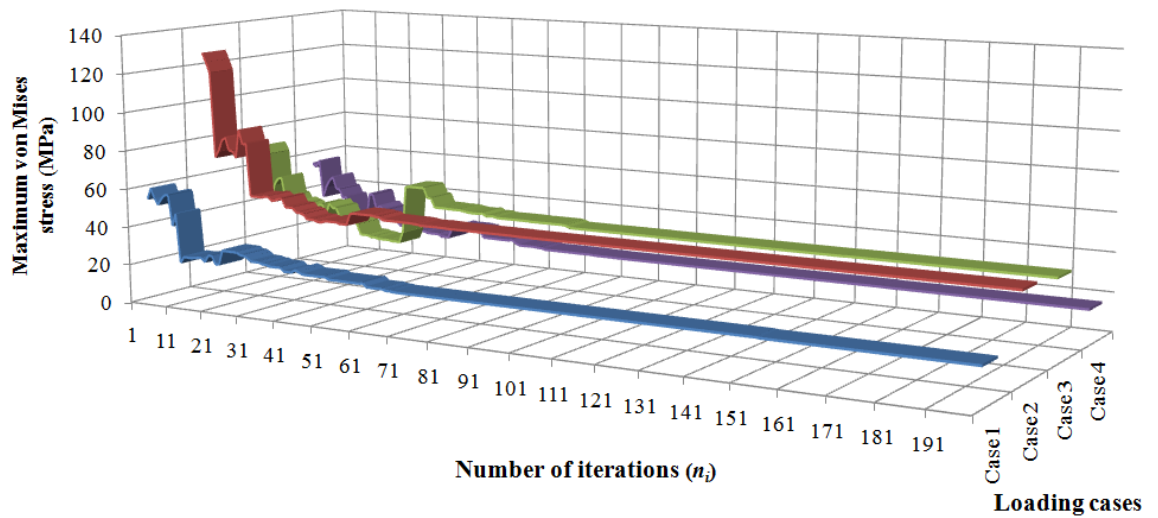


Figure 7.19 – Optimisation convergence history of maximum von Mises stress for four different loading cases

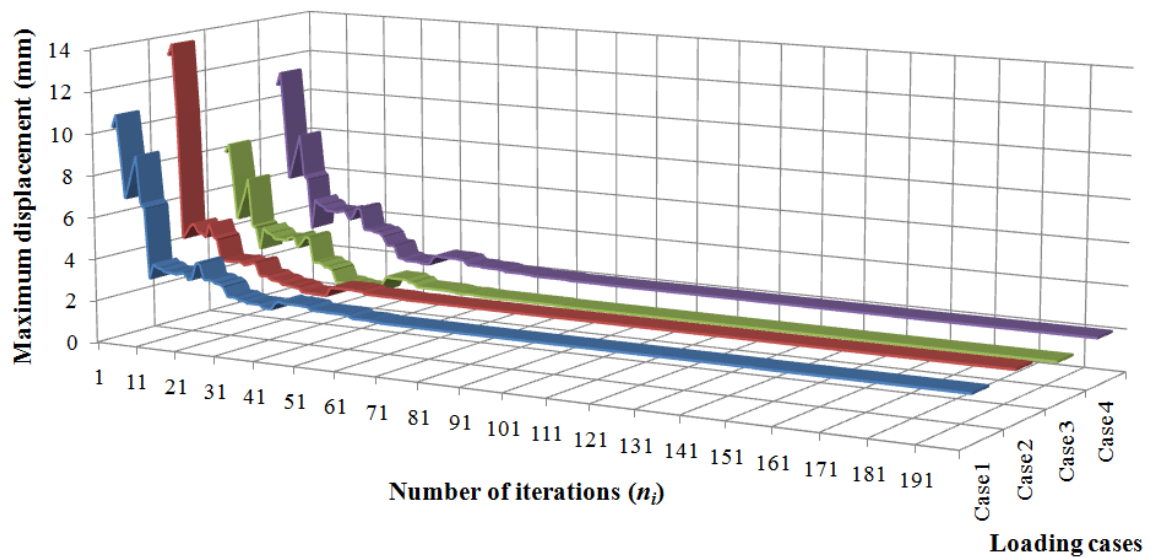


Figure 7.20 – Optimisation convergence history of maximum displacement for four different loading cases

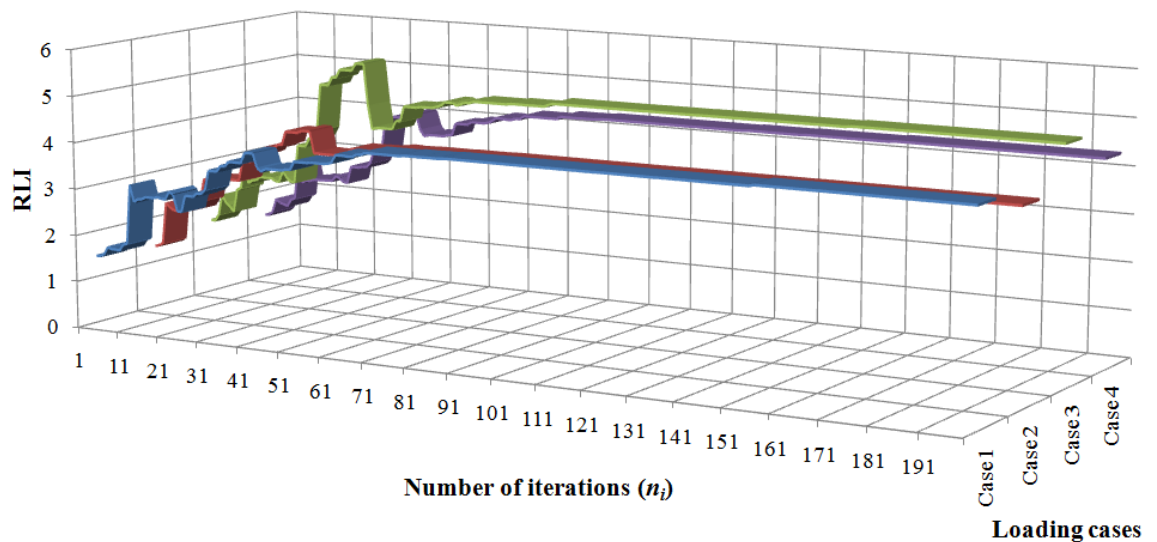


Figure 7.21 – Optimisation convergence history of reliability loading-case index for four different loading cases

Figure 7.18 shows initial fluctuations in the structural mass until attaining a maximum at $n_i = 38$, followed by a steep decrease until $n_i = 40$, due to the high sensitivity of the size to changes in rib height. This is followed by a gradually increase in structural mass, in order to satisfy all the design constraints; e.g., the maximum von Mises stresses, maximum displacements, and reliability loading-case index at each loading-case.

The initial minimal RLI and structural mass are 1.36 and 7.21 kg, respectively. Based on the properties of the BMC material and its application in raised-access floor panels, the values of σ_{lim} and δ_{lim} are 100 MPa and 2.4 mm, respectively. The structural mass is required to be less than 7 kg. From these values (100 MPa, 2.4 mm, and 7 kg) and the equation (4.16) in Chapter 4, the minimum acceptable value of the index is 3.87. This

RLI index shows that the original structure is under-designed for the applied safety index constraints.

The attributes of the initial and optimised designs are given in Table 7.11 and Table 7.12. The optimal design yielded a minimal *RLI* of 3.99 and a structural mass of 6.06 kg. The maximum von Mises stress and maximum displacement showed marked reductions from 126 to 43.4 MPa (loading case 2) and from 13.1 to 2.33 mm (loading case 2), respectively, in the optimised structure, thereby satisfying the target values. To reduce the high von Mises stress in the panel, the total thickness of the panel is increased to the maximum limit (51 mm). The mass is reduced from 7.21 to 6.06 kg, representing a 16% saving in BMC material.

Table 7.11 – Performance of the original design under four different loading cases

	Loading case 1	Loading case 2	Loading case 3	Loading case 4
Maximum von Mises stress (MPa)	52.8	126.0	68.4	53.0
Maximum displacement (mm)	10.1	13.1	7.76	10.6
Structural mass (kg)	7.21	7.21	7.21	7.21
Reliability loading-case index <i>RLI</i>	1.46	1.36	1.63	1.44

Table 7.12 – Performance of the optimised structure under four different loading cases

	Loading case 1	Loading case 2	Loading case 3	Loading case 4
Maximum von Mises stress (MPa)	18.6	43.4	40.7	17.1
Maximum displacement (mm)	2.14	2.33	1.85	2.12
Structural mass (kg)	6.06	6.06	6.06	6.06
Reliability loading-case index <i>RLI</i>	4.30	3.99	4.92	4.34

7.3.6.3 Stress distribution

Figure 7.22–Figure 7.24 show the distribution of the maximum (most positive) (S1) and minimum (most negative) (S3) principal stresses, and the xy -shear stress (τ_{xy}) for the optimised floor panel, respectively. The design solution obtained from finite element modelling consists of 753 nodes.

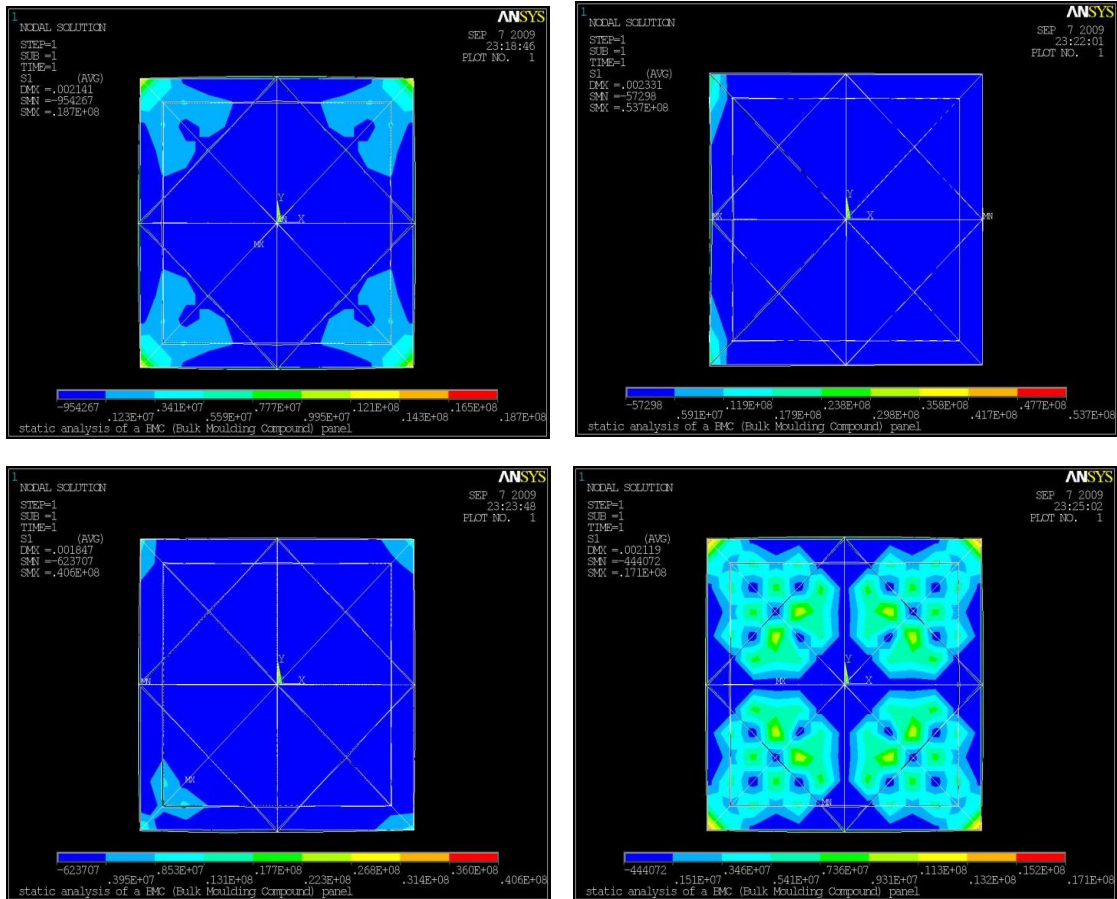


Figure 7.22 – Distribution of the most positive (tensile) stress for the optimised floor panel, for loading cases 1 (top left), 2 (top right), 3 (bottom left), and 4 (bottom right) (unit: Pa)

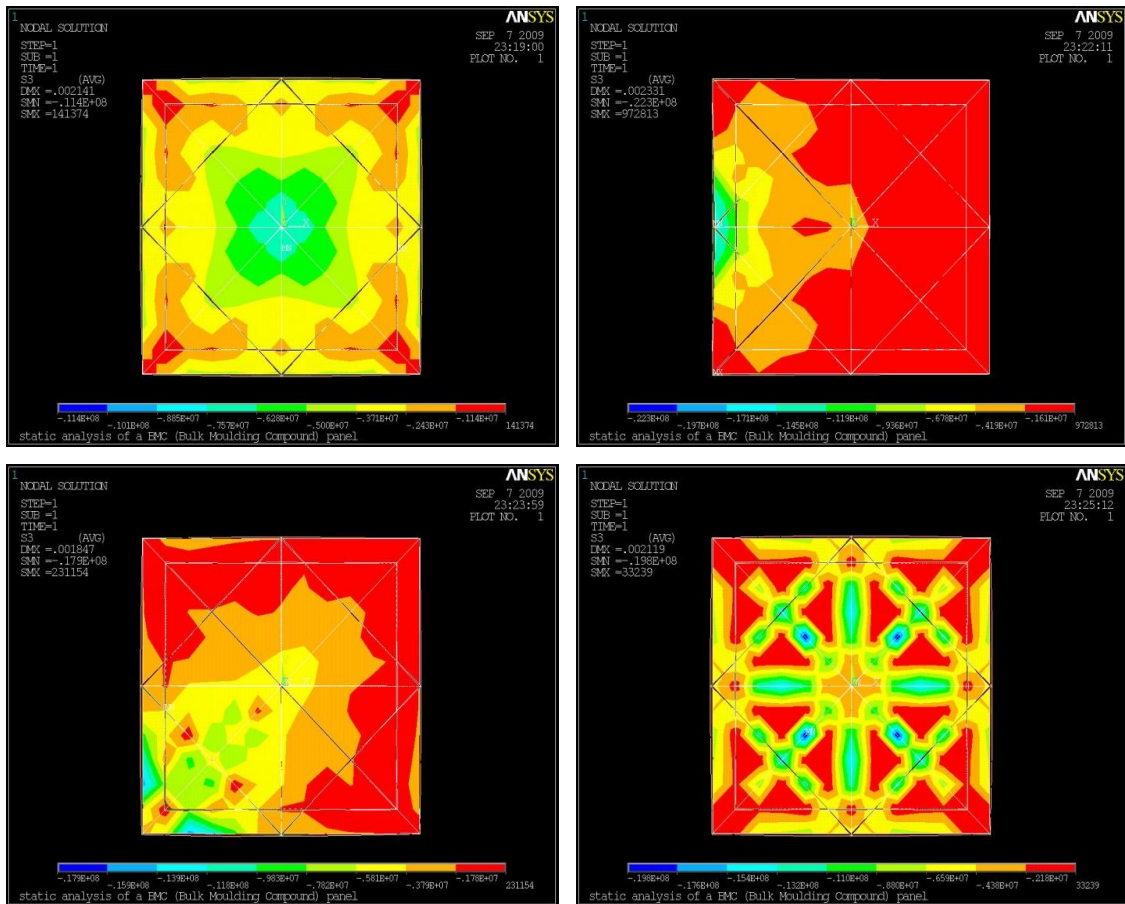


Figure 7.23 – Distribution of the most negative (compressive) stress for the optimised floor panel, for loading cases 1 (top left), 2 (top right), 3 (bottom left), and 4 (bottom right) (unit: Pa)

The maximum principal stress (S1) among the four loading cases varied from -0.95 to 53.7 MPa (Figure 7.22). The minimum principal stress (S3) varied from 0.03 to -22.3 MPa (Figure 7.23). The most positive (tensile) and most negative (compressive) stresses were found for loading case 2, at the point where the load was applied. This result was obtained because the panel is simply supported at the four corners, whereas the concentrated load was applied at the mid-span along an edge. The stresses were below the allowable stress of the material. The xy -plane is shown in Figure 7.24 because it has larger positive and negative values than the xy - and xz -shear planes. The τ_{xy} plots reveal that the shear stress varied from -9.33 to 19.6 MPa; hence, the structure remains safe under the applied loads.

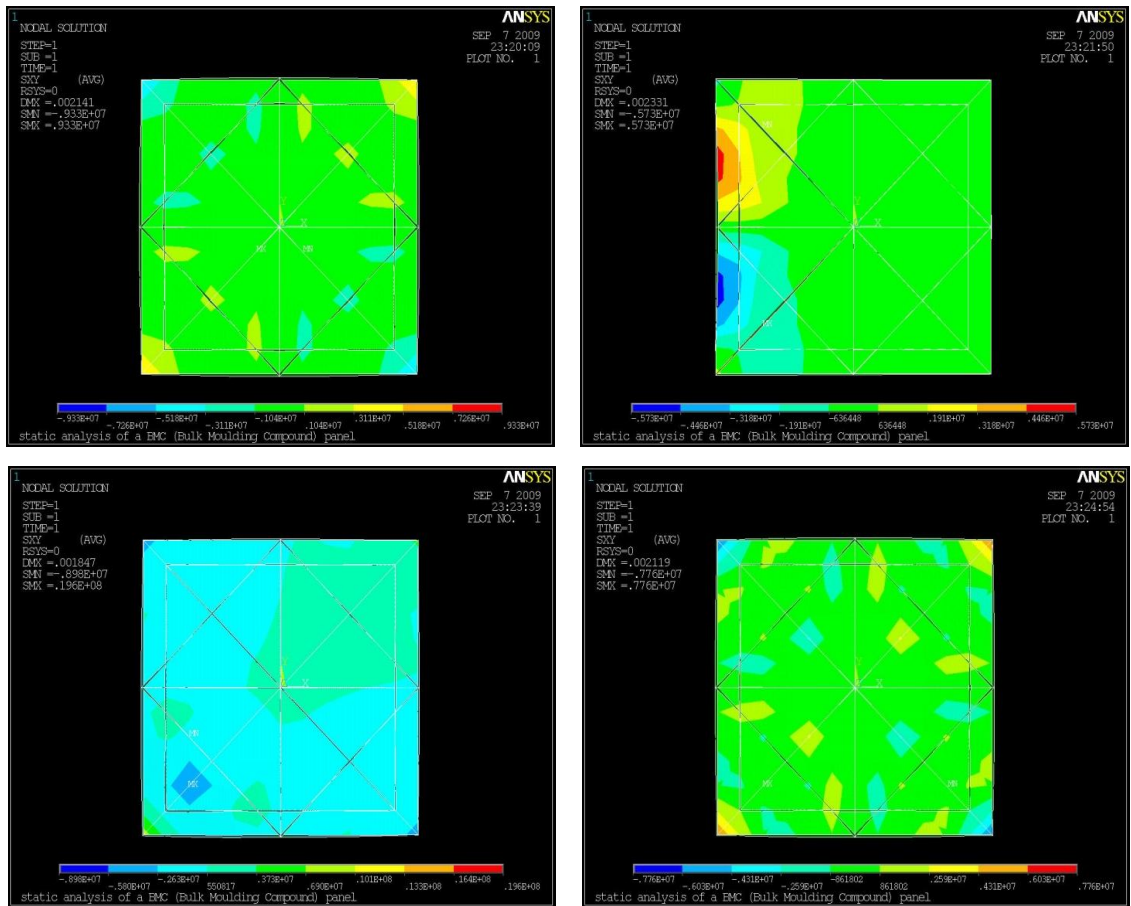


Figure 7.24 – Distribution of τ_{xz} shear stress for loading cases 1 (top left), 2 (top right), 3 (bottom left), and 4 (bottom right) (unit: Pa)

The results show that the reliability-related sizing/shape optimisation method presented in this research can be used to obtain a structurally optimised raised-access floor panel design with BMC material. Figure 7.25 and Figure 7.26 provide a more complete comparison of the initial and optimised designs of the panel for the four loading cases.

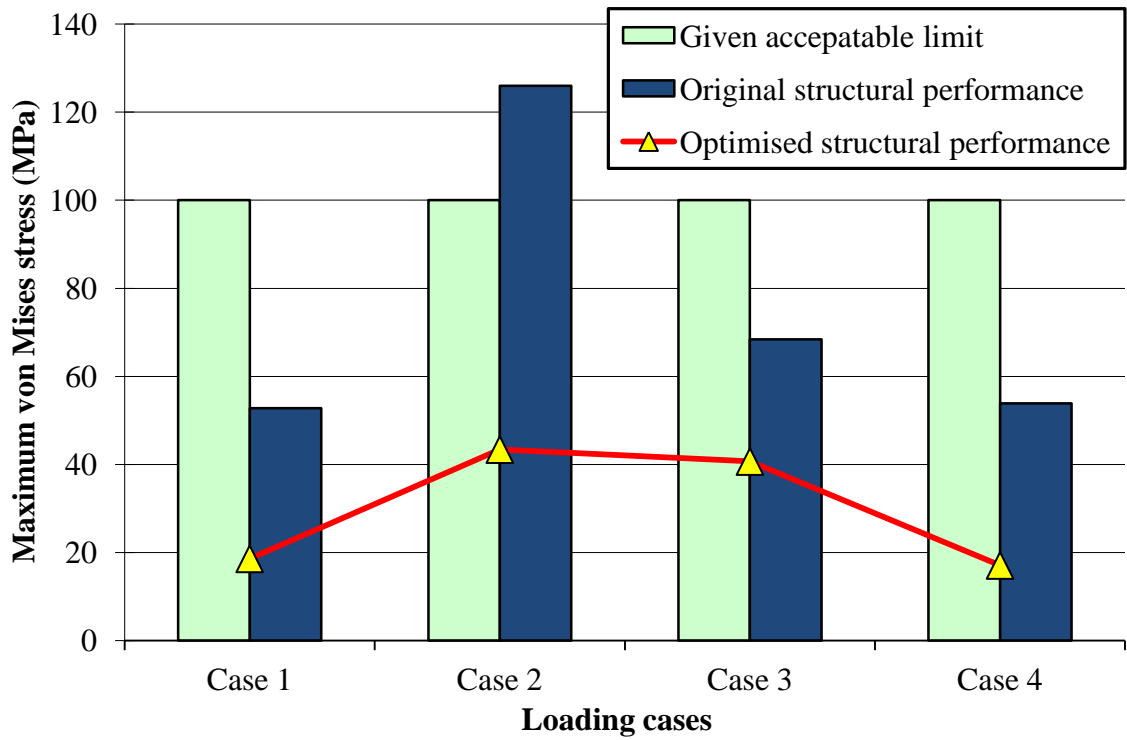


Figure 7.25 – Comparison of maximum von Mises stress for the original and optimised panels

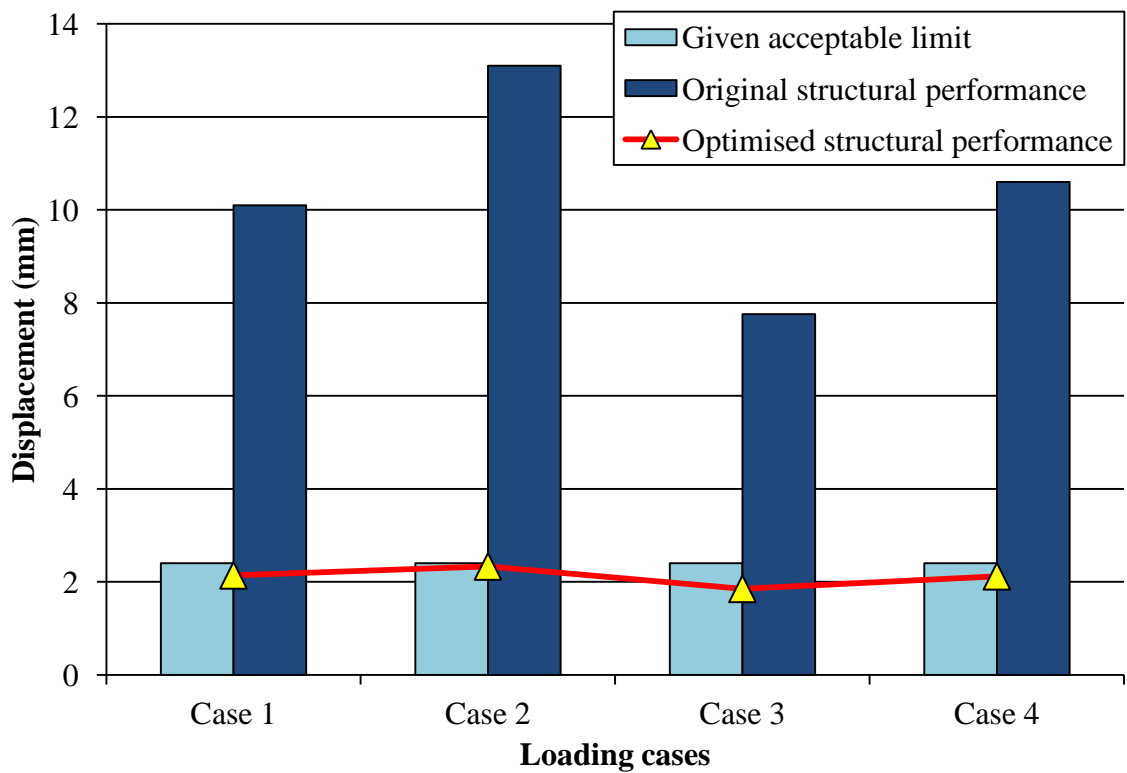


Figure 7.26 – Comparison of maximum displacement for the original and optimised panels

7.4 Summary

In this chapter, a method was presented that combines MOST (a method of multi-objective structural optimisation) with a reliability loading-case index (RLI; for calculating the structural reliability) using a parametric finite element model. The method can be used for reliability-related multi-factor optimisation of the structural performance of three-dimensional structural designs (e.g., mass, RLI, maximum stresses, and maximum deflections) under multi-loading cases.

The effectiveness and efficiency of the method was confirmed by its applications to optimising a star-like truss structure and a raised-access floor panel structure. The results show an overall improvement in the design of both structures, for which the value of RLI is greatly increased. The results also show that the combination of MOST and RLI is highly efficient in terms of optimisation. The proposed method was successful in identifying the optimum design for both case studies, resulting in improved performance for all loading cases.

8 Conclusions and Future Work

8.1 Summary of research

The key findings of this research (drawn from the earlier chapters) are summarised below.

- i) This study demonstrated the capability of the multifactor optimisation of structure techniques (MOST) as a unique optimisation technique. The optimisation technique was coupled with finite element software to determine the system responses as a function of design variables.
- ii) A multi-objective structural design was optimised (i.e., a sliding calliper, which is a component of an automotive braking system). The design considered requirements regarding mechanical strength, stiffness, and structural mass.
- iii) In this research, the MOST technique was extended to solve a multi-disciplinary design which simultaneously considered the amount of electrical power and structural performance. An energy harvesting device was optimised (i.e., a bimorph piezoelectric cantilever beam). The first optimised design was successfully achieved using sizing and shape methods in the optimisation. The design was further optimised by adding and changing the locations of holes, and changing their sizes/shapes, utilising the sizing and shape optimisation method to seek the optimum “topology” of the cantilever beam. The results yielded a better power density compared with the first optimised design.
- iv) A new reliability loading-case index (RLI) was developed, representing a modification of a well-known structural reliability approach—the first-order reliability method (FORM). The new index can be used to calculate the structural reliability. Thus, the MOST technique was extended to automatically accommodate the RLI. This new approach can be employed for reliability-related multifactor optimisation problems, enabling the optimisation of multi-objective, multi-disciplinary, and multi-loading cases, simultaneously.

- v) In this research, an optimisation method was proposed and developed that combines MOST (as a unique method of multi-objective structural optimisation) with a reliability loading-case index (as a means of calculating the structural reliability). This method was successfully applied in optimising a star-like truss structure and a raised-access floor panel structure. The optimised designs yielded significant improvements in structural performance and reliability.

8.2 Conclusions

This research initially sought to assess the effectiveness of MOST as a design optimisation method for multi-objective and multi-loading-case design problems, in which, the analyses considered mechanical strength–stiffness and structural mass. The research presented in this thesis demonstrated the design approach for various categories of problems involving requirements regarding mechanical strength, electrical power, and reliability, aimed at the design optimisation of engineering structures. The effectiveness of MOST was demonstrated in analyses of a sliding caliper and a bimorph cantilever beam. MOST was then extended to accommodate and execute reliability-related multifactor optimisation, and applied to a star-like truss structure and a raised-access floor panel structure, thereby demonstrating its capability in solving multi-objective, multi-disciplinary, and multi-loading-case optimisation problems, simultaneously. The reliability-related multifactor optimisation method, as presented in this thesis, is not limited to mechanical static or dynamic applications: it can also be applied to other fields, such as combining computational fluid dynamics, electromagnetics, and multi-physics applications within an optimisation process. The applications of this approach, as performed in the present research, are summarised below.

- a) The proposed method was successfully applied in optimising a sliding caliper (a component of a vehicle braking system). MOST formed the basis of the sizing and shape optimisation, which aimed to attain a lightweight design. The optimised design yielded a 17% saving in materials while satisfying the deflection and strength requirements. However, this example did not fully demonstrate the effectiveness of MOST as a unique optimisation method, as it considered only a single loading case.

- b) A subsequent multi-objective and multi-disciplinary optimisation demonstrated the effectiveness of MOST for a structural- and energy-optimisation problem. A wireless sensor component, used in energy harvesting, was studied to provide the renewable energy required to transmit data. A piezoelectric element is an excellent transducer in converting vibrational energy to electrical energy, and vice versa. This study analysed a bimorph cantilever beam as a piezoelectric element.

In this research, an equation (equation 6.16 in Chapter 6) was proposed for calculating the power output using a finite element method. The equation needs to be verified to enable its application in further analyses. First, the analysis sought to verify experimental results (Ooi, 2010), theoretical results (Roundy, 2003), and the results of a finite element simulation (current study), considering a rectangular cantilever beam. The results show good agreement between the finite element simulation and the theoretical results, which differ by approximately 4.5% in calculating the maximum power output. This result demonstrates that a finite element simulation can be used to simulate the behaviour of the cantilever beam under various boundary conditions. A comparison of the finite element results and the experimental results reveals that the maximum power output differs by ~20%. This discrepancy reflects the fact that the experimental results were affected by various conditions (e.g., the environment effect and energy lost within the connection). Therefore, the finite element simulation yields accurate and reliable results compared with theoretical values.

Next, a shape optimisation of the cantilever beam was considered using MOST, aiming to maximise the power output while satisfying the design constraints. The optimised result represented a 46% saving in piezoelectric and shim materials, and the maximum output power was increased by 25%. The optimisation was performed by assigning a weighting factor to each objective, which was considered in the MOST. An initial investigation demonstrated the validity of the MOST-optimised structure for the cantilever beam. This result paves the way for the application of MOST in terms of shape optimisation, which is the first stage of optimisation.

The second stage involved the design optimisation and discretisation of the size and shape of a structure, while satisfying the requirements regarding strength

and power density. Additional holes were applied to the domain region of the first-stage optimised design until the maximum output power was attained. Most of the design was based on maximising the power output, the average element stress, and displacement performance, while minimising the structural volume. The trade-off between the structural volume and the output power of a structure represents a great challenge in design optimisation. The removal of material results in reduced structural volume, which may affect the maximum power output. The optimised “topology” structure yielded a further 17.1% saving in build material and an 11.7% increase in power density compared with the first-stage optimised design. The results revealed that the application of MOST in sizing and shape optimisation was successful in optimising the bimorph cantilever beam. However, this example does not demonstrate all of the capabilities of MOST. To fully evaluate the effectiveness of this method, a multi-factor structural optimisation under multi-loading cases was considered in the next two examples.

- c) A structural reliability-related multi-factor optimisation method was developed and successfully applied to optimise a star-like truss structure and a raised-access floor panel structure. The optimisation technique presented here is applicable to multi-objective, multi-disciplinary, and multi-loading-case optimisation problems. The method employs MOST (for multi-objective structural optimisation) combined with a reliability loading-case index (as a way of calculating the structural reliability). Structural reliability is assessed using the widely employed first-order reliability method (FORM), chosen because it introduces a limit state condition in its simplest configuration. However, the limit state condition is not necessary during the optimisation, which greatly simplifies the process. Most of the structural design was based on maximising structural strength and stiffness, without considering the reliability index. The trade-off between the structural configuration and the value of the reliability index for the structure, under each loading case, represents a complication in terms of design optimisation. The use of MOST does not guarantee that every performance and every loading case is optimised, especially in the case of conflict with other objectives and when many loading cases are concurrently considered in an optimisation. In these examples, MOST optimisation satisfied all the design constraints and achieved the optimum solutions. The numerical

examples of the designs validate the effectiveness and efficiency of the proposed method.

8.3 Recommendations for future work

This research highlighted two potential areas of future work: the development of reliability analysis (as a means of calculating the structural reliability in an optimisation process) and improvements to MOST (as a unique method of multi-objective structural optimisation). Although design solutions were attained, there exists scope to improve the reliability-related multi-factor optimisation, as outlined below.

- a) Structural optimisation should be introduced into conceptual design. For example, an innovative design should be sought by optimisation under specified design constraints. This approach would produce new design concepts in engineering field which would be attractive to design engineers. In addition, multi-disciplinary optimisation must be considered whenever possible in conceptual designs in the future research.
- b) This research considered the use of smart materials. In a multi-disciplinary design optimisation, it is possible to further investigate a material which produces the targeted energy in a specific environment. Smart materials have unique properties and are of great interest to researchers in terms of their internal microscopic structure. Thus, an optimisation method should be used to determine the optimum structure of such materials. Future research should consider the combined optimisation of macro structures constructed with smart materials and the micro structures of the smart materials used simultaneously. The application of smart materials in a device used to generate renewable energy in a specific environment is also of interest.
- c) Although structural optimisation is able to solve some structural design problems, a new research direction is to simultaneously consider new conceptual, large-scale, robust and/or reliability-based design problems. The results of the optimisation must be accurate and precise, especially for multi-factor optimisation problems.

In this era of rapidly improving computational power, computer-aided design (CAD) and finite element analysis are important tools. For example, CAD software can be used to perform a structural analysis. CAD software and optimisation procedures are limited by the difficulty of automating the optimisation process, especially in terms of large geometrical changes. Thus, future advances in engineering design optimisation require the development of a method for designing and generating manufacturing data.

- d) The MOST technique can be further enhanced by introducing the topology method into this unique optimisation method. One of the objectives of structural design optimisation is to reduce the material cost by minimising the mass. Future research should seek to control the distribution of high- and low-stress elements by the optimisation procedure.
- e) Ideally, it would be useful to link reliability and optimisation methods using the FORM and MOST techniques, as used as a reliability-related multifactor optimisation method in this research. In addition, a choice of several reliability methods should be implement into the MOST technique, thereby enabling the solving of a specific design problem using a specified reliability method. This would offer an alternative design approach to structural engineers.
- f) Further improvement could be done on the examples presented in this thesis. As mentioned previously, the MOST technique should incorporate the topology optimisation method. In the piezoelectric cantilever beam example, a two-stage optimisation was employed: a sizing and shape optimisation, followed by seeking the optimum “topology” structure. The proposed two-stages optimisation could be improved if a “combined” approach could be devised; i.e., by considering a combined sizing, shape, and topology optimisation method.

For multi-factor optimisation, it is necessary to improve MOST, enabling it to execute fully automatic procedures of structural and reliability optimisation in solving sizing, shape, and topology design problems.

9 References

- Abido, M.A., 2002, Optimal power flow using particle swarm optimization, *International Journal of Electrical Power & Energy Systems* 24(7), pp. 563–571.
- Adeli, H., Kamal, O., 1992, Concurrent analysis of large structures--I. Algorithms, *Computers & Structures* 42(3), pp. 413–424.
- Afonso, A.M.B., Sienz, J., 1999, Investigation of different strategies to solve multicriteria structural shape optimisation problems, *Engineering Design Optimization, Proceedings of 1st ASMO/ISSMO conference*, MCB University press, Ilkley UK.
- Agarwal, H., Mozumder, C., Renaud, J., Watson, L., 2007, An inverse-measure-based unilevel architecture for reliability-based design optimization, *Struct Multidisc Optim* 33(3), pp. 217–227.
- Agarwal, H., Renaud, J., 2004, Reliability based design optimization using response surfaces in application to multidisciplinary systems, *Eng Optim* 36(3), pp. 291–311.
- Aguilar Madeira, J.F., Rodrigues, H.C., Pina, H.L., 2005, Multi-objective optimization of structures topology by genetic algorithms, *Adv Eng Softw* 36(1), *Evolutionary Optimization of Engineering Problems*, pp. 21–28.
- Andy Darvill, available online at <http://home.clara.net/darvill/altenerg/solar.htm>, [accessed on 30th July 2009].
- ANSYS, 2007, Release 11.0 Documentation for ANSYS, ANSYS Ltd.
- Aoues, Y., Chateauneuf, A., 2008, Reliability-based optimization of structural systems by adaptive target safety – Application to RC frames, *Structural Safety* 30(2), pp. 144–161.
- Aoues, Y., Chateauneuf, A., 2010, Benchmark study of numerical methods for reliability-based design optimization, *Struct Multidisc Optim* 41(2), pp. 277–294.
- Atrek, E., Gallagher, R.H., Ragsdell, K.M., Zienkiewicz, O.C. (eds), 1984, *New directions in optimum structural design*, John Wiley & Sons, Chichester.
- Au, S., 2005, Reliability-based design sensitivity by efficient simulation, *Comput Struct* 83(14), pp. 1048–1061.

- Au, S., Beck, J., 2001, Estimation of small failure probabilities in high dimensions by subset simulation, *Probab Eng Mech* 16(4), pp. 263–277.
- Augusti, G., Baratta, A., Casciati, F., 1984, *Probabilistic Methods in Structural Engineering*, Chapman and Hall, New York.
- Barakat, S., Bani-Hani, K., Taha, M.Q., 2004, Multi-objective reliability-based optimization of prestressed concrete beams, *Structural Safety* 26(3), pp. 311–342.
- Benham, P.P., Crawford, R.J., Armstrong, C.G., 1996, Addison Wesley Longman Limited, Singapore, pp. 67–68.
- Bennet, J.A., Botkin, M.E., 1986, *The optimum shape: Automated structural design*, General motors research laboratory symposia series, Plenum press, New York.
- Bert, C.W., Birman, V., 1998, Effects of stress and electric field on the coefficients of piezoelectric materials: one-dimensional formulation, *Mech. Res. Commun.* 25(2), pp. 165–169.
- Beyer, H.G., Schwefel, H.P., 2002, Evolution strategies—a comprehensive introduction, *Nat Comput* 1(1), pp. 3–52.
- Bichon, B., Eldred, M., Swiler, L., Mahadevan, S., McFarland, J., 2008, Efficient global reliability analysis for nonlinear implicit performance functions, *AIAA J* 46(10), pp. 2459–2468.
- Bichon, B., Mahadevan, S., Eldred, M., 2009, Reliability-based design optimization using efficient global reliability analysis, In: 50th AIAA/ASME/ASCE/AHS/ASC structures, structural dynamics, and materials conference, Palm Springs, California, AIAA 2009-2261.
- Bjerager, P., 1988, Probability integration by directional simulation, *Journal of Engineering Mechanics* 114(8), pp. 1285–1302.
- Bonnans, J.F., Gilbert, J., Lemaréchal, C., Sagastizábal, C., 2003, *Numerical optimization*, Springer, Heidelberg.
- Borri, A., Speranzini, E., 1997, Structural reliability analysis using a standard deterministic finite element code, *Structural Safety* 19(4), pp. 361–382.

- Bourinet, J.M., Mattrand, C., Dubourg, V., 2009, A review of recent features and improvements added to FERUM software, In: Proceedings of the 10th International Conference on Structural Safety and Reliability (ICOSSAR'09), Osaka, Japan.
- Box, G.E.P., Wilson, K.B., 1951, On the experimental attainment of optimum conditions, *J R Stat Soc Series B* (13), pp. 1–45.
- Breitung, K., 1994, Asymptotic approximations for probability integrals. In: *Lecture notes in mathematics*, vol 1592. Springer, Berlin.
- BS EN 12825:2001, Raised Access Floor.
- Bugeda, G., Ródenas, J.J., Oñate, E., 2008, An integration of a low cost adaptive remeshing strategy in the solution of structural shape optimization problems using evolutionary methods, *Computers and structures* 86, pp. 1563–1578.
- Caello, C.A.C., 2009. Available online at <http://www.lania.mx/~ccoello/EMOO/EMOObib.html#D> [accessed 20th Sept. 2010].
- Campbell, J.S., Kelliher, D., 2000, Structural shape optimisation of elastic continua: a study on nonlinearity and a 2D benchmark, *Engineering design optimisation*, Proc. Of the 2nd ASMO UK/ISSMO conference, Swansea, UK, pp. 65–72.
- Cardoso, J. B., de Almeida, J.R., Dias, J.M., Coelho, P.G., 2008, Structural reliability analysis using Monte Carlo simulation and neural networks, *Advances in Engineering Software* 39(6), pp. 505–513.
- Chan, K.Y., Skerlos, S., Papalambros, P., 2006, Monotonicity and active set strategies in probabilistic design optimization, *J Mech Des* 128(4), pp. 893–900.
- Chan, K.Y., Skerlos, S., Papalambros, P., 2007, An adaptive sequential linear programming algorithm for optimal design problems with probabilistic constraints, *J Mech Des* 129(2), pp. 140–149.
- Chandu, S., Grandhi, R., 1995, General purpose procedure for reliability based structural optimization under parametric uncertainties, *Adv Eng Softw* 23(1), pp. 7–14.
- Charnes, A., Cooper, W.W., 1959, Chance-constrained programming. *Manage Sci* 6(1), pp. 73–79.

- Chen, X., Hasselman, T., Neill, D., 1997, Reliability-based structural design optimization for practical applications, In: Proceedings of the 38th AIAA structures, structural dynamics, and materials conference, Florida.
- Chen, X., Lind, N.C., 1982, A new method for fast probability integration, paper no. 171, Waterloo, Canada: University of Waterloo.
- Cheng, G., Xu, L., Jiang, L., 2006, A sequential approximate programming strategy for reliability-based structural optimization, *Comput Struct* 84(21), pp. 1353–1367.
- Cheng, J., Li, Q.S., 2008, Reliability analysis of structures using artificial neural network based genetic algorithms, *Computer Methods in Applied Mechanics and Engineering* 197(45-48), pp. 3742–3750.
- Ching, J., Hsieh, Y., 2007a, Approximate reliability-based optimization using a three-step approach based on subset simulation, *J Eng Mech* 133(4), pp. 481–493.
- Ching, J., Hsieh, Y., 2007b, Local estimation of failure probability function and its confidence interval with maximum entropy principle, *Probab Eng Mech* 22(1), pp.39–49.
- Clark, C.S., 1995, *The Lanchester Legacy, a trilogy of Lanchester works, Vol 1*, Butler & Tanner, Frome and London, England, pp.1895–1931.
- Coello, C.A.C., Pulido, G.T., 2001, A micro-genetic algorithm for multiobjective optimization. In: *Evolutionary multi-criterion optimization, First international conference, EMO 2001, Zurich, Switzerland: Springer.*
- Corne, D., Jerram, N.R., Knowles, J., Oates, J., 2001, PESA-II: region-based selection in evolutionary multiobjective optimization, In: *Proceedings of the genetic and evolutionary computation conference (GECCO- 2001), San Francisco, CA.*
- Corne, D.W., Knowles, J.D., Oates, M.J., 2000, The Pareto envelope-based selection algorithm for multiobjective optimization, In: *Proceedings of sixth international conference on parallel problem solving from Nature, Paris, France: Springer.*
- Cornell, 1969, probability-based structural code, *J Amer Concrete Inst* 66(12), pp. 974–985.

- Cox, D., Reid, N., 2000, *The theory of the design of experiments*, Chapman & Hall/CRC, Boca Raton, United States.
- Das, I., Dennis, J. E., 1998, Normal-Boundary Intersection: A New Method for Generating Pareto Optimal Points in Multicriteria Optimization Problems, *SIAM Journal on Optimization* 8(3), pp. 631–657.
- de Weck, O.L., 2004, Multiobjective optimization: History and promise, In Proc. 3rd China-Japan-Korea Joint Symp. Optimization Structural Mech. Syst. Invited Keynote Paper GL2-2, Kanazawa, Japan.
- Deb, K., Pratap, A., Agarwal, S., Meyarivan, T., 2002, A fast and elitist multiobjective genetic algorithm: NSGA-II, *IEEE Trans Evol Comput* 6(2), pp. 182–97.
- Deng, J., 2006, Structural reliability analysis for implicit performance function using radial basis function network, *International Journal of Solids and Structures* 43(11-12), pp. 3255–3291.
- Deng, J., Gu, D.S., Li, X.B., Yue, Z.Q., 2005, Structural reliability analysis for implicit performance functions using artificial neural network, *Structural Safety* 27(1), pp. 25–48.
- Der Kiureghian, A., Dakessian, T., 1998, Multiple design points in first and second-order reliability, *Structural Safety* 20(1), pp. 37–49.
- Der Kiureghian, A., Haukaas, T., Fujimura, K., 2006, Structural reliability software at the University of California, Berkeley, *Structural Safety* 28(1-2), *Structural Reliability Software*, pp. 44–67.
- Der Kiureghian, A., Zhang, Y., 1999, Space-variant finite element reliability analysis, *Comp Methods Appl Mech Eng* 168(1–4), pp. 173–183.
- Der Kiureghian, A., Zhang, Y., Li, C.C., 1994, Inverse reliability problem, *J Eng Mech* 120(5), pp. 1154–1159.
- Díaz, A.R., Bendsøe, M.P., 1992, Shape optimization of structures for multiple loading conditions using a homogenization method, *Structural and Multidisciplinary Optimization* 4(1), pp. 17–22.

- Ditlevsen, O., 1979a, Generalized second moment reliability index, *Journal of structural mechanics* 7(4), pp. 435–451.
- Ditlevsen, O., 1979b, Narrow reliability bounds for structural systems, *Journal of structural mechanics* 7(4), 453–472.
- Ditlevsen, O., Madsen, H., 1996, *Structural reliability methods*, John Wiley & Sons, New York, NY.
- Du, X., Chen, W., 2004, Sequential optimization and reliability assessment method for efficient probabilistic design, *J Mech Des* 126(2), pp. 225–233.
- Edgeworth, F.Y., 1881, *mathematical physics*, P.Keagan, London, England.
- Elhewy, A.H., Mesbahi, E., Pu, Y., 2006, Reliability analysis of structures using neural network method, *Probabilistic Engineering Mechanics* 21(1), pp. 44–53.
- Enevoldsen, I., Sørensen, J., 1994, Reliability-based optimization in structural engineering, *Structural Safety* 15(3), pp. 169–196.
- Engelund, S., Rackwitz, R., 1993, A benchmark study on importance sampling techniques in structural reliability, *Structural Safety* 12(4), pp. 255–276.
- Erbatur ,F., Hasancebi, O., Tutuncu, I., Kilic, H., 2000, Optimal design of planar and space structures with genetic algorithms, *Computers & Structures* 75(2), pp. 209–224.
- Fernandes, L., Figueiredo, I., Júdice, J., Costa, L., Oliveira, P., 1998, Application of genetic algorithms to plate optimization, In: Idelsohn, S.R., Oñate, E., Dvorkin, E., (eds.), *Computational mechanics, new trends and applications*, Barcelona: CIMNE.
- Fiessler, B., Neumann, H.J., Rackwitz, R., 1979, Quadratic limit states in structure reliability, *ASCE J. Eng. Mech. Div.* 105(4), pp. 661–676.
- Flynn, A.M., Sanders, S.R., 2002, Fundamental limits on energy transfer and circuit considerations for piezoelectric transformers, *IEEE Transactions on Power Electronics* 17(1), IEEE, pp. 8–14.
- Fonseca, C.M., Fleming, P.J., 1993, Multiobjective genetic algorithms, In: IEE colloquium on ‘Genetic Algorithms for Control Systems Engineering’ (Digest No. 1993/130), London, UK: IEE.

- Fonseca, C.M., Fleming, P.J., 1995a, Multiobjective optimization and multiple constraint handling with evolutionary algorithms I: A unified formulation, Tech. Rep. 564, University of Sheffield, Sheffield, UK.
- Fonseca, C.M., Fleming, P.J., 1995b, Multiobjective optimization and multiple constraint handling with evolutionary algorithms II: Application example, Tech. Rep. 565, University of Sheffield, Sheffield, UK.
- Foschi, R., Li, H., Zhang, J., 2002, Reliability and performance-based design: a computational approach and applications, *Structural Safety* 24(2–4), pp. 205–218.
- Fourie, P.C., Groenwold, A.A., 2002, The particle swarm optimization algorithm in size and shape optimization, *Structural and Multidisciplinary Optimization* 23(4), pp. 259–267.
- Freudenthal, A., 1956, Safety and the probability of structural failure, *ASCE Trans* 121, pp. 1337–1397.
- Galhardi, M.A., Guilherme, T.H., Junior, V.L., 2008, A review of power harvesting on mechanical vibration using piezoelectric materials and applications, 7th Brazilian Conference on Dynamics, Control and Applications, Brazil.
- Gallas, Q., Wang, G., Papila, M., Sheplak, M., Cattafesta, L., 2003, Optimization of synthetic jet actuators, 41st AIAA Aerospace Sciences Meeting and Exhibit, Reno, NV, USA, AIAA-2003-0635.
- Gasser, M., Schuëller, G., 1997, Reliability-based optimization of structural systems, *Math Methods Oper Res* 46(3), pp. 287–307.
- Gere, J.M., Timoshenko, S.P., 1991, *Mechanics of Materials*, Chapman & Hall, London, UK, pp. 772.
- Gilbert, J.M., Balouchi, F., 2008, Comparison of energy harvesting systems for wireless sensor networks, *International Journal of Automation and Computing* 5(4), pp. 334–347.
- Glynne-Jones, P., Beeby, S.P., James, E.P., White, N.M., 2001, The modelling of a piezoelectric vibration powered generator for Microsystems, *Proceedings of the 11th International Conference on Solid-State Sensors and Actuators, Transducers 2001 and Eurosensors XV, Munich, Germany (2001)*, pp. 46–49.

- Goldberg, D. E., 1989, Genetic algorithms in search, optimisation and machine learning, Addison-Wesley Publishing Company, Reading, UK.
- Goldschmidtboeing, F., Woias, P., 2008, Characterization of different beam shapes for piezoelectric energy harvesting, *Journal of micromechanics and microengineering* 18(10), 104013, 7pp.
- Gollwitzer, S., Kirchgäßner, B., Fischer, R., Rackwitz, R., 2006, PERMAS-RA/STRUREL system of programs for probabilistic reliability analysis, *Structural Safety* 28(1-2), *Structural Reliability Software*, pp. 108–129.
- Griffith, R.E., Stewart, R.A., 1961, A nonlinear programming technique for the optimisation of continuous processing systems, *Management science* 7, pp. 379–392.
- Grooteman, F., 2008, Adaptive radial-based importance sampling method for structural reliability, *Structural Safety* 30(6), pp. 533–542.
- Guo, Y.W., Li, W.D., Mileham, A.R., Owen, G.W., 2009, Applications of particle swarm optimisation in integrated process planning and scheduling, *Robotics and Computer-Integrated Manufacturing* 25(2), pp. 280–288.
- Ha, S.K., Kim, Y.H., 2002, Analysis of a piezoelectric multi-morph in extentional and flexural motions, *Journal of Sound and Vibration* 253(5), pp. 1001–1014.
- Haldar, A., Mahadevan, S., 1995, First-order and second-order reliability method, In: Sundararajan, C., (ed.) *Probabilistic structural mechanics handbook – theory and industrial applications*, New York: Chapman & Hall, pp. 29.
- Haftka, R.T., Gürdal, Z, 1992, *Element of structural optimization*, Kluwer academic press, Dordrecht.
- Hajela, P., Lin, C-y., 1992, Genetic search strategies in multicriterion optimal design, *Struct Optimization* 4(2), pp. 99–107.
- Harper, G.A., 1998, *brakes and friction materials: the history and development of the technologies*, mechanical engineering publications limited, London, England.
- Hartman, D., Neumann, M., 1989, Structural optimization of a box girder bridge by means of the finite strip method, *Computer Aided Optimum Design of Structures*, Eds. Brebbia, C.A., Hernandez, S., pp. 337–346.

- Hasofer, A.M., Lind, N.C., 1974, Exact and invariant second-moment code format, *J. Eng MEch. Div. ASCE* 100(1), pp. 111–121.
- Hill, W.J., Hunter, W.G., 1966, A review of response surface methodology: A literature survey, *Technometrics* 8(4), pp. 571–590.
- Hilton, H., Feigen, M., 1960, Minimum weight analysis based on structural reliability, *J Eerosp Sci* 27(9), pp. 641–652.
- Hinton E., Rao, N.V.R., 1994, Structural shape optimization of shells and folded plates using two noded finite strips, *Computers and Structures* 46, pp. 1055–1071.
- Hinton, E., Rao, N.V.R., 1993, Analysis and shape optimization of variable thickness prismatic folded plates and curved shells. Part II: shape optimization, *Thin Walled Structures* 17, pp.161–183.
- Hohenbichler, M., Rackwitz, R., 1981, Nonnomal dependent vectors in structural reliability, *Journal of the Engineering mechanics Division, ASCE* 107(6), pp. 1227–1238.
- Holland, J.H., 1975, *Adaptations in natural and artificial systems*, MIT Press, London.
- Horn, J., Nafpliotis, N., Goldberg, D.E., 1994, A niched Pareto genetic algorithm for multiobjective optimization, *Proc. 1st IEEE ICEC (Orlando, USA, June 27-29, 1994)*, pp. 82–87.
- Hossain, F., Anagnostou, E. N., Bagtzoglou, A.C., 2006, On Latin Hypercube sampling for efficient uncertainty estimation of satellite rainfall observations in flood prediction, *Computers & Geosciences* 32(6), pp. 776–792.
- Hwang, W.S., Park, H.C., 1993, Finite element modelling of piezoelectric sensors and actuators, *AIAA Journal*, 31(5), pp. 930–937.
- Ikeda, T. 1996, *Foundamentals of piezoelectricity*, Oxford science publications, Oxford.
- Iman, R.L., 1992, Uncertainty and sensitivity analysis for computer modeling applications, *American Society of Mechanical Engineers* 28, pp.153–168.
- Iman, R.L., Conover, W.J., 1982, A distribution-free approach to inducing rank correlation among input variables, *Communications in Statistics Part B. Simulation and Computation* 11(3), pp. 311–334.

- Jacobs, J., Etman, L., van Keulen, F., Rooda, J., 2004, Framework for sequential approximate optimization, *Struct Multidisc Optim* 27(5), pp. 384–400.
- Jakiela, M.J., Chapman, C., Duda, J., Adewuya, A., Saitou, K., 2000, Continuum structural topology design with genetic algorithms, *Computer Methods in Applied Mechanics and Engineering* 186(2-4), pp. 339–356.
- Jang, Y.S., Sitar N., Der Kiureghian, A., 1994, reliability analysis of contaminant transport in saturated porous media, *Water Resources Res* 30(8), pp. 2435–2448.
- Jaynes, E., 1968, Prior probabilities, *IEEE Trans Syst Sci Cybern* 4(3), pp. 227–241.
- Jenkins, W.M., 1991, Towards structural optimisation via the genetic algorithm, *Computers and Structures* 40, pp. 1321–1327.
- Jensen, H., 2005, Design and sensitivity analysis of dynamical systems subjected to stochastic loading, *Computers & Structures* 83, pp. 1062–1075.
- Jensen, H., Catalan, M., 2007, On the effects of non-linear elements in the reliability-based optimal design of stochastic dynamical systems, *Int J Non-Linear Mech* 42(5), pp. 802–816.
- Jensen, H., Valdebenito, M., Schuëller, G., Kusanovic, D., 2009, Reliability-based optimization of stochastic systems using line search, *Comput Methods Appl Mech Eng* 198(49–52), pp. 3915–3924.
- John, S. C., Denis, K., 2000, Structural shape optimisation of elastic continua: A study on nonlinearity and 2D benchmark, *Proceedings of the 2nd ASMO UK/ISSMO conference, Engineering Design Optimisation, Swansea*, pp. 65–72.
- Johnson, E., Proppe, C., Spencer, B.Jr., Bergman, L., Székely, G., Schuëller, G., 2003, Parallel processing in computational stochastic dynamics, *Probab Eng Mech* 18(1), pp. 37–60.
- Kelliher, D., Campbell, J.S., Robinson, J.C., 1999, Structural shape optimisation of two-dimensional continua using a hybrid boundary-element/finite-element method, *Engineering Design Optimization, Proceedings, of 1st ASMO/ISSMO conference, MCB University Press, Ilkley UK*.

- Kennedy, J., Eberhart, R.C., 1995, Particle swarm optimisation, In: Proc. 1995 IEEE Int. Conf. Neural Networks, Perth, Australia, pp. 1942–1948.
- Kharmanda, G., Mohamed, A., Lemaire, M., 2002, Efficient reliability-based design optimization using a hybrid space with application to finite element analysis, *Struct Multidisc Optim* 24(3), pp. 233–245.
- Khayet, M., Abu Seman, M.N., Hilal, N., 2010, Response surface modeling and optimization of composite nanofiltration modified membranes, *Journal of Membrane Science* 349(1-2), pp. 113–122.
- Kim, I.Y., de Weck, O.L., 2005, Adaptive weighted-sum method for bi-objective optimization: Pareto front generation, *Struct. Multidisc. Optim* 29, pp. 149–158.
- Kim, I.Y., de Weck, O.L., 2006, Adaptive weighted-sum method for multiobjective optimization: a new method for Pareto front generation, *Struct. Multidisc. Optim* 31, pp. 105–116.
- Kinkaid, N. M., O'Reilly, O. M., Papadopoulos, P., 2003, Automotive disc brake squeal, *Journal of Sound and Vibration* 267(1), pp. 105–166.
- Kita, H., Yabumoto, Y., Mori, N., Nishikawa, Y., 1996, Multi-objective optimization by means of the thermo-dynamical genetic algorithm, *Parallel Problem Solving from Nature IV*, pp. 504–512.
- Knowles, J.D., Corne, D.W., 2000, Approximating the nondominated front using the Pareto archived evolution strategy, *Evol Comput* 8(2), pp. 149–172.
- Konak, A., Coit, D.W., Smith, A.E., 2006, Multiobjective optimisation using genetic algorithm: A tutorial, *Reliability Eng. & System Safety* 91, pp. 992–1007.
- Koski, J., 1988, Multicriteria truss optimization, *Multicriteria Optimization in Engineering and in the Sciences*, edited by Stadler, New York, Plenum Press.
- Koutsourelakis, P., 2008, Design of complex systems in the presence of large uncertainties: a statistical approach, *Comput Methods Appl Mech Eng* 197(49–50), pp. 4092–4103.

- Krohling, R.A., Knidel, H., Shi, Y., 2002, Solving numerical equations of hydraulic problems using particle swarm optimization, IEEE Congress on Evolutionary Computation, Honolulu, Hawaii USA.
- Kuang, Da., J.H., Zheng., 2005, Strategies based on polar coordinates to keep diversity in multi-objective genetic algorithm, Congress on Evolutionary Computation 2005, pp. 1276–1281.
- Kuschel, N., Rackwitz, R., 1997, Two basic problems in reliability-based structural optimization, *Math Methods Oper Res* 46(3), pp. 309–333.
- Kwak, B., Lee, T., 1987, Sensitivity analysis for reliability-based optimization using an AFOSM method, *Comput Struct* 27(3), pp. 399–406.
- Kymissis, J., Kendall, C., Paradiso, J., Gershenfeld, N., 1998, Parasitic Power Harvesting in Shoes, *iswc, Second International Symposium on Wearable Computers (ISWC'98)*, pp. 132.
- Lam, K.Y., Peng, X.Q., Liu, G.R., Reddy, J.N., 1997, A finite-element model for piezoelectric composite laminates, *Smart Materials and Structures* 6(5), pp. 583–591.
- Lanchester, F.W., 1902, Improvements in the brake mechanism of power-propelled road vehicles, G.B. patent no. 26407.
- Lee, J., Kwak, B., 1995, Reliability-based structural optimal design using the Neumann expansion technique, *Comput Struct* 55(2), pp. 287–296.
- Lee, J.O., Yang, Y.S., Ruy, W.S., 2002, A comparative study on reliability-index and target-performance-based probabilistic structural design optimization, *Computers & Structures* 80(3–4), pp. 257–269.
- Leite, J., Topping, B., 1999, Parallel simulated annealing for structural optimization, *Computers & Structures* 73(1–5), pp.545–564.
- Leland, E.S., Lai, E.M., Wright, P.K., 2007, A self-powered wireless sensor for indoor environmental monitoring, University of California Berkeley.
- Lemaire, M., Pendola, M., 2006, phimeca-soft, *Structural Safety* 28(1-2), *Structural Reliability Software*, pp. 130–149.

- Li, W., Yang, L., 1994, An effective optimization procedure based on structural reliability. *Comput Struct* 52(5), pp. 1061–1067.
- Lin, H.Z., Khalessi, M.R., 2006, General outlook of UNIPASS(TM) V5.0: A general-purpose probabilistic software system, *Structural Safety* 28(1-2), *Structural Reliability Software*, pp. 196–216.
- Lind, N., 1976, Approximate analysis and economics of structures, *ASCE J Struct Div* 102(ST6), pp. 1177–1196.
- Liu, J.S., 1996. PhD Thesis.
- Liu, J.S., Hollaway, L., 1998, Integrated structure-electromagnetic optimization of large reflector antenna systems, *Structural Optimization* 16, pp. 29–36.
- Liu, J.S., Hollaway, L., 2000, Design optimisation of composite panel structures with stiffening ribs under multiple loading cases, *Computers & Structures* 78(4), pp. 637–647.
- Liu, J.S., Lu, T.J., 2001, Optimal design of optical fibre-holding microclips with metamorphic development, *Journal of Micromechanics and Microengineering* 11, pp. 195–201.
- Liu, J.S., Lu, T.J., 2004, Multi-objective and multi-loading optimization of ultralightweight truss materials, *International Journal of Solids and Structures* 41(3–4), pp. 619–635.
- Liu, J.S., Parks, G.T., Clarkson, P.J., 2000, Metamorphic development: a new topology optimization method for continuum structures, *Structural and Multidisciplinary Optimization* 20, pp. 288–300.
- Liu, J.S., Parks, G.T., Clarkson, P.J., 2001, Shape optimisation of axisymmetric cylindrical nozzles in spherical pressure vessels subject to stress constraints, *International Journal of Pressure Vessels and Piping* 78, pp. 1–9.
- Liu, J.S., Parks, G.T., Clarkson, P.J., 2005, Topology/shape optimisation of axisymmetric continuum structures – a metamorphic development approach, *Structural and Multidisciplinary Optimization* 29(1), pp. 73–83.

- Liu, J.S., Thompson, G., 1996, The multi-factor design evaluation of antenna structures by parameters profile analysis, *J. Engng Manufac. Proc Inst. Mech. Eng* 210(B5), pp. 449–456.
- Liu, J.S., Thompson, G., Clarkson, P.J., Parks, G.T., 1999, Design for structural performance by multi-factor optimisation, *Engineering Design Optimization, Proceedings of 1st ASMO UK/ISSMO conference*, MCB University Press, Ilkley UK.
- Liu, P.L., Der Kiureghian, A., 1986, Multivariate distribution models with prescribed marginals and covariances, *Probab Eng Mech* 1(2), pp. 105–112.
- Liu, P.L., Der Kiureghian, A., 1991, Finite-element reliability of geometrically nonlinear uncertain structures, *J Eng Mech ASCE* 117(8), pp. 1806–1825.
- Liu., P.L., Lin, H.Z., Der Kiureghian, A., 1989, CalREL user manual, Report No. UCB/SEMM-89/18, Department of Civil Engineering, University of California, Berkeley.
- Lopes, P.A.M., Gomes, H.M., Awruch, A.M., 2010, Reliability analysis of laminated composite structures using finite elements and neural networks, *Composite Structures* 92(7), pp. 1603–1613.
- Lu, F., Lee, H.P., Lim, S.P., 2004, Modeling and analysis of micro piezoelectric power generators for micro-electromechanical-systems applications, *Smart Materials and Structures* 13(1), pp. 57–63(7).
- Lu, H., Yen, G.G., 2003, Rank-density-based multiobjective genetic algorithm and benchmark test function study, *IEEE Trans Evol Comput* 7(4), pp. 325–343.
- Madsen, H.O., Krenk, S., Lind, N.C., 1986, *Methods of Structural Safety*, Prentice-Hall, Englewood Cliffs, NJ.
- Masmoudi, M., Capek, D., Abdelhedi, R., Halouani, F.El., Wery, M., 2006, Application of surface response analysis to the optimisation of nitric passivation of cp titanium and Ti6Al4V, *Surface and Coatings Technology* 200(24), pp. 6651–6658.
- Mason, W.P., 1950, *Piezoelectric crystals and their application to ultrasonics*, New York: D. Van Nostrand Company, Inc.
- Masters, T., 1993, *Practical neural network recipes in C*, Academic Press, San Diego.

Mateu, L., Moll, F., 2005, Optimum piezoelectric bending beam structures for energy harvesting using shoe inserts, *J. Intell. Material System Structure* 16, pp. 835–845.

MatWeb – Cast iron, available online at <http://www.matweb.com/search/DataSheet.aspx?MatGUID=6291a24572754cae94ff365ed99b96f9>, [accessed 16th Feb 2011].

McCulloch, W.S., Pitts, W., 1943, A logical calculus of ideas immanent in nervous activity, *Bull Math Biophys* 5, pp. 115–133.

Mckay, M.D., Conover, W.J., Beckman, R.J., 1979, A comparison of three methods for selecting values of input variables in the analysis of output from a computer code, *Technometrics* 21, pp. 239–245.

Melchers, R. E., Ahammed , M., 2004, A fast approximate method for parameter sensitivity estimation in Monte Carlo structural reliability, *Computers & Structures* 82(1), pp. 55–61.

Michell, A.G.M., 1904, The limits of economy of material in frame-structures. *Phil. Mag.* 8, pp. 589–597.

Miller, L.M., Emley, N.C., Shafer, P., Wright, P.K., 2008, Strain enhancement within cantilevered, Piezoelectric MEMS Vibrational Energy Scavenging Devices, *Advances in Science and Technology Vol. Smart Materials & Mico/Nanosystems*, 54-pp405–410.

Missoum, S., Ramub, P., Haftka, R., 2007, A convex hull approach for the reliability-based design optimization of nonlinear transient dynamic problems, *Comput. Methods Appl. Mech. Eng.* 196(29-30), pp. 2895–2906.

Moses, F., 1997, Problems and prospects of reliability-based optimization, *Eng Struct* 19(4), pp. 293–301.

Moses, F., Kinser, D., 1967, Optimum structural design with failure probability constraints, *AIAA J* 5(6), pp. 1152–1158.

Murata, T., Ishibuchi, H., 1995, MOGA: multi-objective genetic algorithms, In: *Proceedings of the 1995 IEEE international conference on evolutionary computation*, 29 November–1 December 1995, Perth, WA, Australia: IEEE.

- Murthy, P., Subramanian, G., 1968, Minimum weight analysis based on structural reliability. *AIAA J* 6(10), pp. 2037–2039.
- Nadir, W., Kim, I.Y., de Weck, O.L., 2004, Structural shape optimization considering both performance and manufacturing cost, 10th AIAA/ASSMO Multidisciplinary analysis and optimization conference, 30th Aug. – 1st Sept 2004, Albany New York, 4593.
- Newcomb, T.P., Spurr, R.T., 1969, *Automobiles brakes and braking systems*, R. Bentley Inc., Cambridge, MA.
- Newcomb, T.P., Spurr, R.T., 1989, *A technical history of the motor car*, Adam Hilger, New York.
- Ng, T.H., Liao, W.H., 2005, Sensitivity analysis and energy harvesting for self-powered piezoelectric sensor, *J. Intell. Mater. Syst. Struct* 16, pp. 785–797.
- Ngim, D.B., Liu, J.S., Soar, R.C., 2007, Design optimization for manufacturability of axisymmetric continuum structures using metamorphic development, *International Journal of Solids and Structures* 44(2), pp. 685–704.
- Ngim, D.B., Liu, J.S., Soar, R.C., 2009, Design optimisation of consolidated granular-solid prismatic beam using metamorphic development, *International Journal of Solids and Structures* 46, pp. 726–740.
- Nguyen, X.S., Sellier, A., Duprat, F., Pons, G., 2009, Adaptive response surface method based on a double weighted regression technique, *Probabilistic Engineering Mechanics* 24(2), pp. 135–143.
- Nikolaidis, E., Burdisso, R., 1988, Reliability based optimization: a safety index approach, *Comput Struct* 28(6), pp. 781–788.
- Ogawa, J., Tanaka, H., 2009, Importance sampling for stochastic systems under stationary noise having a specified power spectrum, *Probabilistic Engineering Mechanics* 24(4), pp. 537–544.
- Ohsaki, M., 2001, Random search method based on exact reanalysis for topology optimization of trusses with discrete cross-sectional areas, *Computers & Structures* 79(6), pp. 673–679.

- Olsson, A.M.J., Sandberg, G.E., 2002, On Latin hypercube sampling for stochastic finite element analysis, *Journal of Engineering Mechanics* 128(1), pp. 121–125.
- Omkar, S.N., Mudigere, D., Naik, G.N., Gopalakrishnan, S., 2008, Vector evaluated particle swarm optimization (VEPSO) for multi-objective design optimization of composite structures, *Computers & Structures* 86(1-2), pp. 1–14.
- Ooi, B.L., 2010, Optimisation and frequency tuning concepts for a vibration energy harvester, PhD Thesis, University of Hull.
- Ormoneit, D., White, H., 1999, An efficient algorithm to compute maximum entropy densities, *Econom Rev.* 18, 127–140.
- Oshaki, M., 1995, Genetic algorithm for topology optimisation of trusses, *Computers and Structures* 57, pp. 219–225.
- Pandey, M.K., Tiwari, M.K., Zuo, M.J., 2007, Interactive enhanced particle swarm optimization: a multi-objective reliability application, *Proc. of the Inst. of Mech. Eng. Part O: Journal of Risk and Reliability* 221, pp. 177–191.
- Papadrakakis, M., Lagaros, N.D., 2002, Reliability-based structural optimization using neural networks and Monte Carlo simulation, *Computer Methods in Applied Mechanics and Engineering* 191(32), pp. 3491–3507.
- Papadrakakis, M., Lagaros, N., Plevris, V., 2005, Design optimization of steel structures considering uncertainties, *Eng Struct* 27(9), pp. 1408–1418.
- Papalambros, P.Y., 1995, Optimal design of mechanical components and systems, *J. Vib. Acoust.*, 117(B).
- Pellisetti, M., 2009, Parallel processing in structural reliability, *J Struct Eng Mech* 32(1), pp. 95–126.
- Perez, R.E., Behdinan, K., 2007, Particle swarm approach for structural design optimization, *Computers & Structures* 85(19-20), pp. 1579–1588.
- Piezo System, Inc. CATALOG #7C (2008), available online at <http://www.piezo.com/catalog.html>, [accessed on 31st July 2009].

- Poulin, G., Sarraute, E., Costa, F., 2004, Generation of electrical energy for portable devices comparative study of an electromagnetic and a piezoelectric system, *Sensors and Actuators A: Physical* 116, pp. 461–471.
- Pradlwarter, H.J., Schueller, G.I., 2010, Local domain Monte Carlo Simulation, *Structural Safety* 32(5), Probabilistic Methods for Modeling, Simulation and Optimization of Engineering Structures under Uncertainty in honor of Jim Beck's 60th Birthday, pp. 275–280.
- Rackwitz, R., 1976, Practical probabilistic approach to design, bulletin No. 112 Paris, France: Comité Eur-o-pean du Béton.
- Rackwitz, R., 2001, Reliability analysis--a review and some perspectives, *Structural Safety* 23(4), pp. 365–395.
- Rackwitz, R., Fiessler, B., 1978, Structural reliability under combined load sequences, *Computers & Structures* 9, pp. 489–494.
- Rahami, H., Kaveh, A., Gholipour, Y., 2008, Sizing, geometry and topology optimization of trusses via force method and genetic algorithm, *Engineering Structures* 30(9), pp. 2360–2369.
- Rahman, S., Xu, H., 2004, A univariate dimension-reduction method for multi-dimensional integration in stochastic mechanics, *Probab Eng Mech* 19(4), pp. 393–408.
- Rajagopal, K.R., DebChaudhury, A., Newell, J.F., 1989, Verification of NESSUS code on space propulsion components, In: *Proceedings of the 5th International Conference on Structural Safety and Reliability*, New York: American Society of Civil Engineers, pp. 2299–2306.
- Reddy, M., Grandhi, R., Hopkins, D., 1994, Reliability based structural optimization: a simplified safety index approach, *Comput Struct* 53(6), pp. 1407–1418.
- Reh, S., Beley, J.D., Mukherjee, S., Khor, E.H., 2006, Probabilistic finite element analysis using ANSYS, *Structural Safety* 28(1-2), *Structural Reliability Software*, pp. 17–43.
- Ren, W.X., Chen, H.B., 2010, Finite element model updating in structural dynamics by using the response surface method, *Engineering Structures* 32(8), pp. 2455–2465.

- RG2 BSEN floor panel, Kingspan access floor limited, available online at <http://www.fieldmansaccessfloorsltd.com/Data-Sheets.aspx>, [accessed 18th March 2011].
- Riha, D.S., Hassan, J.E., Forrest, M.D., Ding, K., 2004, Stochastic approach for vehicle crash models, In: Proceedings of the SAE 2004 world congress & exhibition, 2003-01-0460, Detroit, MI.
- Rodriguez, E.A., Pepin, J.W., Thacker, B.H., Riha, D.S., 2002, Uncertainty quantification of a containment vessel dynamic response subjected to high-explosive detonation impulse loading, In: Proceedings of the AIAA/ASME/ASCE/AHS/ASC 43rd structures, structural dynamics, and materials (SDM) conference, AIAA 2002-1567, Denver, CO.
- Rome, L.C., Flynn, L., Goldman, E.M., Yoo, T.D., 2005, Generating electricity while walking with loads, *Science* 309, pp. 1725–1728.
- Rong, J.H., Liang, Q.Q., 2008, A level set method for topology optimization of continuum structures with bounded design domains, *Computer Methods in Applied Mechanics and Engineering* 197(17-18), pp. 1447–1465.
- Roundy, S., 2005, On the effectiveness of vibration-based energy harvesting, *Journal Intell. Material System Structure* 16, pp. 809–823.
- Roundy, S.J., 2003, Energy scavenging for wireless sensor nodes with a focus on vibration to electricity conversion, Ph.D. Dissertation, Department of Mechanical Engineering, University of California, Berkeley.
- Roundy, S.J., Wright, P.K., Rabaey J, 2003, A study of low level vibrations as a power source for wireless sensor node, *Computer Communications* 26(11), pp.1131–1144.
- Royset, J., Der Kiureghian, A., Polak, E., 2001, Reliability-based optimal structural design by the decoupling approach, *Reliab Eng Syst Saf* 73(3), pp. 213–221.
- Royset, J., Polak, E., 2004a, Implementable algorithm for stochastic optimization using sample average approximations, *J Optim Theory Appl* 122(1), pp. 157–184.
- Royset, J., Polak, E., 2004b, Reliability-based optimal design using sample average approximations, *Probab Eng Mech* 19(4), pp. 331–343.

- Saitou, K., Izui, K., Nishiwaki, S., Papalambros, P., 2005, A Survey of Structural Optimization in Mechanical Product Development, *J. Comput. Inf. Sci. Eng.* 5(3), 204 (13 pages).
- Santosh, T.V., Saraf, R.K., Ghosh, A.K., Kushwaha, H.S., 2006, Optimum step length selection rule in modified HL-RF method for structural reliability, *International Journal of Pressure Vessels and Piping* 83(10), pp. 742–748.
- Saravanos, D.A., Heyliger, P.R., Hopkins, D.A., 1997, Layerwise mechanics and finite element for the dynamic analysis of piezoelectric composite plates, *International Journal of Solids and Structures* 34(3), pp. 359–378.
- Sarker, R., Liang, K-H., Newton, C., 2002, A new multiobjective evolutionary algorithm. *Eur J Oper Res* 140(1), 12–23.
- Schaffer, J.D., 1985, Multiple objective optimization with vector evaluated genetic algorithms. *Proc. 1st ICGA (Carnegie-Mellon University, USA, July 24-26)*, pp. 93–100.
- Schuëller, G.I., Pradlwarter, H.J., Beck, J., Au, S., Katafygiotis, L., Ghanem, R., 2005, Benchmark study on reliability estimation in higher dimensions of structural systems—an overview. In: Soize C, Schuëller GI (eds) *Structural dynamics EURO-DYN 2005—Proceedings of the 6th international conference on structural dynamics*. Millpress, Rotterdam, pp 717–722.
- Schuëller, G.I., Bucher, C.G., Bourgund, U., Ouypornprasert, W., 1987, On efficient computational schemes to calculate structural failure probabilities, In: *Lecture notes in engineering, Stochastic Structural Mechanics* 31, Lin, Y.K., Schuëller, G.I., Eds, New York: Springer-Verlag, pp. 388–410.
- Schuëller, G.I., Pradlwarter, H.J., 2006, Computational stochastic structural analysis (COSSAN) - a software tool, *Structural Safety* 28(1-2), *Structural Reliability Software*, pp. 68–82.
- Schuëller, G.I., Stix, R., 1987, A critical appraisal of methods to determine failure probabilities, *Structural Safety* 4(4), pp. 293–309.
- Schutte, J.F., Groenwold, A.A., 2003, Sizing design of truss structures using particle swarms, *Structural and Multidisciplinary Optimization* 25, pp. 261–269.

- Schy, A.A., Giesy, D.P. 1988, Multicriteria Optimization for Design of Aircraft Control Systems, In: Stadler, W. (ed.) Multicriteria Optimization in Engineering and in the Sciences, New York: Plenum, pp. 225–262.
- Shenck, N.S., Paradiso, J.A., 2001, Energy scavenging with shoe-mounted piezoelectrics, IEEE Micro. 21(3), pp. 30–42.
- Shinozuka, M., 1983, Basic analysis of structural safety, J. Struct. Engrg., ASCE 109(3), pp. 721–740.
- Silva, M., Tortorelli, D.A., Norato, J., Bae, Ha-R, 2008, Topology optimization with regards to system reliability, EngOpt 2008 – International conference on engineering optimization, Rio de Janeiro, Brazil.
- Silvern, D., 1963, Optimization of system reliability, AIAA J 1(12), pp. 2872–2873.
- Sitar, N., Cawfield, J.D., Der Kiureghian, A., 1987, First-order reliability approach to stochastic analysis of subsurface flow and contaminant transport, Water Resources Res 23(5), pp. 794–804.
- Sodano, H.A., Inman, D.J., Park, G., 2005a, Generation and Storage of Electricity from Power Harvesting Devices, Journal of Intelligent Material Systems and Structures, 16(1), pp. 67–75.
- Sodano, H.A., Inman, D.J., Park, G., 2005b, Comparison of Piezoelectric Energy Harvesting Devices for Recharging Batteries, Journal of Intelligent Material Systems and Structures, 6(10), pp. 799–807.
- Sodano, H.A., Magliula, E.A., Park, G., Inman, D.J., 2002, Electric power generation using piezoelectric materials, Proc. 13th Int. Conf. on Adaptive Structures and Technologies (Potsdam, Germany), pp. 153–161.
- Sodano, H.A., Park, G., Inman, D.J., 2004, Estimation of electric charge output for piezoelectric energy harvesting, Strain 40, pp. 49–58.
- Solymar, L., 1984, Lectures on electromagnetic theory, Oxford University Press, Oxford, pp. 12.

- Song, J.S., Lee, K.J., 1992, System performance assessment of final repository for radioactive wastes using first-order reliability method, *Waste Management* 12(4), pp. 323–335.
- Sperry, E.A., 1894, The electric brake in practice, *Transactions AIEE* 11, pp.682–728.
- Sperry, E.A., 1895, Electric brake, US patent nos. 534974, 534977.
- Sperry, E.A., 1896, Electric brake, US patent no. 565937.
- Srinivas, N., Deb, K., 1994, Multiobjective optimization using nondominated sorting in genetic algorithms, *J Evol Comput* 2(3), pp. 221–48.
- Stadler, W., 1979, A survey of multicriteria optimization or the vector maximum problem, part I: 1776–1960, *Journal of Optimization Theory and Applications* 29(1), pp. 1–52.
- Stadler, W., 1984, Applications of Multicriteria Optimization in Engineering and the Sciences (A Survey), *Multiple Criteria Decision Making – Past Decade and Future Trends*, edited by M. Zeleny, JAI Press, Greenwich, Connecticut.
- Starner, T., 1996, Human-powered wearable computing, *IBM Systems Journal* 35(3), pp. 618–629
- Stein, M., 1987, Large sample properties of simulations using Latin hypercube sampling, *Technometrics* 29(2), pp. 143–151.
- Stordeur, M., Stark, I., 1997, Low Power Thermoelectric Generator–Self-Sufficient Energy Supply for Micro Systems, *Proc. of 16th International Conference on Thermoelectrics*, pp. 575–577.
- Su, X.T., Yang, Z.J., Liu, G.H., 2010, Monte Carlo simulation of complex cohesive fracture in random heterogeneous quasi-brittle materials: A 3D study, *International Journal of Solids and Structures* 47(17), pp. 2336–2345.
- Switzky, H., 1965, Minimum weight design with structural reliability, *J Aircr* 2(3), pp. 228–232.
- Taflanidis, A., Beck, J., 2008a, An efficient framework for optimal robust stochastic system design using stochastic simulation, *Comput Methods Appl Mech Eng* 198(1), pp. 88–101.

- Taflanidis, A., Beck, J., 2008b, Stochastic subset optimization for optimal reliability problems, *Probab Eng Mech* 23(2–3), pp. 324–338.
- Tamaki, H., Mori, M., Araki, M., Mishima, Y., Ogai, H., 1994, Multi-criteria Optimization by genetic algorithms: A case of scheduling in hot rolling process, *Proc. APORS'94* (Fukuoka, Japan, July 26-29, 1994), pp. 374–381.
- Tekiner, H., Coit, D.W., Felder, F.A., 2010, Multi-period multi-objective electricity generation expansion planning problem with Monte-Carlo simulation, *Electric Power Systems Research* 80(12), pp. 1394–1405.
- Thacker, B.H., Nicolella, D.P., Kumaresan, S., Yoganandan, N., Pintar, F., 2001, Probabilistic finite element analysis of the cervical spine, *Math. Modeling and Sci. Computing* 13, pp. 12–21.
- Thacker, B.H., Riha, D.S., Fitch, S.H.K., Huyse, L. J., Pleming, J.B., 2006, Probabilistic engineering analysis using the NESSUS software, *Structural Safety* 28(1-2), *Structural Reliability Software*, pp. 83–107.
- Thacker, B.H., Rodriguez, E.A., Pepin, J.E., Riha, D.S., 2003, Uncertainty quantification of a containment vessel dynamic response subjected to high-explosive detonation impulse loading, In: *IMAC-XXI: conference & exposition on structural dynamics*, No. 261, Kissimmee, FL.
- The Access Flooring Company, 2008, *Understanding raised floor systems for the specifier* (2008), Edenbridge Kent.
- Thompson, G., Goeminne, J., 1993, The design review of engineering systems including maintainability and reliability using parameter profiles. *Int. Conf. Eng. Design*. The Hague, Netherlands.
- Toyota, available online at http://www.toyota.co.uk/cgi-bin/toyota/bv/generic_editorial.jsp?navRoot=toyota_1024_root&noLeftMenu=true&fullwidth=TRUE&nodiv=TRUE&edname=HSD_Landing&zone=Zone+See+the+Range&id=HSD_Logo, [Accessed 19th Feb 2011]
- Tu, J., Choi, K.K., Park, Y.H., 2001, Design potential method for robust system parameter design, *AIAA J* 39(4), pp. 667–677.

- Tvedt, L., 2006, Proban - probabilistic analysis, *Structural Safety* 28(1-2), Structural Reliability Software, pp. 150–163.
- Tzou, H.S., Tseng, C.I., 1990, Distributed piezoelectric sensor/actuator design for dynamic measurement/control of distributed parameter systems: A piezoelectric finite element approach, *Journal of Sound and Vibration* 138(1), pp. 17–34.
- Umesha, P., Venuraju, M., Hartmann, D., Leimbach, K., 2005, Optimal design of truss structures using parallel computing, *Struct. Multidisc. Optim.* 29(4), pp. 285–297.
- Valdebenito, M.A., Schuëller, G.I., 2010b, Efficient strategies for reliability-based optimization involving non linear, dynamical structures, *Comput Struct* (in press).
- Valdebenito, M.A., Schuëller, G.I., 2010a, A survey on approaches for reliability-based optimization, *Struct. Multidisc. Optim.* 42, pp. 645–663.
- van Keulen, F., Vervenne, K., 2004, Gradient-enhanced response surface building, *Struct Multidisc Optim* 27(5), pp. 337–351.
- Vanmarcke, E.H., 1973, Matrix formulation of reliability analysis and reliability-based design, *Computers & Structures* 3(4), pp. 757–770.
- Venkataraman, S., Haftka, R.T., 2004, Structural optimization complexity: what has Moore's law done for us?, *Structural and Multidisciplinary Optimization* 28(6), pp. 375-387.
- Venter, G., Sobieszczanski-Sobieski, J., 2004, Multidisciplinary optimisation of a transport aircraft wing using particle swarm optimisation, *Struc. Multidisc. Optim.* 26, pp. 121–131.
- Veritas Sesam Systems, 1991, **PROBAN**, Houston, Texas: Veritas Sesam Systems.
- Wahab, M.A., 2008, *Dynamics and vibration an introduction*, pp.273.
- Wang, J., Zhai, Z., Jing, Y., Zhang, C., 2010, Particle swarm optimization for redundant building cooling heating and power system, *Applied Energy* 87(12), pp. 3668–3679.
- Wang, L., Grandhi, R., 1994, Efficient safety index calculation for structural reliability analysis, *Computers and Structures.* 52(1), pp. 103–111.

- Wang, S.Y., 2004, A finite element model for the static and dynamic analysis of a piezoelectric bimorph, *International Journal of Solids and Structures* 41(15), pp. 4075–4096.
- Watkins, R.I., Morris, A.J., 1987, A multicriteria objective function optimization scheme for laminated composites for use in multilevel structural optimization schemes, *Computer Methods in Applied Mechanics and Engineering* 60(2), pp. 233–251.
- Williams, C.B., Yates, R.B., 1996, Analysis of a micro-electric generator for microsystem, *Sensor & Actuators A52*, pp. 8–11.
- Wilson, R. B., 1963, A Simplicial Method for Convex Programming, PhD thesis, Harvard University.
- Wu, S.J., Yu, X., Hu, Z.H., Zhang, L.L., Chen, J.M., 2009, Optimizing aerobic biodegradation of dichloromethane using response surface methodology, *Journal of Environmental Sciences* 21(9), pp. 1276–1283.
- Wu, Y. T., Wirsching, P. H., 1987, A new algorithm for structural reliability estimation, *J. Eng. Mech. Division*. 113, pp. 1319–1336.
- Wu, Y., 1994, Computational methods for efficient structural reliability and reliability sensitivity analysis, *AIAA J* 32(8), pp. 1717–1723.
- Wu, Y.T., 1984, Efficient methods for mechanical and structural reliability analysis and design, Ph.D. Thesis, Tucson, Arizona: University of Arizona.
- Wu, Y.T., Shin, Y., Sues, R.H., Cesare, M.A., 2006, Probabilistic function evaluation system (ProFES) for reliability-based design, *Structural Safety* 28(1-2), *Structural Reliability Software*, pp. 164–195.
- Wu, Y.T., Torng, T.Y., Khalessi, M.R., 1990, A new iteration procedure for efficient structural reliability analysis, *Proc. First Int. Symp, On Uncertainty Modeling and Analysis*, IEEE.
- Xiang, Y., Liu, Y., 2011, Application of inverse first-order reliability method for probabilistic fatigue life prediction, *Probabilistic Engineering Mechanics* 26(2), pp. 148–156.

- Xu, H., Rahman, S., 2004, A generalized dimension-reduction method for multi-dimensional integration in stochastic mechanics, *Int J Numer Methods Eng* 61(12), pp. 1992–2019.
- Xu, S.X., Koko, T.S., 2004, Finite element analysis and design of actively controlled piezoelectric smart structures, *Finite Element in Analysis and Design* 40(3), pp. 241–262.
- Yang, J.S., Nikolaidis, E., 1991, Design of aircraft wings subjected to gust loads—a safety index based approach, *AIAA J* 29(5), pp. 804–812.
- Yang, R., Gu, L., 2004, Experience with approximate reliability-based optimization methods, *Struct Multidisc. Optim* 26(1–2), pp. 152–159.
- Yang, Z.J., Su, X.T., Chen, J.F., Liu, G.H., 2009, Monte Carlo simulation of complex cohesive fracture in random heterogeneous quasi-brittle materials, *International Journal of Solids and Structures* 46(17), pp. 3222–3234.
- Yao, L.Q., Lu, L., 2003. Hybrid-stabilized solid-shell model of laminated composite piezoelectric structures under non-linear distribution of electric potential through thickness, *International Journal for Numerical Methods in Engineering* 58(10), pp. 1499–1522.
- Yen, G.G., Lu, H., 2003, Dynamic multiobjective evolutionary algorithm: adaptive cell-based rank and density estimation, *IEEE Trans Evol Comput* 7(3), pp. 253–274.
- Youn, B., Choi, K., Park, Y., 2003, Hybrid analysis method for reliability-based design optimization, *J. Mech. Des.* 125(2), pp. 221–232.
- Zadeh, L., 1963, Optimality and Non-Scalar-Valued Performance Criteria, *IEEE Trans Autom. Control* 8, pp. 59–60.
- Zhang, F., Lu, Z.Z., Cui, L.J., Song, S.F., 2010, Reliability Sensitivity Algorithm Based on Stratified Importance Sampling Method for Multiple Failure Modes Systems, *Chinese Journal of Aeronautics* 23(6), pp. 660–669.
- Zhang, J., Foschi, R., 2004, Performance-based design and seismic reliability analysis using designed experiments and neural networks, *Probab Eng Mech* 19(3), pp. 259–267.

Zienkiewicz, O.C., Campbell, J.S., 1973, Shape optimization and sequential linear programming, Optimum Structural Design, Eds. Gallagher, R.H., Zienkiewicz, O.C., Chapter 7, John Wiley, Chichester.

Ziha, K., 1995, Descriptive sampling in structural safety, Structural Safety 17(1), pp. 33–41.

Zitzler, E., Laumanns, M., Thiele, L., 2001. SPEA2: improving the strength Pareto evolutionary algorithm, Swiss Federal Institute Technology: Zurich, Switzerland.

Zitzler, E., Thiele, L., 1999, Multiobjective evolutionary algorithms: a comparative case study and the strength Pareto approach, IEEE Trans Evol Comput 3(4), pp. 257–271.

Zou, T., Mahadevan, S., 2006, A direct decoupling approach for efficient reliability-based design optimization, Struct Multidisc Optim 31(3), pp. 190–200.

10 Appendices

Appendix A – Example of reliability-related multi-factor optimisation

This document presents the optimised result extracted from the analysis. The reliability loading-case index is provided in section b).

a) Result of static analysis

The following example is the static analysis extracted from the optimised result for the truss structure.

```
**** CENTER OF MASS, MASS, AND MASS MOMENTS OF INERTIA ****
CALCULATIONS ASSUME ELEMENT MASS AT ELEMENT CENTROID
TOTAL MASS = 4.8171 Structural mass (kg)

```

CENTER OF MASS MASS	MOM. OF INERTIA ABOUT ORIGIN	MOM. OF INERTIA ABOUT CENTER OF
XC = -0.28810E-17	IXX = 0.2873	IXX = 0.1837
YC = -0.14405E-17	IYY = 0.2873	IYY = 0.1837
ZC = 0.14664	IZZ = 0.3376	IZZ = 0.3376
	IXY = 0.000	IXY = 0.1999E-34
	IYZ = 0.000	IYZ = -0.1018E-17
	IZX = -0.5204E-17	IZX = -0.7239E-17

***** POST1 ELEMENT TABLE LISTING *****

STAT ELEM	CURRENT AXSTRESS
1	-0.25173E+08
2	-0.25173E+08
3	-0.25173E+08
4	-0.25173E+08
5	-0.25173E+08
6	-0.25173E+08
7	-0.25173E+08
8	-0.25173E+08
9	-0.25173E+08
10	-0.25173E+08
11	-0.25173E+08
12	-0.25173E+08
13	-0.25173E+08
14	-0.25173E+08
15	-0.25173E+08
16	-0.25173E+08
17	0.42834E+08
18	0.42834E+08
19	0.42834E+08
20	0.42834E+08

Loading case 1

Axial stress (MPa)

Negative = compression stress

Positive = tensile stress

```

21  0.42834E+08
22  0.42834E+08
23  0.42834E+08
24  0.42834E+08
25 -0.37559E+08
26 -0.37559E+08
27 -0.37559E+08
28 -0.37559E+08
29 -0.37559E+08
30 -0.37559E+08
31 -0.37559E+08
32 -0.37559E+08

```

```

MINIMUM VALUES
ELEM      28
VALUE -0.37559E+08

```

```

MAXIMUM VALUES
ELEM      19
VALUE  0.42834E+08

```

```

***** POST1 NODAL DEGREE OF FREEDOM LISTING *

```

Loading case 1
Displacement (m)

```

LOAD STEP=      1  SUBSTEP=      1
TIME=      1.0000  LOAD CASE=      0

```

```

THE FOLLOWING DEGREE OF FREEDOM RESULTS ARE IN THE GLOBAL
COORDINATE SYSTEM

```

NODE	UX	UY	UZ	USUM
1	0.0000	0.0000	0.0000	0.0000
2	0.0000	0.0000	0.0000	0.0000
3	0.0000	0.0000	0.0000	0.0000
4	0.0000	0.0000	0.0000	0.0000
5	0.0000	0.0000	0.0000	0.0000
6	0.0000	0.0000	0.0000	0.0000
7	0.0000	0.0000	0.0000	0.0000
8	0.0000	0.0000	0.0000	0.0000
9	0.17351E-04	0.41890E-04	-0.23349E-04	0.51001E-04
10	0.41890E-04	0.17351E-04	-0.23349E-04	0.51001E-04
11	0.41890E-04	-0.17351E-04	-0.23349E-04	0.51001E-04
12	0.17351E-04	-0.41890E-04	-0.23349E-04	0.51001E-04
13	-0.17351E-04	-0.41890E-04	-0.23349E-04	0.51001E-04
14	-0.41890E-04	-0.17351E-04	-0.23349E-04	0.51001E-04
15	-0.41890E-04	0.17351E-04	-0.23349E-04	0.51001E-04
16	-0.17351E-04	0.41890E-04	-0.23349E-04	0.51001E-04
17	-0.20329E-19	-0.20329E-19	-0.32963E-03	0.32963E-03

```

MAXIMUM ABSOLUTE VALUES
NODE      14      12      17      17
VALUE -0.41890E-04 -0.41890E-04 -0.32963E-03 0.32963E-03

```

***** POST1 ELEMENT TABLE LISTING *****

STAT	CURRENT
ELEM	AXSTRESS
1	-0.29570E+08
2	-0.99977E+07
3	-0.99975E+07
4	-0.29569E+08
5	0.20316E+08
6	-0.31212E+08
7	0.50237E+08
8	-0.19402E+08
9	0.76649E+08
10	-0.57019E+08
11	-0.57020E+08
12	0.76645E+08
13	-0.19402E+08
14	0.50237E+08
15	-0.31210E+08
16	0.20316E+08
17	0.17012E+08
18	-0.12657E+07
19	-0.31107E+08
20	-0.66299E+08
21	-0.66298E+08
22	-0.31107E+08
23	-0.12661E+07
24	0.17011E+08
25	-0.14916E+08
26	-0.69033E+07
27	0.14193E+08
28	0.42704E+08
29	-0.85072E+08
30	0.42705E+08
31	0.14193E+08
32	-0.69031E+07

Loading case 2
Axial stress (MPa)
Negative = compression stress
Positive = tensile stress

MINIMUM VALUES
ELEM 29
VALUE -0.85072E+08

MAXIMUM VALUES
ELEM 9
VALUE 0.76649E+08

***** POST1 NODAL DEGREE OF FREEDOM LISTING *****

LOAD STEP= 1 SUBSTEP= 1
TIME= 1.0000 LOAD CASE= 0

Loading case 2
Displacement (m)

THE FOLLOWING DEGREE OF FREEDOM RESULTS ARE IN THE GLOBAL
COORDINATE SYSTEM

NODE	UX	UY	UZ	USUM
1	0.0000	0.0000	0.0000	0.0000
2	0.0000	0.0000	0.0000	0.0000
3	0.0000	0.0000	0.0000	0.0000
4	0.0000	0.0000	0.0000	0.0000
5	0.0000	0.0000	0.0000	0.0000
6	0.0000	0.0000	0.0000	0.0000
7	0.0000	0.0000	0.0000	0.0000
8	0.0000	0.0000	0.0000	0.0000
9	-0.35212E-04	0.11746E-03	0.11415E-03	0.16753E-03
10	-0.29356E-04	0.12476E-03	0.60403E-04	0.14169E-03
11	0.27767E-04	0.14996E-03	0.53618E-04	0.16166E-03
12	-0.17940E-03	0.43309E-03	-0.83354E-03	0.95632E-03
13	-0.12568E-03	0.86399E-04	0.53640E-04	0.16167E-03
14	-0.67463E-04	0.10898E-03	0.60399E-04	0.14169E-03
15	-0.58159E-04	0.10795E-03	0.11416E-03	0.16754E-03
16	-0.48994E-04	0.11828E-03	0.14101E-03	0.19046E-03
17	-0.44972E-04	0.10857E-03	0.45342E-04	0.12596E-03

MAXIMUM ABSOLUTE VALUES

NODE	12	12	12	12
VALUE	-0.17940E-03	0.43309E-03	-0.83354E-03	0.95632E-03

EXIT THE ANSYS POST1 DATABASE PROCESSOR

b) Reliability loading-case index result

The initial and optimised results are shown below, including each iterative solution obtained as part of the optimisation process. Therefore, all the intermediate results can be examined. The following document is an example of the initial and optimised results for the truss structure.

i) Initial design

Number of objectives: 4
Number of loading cases: 2

NUMBER OF ROW IS M= 4 NUMBER OF COLUMN IS N= 2

DATA BY STRUCTURAL AND RELIABILITY ANALYSIS

	LC1	LC2
AxiStr	0.688E+08	0.133E+09
Disp	0.797E-03	0.446E-02
Mass	0.648E+01	0.648E+01
RLI	0.324E+01	0.281E+01

Result of particular performance and loading cases, for axial stress, displacement, mass, and RLI. Second and third columns represent loading cases 1 and 2, respectively.

at the 0 F(X)=-.475357E+02
0.1000E+00 0.5000E-01 0.1000E-03 0.1000E-03 0.1000E-03
0.2500E+00

Design variables

ii) Optimised design

DATA BY STRUCTURAL AND RELIABILITY ANALYSIS

	LC1	LC2
AxiStr	0.428E+08	0.851E+08
Disp	0.330E-03	0.956E-03
Mass	0.482E+01	0.482E+01
RLI	0.355E+01	0.328E+01

Objective no change in a complete cycle, stop here

at the 16 F(X)=-.554177E+02
0.2396E+00 0.1754E+00 0.5128E-04 0.7919E-04 0.1248E-03
0.2054E+00

Total number of complete iterations

Appendix B - Multifactor optimisation of structure technique (MOST): optimisation flow procedure

In Chapter 4.4, the development of multifactor optimisation of structure technique (MOST) is discussed. This appendix provides a general summary of MOST procedure as a complementary section to Chapter 4.4, and describes the structural analysis and optimisation flows in detail.

Basically, a recurring iterative process is required before an optimum solution can be found in a given optimisation. The MOST technique focuses on the use of finite element analysis for structural optimisation. The optimisation process involves seven fundamental steps, which are listed below and explained in the following paragraphs:

- i) Model generation (initial design)
- ii) Initial design analysis results (output file)
- iii) MOST optimisation setup
- iv) Optimisation loop
 - a) Performance analysis (structural and other disciplinary analyses)
 - b) Performance improvement by changing the structural variables
 - c) Convergence checking
- v) Optimum design

Step (i) involves the initial design. In generating the model, the input files can be created from the graphical user interface or in the text mode using ANSYS, with the latter method being the most convenient. The input file consists of the material properties, constraints, boundaries conditions, element type and size, loading cases, etc. For the generation of the model, finite element software (i.e., ANSYS) is used.

Step (ii) is concerned with the analysis results (i.e., the ANSYS output file). For the structural analysis, the mass is written into this file, as are the stresses and displacements of each node and/or element. The maximum stress and maximum displacement are of interest in designs where these values cannot be exceeded on specified requirements. Others performance factors can also be written into the output file (e.g., the frequency of the design).

Step (iii) is the MOST optimisation setup, which is an important part of the optimisation process. First, the constraints of each design variable are considered, with the aim that each design variable meets the specific requirements (e.g., the cross-sectional area of a truss member cannot be bigger or smaller than specified values). Next, the lowest acceptable limit and the best expected values for each objective under each loading case must be specified. These objectives are forced to approach the best expected values by the MOST technique until convergence is attained. More specifically, these are the optimisation objectives to be achieved (e.g., one objective might be that the structural maximum stress is smaller than the yield stress by a factor of X).

Finally, the weighting factor, the performance parameter, and the loading case are assigned a weighting factor according to their importance. The sum of the performance parameters weighting factors is equal to 1, as is the sum of the loading case parameters weighting factors. For example, consider a structural analysis related to a problem that requires the minimisation of a structural mass under two loading cases, in which the design constraints must satisfy all the specified design requirements. To assign the weighting factor, the mass performance parameter is given a high factor and the weighting factor of the loading case parameter is evenly divided between the two loading cases.

This document is written in a text file rather than in FORTRAN, in order to avoid the errors that arise from compiling FORTRAN, related to changes in the weighting factor. For each optimisation, this document is unchanged until a complete optimisation is obtained (i.e., until convergence has been attained). This file is later read by the MOST optimisation procedure.

Step (iv), the optimisation loop, comprises three important steps: (a) performance analysis, (b) performance improvement, and (c) convergence. These three steps are defined in detail below.

In step (a), the MOST technique is used to analyse the structural performance and other disciplinary performance (if any). The result is assessed by using a matrix system—the performance data matrix (PDM). An $m \times n$ matrix (d_{ij}), the so-called PDM, is defined by a set of performance parameters P_i ($i = 1, 2, \dots, m$) and loading case parameters C_j ($j = 1, 2, \dots, n$). Thus, the data point d_{ij} is the i -th performance P_i of the structure for loading case C_j . The data points of the matrix are obtained by a finite element analysis

of the structure including any other disciplinary analyses. The matrix lists every performance parameter of the system for each individual loading case (see Table B.1).

Table B.1 – Performance data matrix

	C_1	C_2	...	C_n
P_1	d_{11}	d_{12}	...	d_{1n}
P_2	d_{21}	d_{22}	...	d_{2n}
\vdots	\vdots	\vdots		\vdots
P_m	d_{m1}	d_{m2}	...	d_{mn}

The PDM is assessed by using a parameter profile matrix (PPM) to review the profile of the performances for different loading cases (see Table B.2). The PPM assesses the character of the structure/system with respect to the actual performances relative to their acceptable limits and to the best values of the performances.

Table B.2 – Parameter profile matrix

	C_1	C_2	...	C_n
P_1	D_{11}	D_{12}	...	D_{1n}
P_2	D_{21}	D_{22}	...	D_{2n}
\vdots	\vdots	\vdots		\vdots
P_m	D_{m1}	D_{m2}	...	D_{mn}

The data point D_{ij} in the PPM is a non-dimensional number (range, 0–10) which is determined by the closeness of the actual performance d_{ij} to the acceptable limit and by the best values of the performance. In principle, the data point D_{ij} for a given acceptable limit (e.g., the lower limit) is calculated as follows:

$$D_{ij} = \left(\frac{d_{ij} - l_{ij}}{b_{ij} - l_{ij}} \right) \times 10 \quad (\text{B.1})$$

where d_{ij} is the actual performance value taken from the PDM, and l_{ij} and b_{ij} are the lower limit and the best value, respectively. Equation (B.1) is valid for $l_{ij} < d_{ij} < b_{ij}$; for $d_{ij} > b_{ij}$, $D_{ij} = 10$; and for $d_{ij} < l_{ij}$, $D_{ij} = 0$.

Information obtained from the PPM allows the whole system to be evaluated. The system can be further analysed using the parameter performance index (PPI) and the case performance index (CPI). The system can be reviewed by using the information contained in the indices; i.e., a comparison of PPIs indicates whether the system performs better with respect to some performances than to others, and a comparison of CPIs shows whether the system performs better under certain loading cases than under others. The highest values for PPI and CPI are 10. PPI and CPI values close to 10 indicate good designs, whereas values close to 0 indicate poor designs. PPI and CPI are defined as follows:

$$\begin{aligned} PPI_i &= Z_i \times n \quad i = 1, 2, \dots, m \\ CPI_j &= N_j \times m \quad j = 1, 2, \dots, n \end{aligned} \quad (\text{B.2})$$

where

$$Z_i = \frac{1}{\sum_{j=1}^n \left(\frac{1}{D_{ij}} \right)} \quad \text{and} \quad N_j = \frac{1}{\sum_{i=1}^m \left(\frac{1}{D_{ij}} \right)} \quad (\text{B.3})$$

The mean and standard deviation (SD) are calculated for each parameter and each loading case for every column and row of the PPM matrix. The SD is a measure of the degree of dispersion of the data around the mean. A well-designed system should have low SDs and high means (close to 10). High SDs indicate that the system is likely to have significant problematic areas.

The mean values, CPIs, PPIs, and SDs provide an overall performance assessment for the system and loading cases. The mean values are not used directly to rate the performance, because high scores may hide low scores. These indices are calculated by summing the inverse of the data points as a performance rating. To simplify the calculations, the performance indices are recalculated into the range 0–10, enabling different loading cases and parameters to be compared, thereby providing an overall perspective of the characteristics of the system.

To evaluate the design, an overall performance index (OPI) is presented to formulate the performances and loading cases, which provides a quantitative assessment of the system. The OPI function, which lies in the range 0–100, is expressed as follows (for an un-weighted case):

$$OPI = \frac{100}{m \times n} \sum_{i=1}^m \sum_{j=1}^n PPI_i \times CPI_j \quad (B.4)$$

In step (b), the system analyses the performance based on OPI, by comparing a previous iteration and the current results. If the current OPI value is better than the previous value, the system proceeds to the next step (i.e., it generates an input file for ANSYS). Conversely, if the current OPI value is worse than the previous value, the system continues to seek a better solution until the new OPI value is better than the previous value.

Step (c) involves the optimisation process to determine if a better design can be sought or not by further improving the OPI function.

Steps (a) to (c) are repeated until the design satisfies all the chosen constraints and until it cannot be improved any more by any further iterations.

Step (v), which is the last stage in the optimisation process, is the attainment of the optimum solution.

To illustrate the MOST optimisation procedure, a flow chart is included to explain in detail how an optimum solution is achieved for a design problem (Figure B.1).

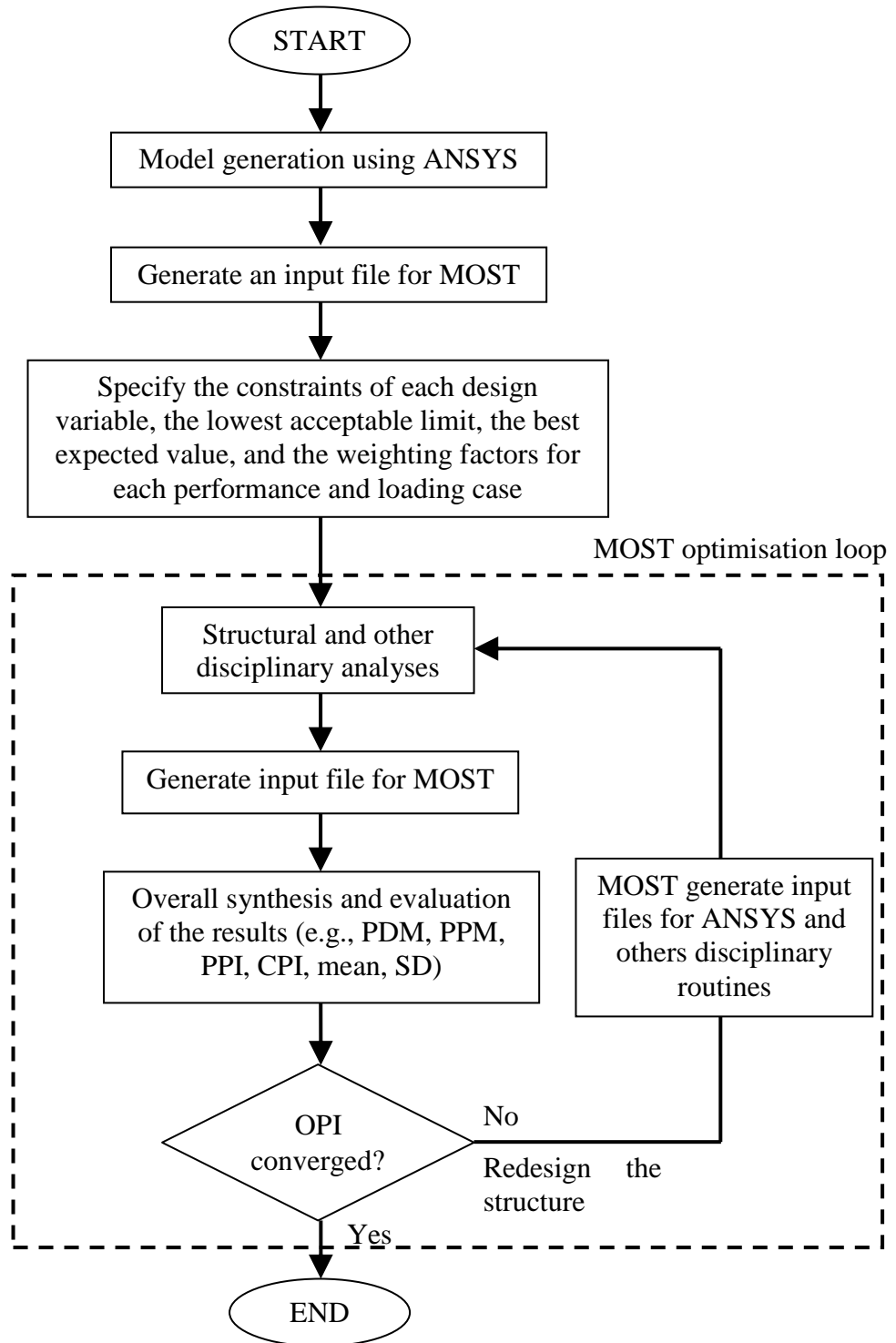


Figure B.1 – Implementation flow chart of the MOST optimisation technique

Appendix C – Piezoelectric generator

Chapter 6 discussed the development of a simulation method for piezoelectric generators, although without providing details of the derivation of the model. This appendix is intended to complement Chapter 6, and describes in detail the model of the piezoelectric generator.

a) Mechanical derivation

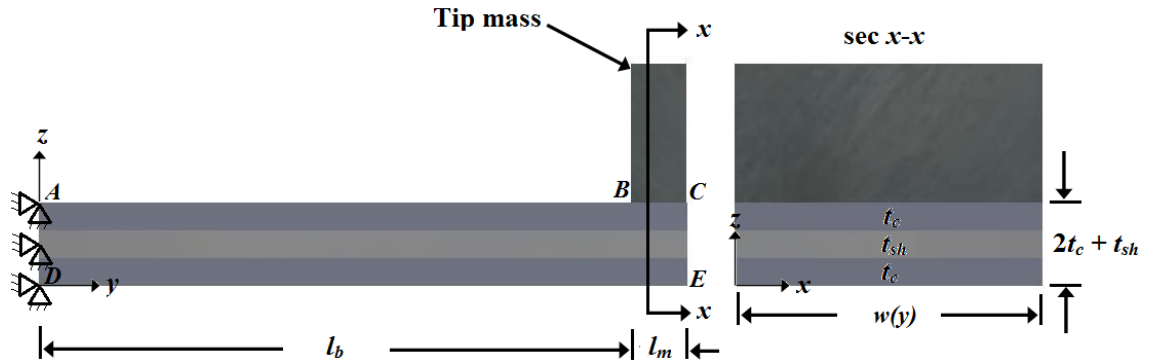


Figure C.1 – Details of the piezoelectric cantilever beam

By using an analytical calculation, the effective moment of inertia (I) of the cantilever beam is defined as follows:

$$I = \left[\frac{2wt_c^3}{12} + \frac{1}{2}wt_c(t_c + t_{sh})^2 \right] + \left[\frac{wt_{sh}^3}{12} \left(\frac{Y_c}{Y_{sh}} \right) \right] \quad (C.1)$$

where w is the beam width, t_c is the thickness of the piezoelectric material, t_{sh} is the thickness of the centre shim material, Y_c is the Young's modulus of the piezoelectric material, and Y_{sh} is the Young's modulus of the centre shim material. This equation is valid in calculating the effective moment of inertia, based on the rectangular shape shown in Figure C.1. The setup of the piezoelectric generator is shown in Figure C.2.

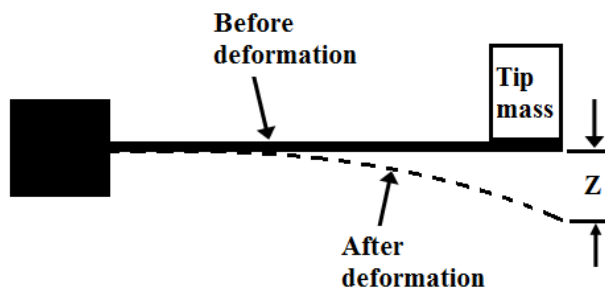


Figure C.2 – Piezoelectric bender

A tip mass is applied to the free end of the beam, which comprises three layers: the top and bottom layers of piezoelectric material, and a middle layer (a brass shim). The electrode, used to produce energy, is connected to the top and bottom surfaces. The electrode length (l_e ; not shown in Figure C.2) is always equal to or less than the beam length (l_b). When the beam is deformed, a stress is induced on the top and bottom surfaces. For the piezoelectric generator, stress and strain are the main concerns. The stress and strain in a piezoelectric material are the ***average element stress and strain***. Therefore, the average element stress in the piezoelectric material covered by the electrode is as follows:

$$\sigma_{ave} = \frac{1}{l_e} \int_0^{l_e} \frac{M(x)b}{I} dx \quad (C.2)$$

If the piezoelectric cantilever beam has a rectangular shape, the average element stress can be calculated using equation (C.1), as can the bending moment of the beam. However, if the beam is an irregular shape, it becomes difficult to calculate the second moment of the area. Finite element analysis can be used to obtain the solution of the average element stress for each analysis, meaning that the second moment of the area is not necessary to calculate the average element stress of the beam, especially in the case of an irregular shape. Consequently, the average element stress (σ_{ave}) can be stated as follows:

$$\sigma_{ave} = \frac{1}{n_c} \sum_{c=1}^{n_c} \sigma_c \quad (C.3)$$

where n_c is the number of piezoelectric material elements. This approach assumes that all the elements are of equal size. Roundy (2003) stated that the tip deflection of the cantilever beam is related to the average strain in the piezoelectric material. By utilising Hooke's Law for elastic material (Benham *et al.*, 1996), the average element stress from finite element analysis, and the Roundy method, the relationship among these factors (b^*) can be defined as follows:

$$b^* = \frac{\sigma_{ave}}{Y_{czt}} \quad (C.4)$$

b) Derivation of electrical energy

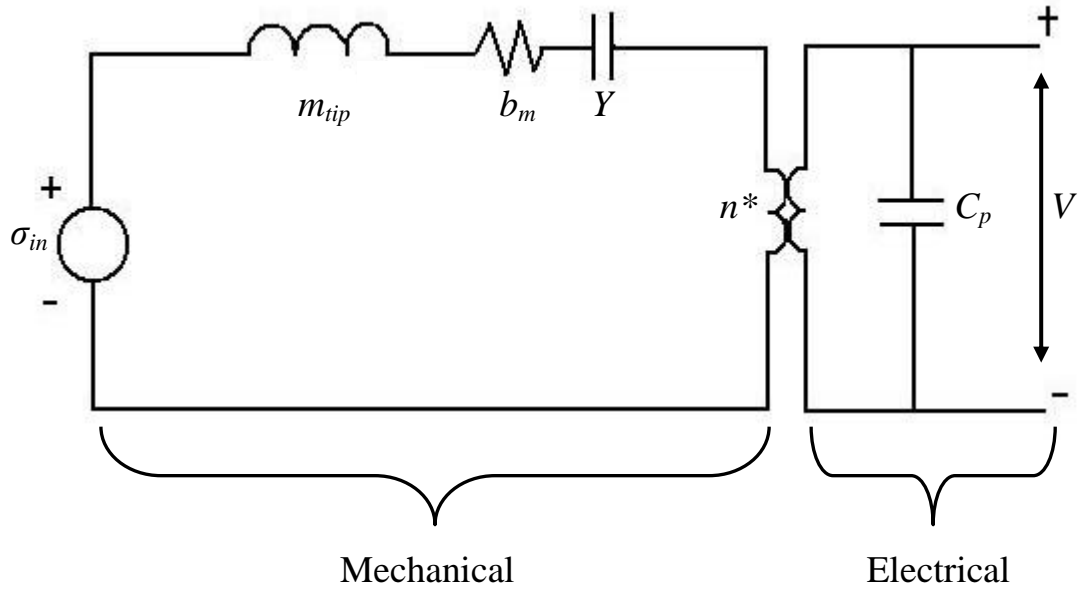


Figure C.3 – Circuit representation of a piezoelectric bimorph cantilever beam

Figure C.3 shows the mechanical side of the piezoelectric cantilever beam and the voltage generated from vibrations, where σ_{in} is the input vibration stress, m_{tip} is the effect of mass or the inertia term, b_m is the resistive element of damping, Y is the stiffness element, n^* is the effective number of turns for the transformer, C_p is the capacitance of the piezoelectric element, and V is the voltage of the system.

The basic derivation is based on Roundy (2003). The piezoelectric elements can be easily applied to the mechanical and electrical sides of the piezoelectric system as circuit elements. The system equations can be obtained by applying Kirchoff's Voltage Law (KVL) and Kirchoff's Current Law (KCL). The mechanical side consists of stress/strain relationships for circuit elements.

The stress across the element is the stress developed as a result of flexing of the beam. σ_{in} is an equivalent stress which represents an input vibration; m represents the inertia term. Thus, the relationships for these two elements are as follows:

$$\sigma_{in} = \frac{m_{tip}}{b^{**}} \dot{y} \quad (C.5)$$

$$\sigma_m = \frac{m_{tip}}{b^{**}} \ddot{z} \quad (C.6)$$

where $b^{**} = \frac{m_{tip}(\dot{y} + \ddot{z})}{\sigma_{ave}}$, relating the vertical force to the average element stress.

The resistive element of damping (b_m) relates stress to tip displacement (unit: Ns/m³). Therefore, the stress/strain relationship for the damping element (σ_{bm}) is as follows:

$$\sigma_{bm} = \frac{b_m}{b^*} \dot{\delta} \quad (C.7)$$

where $\dot{\delta}$ is the rate of change of displacement. The piezoelectric generator is modelled as a transformer (Flynn and Sanders, 2002). The constitutive equations for a piezoelectric material are as follows (Ikeda, 1996):

$$\delta = \sigma/Y + dE \quad (C.8)$$

$$D = \varepsilon E + d\sigma \quad (C.9)$$

where δ is mechanical strain, σ is mechanical stress, Y is the modulus of elasticity, d is the piezoelectric strain coefficient, E is the electric field, D is electric displacement, and ε is the dielectric constant of the piezoelectric material. The transformer relates stress to the electric field at zero strain or relates electrical displacement to strain for a zero electric field, as follows:

$$\sigma_t = -dY_c E \quad (C.10)$$

$$D_t = -dY_c \delta \quad (C.11)$$

The equivalent turn's ratio for the transformer is then $-dY$; however, the current is $\dot{q} = n^* l_e w \dot{D}$ and the voltage is $V = Et_c$. Hence, the equations for the transformer (σ_t) can be written as follows:

$$\sigma_t = \frac{-dY_c}{t_c} V \quad (C.12)$$

$$q_t = -dY_c n^* l_e w \delta \quad (C.13)$$

Applying KVL to the circuit shown in Figure C.3 yields the following equation:

$$\sigma_{in} = \sigma_m + \sigma_{bm} + \sigma_t \quad (C.14)$$

Substituting equations C.5–C.7, C.12, and Hooke's Law ($\sigma_y = Y_c \delta$) into equation C.14 and rearranging the terms, the mechanical dynamics of the system with an electrical coupling term yields the following third-order equation:

$$\ddot{\delta} = -\frac{Y_c b^* b^{**}}{m_{tip}} \delta - \frac{b_m b^{**}}{m_{tip}} \dot{\delta} + \frac{dY_c}{t_c} \frac{b^* b^{**}}{m_{tip}} V + b^* \ddot{y} \quad (C.15)$$

The damping coefficient (c) is the product of the resistive element (b_m) and b^{**} . The effective spring constant, K_{sp} , is equal to Yb^*b^{**} and has units of force and displacement, which relates tip force to tip displacement. $K_{sp} = Yb^*b^{**}$ and the damping coefficient is substituted into equation C.15, yielding the following:

$$\ddot{\delta} = -\frac{k_{sp}}{m_{tip}}\delta - \frac{c}{m_{tip}}\dot{\delta} + \frac{k_{sp}d}{m_{tip}t_c}V + b^*\ddot{y} \quad (C.16)$$

Equation C.16 is part of the dynamic model. Applying KCL to the electrical side, the generator represents a complete dynamic model. From the KCL rules, the current in the transformer is equal to the current through the capacitor, as follows:

$$\dot{q}_t = \dot{q}_{C_p} \quad (C.17)$$

where \dot{q}_t is the current through the transformer (equation C.13) and \dot{q}_{C_p} is the current through the capacitor C_p . The capacitance of the piezoelectric is defined as:

$$C_p = \int_0^{l_e} \frac{n\epsilon w(x)}{t_c} dx \quad (C.18)$$

By using $\rho = m/v$ (density = mass/volume), equation C.18 can be written as follows:

$$C_p = \frac{n\epsilon m_c}{\rho t_c^2} \quad (C.19)$$

where n is the number of layers of piezoelectric material (here, $n = 2$), m_c is the mass of a single layer of piezoelectric material, ρ is the density of the piezoelectric material, and ϵ is the dielectric constant. Substituting equations C.13 and C.18 into equation C.17 and rearranging the terms, we have:

$$\dot{V} = -\frac{dY_c t_c}{\epsilon} \dot{\delta} \quad (C.20)$$

By rearranging equations C.16 and C.20, the dynamic model of the system is obtained as follows:

$$\begin{bmatrix} \dot{\delta} \\ \ddot{\delta} \\ \dot{V} \end{bmatrix} = \begin{bmatrix} 0 & 1 & 0 \\ -\frac{k_{sp}}{m_{tip}} & -\frac{c}{m_{tip}} & \frac{k_{sp}d}{m_{tip}t_c} \\ 0 & -\frac{dY_c t_c}{\epsilon} & 0 \end{bmatrix} \begin{bmatrix} \delta \\ \dot{\delta} \\ V \end{bmatrix} + \begin{bmatrix} 0 \\ b^* \\ 0 \end{bmatrix} \ddot{y} \quad (C.21)$$

Equation C.21 is an open circuit, meaning that no power is transferred. Figure C.4 shows the circuit with a simple resistor as a load.

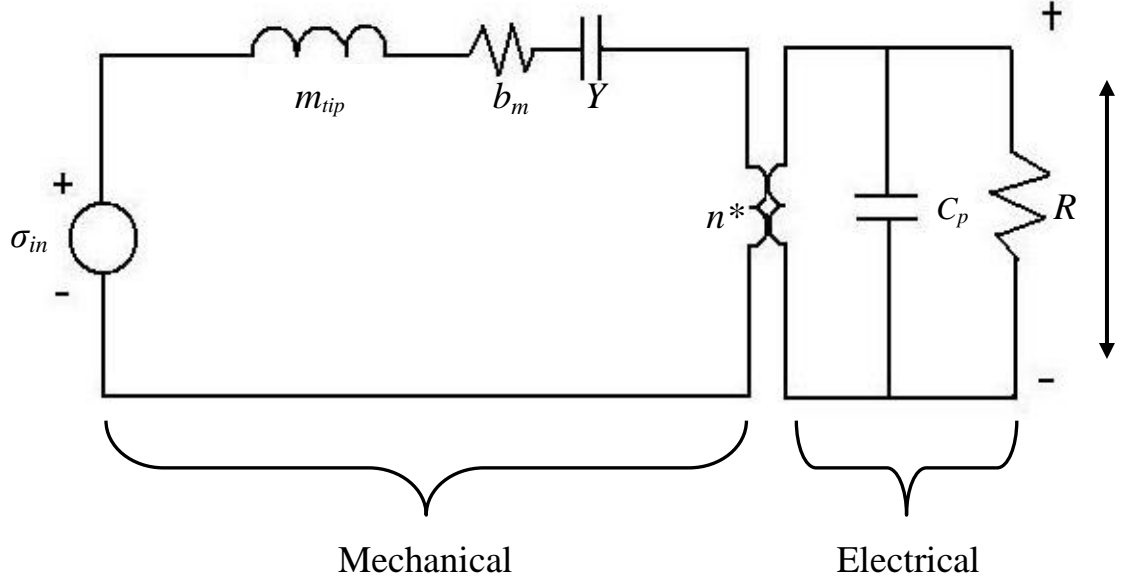


Figure C.4 – Circuit representation of a piezoelectric bimorph with a resistive load

Equation C.22 is similar to equation C.17, although with a minor change on the electrical side. Applying KCL to the electrical side of the circuit, we have

$$\dot{q}_t = \dot{q}_{C_p} + \dot{q}_R \quad (\text{C.22})$$

where \dot{q}_R is the current through the resistor R . The current through the resistor and the capacitor is shown in equation C.23, and the new system model in state space is expressed in equation C.24:

$$\dot{V} = -\frac{dY_{ctc}}{\varepsilon} \delta - \frac{1}{RC_P} V \quad (\text{C.23})$$

$$\begin{bmatrix} \dot{\delta} \\ \ddot{\delta} \\ \dot{V} \end{bmatrix} = \begin{bmatrix} 0 & 1 & 0 \\ -\frac{k_{sp}}{m_{tip}} & -\frac{c}{m_{tip}} & \frac{k_{sp}d}{m t_c} \\ 0 & -\frac{dY_{ctc}}{\varepsilon} & -\frac{1}{RC_P} \end{bmatrix} \begin{bmatrix} \delta \\ \dot{\delta} \\ V \end{bmatrix} + \begin{bmatrix} 0 \\ b^* \\ 0 \end{bmatrix} \dot{y} \quad (\text{C.24})$$

By taking the Laplace transform of equations C.16 and C.23, and rearranging the yield term, we have:

$$V \left[s^3 + \left(\frac{1}{RC_P} + \frac{c}{m_{tip}} \right) s^2 + \left(\frac{k_{sp}}{m_{tip}} \left(1 + \frac{d^2 Y_c}{\varepsilon} \right) + \frac{c}{m_{tip} RC_P} \right) s + \frac{k_{sp}}{m RC_P} \right] = -\frac{Y_c d t_c b^*}{\varepsilon} A_{in} \quad (\text{C.25})$$

Equation C.25 can be solved for the output voltage by making suitable substitutions, such as:

$$k = \sqrt{\frac{d^2 Y_c}{\varepsilon}} \quad (C.26)$$

$$\omega_n = \sqrt{\frac{k_{sp}}{m}} \quad (C.27)$$

$$\zeta = \frac{c}{2m\omega_n} \quad (C.28)$$

Using equations C.26–C.28, the voltage equation is as follows:

$$V = \frac{-j\omega \frac{Y_c dt_c b^*}{\varepsilon}}{\left[\frac{1}{RC_p} \omega_n^2 - \left(\frac{1}{RC_p} + 2\zeta \omega_n \right) \omega^2 \right] + j\omega \left[\omega_n^2 (1+k^2) + \frac{2\zeta \omega_n}{RC_p} - \omega^2 \right]} A_{in} \quad (C.29)$$

The power transferred to the load is simply V^2/R . By using the solution of the average element stress and the vertical tip displacement, the power output for the piezoelectric cantilever beam (vibrating at its resonance frequency) is as follows:

$$P = \frac{1}{2\omega_n^2} \frac{RC_p^2 \left(\frac{dt_c \sigma_{ave}}{\varepsilon z_t} \right)^2}{(4\zeta^2 + k^4)(RC_p \omega_n)^2 + 4\zeta k^2 (RC_p \omega_n) + (2\zeta)^2} A_{in}^2 \quad (C.30)$$

By taking the differential of equation C.30 with respect to R , setting the results equal to zero and solving for R . The optimum load resistance is as follows:

$$R_{opt} = \frac{1}{\omega_n C_p} \frac{2\zeta}{\sqrt{4\zeta^2 + k^4}} \quad (C.31)$$